STRUCTURE, PROPERTIES AND APPLICATIONS OF CONDUCTING POLYMERS CONTAINING ORGANO Fe(II)/Fe(III) COMPLEXES

A THESIS SUBMITTED TO THE UNIVERSITY OF PUNE FOR THE DEGREE OF DOCTOR OF PHILOSOPHY IN CHEMISTRY

BY

SANTHOSH PAUL

POLYMER SCIENCE AND ENGINEERING DIVISION

NATIONAL CHEMICAL LABORATORY (NCL)

PUNE – 411008, INDIA.

MAY 2007

राष्ट्रीय रासायनिक प्रयोगशाला
(वैज्ञानिक तथा औद्योगिक अनुसंधान परिषद)
डॉ. होमी भाभा मार्ग पुणे - 411 008. भारत
NATIONAL CHEMICAL LABORATORY
(Council of Scientific & Industrial Research)
Dr. Homi Bhabha Road, Pune - 411 008. India.

CERTIFICATE

Certified that the work incorporated in this thesis entitled **"Structure, Properties and Applications of Conducting Polymers Containing Organo Fe(II)/Fe(III) complexes"** submitted by Mr. Santhosh Paul, was carried out by him under my supervision/guidance at the Polymer Science and Engineering Division, National Chemical Laboratory, Pune – 411008. Such material as has been obtained from other sources has been duly acknowledged in this thesis.

May, 2007.

Dr. S. Radhakrishnan
Research Guide.

☎ FAX WEBSITE
Communication Channels
NCL Level DID : 2590
NCL Board No. : +91-20-25902000
EPABX : +91-20-25893300
+91-20-25893400
Director's Office : +91-20-25893355
COA's Office : +91-20-25893619
COS&P's Office : +91-20-25893008
www.ncl-india.org

DECLARATION

I hereby declare that the work incorporated in the thesis entitled **"Structure, Properties and Applications of Conducting Polymers Containing Organo Fe(II)/Fe(III) Complexes"** submitted for the degree of Doctor of Philosophy to the university of Pune, has been carried out by me at the National Chemical Laboratory, Pune under the supervision of Dr. S. Radhakrishnan. The work is original and has not been submitted in part or full by me for any other degree or diploma to this or any other university.

May–2007

National Chemical Laboratory,
Pune-8.

Santhosh Paul
Research student.

Acknowledgements

A journey is easier when you travel together. At this moment, I feel the great value of interdependence than only independence. This thesis is the product of four years of hard work whereby I have been accompanied and supported by many people. It is a pleasant aspect that I have now the opportunity to express my gratitude for all of them.

The first person, I would like to thank is my research supervisor and a sagacious scientist **Dr. S. Radhakrishnan**. His overly enthusiasm and integral view on research and his mission for providing 'only high-quality work and not less', has made a deep impression on me. I owe him lots of gratitude for having me shown this way of research. He could not even realize how much I have learned from him: personal discipline, self-dependency and simplicity.

I wish to express my warm and sincere thanks to **Director, NCL**, for permitting me to do this research work and providing me the excellent facilities. This also extends to Pune University for allowing me to register and submit thesis.

I owe my heartiest gratitude to **Dr. N. N. Chavan**, who gave me the opportunity to work with him and assisted me to complete the synthesis work.

I warmly thank **Dr. M. Muthukrishnan**, who gave me untiring help during my difficult moments of Ph.D tenure. This equally extends to Dr. T. P. Mohandas for providing me the space and use facilities in his lab unconditionally at any time.

My seniors and contemporary colleagues in the lab: Dr. S. D. Deshpande, Dr. Rahul Patil, Dr. V. Sreejith, Dr. A. Adhikari, Dr. S. Kanagoakar, Dr. S. B. Kar, Dr. S. Subramanyam Mr. Francis Amalraj, Pradip Sonawane, V. V. Radhakrishnan, B. T. S. Ramanujam, Narendra Sonawane, Anshuman Duarah, Michael Joseph and M. P. Raut, all gave me the feeling of being at home at work.

My special thanks goes to Mr. R. Harikrishna and Shijo K. Cherian for being with me, understanding and cooperating to great extend.

During this work I have collaborated with many colleagues for whom I have great regard, and I wish to extend my warmest thanks to all those who have helped me with my work.

Additional energy and vitality for this research was provided externally through my involvement in occasional get together with friends, social interactions and activities. I thank you all for having shared many experiences and thoughts with me throughout the last years. The principle, to see the good in everything and be a constructive part of the whole, made me feel responsible.

I owe my loving thanks to my parents, **P. V. Poulose** and **K. O. Annie**. They missed their son for quite some time due to my research outside the hometown. Without their encouragement, prayer and understanding, it would have been impossible for me to finish this work. My special gratitude is due to my brother Justin Paul and his family for their loving support.

The financial support provided by CSIR, New Delhi is greatly acknowledged.

The chain of my gratitude would be definitely incomplete if I would forget to thank the first cause of this chain, using Aristotle's words, The Prime Mover. My deepest and sincere gratitude for inspiring and guiding this humble being.

THIS WHOLE WORK IS DEDICATED TO THE HANDS OF ALMIGHTY GOD.

National Chemical Laboratory
Pune 411008. Santhosh Paul.

CONTENTS

LIST OF ACRONYMS

Ar	- Aromatic
BE	- Binding Energy
CO	- Carbon Monoxide
CP	- Conducting Polymer
Cp	- Cyclopentadiene
CV	- Cyclic Voltammetry
DCM	- Dichloromethane
DMSO	- Dimethyl Sulphoxide
DSC	- Differential Scanning Calorimetry
d-value	- Inter-planar Distance
Ea	- Activation Energy
ECP	- Electronically Conducting Polymer
EDAX	- Electron Dispersion X-ray Microanalysis
eV	- Electron Volt
Fc	- Ferrocene
$FeCl_3$	- Ferric Chloride
FePcTSA	- Iron(III)phthalocyanine-4,4',4'',4'''-tetrasulfonic acid,compound with oxygen monosodium salt hydrate
FeTPP-Cl	- 5,10,15,20-tetraphenyl-21H,23H-porphineiron(III) chloride
FTIR	- Fourier Transform Infrared
GFAAS	- Graphite Furnace Atomic Absorption Spectroscopy
H_2SO_4	- Sulfuric Acid
^{1}HNMR	- Proton Nuclear Magnetic Resonance
ICP	- Inherently Conducting Polymer.
KBr	- Potassium Bromide
KCl	- Potassium Chloride
MEMs	- Microelectromechanical System

MOSFET	- Metal Oxide Semiconductor Field Effective Transistor
m.p.	- Melting point
$(NO)_x$	- Nitric Oxide
OD	- Optical Density
PA	- Polyacetylene
PEO	- Polyethylene Oxide
PET	- Polyethylene Terephthalate
ppm	- Parts per Million
PPy	- Polypyrrole
Pt	- Platinum
Py	- Pyrrole
RT	- Room Temperature
SCE	- Standard Calomal Electrode
TBAP	- Tetrabutylammonium Perchlorate
TEM	- Transmission Electron Microscopy
TGA	- Thermogravimmetric Analysis
TLC	- Thin Layer Chromatography
UV-Vis.	- Ultra Violet–Visible
XRD	- X-Ray Diffraction.

LIST OF SYMBOLS

I	- Current
E	- Potential
P	- Resistivity
R	- Resistance.
R_0	- Initial Resistance
ΔR	- Change in Resistance
σ	- Conductivity
Ω	- Ohm
KΩ	- Kilo Ohm
MΩ	- Mega Ohm
mA	- milli Ampere
I	- Current
S/cm	- Siemens per Centimeter
V	- Voltage
mV	- milli Volt
μV	- micro Volt
K^{-1}	- Kelvin Inverse
T	- Temperature
^{0}C	- Degree Centigrade
S	- Sensitivity Factor
%	- Percentage
μm	- micro meter
mg	- milli gram
g	- gram
t	- Time
h	- Hour
s	- Second
ml	- milli Liter
μl	- micro Liter

λ_{max}	- Wavelength of Maximum Absorption
υ_{max}	- Wavenumber of Maximum Transmission
nm	- Nano meter
[C]	- Polymer Conversion
% T	- Percentage Transmission
Ea	- Activation Energy
t_{50}	- Response Time of Sensor
dR	- Change in Resistance
dt	- Change in Time
MHz	- Mega Hertz
d	- Doublet in NMR
s	- Singlet in NMR
t	- Triplet in NMR
m	- Multiplet in NMR
T_m	- Melting Temperature
T_g	- Glass Transition Temperature
J/g	- Joule per gram
ΔH_m	- Enthalpy Change During Melting
ΔH_c	- Enthalpy Change During Crystalisation

CHAPTER I

INTRODUCTION

1.1. Conducting Polymers History

The past decade has witnessed tremendous advances in the development of organic conductive molecular and polymeric materials and this field continues to be of great scientific and commercial interest. This field of science flourished by discovering new π-conjugated materials and by tailoring their electrical conductivity by doping from semi conductive to metallic and even super conductive regime.

Polymer synthesis in the 1950's was dominated by Karl Zieglar and Giulio Natta, whose discovery of polymerization catalysts was important for the development of polyethylene and the modern 'plastic' industry. Theses were insulating polymers. The well known conducting polymer viz. polyacetylene (PA), was also first synthesized using these type of catalysts in 1974 when Ito and Shirakawa [1] synthesized films of PA following a modified Natta route. These free standing films however were found to be intrinsically semiconducting with an energy gap of 1.4 eV [2]. In 1976, Hideki Shirakawa, Alan Mac Diarmid and Alan J. Heeger discovered conducting polyacetylene and the ability to dope this polymer over the full range from insulating to metallic states [3, 4]. The importance of this discovery was recognized in 2000 when the Nobel Prize for Chemistry was awarded to the scientists, who discovered electrically conducting PA [5]. Leading from this break through, many other small conjugated molecules were found to polymerize with improved or desired properties, which began to attract the attention of synthetic chemists in the 1980's. The archetype of conducting polymer viz. polyacetylene, becomes very highly conducting on doping in comparison with other conjugated polymers, but its environmental instability, insolubility, infusibility and lack of processability are obstacles to technological applications. Polymers containing heterocyclic units in the backbone, which have notable electrical conductivities, offer increased stability and processability in both the neutral and doped states when compared with polyacetylene.

Conducting polymers have become valuable for electronic components of the modern age, because they possess a broad range of applications in thin film transistors [6], batteries [7–9], chemical sensors [10–13], antistatic coatings [14], electronic chips and other molecular level electronics [15, 16], electromagnetic shielding [17], artificial muscles [18], LED's [19], bio-sensors [20–22], fuel cells [23], photo voltaic cells [24],

corrosion coatings [25, 26]; therefore they render tremendous future marketing opportunities. Fig. 1.1. gives the structure of a few inherently conducting polymers.

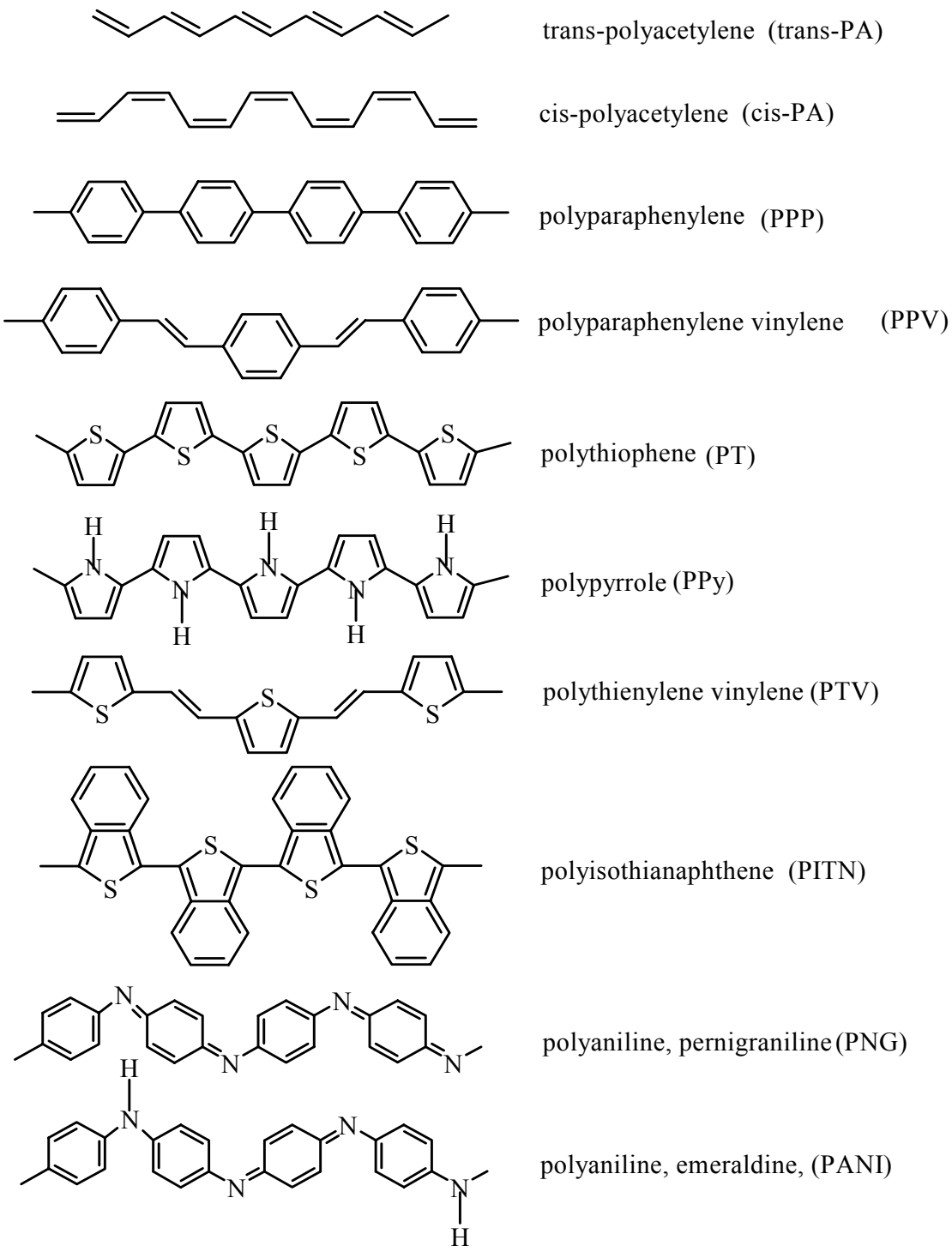

Fig. 1.1. Examples of a few inherently conducting polymers.

1.2. Classification of Conducting Polymers

Electrically conducting polymers are classified into different types on the basis of the conduction process [27] as follows:

a. Polymeric charge transfer complexes.
b. Organometallic polymeric conductors.
c. Conducting polymer composites.
d. Highly conjugated polymers.

1.2.A. Polymeric Charge Transfer Complexes

These are formed by the addition of acceptor like molecules to insulating polymers forming complexes known as conducting charge transfer complexes. The theory for the charge transfer complexes was proposed by Mulliken [28, 29] and Dewar [30]. However, reasons for high conductivity in polymeric charge-transfer complexes and radical-ion salts are still somewhat obscure. It is likely that in polymeric materials, the donor-acceptor interaction promotes orbital overlap, which contributes to alter molecular arrangements, and enhanced electron delocalization.

1.2.B. Organometallic Polymeric Conductors

These are obtained by adding organometallic groups to polymer molecules [31]. The metal d-orbitals may overlap π-orbitals of the organic structure increasing electron delocalization. The d-orbitals may also bridge adjacent layers in crystalline polymers such as in poly (ferrocenylene) to give conducting property to it. Metallophthalocyanines and their polymers are also from this class of material. They possess a strong potential for future applications, for example in molecular wires, antistatic foils, fibers and xerography.

1.2.C. Conducting Polymer Composites

Conducting polymer composites are mixtures/blends of conductive particles and polymers. These are phase separated materials with conducting phase dispersed in an insulating matrix. Various moulding, casting and extrusion techniques are normally used to make these composites.

1.2.D. Highly Conjugated Polymers

These are the main materials of interest in the current studies. An organic polymer that possesses the electrical, electronic, magnetic and optical properties of a metal while retaining the mechanical properties, processibility etc. commonly associated with a conventional polymer, is termed as an "intrinsically conducting polymer" (ICP) more commonly known as "synthetic metal" [32]. The unique electronic properties of the conjugated polymers are derived from the presence of π - electrons, the wave functions of which are delocalized over a long portion of the polymer chain when the molecular structure of the backbone is planar. It is therefore necessary that there are no large torsion angles at the bonds, which would decrease the delocalization of the π - electrons system [33].

In conjugated polymers, the chemical bonding leads to one unpaired electron (the π-electron) per carbon atom. More over, π- bonding, in which the carbon orbitals are in the sp^2p_z configuration and in which the orbitals of successive carbon atoms along the back bone overlap, leads to electron delocalization along the backbone of the polymer. This electronic delocalization provides the 'high way' for charge mobility along the backbone of the polymer chain. In other words, the infinitely long one dimensional arrangement of π- electrons forms a half filled band, or that the highest occupied (HO) and the lowest unoccupied (LU) π- electron bands merge with each other, leading to a metallic behavior.

The classic example is polyacetylene, in which each carbon is σ- bonded to only two neighboring carbons and one hydrogen atom with one π- electron on each carbon. If the C-C bond lengths were equal, the chemical formula, $-(CH)_n$ with one unpaired electron per formula unit would imply a metallic state. The easy conversions to the metallic state on doping together with a variety of studies of the neutral polymer have eliminated the antiferromagnetic Mott insulator as a possibility.

Although many polymers fall under this class of material, the main polymer which is studied in the present work, is polypyrrole (PPy) doped with ferrocene, iron phthalocyanine, iron porphyrin and its random co-polymer with ferrocene derivative. Hence, a brief survey of polypyrrole and pyrrole co-polymer is given in the following sections.

1.3. Polypyrrole

Amongst all known conducting polymers, PPy is the most frequently used in commercial applications, due to the long-term stability of its conductivity and the possibility of forming homopolymers or composites with optimal mechanical properties [34]. Pyrrole was first synthesized in 1916 by the oxidation of pyrrole with H_2O_2 to give an amorphous powdery product known as pyrrole black [35]. There are three methods generally used to prepare polypyrrole: (i) chemical polymerization in solution [36–38], (ii) chemical vapor deposition (CVD)/ vapor phase polymerization [39, 40], and (iii) electrochemical polymerization [41–43]. The chemically prepared materials are of lower quality as compared to those obtained from electrochemical route. However, chemical methods have some potential advantages such as ease in modification of structure, mass production, short reaction time, preparation of composites and low cost. In 1979, electrochemical technique to synthesize PPy becomes a useful tool to obtain highly conducting freestanding materials. Chemical and electrochemical methods of synthesis have since then been improved in order to optimize the physical and chemical properties of these materials.

The charge carriers within PPy have been identified as polarons and bipolarons. Charge transport in PPy is made up of two components; intrachain charge transport, which consists of the movement of charge along the PPy chains (which usually requires little energy), and interchain charge transport. The later requires considerably more energy and involves the hopping of charge to neighboring chains.

1.3.A. Chemical Synthesis

Polypyrrole can be synthesized in various solvents with different oxidizing agents. In general, pyrrole blacks have been prepared in the presence of various oxidizing agents like hydrogen peroxide, lead dioxide, ferric chloride, nitrous acid, quinones or ozone. The materials obtained by this methods have resulted mainly in insulating materials with room temperature conductivity typically on the order of 10^{-10} to 10^{-11} S/cm [44–46], which on doping with halogenic electron acceptors give a conductivity of about 10^{-5} S/cm. In this sense, a lot of efforts have been made to get highly conducting polypyrrole. One of the great advantages of polypyrrole from synthetic point of view concerns the low

oxidation potential of the pyrrole monomer [47]. Several metallic salts have been employed to polymerize pyrrole such as $FeCl_3$, Fe $(NO_3)_3$, Fe $(ClO_4)_3$, K_3Fe $(CN)_6$, $CuCl_2$, $CuBr_2$ etc. with conductivity's ranging between 10^{-5} to 10^2 S/cm. A typical polypyrrole synthesis procedure in various solvents with anhydrous $FeCl_3$ salt is as follows: In case of $FeCl_3$, the polymerization process is summarized below [48, 49]: 2.695 g (+0.2%) anhydrous iron(III) chloride was dissolved in 50 ml double distilled water in each of the reaction vessels. 0.50 ml freshly vacuum distilled pyrrole (corresponding to an initial mole ratio iron(III)/pyrrole of 2.30) was added to each solution and the polymerization allowed to proceed at 19.0 + 0.5 °C for various time intervals with constant gentle agitation. In each case, the reaction was terminated by vacuum filtration of the product. The resulting black powder was washed with copious quantities of water until the washings were clear and then dried under vacuum (10^{-3} Torr) at room temperature for at least 40 hours. The polymerization scheme is given below:

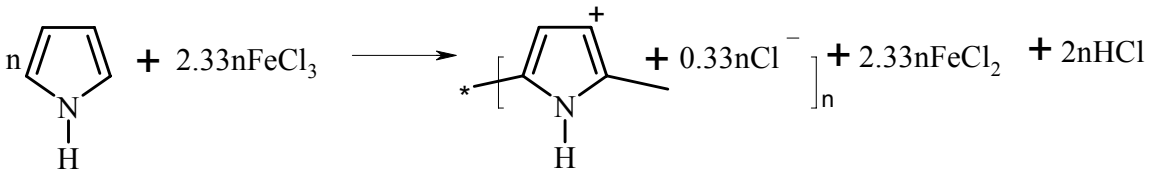

It is believed that for initial mole ratios nFe/n_m greater than 2.33, there is competitive incorporation of iron-based counter-ions such as $FeCl^{4-}$ in addition to the chloride counter-ion. Pron et al. [50] have reported that further doping of polypyrrole prepared by a similar route can be achieved by exposure to iron(III) chloride in nitromethane, resulting in the incorporation of iron-based species. The highest conductivity value obtained by using methanol solution was 190 S/cm. It was found that by controlling the oxidation potential of the solution, the conductivity can be increased up to 220 S/cm. Low temperatures (0-5°C) are the most appropriate for obtaining the best conductivities in aqueous solutions of ferric salts [51]. A similar behaviour of the chemical oxidation of pyrrole in organic solvents has been reported [52]. This seems to suggest that lowering the reaction rate results in an increasing conductivity of the polymer.

Yoshikawa et al. [53] have found that highly conductive PPy could be obtained if the oxidation potential of the aqueous solution is controlled to the optimum value during

chemical polymerization by adding a suitable amount of $FeCl_2$. In this way PPy having conductivity of more than 200 S/cm was prepared [54]. Apart from the metallic salts, simultaneous chemical synthesis and doping of PPy has been achieved, using a halogenic electron acceptor such as bromine or iodine dissolved in different solvents. PPy-I_2 and PPy-Br_2 have conductivities around 1 to 30 S/cm [55]. CuCl-$AlCl_3$-O_2 is a typical catalytical system applied to synthesize PPy chemically [56] in mass quantities. The oxidation states of PPy are shown in Fig. 1.2.

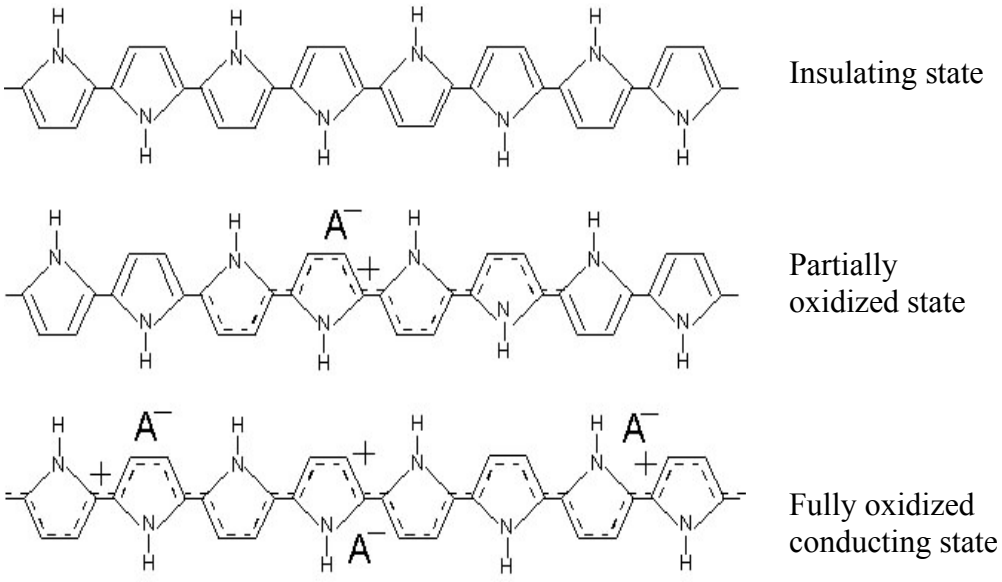

Fig. 1.2. Various oxidation states from insulating to conducting polypyrrole

1.3.B. Electrochemical Polymerization

It has been observed that, with the exception of polyacetylene, most of the conducting polymers can be electrochemically produced by anodic oxidation. More over, in contrast to chemical methods, the conducting films are formed directly on the electrode. This stimulated research teams in the field of electrochemistry to study the electro synthesis of these materials.

The electrochemical preparation of polypyrrole in aqueous solution has been reported first by Diaz et al. [57]. According to them, the electro synthesis of PPy film proceeds via the oxidation of pyrrole at the platinum electrode to produce an unstable π-radical cation which then reacts with the neighboring pyrrole species. Electro polymerization of pyrrole

can be performed in both aqueous and non-aqueous media, such as acetonitrile, propylene carbonate, and dichloromethane etc [58–60]. There are some advantages in doing electropolymerization of PPy in aqueous systems, which are: i) it permits the use of a variety of ions as dopant, ii) in most cases the standard electrode potential of a redox couple is measured in aqueous solutions, and iii) water possesses favorable aspects [61] for future industrial applications of electrochemically grown polypyrrole films. However, with increasing nucleophilicity of solvent, the film growth is inhibited due to the interaction of the solvent with the primary products of monomer oxidation. The film does not form in such nucleophilic aprotic solvents as dimethlyformamide, dimethyl sulfoxide, hexa methylphosphonamide, unless the nucleophilicity of solvent is reduced by addition of a protic acid [62]. Apart from that, the side reactions occurring on the film surface can affect electropolymerization in these solvents. According to the extensively used procedure of Diaz, 2% of water in acetonitrile solution results in better PPy films with improved properties (adhesion to electrode, uniformity) [63]. However, a high content of water in the electrolyte (over 20%) results in deterioration of the film properties such as tensile strength and conductivity.

In a typical preparation, acetonitrile solution containing 0.1 M $TEATBF_4$ plus ca.0.02 M pyrrole is employed. The oxygen in the solution is swept out by bubbling an inert gas through solution prior to the electrolysis, because films prepared in the presence of oxygen have inferior properties [64]. Using a current density of 0.22 mA/cm^2 films having thickness of 10-200 μm were prepared by Diaz and Kanazawa, which could be physically separated from the electrode. Wernet et al. reported that the conductivities of polypyrrole containing alkylsulfonate varied from 1 to 160 Scm^{-1}. It has been established that during electrochemical polymerization of pyrrole in acetonitrile solution or in aqueous solution, 2 electrons are transferred from pyrrole to the Pt anode [65] and the pyrrole units are α,α-linked to form the polymer with the elimination of 2 H per pyrrole unit. Even when if runs the polymerization in a neutral supporting electrolyte solution, the solution at the vicinity of the anode becomes acidic during polymerization [66]. The reactivity can be explained in terms of the competition mechanism of oxidation between pyrrole and anion. When the on-set potential of oxidation current of pyrrole is inferior to the standard electrode potential of anion, the formation of pyrrole cation should dominate

over the oxidation of the anion, resulting in the electrodeposition of pyrrole [67]. In the other case, the oxidation of anion should prevail over that of pyrrole, which makes difficult the formation of pyrrole cation leading to the film formation. Although a kinetic discussion requires studies of elementary processes of the polymerization, the above intepretation could be endorsed at least qualitatively by the Marcus Levich theory of the electron transfer [68], which tells that a rate constant of the electrode reaction depends on the over potential (difference between electrode potential and standard electrode potential) and the reorganization energy.

According to Rodriguez et al. [69] the electrochemical method is most useful since it permits direct grafting of the conducting polymers onto the electrode surface, which can be of special interest for electrochemical applications. As the electrical potential needed for monomeric oxidation is significantly higher than the charging (or doping) of the finally formed polymer, the polymer is obtained in its conducting (doped) state. The film thickness can be easily controlled by the electrical charge employed during polymerization. Also, the electrochemical generation of conducting PPy is a fast, easy and clean method to obtain highly conducting PPy materials. Another characteristic of electrochemical polymerization of pyrrole arises from the special features of its oxidation process. Electropolymerization of pyrrole and similar monomers differs from the other polymerization reactions. In the common electrochemically induced polymerization process, the electrode triggers chain growth and consequently, the process requires little electricity [70, 71]. By contrast, in the anodic oxidation of pyrrole to produce polypyrrole, the charged species of precursor initially formed by the continuous oxidation of the neutral monomer at the anode surface [72]. In consequence, several electrochemical and chemical competitive reactions are possible near the electrode surface.

The oxidation of pyrrole to polypyrrole is irreversible. The mechanism of this reaction was extensively studied; yet the problem still remains not fully resolved. Among the mechanisms proposed, two different theories have gained the greatest interest. One of those is the oxidative coupling of monomer molecules is shown in Fig. 1.3. [73]. The first stage of the reaction is the electrode oxidation of monomer molecules yielding radical cations with the radical state delocalized over the pyrrole ring (B). The maximum spin

density is at the α-position [74]; hence, of the three possible resonance states, (C), (D) and (E), the latter is the most stable. The radical cations dimerise and expel two protons. The dimers, owing to stronger conjugation, are more readily oxidized under the given reaction conditions than the monomer. The chain growth proceeds by addition of a newly formed radical cation to an oligomeric one.

1) Monomer Oxidation

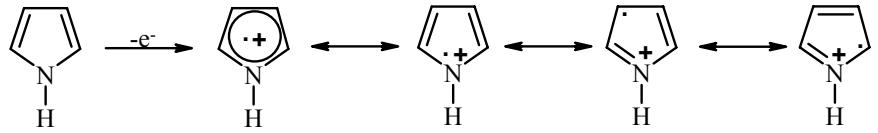

2) Coupling (Dimerisation of cation radicals)

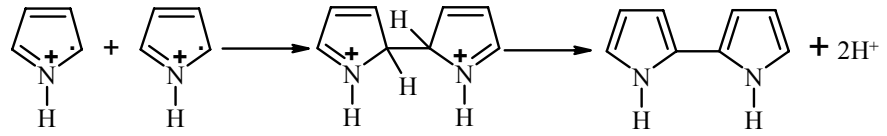

3) Chain growth

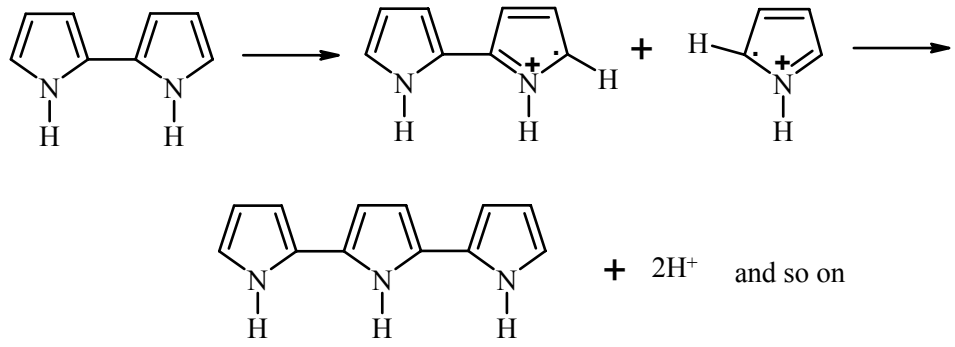

Fig. 1.3. Oxidative coupling mechanism for Polypyrrole

The second most widely discussed mechanism is the free radical reaction is shown in Fig. 1.4. This scheme implies that formation of a radical cation on the anode is followed by the loss of proton and attack of the radical on the neutral monomer. After re-oxidation of the dimeric radical and proton loss, the dimeric molecule can experience subsequent oxidation, which results in chain growth.

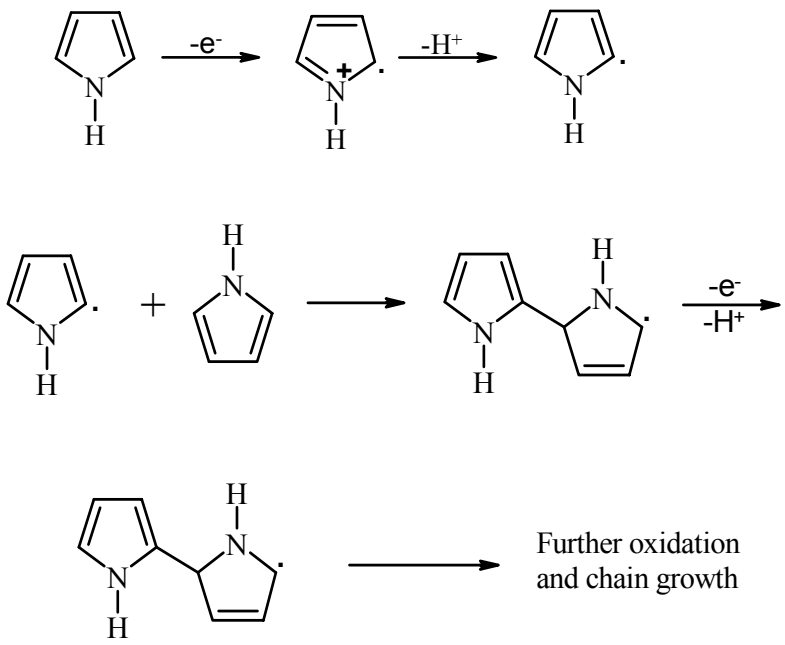

Fig. 1.4. Radical Mechanism for polypyrrole synthesis

1.4. The Concept of Doping

Conjugated organic polymers as such are either electrical insulators or semiconductors. The physical properties of these polymers are altered drastically upon addition of donors or acceptors [75]. Those polymers that can have their conductivity increased by several orders of magnitude from the semiconductive regime are referred to as electronically doped conducting polymers. There are various doping mechanisms were suggested for semiconducting polymers [76, 77]. Besides, the conductivity along the conjugated π-system of a chain, which is accepted as the most important factor; for the overall conductivity, hopping between the chains must be considered, because, in principle, one has to deal with finite polymeric chains that do not percolate the sample. Furthermore, so-called "defects" (sp^3-carbons, β-1inkage, cross-linking, strongly twisted segments, etc.) make hopping necessary to ensure conductivity, because they interrupt the π-conjugation. Hopping is expected to be the rate limiting factor for the electrical conductivity for energetical reasons [78]. The conductivities of the doped polymers are compared with metals and insulators in Fig. 1.5.

The conductivity attainable by an electronic polymer has been increased an infinite number of times as in the discovery of superconductivity in regioregular poly(3-hexylthiophene) [79–81]. The electrical conductivity results from the existence of charge carriers (through doping) and from the ability of those charge carriers to move along the π- bonded 'high way'. So doping is a phenomenon of charge injection onto conjugated semiconducting macromolecular chains.

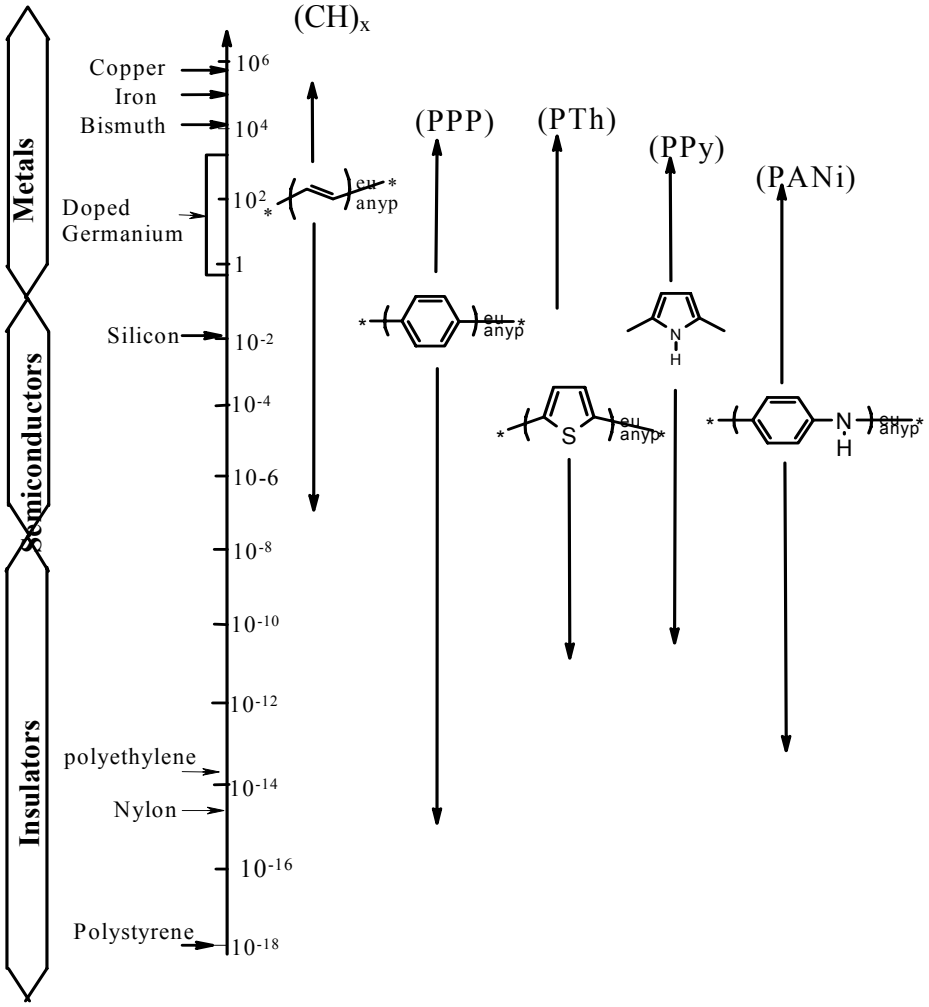

Fig. 1.5. Conductivities of main ECPs compared with other classical conductors, semiconductors and insulators. The arrows indicate the ranges of conductivity from the dedoped state (lower value) to the doped state (upper value).

The concept of doping is the unique one, which distinguishes conducting polymers from all other type of polymers. Because of electron–lattice interactions, structural distortions occur, leading to generation of polarons, bipolarons, and solitons. Suitable oxidation (p-doping) and reduction (n-doping) of certain polymers have been demonstrated to result in

a wide range of electrical conductivity σ from 10^{-13} to 10^{5} S/cm. In comparison, copper has a room temperature σ of 6 X 10^{5} S/cm. Application of statistical mechanics allows calculation of the density of polarons, bipolarons and solitons and the density of electrons and holes in the energy band states. As the doping level is increased, the concentration of polarons goes up and they become crowded together, close enough for bipolaron formation to occur. It is at this point in the doping process that the conductivity undergoes a marked increase. Once the radical components of the polarons have combined to form π bonds, the remaining positive charges achieve high mobility along the chain. Doping of polymers may be carried out by the following methods: i) Gaseous doping ii) Solution doping iii) Electrochemical doping iv) Self-doping v) Radiation induced doping vi) Ion exchange doping. Various doping mechanisms are summarized as follows:

1.4.A. Chemical Doping by Charge Transfer

The redox reaction mechanism is given below with the following example [82, 83]:

a) p-type:

$$(\pi\text{-polymer})_n + 3/2ny(I_2) \longrightarrow [(\pi\text{-polymer})^{+y}(I_3^-)_y]_n$$

b) n-type:

$$(\pi\text{-polymer})_n + [Na^+(Naphthalide)^-]_y \longrightarrow [(Na^+)_y(\pi\text{-polymer})^{-y}]_n + (naphth)^0$$

1.4.B. Electrochemical Doping

Electrochemical doping is illustrated with the following example:

a) p-type:

$$(\pi\text{-polymer})_n + [(Li^+)BF_4^-]_{solution} \longrightarrow [(\pi\text{-polymer})^{+y}(BF_4^-)_y]_n + Li\ (electrode)$$

b) n-type:

$$(\pi\text{-polymer})_n + Li\ (electrode) \longrightarrow [(Li^+)_y(\pi\text{-polymer})^{-y}]_n + [(Li^+)BF_4^-]_{solution}$$

1.4.C. Photodoping

The semiconducting polymer is locally oxidized and (near by) reduced by photo absorption and charge separation (electron hole pair creation and separation into free carriers):

$$(\pi\text{-polymer})_n + h\upsilon \longrightarrow [(\pi\text{-polymer})^{+y} + (\pi\text{-polymer})^{-y}]_n$$

1.4.D. Charge Injection at a Metal-semiconducting Polymer (MS) Interface

Electrons and holes can be injected from metallic contacts into the π* and π-bands respectively [84]:

a) hole injection into an otherwise filled π-band

$$(\pi\text{-polymer})_n - y(e^-) \longrightarrow (\pi\text{-polymer})^{+y}]_n$$

b) electron injection into an empty π* band

$$(\pi\text{-polymer})_n + y(e^-) \longrightarrow (\pi\text{-polymer})^{-y}]_n$$

The effect of doping and allied application is shown in Fig. 1.6.

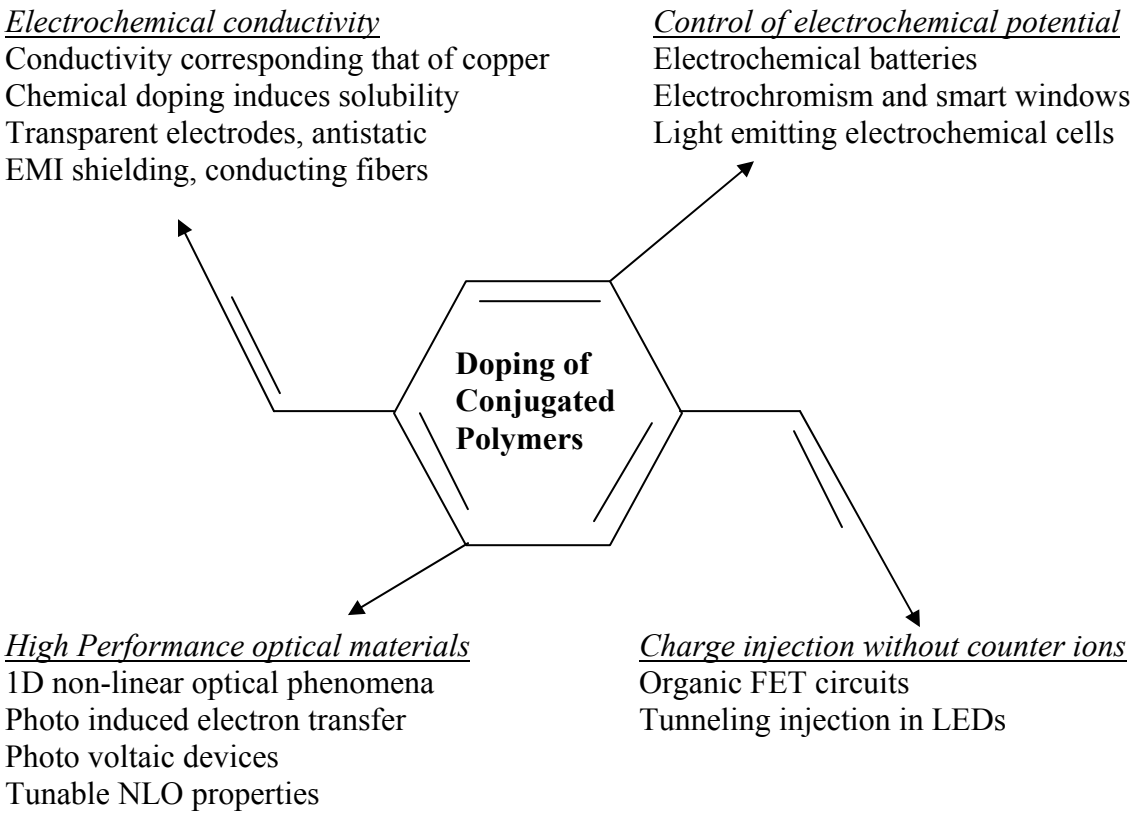

Fig. 1.6. Doping and related applications of conducting polymers

1.5. Co-polymer Synthesis with Pyrrole

Co-polymerization is a process in which two or more monomers are incorporated as integral segments of a polymer. In general, copolymers possess physical and mechanical properties intermediate between both homopolymers. The magnitude of the numerical values of these properties are generally dependent on the concentration of the monomer

units incorporated into the copolymer. The primary advantage of copolymerization is that it leads to a homogeneous material, the properties of which can be regulated by adjusting the ratio of the concentration of monomers in the feed. One of the important goals of research on conducting polymers is to synthesis small gap conjugated polymers, and since copolymerization can influence the band gap [85, 86]. The reactivity of pyrrole and thiophene during copolymerization with their derivatives depends strongly on the oxidation potentials of the monomers. In general, there are four kinds of copolymers:

i) Random copolymer

The arrangement of monomer units is in a statistically random placement along a chain.

–A–B–A–A–AA–B–A–A–B–B–

ii) Alternating copolymer

The two types of monomeric units alternate regularly in the polymer chain.

–A–B–A–B–A–B–A–B–A–B–A–B–

iii) Block copolymers

It composed of long, linear sequence of one monomer unit followed by long linear segment of another.

–A–A–A–A–A–B–B–B–B–B–B–B–A–A–A–A–

iv) Graft copolymers

One homopolymer is attached at various, generally random, points along the back bone of another homopolymer.

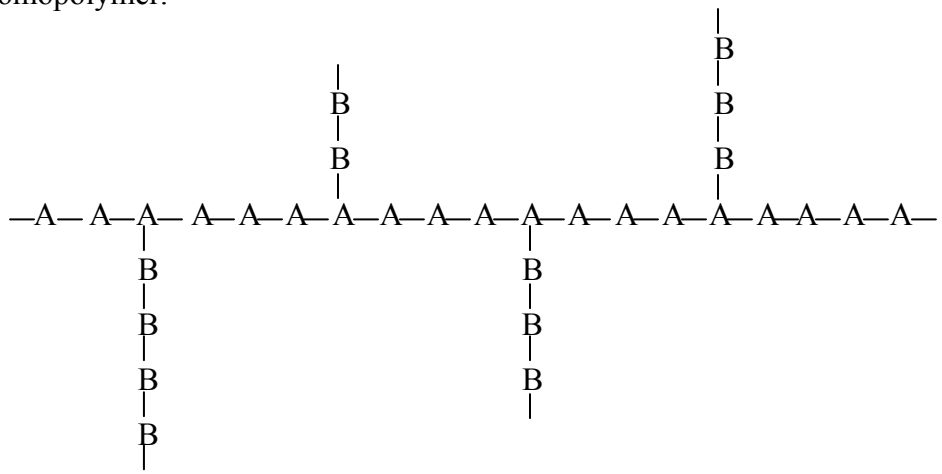

1.5.A. Polypyrrole and Polythiophene Copolymers

In the oxidative copolymerization of one heterocyclic monomer with another, a crucial parameter is the oxidation potential of the monomer. Because it determines which monomer will oxidize first and the stability of the intermediate species. Inganas et al. [87] first prepared random co-polymers of thiophene and pyrrole. The composition of the copolymer depends on applied potential and feed ratio. Thiophenes and pyrroles were extensively studied for copolymerization [88, 89]. By its very nature, copolymerization offers the unique capability or opportunity to design and construct molecules with special electronic properties. Copolymerization enables the molecular architect or tailor to incorporate various molecules; eg. biological components into electroactive polypyrrole and polythiophene.

It is virtually impossible to prepare alternating copolymers by the direct oxidative copolymerization of two heterocyclic monomers because each monomer would have to be incapable of homopolymerizing and could only react with each other. Some polycondensations yield alternating structures, but the most efficient route is to homopolymerize a dimer comprising both monomer units. Naitoh [90] prepared alternating copolymers of thiophene and pyrrole by synthesizing and electrochemically polymerizing 2,2'-thienylpyrrole.

Thiophene/styrene block copolymers were reported by Olinga [91]. In case of grafted copolymers, the main problem is very low yield. The low percolation thresholds observed for composites of polythiophenes and vinyl polymers suggest that highly conducting and processable materials may be prepared by graft copolymerization. Polythiophene-polyvinyl alcohol graft copolymers were reported by Wakabayashi et al. [92].

Pyrrole is a very reactive monomer, forming random copolymers when present during the oxidation of several monomers with widely different structures. Polypyrrole copolymers with perfectly alternating units of pyrrole with another single heterocycle are rare. Kowalik et al. reported alternate copolymers of pyrrole and benzoquinone [93].

A number of techniques for the preparation of polymers with desired end groups have been developed. Living polymerization is widely used polymerization technique to synthesize polymers with desired structure. Living polymerizations are chain growth reactions that proceed in the absence of irreversible chain transfer and chain termination.

The final average molecular weight of the polymer can be adjusted by varying the initial monomer/initiator ratio, while maintaining a narrow molecular weight distribution (Mw/Mn/1.5). Hence, polymers can be end-functionalized and block copolymerized with other monomers. Thus, it has opened new pathways to create many new materials with vastly differing properties by varying the topology of the polymer (comb, star, dendritic, etc.), the composition/architecture of the polymer (random, periodic, graft, etc.), or the functional groups at various sites of the polymer (end, center, side) [94]. Telechelic polymers and macromonomers can be used as cross-linkers, chain extenders, and precursors for block and graft copolymers.

The block copolymers of PPy was synthesized with α,ω–diamine polydimethylsiloxane with very high conductivity (4000 S/cm) [95]. Immobilization of enzymes in polypyrrole block copolymers [96] and thiophene ended polystyrene with polypyrrole were reported by Toppare et al. [97].

Graft copolymerization of pyrrole takes place, but the problem is that it is difficult or next to impossible to determine the extend of grafting. In conventional graft copolymerization, the graft copolymer is readily separated from the homopolymers and characterized. Pyrrole is so reactive and its copolymers and homopolymers are insoluble, characterization of its graft copolymers is a formidable problem for researchers preparing these materials. Pyrrole/styrene graft copolymers [98] were synthesized by different methods like atom transfer radical polymerization technique [99] etc.

1.5.B. Random Copolymerization of Pyrrole with Ferrocenyl Derivatives

More emphasis has been given on this topic because the random copolymerization is one of the research areas explained in chapter 6 where a ferrocene derivativatised pyrrole has been synthesized and co-polymerized with pyrrole. The specific objective here being the preparation of redox-active films of ferrocene co-valently bonded to polypyrrole. A high degree of conjugation is expected for the copolymer of pyrrole when attached with ferrocenyl derivative, which is utilized for the detection of CO gas.

In 1988, Skotheim and co-workers [100] established the first general procedure for dithering a ferrocene moiety to either the 3-alkyl or the 1-alkyl of pyrrole and the copolymerization of ferrocene derivatised pyrrole (Fc-P) with pyrrole [101, 102].

Depositing films of these copolymers on the surface of an electrode converts it into a derivatised electrode that is useful for reoxidising reduced flavin enzymes, such as glucose oxidase. The immobilized ferrocene molecules serve as a shuttle for electron transport between the enzyme catalytic centre and the electrode surface. Cyclic voltammetry of these modified films show two different redox processes, which corresponds to the reduction/oxidation of the polypyrrole back bone and the ferrocene moiety, respectively. It also confirms that the concentration of ferrocene in the film can be controlled by the composition of the feed. Skotheim et al. [103] prepared LB copolymer films by polymerizing mixtures of pyrrole, 3-hexadecylpyrrole and ferrrocene-3-alkylpyrrole (Fc-P) (2500:5:1) at the air-water interface, with the subphase containing $FeCl_3$. It is possible to synthesize ferrocene-PPy copolymers via plasma polymerization technique. The report claiming a good homogeneous and continuous polymer film of Fc-PPy were deposited on the electrode [104].

1.6. Functionalisation of Conducting Polymers

Both chemically and electrochemically synthesized polypyrroles are typically insoluble in water and organic solvents and due to strong intermolecular and intramolecular interactions of their polymer chains, are infusible. Over the past decade, research to overcome this serious hindrance to their processability and subsequent utilization has been intense. It has proven possible to add a wide range of additional functionalities to the parent polymer structure, opening up an exciting array of potential applications for these materials. The present work addressed this issue and functionalized conducting polymer with ferrocene, iron phthalocyanine, iron porphyrin and ferrocenyl derivatised pyrrole copolymer to focus on mainly its interaction with polypyrrole, the structural variations with specific dopants and its chemical sensitivity to carbon monoxide gas etc. Organic CPs having flexible and adjustable chemical properties are great candidate materials to chemically and biologically respond to specific target analytes. Plain CP films exhibit very weak selectivity and sensitivity towards organic molecules or chemical gases such as alcohols, CO, $(NO)_x$ etc. On the other hand, polymer specificity can be modulated when the CP backbones are properly substituted with functional groups chosen ad hoc [105]. This is likely to allow selective partitioning of target analytes. The

strategy of using properly functionalized organic semiconductors also can be followed to obtain specific recognition involving iron phthalocyanine, ferrocene, iron porphyrin etc. doped PPy for CO sensing.

Two distinct approaches to achieving this additional functionality have been successfully employed, namely:

i) Covalent attachment of specific groups to the PPy back bone (either pre or post polymeriztaion)

ii) Incorporation of specific dopant anions.

There are three different methods used to obtain functional molecules incorporating conducting polymers, namely (a) Electrochemical polymerization (b) Chemical polymerization and (c) Photopolymerization. Amongst them, one of the most fascinating methods is electrochemical polymerization to incorporate the functional molecule in the conducting polymer especially as a dopant [106]. An important break through in polypyrrole chemistry was the discovery by Lee et al. in 1995 of a chemical polymerization route to an unsubstituted polypyrrole that was soluble in organic solvents [107]. Chemical polymerization methods are also available for preparation of functionalized conducting polymers. The vapor/liquid interface chemical polymerization is used to obtain a thin and highly transparent membrane (film). Bulk chemical polymerization is another way of getting a functional molecule incorporating conducting polymer membrane as well as simple conducting polymer, utilizing an appropriate support. Compared with electrolytic method, chemical polymerization methods, yields materials having lower conductivities of resulting conducting polymers. Shimidzu et al. [108] reported that visible light irradiation of an aqueous pyrrole solution in the presence of $[Ru(bipy)_3]^{2+}$ (bipy = 2,2'-bipyridine) as the photosensitizer and $[CoCl(NH_3)_5]^{+2}$ as a sacrificial oxidant led to the deposition PPy.Cl. This powdery product exhibited a relatively low conductivity compared with PPy.Cl prepared via standard chemical or electrochemical methods.

In 1989, Roncali and co-workers reported the synthesis of poly[3-(3,6-dioxaheptyl)thiophene] and examined its voltammetric properties in the presence of Bu_4N^+ and Li^+ electrolytes [109]. This was said to be the first conjugated polymer system with a covalently attached functional group for ion complexation [110]. Pyrroles can be

functionalized by attaching side chains like flexible alkyl or alkoxy groups or ferrocenyl derivatives at either three ring position or N–centre for specific applications; which markedly enhance their solubility and processability in organic solvents. Covalent binding of more sophisticated substituents to PPy can provide a wide range of other attributes.

In the present case, particular emphasis is given on selected dopants and derivatised polypyrrole specially for sensing capabilities. The usual approach has been to synthesize a monomer or dimer containing the appropriate recognition group; this is subsequently oxidized to produce the conducting polymer [111]. A draw back of this approach for functionalization of polymers is that the synthesis of initial substituted monomer may be complex and time consuming. In addition, subsequent oxidation to the desired polymer may prove difficult due to steric hindrance by the functional group, or electronic effects that shift the oxidation potential of the monomer. A significant development, therefore, a route involving the facile modification of pre-formed polypyrroles containing good leaving groups such as N-hydroxysuccinamide [112]. Using this approach, crown ethers and other electroactive groups such as ferrocene, as well as oligonucleotides, have been covalently attached to the pyrrole rings [113]. This generic approach should be extendable to analogous polythiophenes and polyanilines. Another significant development has been the synthesis of chiral polypyrroles [114, 115]. It should also be noted that, unlike analogous substituted polythiophenes where routes to regioregular polymers have been developed. First such regiospecific polymerization was reported by McCullough and Lowe [116] in 1992.

1.7. Charge Transport Processes in Conducting Polymers

The electrical properties of conducting materials are important because they determine:

i) the ability to transport information from one part of the structure to another. ii) the ability to store information. iii) the ability to trigger responses. iv) the ability to store and convert energy [117]. Electrical conductivity in PPy involves movement of positively charged carriers or electrons along polymer chains and hopping of these carriers between the chains. It is generally believed that the intrachain hopping resistance is much greater than the interchain transport resistance.

There are several models were suggested for the electrical conduction in conducting polymers. The central issue relates to the strength of the electron–electron interactions relative to the bandwidth, relative to the electron-phonon interaction, and relative to the strength of the mean disorder potential. Strong electron-electron interactions (electron-hole attraction) lead to the creation of localized and strongly correlated negative and positive polaron pairs: neutral polaron excitons. Well-screened electrons and holes with associated lattice distortions (charged polarons), on the other hand, are more appropriately described using a band picture supplemented by the electron-phonon interaction.

The electronic structure of conjugated polymers was described by SSH [118] in terms of a quasi-one-dimensional tight binding model in which the σ-electrons are coupled to distortions in the polymer backbone by the electron-phonon interaction. In the SSH model, photoexcitation across the π–π^* band gap creates the self-localized, nonlinear excitations of conducting polymers: solitons (in degenerate ground-state systems), polarons, and bipolarons [119]. This tendency towards delocalization is limited by disorder (which tends to localize the wave functions) and by the Coulomb interaction, which binds electrons when transferred to a nearby repeat unit to the positive charge left behind, i.e., to the "hole". Since the typical bandwidths and band gaps are all in the electron volt range, one can start with a one-electron band approach and treat the Coulomb energy as a perturbation. In general, one can expect both "Wannier-like" excitons and "Frenkel-like" excitons for electrons and holes originating from different bands in the same polymer. The most widely used model for electronic conduction is the one-electron band model, discovered by Rudolph Peierls (the "Peierls Instability"). This is based on extending the simple model of a bond between two atoms over whole crystalline solid.

The two electrons go into the lower energy orbital (M.O.Theory). The (now filled) lower-energy orbital is a bonding orbital and the high-energy (empty) orbital is an antibonding orbital (Fig.1.7).

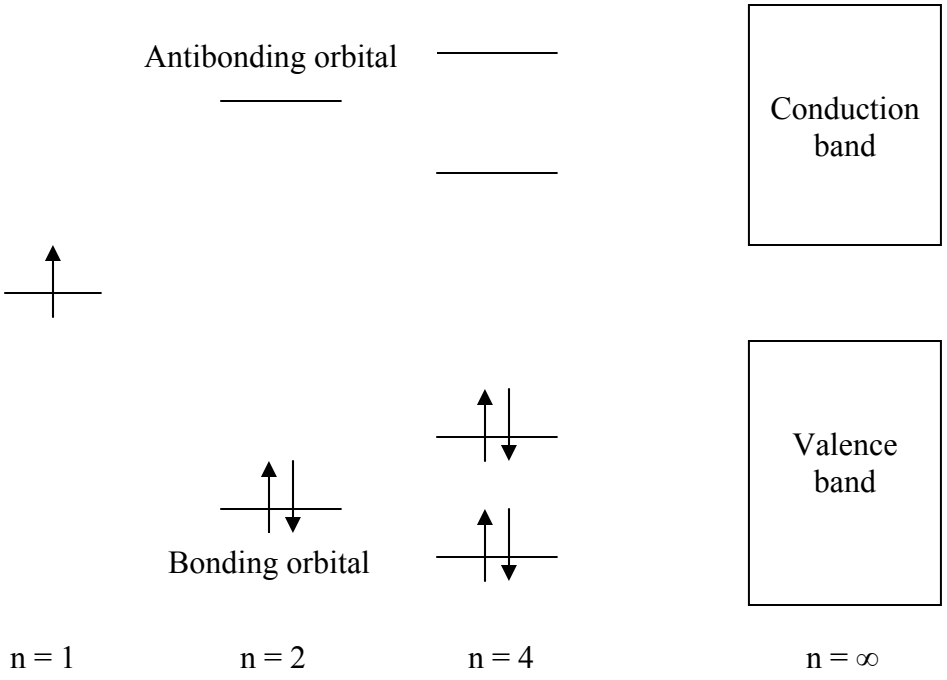

Fig. 1.7. One electron band model for electrical conduction

The magnitude of the conductivity is determined by the number of charge carriers available for conduction and by the rate at which they move. In order to consider the effect of temperature on the electrical conductivity of the three main classes of materials (metals, semiconductors and insulators), it is therefore necessary to consider its effect on both charge carrier concentration and mobility. In a semiconductor, the same is true, but also the charge carrier concentration increases with increasing temperature. Since the charge carrier concentration is much more temperature dependent than the mobility; it is the dominant factor and conductivity increases with increasing temperature.

Hopping or tunneling is the major electron transport process in conducting polymers. A model used to describe the conduction process is the conduction model envisioned by Mott and Davis [120]. When applied to conducting polymers, it assumes that electron transport originates from localized or fixed states within the polymer chain. The charge transfer between the chains takes place by hopping, referred to as phonon assisted hopping between two localized states. Lattice vibrations enhance this process of tunneling from one localized state to another. Plots of dc conductivity versus temperature can be parameterized by fitting Mott's Variable Range Hopping (VRH) Conduction Model. Most conducting polymers have shown a temperature dependence of dc

conductivity consistent with the VRH conduction process, obeying the following relationship:

$$\sigma = \sigma_0 \exp. [-(T_0/T)^{1/4}] \text{ [S/cm]} \text{ ----------(1)}$$

Mott's parameters are listed as follows:

$$\sigma o = e^2 R^2 \nu_{ph} N (E_F) \text{ ----------(2)}$$

$$T_o = \lambda \alpha^3 / k N (E_F) \text{ ----------(3)}$$

$$R = [9/8\pi R^3 N(E_F)]^{1/4} \text{ (cm) ----------(4)}$$

$$W = [3 / 4\pi R^3 N (E_F)] \text{ (eV) ----------(5)}$$

Where σ is the conductivity of the sample at temperature T (K), σo is the pre-exponential factor (S/cm), T_o is the characteristic temperature (K), e is the electronic charge (1.602 X 10^{-19} C), k is the Boltzmann's constant (8.616 X 10^{-5} eV/K), R is the average hopping distance (cm), ν_{ph} is the phonon frequency (10^{13} Hz), N (E_F) is the density of localized states at the Fermi level (cm^{-3}/eV), λ is the dimensional constant (18.1), α is the coefficient of exponential decay of the localized states (cm^{-1}) and W is the hopping activation energy (eV).

Taking the natural logs on both sides of equation (1), the following relationship is obtained:

$$\ln \sigma = \ln \sigma o - (To) \text{ X } (T)^{-1/4} \text{ ----------(6)}$$

The straight line nature of the ln σ versus $T^{-1/4}$ plots justifies the validity of VRH conduction process represented by equation (1) for conducting polymers.

1.8. Sensors

1.8.A. Sensors in General

Fifty years ago, Bardeen et al. discovered [121] that gas adsorption onto a semiconductor produces a conductance change; from that time, a great amount of research was carried out in order to realize commercial semiconducting devices for gas detection. In the second half of 20th century, the interest in the development of electric sensing devices has considerably increased. In the 1960s, the technique of chemical sensors has grown

rapidly and gave the possibility for direct detection of various ions molecule types with certain selectivity limits. The research and development of conventional macrosensors soon turned in the direction of microsensors as a result of the miniaturization in microelectronics and expanding applications in biology, medicine, safety, environmental protection etc. various material structures are used in sensors, depending on the nature of the quantity to be measured.

In recent years, polymeric materials have conquered a large part of sensorics: almost half of the promising chemical sensors are now a day based on polymers. Both large categories of materials, viz., inorganic and organic types, used in the fabrication of sensors. Inorganic materials include single crystals such as quarts, silicon, compound semiconductors; polycrystalline and amorphous materials such as ceramics, glasses, and their composites and metals. Organic materials applied in sensors are mainly polymers; however, lipids, enzymes and biochemical compounds have also found an expanding use recently. A general structure and operation scheme of polymer based sensor is shown in Fig. 1.8.

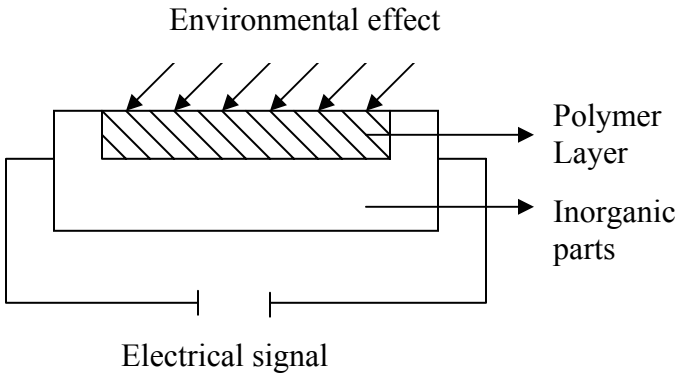

Fig. 1.8. A general schematic diagram of polymer based sensor.

1.8.B. Types of Sensors

The most important structures can be categorized into the following groups:

1.8.B.a. Impedance Type

The structure and operation principles of impedance type sensors are the most simple. Measurand changes alter the permittivity and/or resistivity of the polymer layer, which in turn produces the variation of capacitance and/or resistance values of the sensor [122].

1.8.B.b. Semiconductor Based Sensors

Semiconductor based sensors use silicon or compound semiconductors for fabricating inorganic parts. Sensitive polymer layers may be insulating, semiconducting or conductive materials in these structures.

1.8.B.b.i. Field Effective Sensors

In sensitive electronic devices based on the field effect principle, the semiconductor surface potential is modulated by potential or electric charge variations elsewhere in the structure, usually called a gate, which is actually an insulator-(metal)-sensitive polymer-environment interface (MOSFET) [123]. In the sensor FET devices, the gate metallization and/or polymer coating environment interaction produce the controlling potential, which is the function of the quantity to be measured and can be detected only as a potential difference according to a reference.

1.8.B.b.ii. Other Semiconductor Sensors

Metal semiconductor diodes, the so called Schottky-barrier devices, build up from n-GaAs and discontinuous platinum films can be used as detectors of different gases over a wide range of temperatures. Sensitivity of the device can be measured by the change of capacitance when it is exposed to gases [124]. Interesting device structures can be fabricated using semiconducting or conducting polymers, which can change their resistivity value under different environmental conditions (exposure to gases, solutions etc.). Such devices also use silicon based structures, but the polymer here is an active part of the devices, not only an operation modifying layer or membrane. Fig. 1.9. shows a silicon/(conducting polymer)/gold metallization device structure, which can be used as a diode that changes its characteristics as a function of the quantity to be measured [125].

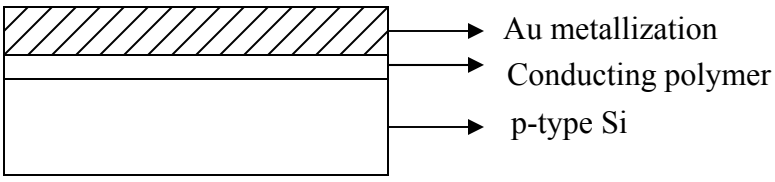

Fig. 1.9. A general schematic diagram for semiconductor sensor device.

1.8.B.c. Resonant Sensors

Resonant sensors generally have an electromechanical resonant frequency, which is a function of the measurand. The output is a quasidigital frequency signal, which is much less prone to noise and interference and can be measured directly in digital systems. This is a great advantage over conventional analog systems. A common approach for obtaining a frequency output is the use of electronic oscillators in which the sensor element itself is the frequency determining element.

Resonant sensors that apply sensitive polymer layers consist of an inorganic resonator covered by the polymer film. The polymer acts as a selective sorbent that absorbs or adsorbs particles from the surroundings. The sensors operation is based on the gravimetric principle: mass and density change due to the adsorption and absorption results varies in acoustic wave propagation properties; therefore, a shift in the oscillation frequency can be detected [126]. The selectivity is determined by the polymer material.

1.8.B.d. Electrochemical Sensor

Electrochemical sensors are widely used as sensors for the measurement of chemical quantities, typically ion or gas molecule concentrations in different media. In the simplest case, an electrochemical cell consists of a minimum of two electrodes and an ionic conductive material between them. The operation of the sensors is based on the reactions and their equilibria at the interfaces between electronic and ionic conductors on the electrode surfaces [127]. A typical electrochemical sensor representation is given in Fig. 1.10. These are classified into:

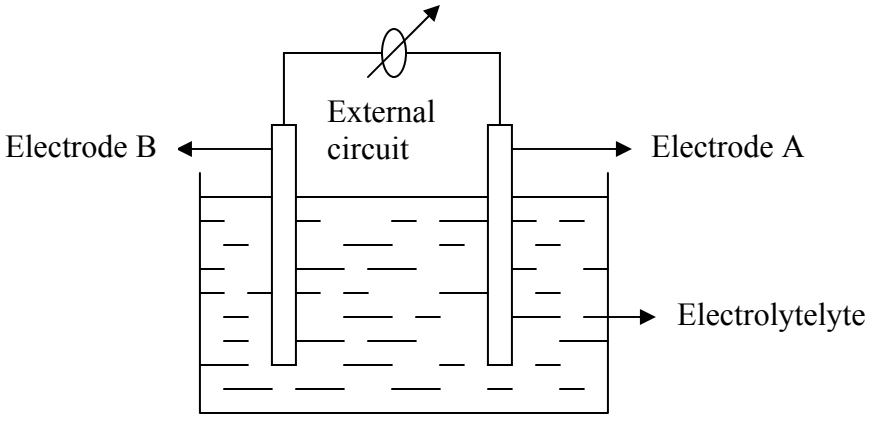

Fig. 1.10. A general schematic representation of an electrochemical sensor.

1.8.B.d.i. Potentiometric Sensors

Here, the potential difference between the reference electrode and working electrode is measured without polarizing the electrochemical cell, i.e. very small current is allowed. In that case, the equilibrium electrode potential difference can be monitored. Application of electroconducting conjugated polymers (ECPs) results in many new possibilities to build up electrochemical sensors. In these materials, a semiconducting polymer contains ionic dopant/or specific molecules covalently grafted to the ECP [128]. The great perspective for ECPs is the phenomenon that the ion exchange or ion sorption occurs directly in the electroconductive material. The ion exchange process directly changes the doping level and also the conductivity and work function of the semiconducting polymer. Thus, ECPs can be used directly as sensitive electrodes.

1.8.B.d.ii. Amperometric Sensors

In amperometry, the signal of interest is a current that linearly dependent upon the concentration of the analyte. As the sensing species approach the working (or sensing) electrode, electrons are catalytically transferred from the analyte to the working electrode. The direction of flow of electrons depends upon the properties of the analyte and can be controlled by the electric potential applied to the working electrode. If a constant potential difference is maintaine by the external circuit, a continuous flow can be measured [129].

1.8.B.d.iii. Voltammetric Sensors

The amperometric method is a special case of the voltametric measurements, where the whole potential-current diagrams are used for the analysis. Any reaction at the electrode surface can usually be detected as a current superimposed to the base current due to double layer charging. Thus, in these voltammograms, current peaks can be observed. The peak potential values can be used for qualitative analysis and the height of the peaks is a function of analyte concentration [130].

1.8.B.d.iv. Conductometric Sensors

These are based on the measurement of electrolyte conductivity, which is changed when the material is exposed to a different environment. The sensing effect is based on the change of the number of mobile charge carriers in the electrolyte [131].

1.8.B.e. Calorimetric Sensors

Calorimetric sensors (often called pellistors) widely used for the detection of relative gas components. It generally utilizes the heat generation or consumption during catalytic chemical reactions of reactive gas molecules for their detection [132]. The sensor consists of a substrate that is heated continuously by the heating resistor, its temperature is different from the ambient temperature. This temperature difference results in a heat flow from the substrate to the environment. In a stationary state, the temperature difference is constant, and the power dissipation is equal to the heat flow. The temperature of the substrate is monitored using a temperature sensor (thermistor, thermoelement, Pt-resistor). The polymer catalyst coating can adsorb and absorb gas components from the environment, which can take part in catalytic chemical reactions. The reaction heat generated or consumed by the chemical reaction can disturb the stationary state heat flow from the sensor to the environment and a temperature change can be detected. Although the conjugated polymer's absorption characteristics are largely determined by the local electronic structure, the sensitivity of the band gap to the polymer's conformation provides a useful means to create this type of sensor.

1.8.B.f. Fiber Optic Sensors

In optical communication links, it is optical fiber that provides the transmission channel. Optical fiber can be made basically from two materials: silica glass (SiO_2) and plastic polymer, generally polymethyl methacrylate (PMMA). The major advantages of these sensors are: low signal attenuation, high information transfer capacity, elimination of electromagnetic interference problems, non-corrosive, flexible and bio-compatible. The operation is based on special change caused by different physical and chemical effects at the tip of the sensor [133].

1.8.C. Sensing Effects and Operation

Depending on this, the sensing effects in polymers can be classified as follows:

i) dielectrics ii) conductive composites iii) electrolytes iv) sorbents v) membranes with receptor molecules vi) permselective membranes vii) ion exchange membranes viii) optically sensitive polymers ix) electroconductive conjugated polymers

Since our investigation is based on functionalized electroconductive conjugated polymers, it is necessary to have a close look on these materials.

1.8.D. Conducting Polymer Based Chemical Sensors

Electronically conducting and semiconducting polymers have attracted a great deal of interest as sensing layers applied in sensors. When considering new sensory technologies one should look to nature for guidance. Many insects can detect chemical signals with perfect specificity and incredible sensitivity. Mammalian olfaction is based on an array of less discriminating sensors and a memorized response pattern to identify a unique odor. It is important to recognize that the extraordinary sensory performance of biological systems does not originate from a single element. In reality, their performance is derived from a completely interactive system wherein the receptor is served by analyte delivery and removal mechanisms, selectivity is derived from receptors, and sensitivity is the result of analyte-triggered biochemical cascades. Clearly, optimal artificial sensory systems should also display all of these features.

Considering these facts it would be useful to study systems like ferrocene, its derivatives, iron phthalocyanine and iron porphyrin with polypyrrole to detect carbon monoxide gas in ppm level. Recently, there has been considerable interest in exploiting metal co-ordinating macrocycles [134–136] and metallocene [137, 138] compounds such as porphyrin, phthalocyanines, ferrocenes and doped conductive polymers [139–141] for gas sensors [142–146], which are mainly associated with detection of organic solvent vapors, ammonia, chlorine and other similar hazardous gases. The electrical, optical, and electrochemical properties of these materials can vary enormously as a result of the functional groups [147–152].

Polypyrrole is a potential candidate among the known conducting polymer family for variety of reasons such as long-term stability of its conductivity and the possibility of

forming copolymers or composites with optimal mechanical properties. Besides having well-known p-type conjugated polymers, polypyrrole was chosen as the host matrix because of its easy chemical preparation/modification, good environmental and thermal stability, and excellent performance at room temperature.

A key advantage of conducting polymer (CP) based sensors over devices using small molecule (chemosensor) elements is the potential of the CP to exhibit collective properties that are sensitive to very minor perturbations. In particular, the CP's transport properties, electrical conductivity or rate of energy migration, provide amplified sensitivity [153]. Fluorescence is a widely used and rapidly expanding method in chemical sensing. There are advantages of using CPs in fluorescent sensory schemes due to amplification resulting from efficient energy migration. The combination of amplification and sensitivity in CP-based sensors is evolving to produce new systems of unparalleled sensitivity [154].

Studies of cross-reactive (low specificity) arrays of CPs have also been fruitful, and these "electronic nose" or "electronic tongue" devices mimic mammalian sensory systems. A number of approaches have been published where CPs are used to detect various toxic gases, chemical vapours and in bio systems like protein-ligand interactions and single-stranded DNA (sDNA) [155].

A short description for the metallic macrocycles used in this work is given below:

a) Ferrocene

Ferrocene is the prototypical metallocene, a type of organometallic chemical compound consisting of two cyclopentadienyl rings bound on opposite sides of a central metal atom. The central iron atom in ferrocene is normally considered to be in the +2 oxidation state. Each cyclopentadienyl ring is then allocated a single negative charge - this extra electron goes into a π orbital, bringing the number of π-electrons on each ring to six, and thus making them aromatic. These twelve electrons (six from each ring) are then shared with the metal via covalent bonding, which, when combined with the six d-electrons the iron has of its own, results in the iron having an 18-electron, inert gas electron configuration. This configuration makes ferrocene particularly stable. Ferrocene is an air stable orange solid that readily sublimes in vacuum or when heated. As expected for a symmetric and uncharged species, ferrocene is soluble in normal organic solvents, such as benzene, but

is insoluble in water. Ferrocene undergoes many reactions characteristic of aromatic compounds, enabling the preparation of derivatives (substituted ferrocenes). Unlike the majority of aromatic hydrocarbons, ferrocene undergoes a one-electron oxidation at a low potential, around 0.5 V vs. a saturated calomel electrode (SCE) (N.B. electron rich aromatic amines such as aniline, the heterocycles pyrrole and thiophene can be oxidized with ease by electrochemical means). Ferrocene can be oxidized using $FeCl_3$ to give the blue-colored ferrocenium ion, $[Fe(C_5H_5)_2]^+$, which is often isolated as its $[PF_6]^-$ salt. Ferrocenium salts are sometimes used as oxidizing agents, in part because the redox product ferrocene is so inert and readily separated from the products

b) Porphyrin

Porphyrin is an organic compound which is aromatic and heterocyclic since its chemical structure essentially consists of four pyrrole rings joined together by four methine (=CH–) group to form a larger macrocycle ring. A porphyrin with an iron atom of the type found in hemoglobin or certain cytochromes is called heme. The macrocycle, therefore, is highly conjugated, and consequently deeply coloured, hence the name porphyrin. There are a lot of interesting applications of porphyrins and other tetrapyrroles (chlorins and bacterioclorins) in chemical and biomedical research (for example, photodynamic Therapy (PDT), Model systems of photochemical reaction centers, biomimetic models of several enzymes (catalases, cytochromes etc.), catalysis (especially with Mn, Fe and Pd metalloporphyrins), sensors and biosensors.

c) Phthalocyanine

A phthalocyanine is a macrocyclic compound having an alternating nitrogen atom-carbon atom ring structure. Th molecule is able to coordinate hydrogen and metal cations in its center by coordinate bonds with the four isoindole nitrogen atoms. The central atoms can carry additional ligands. Most of the elements have been found to be able to coordinate to the phthalocyanine macrocycle. Therefore, a variety of phthalocyanine complexes exist. A phthalocyanine macrocycle consists of four identical corners. Phthalocyanine (Pc) is a beautifully symmetrical 18 p-electron aromatic macrocycle, closely related to the naturally occuring porphyrins. Like the porphyrins, the Pc macrocycle can play host to over seventy different metal ions in its central cavity. Since its discovery over seventy

years ago, Pc and its derivatives have been extensively used as colorants (dyes or pigments). More recently they have been employed in several 'hi-tech' applications such as the photoconducting material in laser printers and the light absorbing layer in recordable CDs. They are also used as photosensitizers in laser cancer therapy, as nonlinear optical materials and as industrial catalysts. Many types of chemical sensor based on phthalocyanines have been proposed - including thin film resistive devices, FET sensors and Langmuir-Blodgett films etc.

1.8.D.a. Polypyrrole Gas Sensors

The system undertaken to study in this research is polypyrrole and so it should be require to have a look at PPy based toxic gas sensors. The first evaluation of electronically conductive polymers (ECPs) as sensitive components in chemical sensors are based on their redox interaction with some gases, including a variation of the doping level, resulting in a quiet straight forward conductance monitoring of gas sensor response over several orders of magnitude [156]. Integrated electrodes covered by a PPy film have been tested by Miasik et al. for the detection of NH_3, NO_2, H_2S gases [157]. Since PPy is p-doped, electron donating gases like ammonia reduces the carrier density; hence, there is a resistance increase on exposure to ammonia [158]. In contrast, NO_2 withdraws electron density and increases conductivity [159]. Yoneyama et al. have shown that electropolymerized PPy films exhibit noticeable gas sensitivities to electron acceptor gases such as PCl_3, SO_2 and NO_2 at room temperature (RT), especially when PPy is reduced electrochemically before exposure [160]. Weddingen [161] reported that the selectivity and sensitivity of gases like O_2, CO, CO_2, NO, SO_2, H_2, CH_4 and NH_3 can be highly influenced by functionalization of conducting polymer. PPy doped with amphiphilic anions exhibits an electrochemical behaviour very sensitive to the water content of the cycling electrolyte. This has been shown by Bidan et al. [162] for self doped PPy or by Huan et al. in the case of dodecylsulphonate doped PPy [163].

Another promising assembly for ECP based chemical sensors is their arrangement in a field effective transistor (FET) device [164]. Such electronic devices operating in the solid state have been developed by Janata et al. for gas sensor applications. They showed that a poly(N-methylpyrrole) based FET responds to lower aliphatic alcohols at room

temperature and with a time response of seconds [165]. It is clear from the above discussions that the sensory response to a given analyte depends strongly on the nature of the dopant species associated with the conducting polymer. Analyte specificity can be achieved by the judicious selection of dopants, functionalization or the development of copolymer.

1.8.D.b. Carbon Monoxide Gas Sensors

Our research work is fully concentrated on the development of functionalized PPy material, which is expected to be highly sensitive and quick response to CO gas as low ppm as possible. So, a brief overview of toxic carbon monoxide gas and conducting polymer sensors for CO detection is given:

CO is odorless, colorless and tasteless gas produced from the incomplete combustion or burning of any fuel. The poisonous effect of carbon monoxide is exercised through the blood owing to the great affinity of the gas for hemoglobin (binds 300 times faster than that of oxygen), which results in the formation of carboxyhemoglobin. The carboxy-hemoglobin is entirely incapable of carrying oxygen to the tissues, and according to the amount of hemoglobin thus inactivated (or percentage saturation), the individual exhibits illness of proportionate severity; if the percentage saturation becomes sufficiently high, death ensues [166].

Unfortunately there are only a few reports available in the literature regarding the CO sensor based on conducting polymers. That too is very slow in response characteristics and change during exposure to the gas molecule is less. Liu et al. [167] reported the electrochemically grown PPy film doped with nickel phthalocyanine tetrasulphonated tetra sodium salt on interdigited electrode used for CO sensor applications. There are a few reports related to the CO sensitivity with functionalized polyaniline [168]. Dendritic carbosilanes with periphery ferrocenyl groups have also been used for sensing CO monoxide by monitoring the conductivity changes of the dendritic film [169].

1.9. Aim and Scope of the Present Work

The conjugated conducting polymers are closely associated with sensor technology because of the wide range of available materials and the possibility of achieving rapid selective sensitivity towards gases by the functionalization of these polymers by

introducing certain groups. There are not many reports available in the literature on carbon monoxide sensor based on conjugated conducting polymers. Ionic conducting polymers have been used in electrochemical type sensors but these are slow, these do not have long shelf life, the relative humidity affects these and as such these are not amenable for miniaturizing. There is tremendous need for sensors, which are fast, low cost, operating at room temperature and in dry atmosphere. Conducting polymers cannot be used directly without modification for this application because there does not appear to be any strong interaction between CO and ICP. In order to make them more sensitive, functional groups chosen from Fe-complexes are aimed to be incorporated in polypyrrole. In order to incorporate the chosen moieties such as ferrocene, there are several routes viz. electrochemical, in situ chemical polymerization, derivitize ferrocene so as to make a co-monomer and polymerize pyrrole in presence of these to give main chain modified PPy. Hence, detailed studies on functionalization of polypyrrole both by chemical as well as electrochemical route with ferrocene, iron phthalocyanine and iron porphyrin for CO were undertaken and completed.

The PPy was selected from the whole range of conducting polymers for carbon monoxide gas sensing application mainly because of the following reasons:

Polypyrrole (PPy) provides a unique substrate for the design of surface materials with specific electrochemical properties. Redox species can be incorporated in the polymer matrix utilizing their own chemical reactivities to effect the tailoring of surface catalyst or redox couple probes for electroanalytical techniques on a versatile electrode surface. The other specialty of PPy are:

i) Inherently conducting polymer
ii) Easy to synthesis
iii) Surface charge characteristics can be easily modified by changing the dopant anion, incorporated into the material during synthesis
iv) Excellent performance at RT
v) Chemical specificity for sensors
vi) High sensitivity and good reproducibility

In the present investigation, two methods of synthesizing functionalized conducting polymers were employed, namely i) Chemical polymerization and ii) Electrochemical

polymerization. The polymers synthesized by these methods if used in surface cell, they are expected to show good chemical sensitivity. The latter synthesis method gives polymeric materials in its highly doped states due to the presence of dopant ions in the polymeric films itself. Obviously, these materials will show higher conductivities than that by earlier method i.e. chemical polymerization.

It is well known that iron complexes are more prone to interact with carbon monoxide gas. The present investigation is the incorporation of iron complexes into polypyrrole is expected to provide very good pathway for sensing specifically to CO. The reversible redox property and cyclic stability of these polymers would make them useful as active components in sensors, switches, diodes, and memory devices. Hence, it is indicated that organo iron(II)/(III) complexes with polypyrrole is potential candidates for the electronic, opto-electronic and molecular electronic applications.

1.10. References

[1] T. Ito, H. Shirakawa, S. Ikeda, J. Polym. Sci. Chem. 12 (1974) 11.

[2] H. Shirakawa, T. Ito, S. Ikeda, Polym. J. 4 (1973) 460.

[3] H. Shirakawa, E. J. Louis, A.G. MacDiarmid, C. K. Chiang, A. J. Heeger, J. Chem. Soc. Chem. Comm. (1977) 578.

[4] C. K. Chiang, M. A. Druy, S. C. Gau, A. J. Heeger, E. J. Louis, A. G. MacDiarmid, J. Am. Chem. Soc. 100 (1978) 1013.

[5] C. K. Chiang, C. R. Fincher, Jr. Y. W. Park, A. J. Heeger, H. Shirakawa, E. J. Louis, S. C. Gau, A. G. MacDiarmid, Phys. Rev. Lett. 39 (1977) 1098.

[6] L. Torsi, A. Dodabalapur, Anal. chem. (2005) 381A.

[7] H. Munstedt, G. Kohler, H. Mohwald, D. Naegde, R. Fly, G. Bitthin, E. Meissner, Synth.Met. 18 (1987) 259.

[8] J. W. Lee, B. N. Popov, J. Power Sources 161 (2006) 565.

[9] J. Wang, J. Chen, C. Y. Wang, D. Zhou, C. O. Too, G. G. Wallace, Synth. Met. 153 (2005) 117.

[10] G. G. Wallace, M. Smith, H. Zhao, 18(4) (1999) 245.

[11] S. Cosnier, B. Galland, C. Gondran, A. Le Pellece, Electroanalysis, 10 (1998) 808.

[12] C. Kranz, H. Wohlschlager, H. L. Schmidt, W. Schuhmann, Electroanalysis, 10 (1998) 546.

[13] H. Korri–Youssofi, F. Garnier, P. Srivasta, P. Godillor, A. Yassar, J. Am. Chem. Soc. 119 (1997) 7388.

[14] F. M. Huijs, F. F. Varcauteren, G. Hadziioannou, Synth. Met. 125 (2002) 395.

[15] J. H. Schon, A. Dodabalapur, Z. Bao, C. Kloc, O. Schenker, B. Batlogg, Nature 410 (2001) 189.

[16] http://www.research.philips.com/pressmedia/background/polymerelec/appl.html.

[17] O. Yavuz, M. K. Ram, M. Aldissi, P. Poddar, H. Srikanth, Synth. Met. 151 (2005) 211.

[18] W. Lu, E. Smela, P. Adams, G. Zuccarello, B. R. Mattes, Chem. Mater. 16 (2004) 1615.

[19] J. H. Burroughes, D. D. C. Bradley, A. R. Brown, R. N. Marks, R. H. Friend, P. L. Burn, A. B. Holmes, Nature 347 (1990) 539.

[20] S. Geetha, C. R. K. Rao, M. Vijayan, D. C. Trivedi, Anal. Chim. Acta 568 (2006) 119.

[21] L. Liu, N. Q. Jia, Q. Zhou, M. M. Yan, Z. Y. Jiang, Mat. Sci. Eng. C 27 (2006) 57.

[22] A. Ramanavicius, A. Kausait, A. Ramanavicien, Sens. Actuators B 111–112 (2005) 532.

[23] C. Feng, P. C. H. Chan, I. M. Hsing, Electrochem. Commun. 9 (2007) 89.

[24] S. W. Oh, H. W. Rhee, Y. C. Kim, J. K. Kim, J. W. Yu, Curr. Appl. Phys. 6 (2006) 739.

[25] E. Hur, G. Bereket, Y. Sahin, Mater. Chem. Phys. 100 (2006) 19.

[26] M. A. Lucio Garcya, M. A. Smit, J. Power Sources 158 (2006) 397.

[27] A. M. Hermann, Appl. Phys. Commun. 3(1&2) (1983) 59.

[28] R. S. Mulliken, J. Am. Chem. Soc. 72 (1950) 600; and 74 (1952) 811.

[29] R. S. Mulliken, J. Chem. Phys. 19 (1951) 514.

[30] M. J. S. Dewar, H. Rogers, J. Am. Chem. Soc. 84 (1962) 395.

[31] H. Funaki, K. Aramaki, H. Nishihara, Synth. Met. 74 (1995) 59.

[32] R. Patil, E. Matveeva, V. Parkhutic, J. Appl. Polym. Sci. 85 (2002) 1904.

[33] W. R. Salaneck, S. Stafstrom, J. L. Bredas, Conjugated polymer surfaces and interfaces, chapt.4, Cambridge University Press (1996).

[34] G. B. Street, in "Handbook of Conducting Polymers" Ed. T. A. Skotheim, Page 673, Marcel Dekker, New York, 1986.

[35] A. Angeli, Gazz. Chim. Ital. 46 (1916) 279.

[36] M. Salmon, K. Kanazawa, A. F. Diaz, M. Krounbi, J. Polym. Sci., Polym. Lett. 22 (1982) 187.

[37] S. Machida, S. Tasaka, S. Miyata, Polym. Prepr. Jpn. 36 (1987) 806.

[38] M. Aizawa, H. Shinohara, H. Shirakawa, Polym. Prepr. Jpn. 33 (1984) 495.

[39] K. Yoshino, H. Hayashi, R. Sugimoto, Jpn. J. Appl. Phys. 23 (1984) L899.

[40] S. Radhakrishnan, D. R. Saini, Synth. Met. 58 (1993) 243

[41] K. Kanazawa, A. F. Diaz, W. D. Gill, P. M. Grant, G. B. Street and G. P. Gardini, Synth. Met. 1 (1979/1980) 329.

[42] M. Ogasawara, K. Funahashi, T. Demura, T. Hagiwara, K. Iwata, Synth. Met. 14 (1986) 61.

[43] M. Satoh, K. Kaneto, K. Yoshino, Synth. Met. 14 (1986) 289.

[44] G. P. Gardini, Adv. Hetrocycl. Chem. 15 (1973) 67.

[45] M. Salmon, K. K. Kanazawa, A. F. Diaz, M. Krounbi, J. Polym. Sci., Polym. Lett**.** Ed. 20 (1982) 187.

[46] H. S. Nalwa, L. R. Dalton, W. F. Schmidt, J. G. Rebe, Polym. Commun**.** 27 (1985) 240.

[47] J. W. Loveland, G. R. Dimeler, Anal. Chem. 33 (1961) 1196.

[48] S. Machinda, S. Miyata, Synth. Met. 31 (1989) 311.

[49] S. P. Armes, Synth. Met. 20 (1987) 365.

[50] A. Profi, Z. Kucharski, C. Budrowski, M. Zagrska, S. Krichene, J. Suwalski, G. Dehe, S. Lefrant, J. Chem. Phys. 83 (11) (1985) 5923.

[51] V. Bochi, G. P. Gardini, J. Chem. Soc., Chem. Commun. 148 (1986).

[52] R. E. Myers, J. Electron. Mater. 15 (1986) 61.

[53] T. Ikegami, S. Machida, S. Miyata, T. Yoshikawa, Polym. Prep. Japan 37 (1988) 738.

[54] S. Machida, S. Miyata, Polym. Prep. Jpn. 36 (1987) 1886.

[55] A. D. Olio, G. Dascola, V. Varacca, V. Bocchi, Compt. Trend. (Paris) C267 (1968) 433.

[56] N. Toshima, Tayanagi, J. Chem. Lett. 1369 (1990).

[57] A. F. Diaz, K. K. Kanazawa, G. P. Gardini, J. Chem. Soc.; Chem. Commun. (1979) 635.

[58] S. Asavapiriyanont, G. K. Chandler, G. A. Gunawardena, D.J. Pletcher, Electroanal. Chem. 177 (1984) 229.

[59] W. Wernet, M. Monkenbusch, G. Wegner, Makromol. Chem., Rapid commun. 5 (1984) 1574.

[60] B. R. Scharifker, E. G. Pastoriza, J. Marino, J. Electroanal. Chem**.** 300 (1991) 85.

[61] M. Yamaura, K. Sato, T. Hagiwara, Synth. Met. 41 (1991) 439.

[62] A. F. Diaz, J. C. Lacroix, New J. Chem. 12 (1988) 171.

[63] A. J. Downard, d. Pletcher, J. Electroanal. Chem. 206 (1986) 139.

[64] R. A. Saraceno, J. G. Pack, A. G. Ewing, J. Electroanal. Chem. 197 (1986) 265.

[65] G. B. Street, in T. A. Skotheim (ed.) Handbook of Conducting Polymers, Marcel Dekker Inc., New York, Vol. 1, p.268-270.

[66] S. Asavapiriyonont, G. K. Chandler, G. A. Gunawardena, D. Pletcher, J. E1ectroanal. Chem. 177 229 (1984).

[67] M. Takakubo, Synth. Met. 18 (1987) 53.

[68] R. A. Marcus, J. Phys. Chem. 67 (1963) 853.

[69] "Polypyrroles: From basic research to technological applications" by Rodriguez, J.; Grande, H.-J.; and Otero, T.F., Handbook of organic conductive Molecules and Polymers : Vol.2, Ed. H. S. Nalwa; John Wiley & sons. 1997.

[70] T. F. Otero, Macromol. Chem., Rapid Commun. 5 (1984) 125.

[71] S. Sanyal, R. C. Bhakta, B. Nayak, Macromolecules 18 (1985) 1314.

[72] A. Diaz, Chem. Scripta 17 (1986) 145.

[73] E. M. Genies, G. Bidan, A. F. Diaz, J. Electroanal. Chem. 149 (1983) 101.

[74] R. J. Walton, J. Bargon, Tetrahedron, 40 (1984) 3963.

[75] A. J. Heeger, S. Kivelson, J. R. Schrieffer, W. P. Su, Rev. Mod. Phys. 81 (1988) 60.

[76] J. P. Louboijtin, F. Beniere, Phys. Chew. Solids 43 (1982) 233.

[77] K. Harigaya, Y. Wada, Synth. Met. 41-43 (1991) 3579.

[78] R. R. Chance, D. S. Boudreaux, J. L. Bredas, R. Silbey in T. A. Skotheim, M. Dekker (Eds.) "Handbook of Conducting Polymers", New York and Basel 1986.

[79] G. Horrowitz, D. Fichou, X. Peng, P. Delannoy, J. Appl. Phys. 67 (1990) 528.

[80] F. Garnier, G. Horrowitz, X. Peng, D. Fiehou, Adv. Mat. 2 (1990) No. 12 592.

[81] G. Horrowitz, D. Fichou, X. Peng, F. Gamier, Synth. Met 41-43 (1991) 1127.

[82] C. K. Chiang, S. C. Gau, C. R. Fincher Jr., Y. W. park, A. G. MacDiarmid, Appl. Phys. Lett. 33 (1978) 18.

[83] H. Shirakawa, E. J. Louis, A. G. MacDiarmid, C. K. Chiang, A. J. Heeger, Chem. Commun. (1978) 578.

[84] A. J. Heeger, Curr. Appl. Phys. 1 (2001) 247.

[85] A. K. Bhakhashi, C. M. Liegener, J. Ladik, M. Seel, Synth. Met. 30 (1989) 79.

[86] A. K. Bhakhashi, J. Chem. Phys. 96 (1992) 2339.

[87] O. Inganas, B. Liedberg, W. Chang-Ru, Synth. Met. 11 (1985) 239.

[88] J. P. Ruiz, A. D. Child, K. Nayak, D. S. Marynick, J. R. Reynolds, Synth. Met. 41-43 (1991) 783.

[89] H. S. Nalwa, Synth. Met. 35 (1990) 387.

[90] S. Naitoh, Synth. Met. 18 (1987) 237.

[91] B. Francois, T. Olinga, Synth. Met. 55-57 (1993) 3489.

[92] M. Wakabayashi, Y. Miyazaki, T. Kanbara, K. Osakada, T. Yamamota, A. Ishibashi, Synth. Met. 55-57 (1993) 3632.

[93] A. Kowalik, H. T. Nguyen, L. M. Tolbert, Synth. Met. 41-43 (1991) 435.

[94] O. W. Webster, Science 251 (1991) 887.

[95] N. Kyzylcan, N. Kokenz, B. Ustamehmetoglu, A. Akar, Eur. Poly. J. 42 (2006) 2361.

[96] A. Gursel, S. Alkan, L. Toppare, Y. Yagcy, React. Funct. Polym. (2003) 57.

[97] S. Alkan, L. Toppare, Y. Hepuzer, Y. Yagci, Synth. Met. 119 (2001) 133.

[98] A. I. Nazzal, G. B. Street, J. Chem. Soc., Chem. Commun. 375 (1985).

[99] S. Tarkuc, E. Sahin, L. Toppare, D. Colak, I. Cianga, Y. Yagci, Polymer 47 (2006) 2001.

[100] T. Inagaki, M. Hunter, X. Q. Yang, T. A. Skotheim, Y. Okamoto, J. Chem. Soc., Chem. Commun. 126 (1988).

[101] T. Inagaki, T. A. Skotheim, H. S. Lee, Y. Okamoto, L. samuelson, S. Tripathy, Synth. Met. 28 (1989) C245.

[102] A. Merz, R. Baumann, A. Haimerl, Makromol. Chem., Macromol. Symp. 8 (1987) 61.

[103] T. A. Skotheim, H. S. Lee, P. D. Hale, H. I. Karan, J. Okamoto, L. samuelson, S. Tripathy, Synth. Met. 42 (1991) 1433.

[104] F. Nastasea, D. Mihaiescub, C. Nastasea, C. Mireac, I. Burzob, Ioan Stamatin, Composites: Part A 36 (2005) 503.

[105] R. A. Bissell, K. C. Persaud, P. Travers, Phys. Chem. Chem. Phys. 4 (2002) 3482.

[106] T. Iyoda, A. Ohtani, T. Shimidzu, Honda, Synth. Met. 18 (1987) 725.

[107] H. J. Anderson, C. E. Loader, R. X. Xu, N. Lee, N. J. Gogan, R. McDonald, L. G. Edwards, Can. J. Chem. 63 (1985) 896.

[108] H. Segawa, T. Shimidzu, K. Honda, J. Chem. Soc., Chem. Commun. 132 (1989) .

[109] H. K. Youssoufi, A.Yassar, S. Bayteche, M. Hmyene, F. Garnier, Synth. Met. 67 (1994) 251.

[110] D. T. McQuade, A. E. Pullen, T. M. Swager, Chem. Rev. 100 (2000) 2537 and references therein.

[111] S. J. Higgins, Chem. Soc. Rev. 26 (1997) 247 and references cited there in.

[112] P. Godillot, H. K. Youssoufi, P. Srivastava, A. El-Kassmi, F. Garnier, Synth. Met. 83 (1996) 117.

[113] F. Garnier, H. K. Youssoufi, P. Srivastava, B. Mandrand, T. Delair, Synth. Met. 100 (1999) 89.

[114] R. L. Elsenbaumer, H. Eckhardt, Z. Iqbal, J. Toth, R. H. Baughman, Mol. Cryst. Liq. Cryst. 118 (1985) 111.

[115] D. Delabouglise, F. Garnier, Synth. Met. 39 (1990) 117.

[116] R. D. McCullough, R. D. Lowe, J. Chem Soc. Chem. Commun. (1992) 70.

[117] G. G. Wallace, G. M. Spinks, L. A. P. Kane-Maguire, P. R. Teasdale, Conductive electroactive polymers, 2nd ed., Ch. 3, p-89, CRC press, LLC, Florida, US.

[118] W. P. Su, J. R. Schrieffer, A. J. Heeger, Phys. Rev. Lett. 42 (1979) 1698.

[119] A. J. Heeger, S. Kivelson, J. R. Schrieffer, W. P. Su, Rev. Mod. Phys. 60 (1988) 781.

[120] N. F. Mott, E. A. Davis, "Electronic Process in Non-crystalline Materials", Clarendon Press, Oxford (1979).

[121] W. H. Brattain, J. Bardeen, Bell Syst. Tech. J. 32 (1953) 1.

[122] Y. Li, M. J. Yang, G. C. Miceli, N. Camaioni, Synth. Met. 128 (2002) 293.

[123] S. Zhao, J. K. O. Sin, B. Xu, M. Zhao, Z. Peng, H. Cai, Sens. Actuators B 64 (2000) 83.

[124] L. M. Lachuga, A. Calle, D. Golmayo, F. Brions, J. D. Abajo, G. J. De-La Campa, Sens. Actuators B 1 (1990) 368.

[125] B. Remaki, D. Jullien, C. Jouve, Sens. Actuators A 33 (1992) 85.

[126] C. De Angelis, V. Ferrari, D. Marioli, E. Sardini, M. Serpelloni, A. Taroni, Sens. Actuators A in press (2006).

[127] A. Ramanavi¡cius, A. Malinauskas, Electrochim. Acta 51 (2006) 6025.

[128] G. Bidan, Sens. Actuat. B, Chem. 6 (1992) 45.

[129] J. Rick, T. C. Chou, Biosens. Bioelectron. 22 (2006) 329.

[130] V. Parra, A. A. Arrieta, J. A. F. Escudero, M. L. R. Mendez, J. A. De Saja, Sens. Actuators B 118 (2006) 448.

[131] M. De Wit, E. Vanneste, H. J. Geise, L. J. Nagels, Sens. Actuators B 50 (1998) 164.

[132] A. Chatterjee, T. Balaji, H. Matsunaga, F. Mizukami, J. Mol. Graph. Model. 25 (2006) 208.

[133] D. Jose, M. S. John, P. Radhakrishnan, V. P. N. Nampoori, C. P. G. Vallabhan, Solid Films 325 (1998) 264.

[134] S. Ching, C.M. Elliott, Langmuir 15 (1999) 1491.

[135] H. Scheytza, H-U. Reissig, O. Rademacher, Tetrahedron 55 (1999) 4709.

[136] Q. Wang, L. Wang, L. Yu, J. Am. Chem. Soc. 120 (1998) 12860.

[137] S. Barlow, H. E. Bunting, C. Ringham, J.C. Green, G.U. Bublitz, S.G. Boxer, J.W. Perry, S. R. Marder, J. Am. Chem. Soc. 121 (1999) 3715.

[138] G. E. Southard, M. D. Curtis, Organometallics 20 (2001) 508.

[139] M. Di Guilio, G. Micocci, R. Rella, P. Siciliano, A. Tepore, Sens. and Actuat. B, Chem. 23 (1995) 193.

[140] V. Casey, J. Cleary, G. D. Arcy, J. B. McMonagle, Sens. and Actuat. B 96 (2003) 114.

[141] U. Storm, O. Bartels, J. Binder, Sens. and Actuat. B, Chem. 77 (2001) 529.

[142] A. C. Partridge, M. L. Jansen and W. M. Arnold, Materials Science and Engineering C 12 (2000) 37.

[143] S. Ampuero and J.O. Bosset, Sens. and Actuators. B 94 (2003) 1.

[144] S.Radhakrishnan and S.D.Deshpande, Materials Lett., 48 (2001) 144

[145] G. Sberveglieri, Sens. and Actuat. B, 23 (1995) 103.

[146] S.Radhakrishnan and S.D.Deshpande, Sensors , 2 (2002) 185

[147] L. S. Roman, M. R. Andersson, T. Yohannes, O. Inganas, Adv. Mater. 9 (1997) 1164.

[148] J. J. M. Halls, K. Pichler, R. H. Friend, S. C. Moratti, A. B. Holmes, Appl. Phys. Lett. 68 (1996) 3120.

[149] M. Kakimoto, H. Kashihara, T. Kashiwagi, T. Takiguchi, J. Ohshita, M. Ishikawa, Macromolecules 30 (1997) 7816.

[150] S. Morita, S. Kiyomatsu, X.H. Yin, A.A. Zakhidov, T. Noguchi, T. Ohnishi, K. Yoshino, J. Appl. Phys. 74 (1993) 2860.

[151] K. Yoshino, X.H. Yin, S. Morita, T. Kawai, A.A.Zakhidov, Solid State Commun. 85 (1993) 85.

[152] G. Yu, K. Pakbaz, A.J. Heeger, Appl. Phys. Lett. 64 (1994) 3422.

[153] T. M. Swager, Acc. Chem. Res. 31 (1998) 201.

[154] J. S. Yang, T. M. Swager, J. Am. Chem. Soc. 120 (1998) 5321.

[155] J. T. Sedjic, H. Peng, P. A. Kilmartin, M. B. Cannell, G. A. Bowmaker, R. P. Cooney, C. Coeller, Synth. Met. 152 (2005) 37.

[156] Nylander, M. Armgarth, I. Lundstrom, Anal. Chem. Symp. Ser. 17 (1983) 203.

[157] J. Miasik, A. Hooper, B. Tofield, J. Chem. Soc., Faraday Trans. I 82 (1986) 1117.

[158] M. Brie, R. Turcu, C. Neamtu, S. Pruneanu, Sens. Actuators B 37 (1996) 119.

[159] T. Hanawa, S. Kuwabata, H. Yoneyama, J. Chem. Soc., Faraday Trans. 1 84 (1988) 1587.

[160] T. Hanawa, H. Yoneyama, Synth. Met. 30 (1989) 341.

[161] G. Weddingen, Ext. abstract, ICSM '88, Santa Fe, NM, June 26 – july 2 (1988) p.271.

[162] G. Bidan, B. Ehui, M. Lapokowski, J. Phys. D: Appl. Phys. 21 (1988) 1043.

[163] L. Hwang, J. Ko, H. Rhee, C. Kin, Synth. Met. 55–57 (1993) 3671.

[164] A. Tsumura, H. Koezuka, S. Tsunoda, T. Ando, Its application to the field effective transistor, Chem. Lett. (1986) 863.

[165] M. jasowicz, J. Janata, Anal. Chem. 58 (1986) 514.

[166] R. C. Frederick, The Analyst, LVI (1931) 561.

[167] D. M. Liu, J. A. Hernandez, K. P. Kamloth, H. D. Lies, Sens. Actuators B 41 (1997) 203.

[168] V. Dixit, S. C. K. Misra, B. S. Sharma, Sens. Actuataors B 104 (2005) 90.

[169] B. W. Koo, C. K. Song, C. Kim, Sens. Actuators B 77 (2001) 432.

CHAPTER II

EXPERIMENTAL

2.1. Introduction

The experimental procedure followed for the synthesis and characterization of polypyrrole functionalized with organo iron complexes such as ferrocene, ferrocene derivatives, iron phthalocyanine and iron porphyrin are described in this chapter. Two methods were adopted for the functionalisation of polypyrrole viz. i) Chemical synthesis method and ii) Electrochemical method. The details for the individual cases are given in the respective chapters. The work mentioned in this chapter covers the techniques used for characterization of ferrocenyl derivatised monomer synthesis, functionalised polypyrrole synthesized in bulk as well as in film form using ^{1}HNMR, UV-Vis., FT-IR spectroscopy, X-ray diffraction studies, TGA, GFAAS, EDAX, DSC, Single crystal XRD, elemental analysis, cyclic voltametry etc. In addition to that, this chapter describes the experimental procedure for synthesis of the functionalisation of PPy with various Fe(II)/Fe(III) complexes in detail. It also deals with the detailed procedure for the preparation of various types of samples, surface cell configuration, properties measurement techniques used for studies on electrical properties, electrochemical methods, carbon monoxide gas sensitivity etc.

2.2. Chemicals Used

The specifications for chemicals and materials used and their sources are given in Table 2.1.

Chemical/Material	Acronym	Source
Pyrrole, A.R.	-	e-Merck Ltd., India
Anhydrous ferric chloride, purified	$FeCl_3$	Merck Ltd., India
Methanol, anhydrous (specially dried)	CH_3OH	Merck Ltd., India
Poly(ethylene)oxide	PEO	BDH, England
Cupric chloride, GR	CuI	Merck Ltd., India
Dichloromethane, HPLC grade	DCM	Merck Ltd., India

Silica gel, (column chromatography grade)	-	Spectrochem Ltd., India
Acetonitrile, HPLC grade	CH_3CN	Merck Ltd., India
Potassium phosphate, tribasic	K_3PO_4	Aldrich, Germany
n-Dodecane, LR	-	S.D. Fine Chem., India
1,4-Dioxane, AR	-	Spectrochem Ltd., India
4-bromo benzaldehyde (synthesis grade)	-	Spectrochem. Ltd., India
Tetrabutyl ammonium perchlorate, electrochemical grade	TBAP	Fluka, Switzerland
Sodium nitrate, purified	$NaNO_3$	Merck Ltd., India
Diethyl ether (stabilized)	-	Merck Ltd., India
Agar powder	-	Spectrochem Ltd., India
Ferrocene	-	Aldrich Germany
5,10,15,20-tetraphenyl-21H,23H-porphyrin iron(III) chloride	-	Aldrich, Germany
Iron(III) phthalocyanine-4,4',4'',4'''-tetrasulphonic acid, mono sodium salt, compounded with oxygen, hydrate	-	Aldrich, Germany
N,N,N',N'-tetramethyl diamino methane, synthesis grade	-	e-Merck Ltd., India
Cuprous iodide, extra pure	CuI	Lobha Chem., India
Trans-1,2-diaminocyclohexane	-	Aldrich, Germany
Orthophosphoric acid	-	Merck Ltd., India
Glacial acetic acid, AR	CH_3COOH	Spectrochem Ltd., India
Sodium hydroxide pellets, GR	NaOH	Merck Ltd., India
Sodium sulphate, anhydrous, GR	$NaSO_4$	Merck Ltd., India
Chloroform-d	$CDCl_3$	Aldrich, Germany
Methyl iodide, (synthesis grade)	CH_3I	S.D. Fine Chem., India
Deuterium oxide	D_2O	Aldrich, Germany

Triphenyl phosphine, (synthesis grade)	TPP	Spectrochem Ltd., India
Ethanol (Absolute)	CH_3OH	SRL Ltd., India
(Methyl sulphoxide)-d6	DMSO	Aldrich, Germany
Tetrahydrofuran, GR	THF	Merck Ltd., India
n-butyl lithium/hexane	-	Chemetall, Germany
Hydrochloric acid, GR	HCl	Merck Ltd., India
Ethyl acetate, GR	-	Merck Ltd., India

Table 2.1: Specifications of chemicals and polymeric materials used for the experiments.

2.3. Drying of Organic Solvents

2.3.A. Diethyl Ether

Diethyl ether was dried for 24 h with anhydrous calcium chloride, filtered and dried further by adding sodium wire until it remains bright. The ether is stored in a dark cool place, until distilled from sodium before use [1].

2.3.B. Alcohols (Methanol and Ethanol)

Refluxed with calcium oxide powder for 3 h and then filtered and distilled before use [1].

2.3.C. Tetrahydrofuran

Benzophenone was added into ordinary THF and then sodium wire was pressed into it. stoppered it loosely and kept in a dark place for over night, when the content go deep blue indicating that peroxides and water has been removed. It is distilled under nitrogen in a pre-baked flask containing freshly extruded sodium wire. THF was then fractionally distilled, degassed and stored above calcium hydride [1].

2.4. Separation Techniques

2.4.A. Thin Layer Chromatography (TLC)

Thin layer chromatography (TLC) [1] is a widely-used chromatography technique, used to separate chemical compounds. It involves a stationary phase consisting of a thin layer of adsorbent material, usually silica gel, alumina, or cellulose immobilised onto a flat, inert carrier sheet. A liquid phase consisting of the solution to be separated dissolved in a

solvent is drawn through the plate via capillary action, separating the experimental solution. The main advantages of TLC is faster runs, better separation and the choice between different stationary phases. Because of its simplicity and speed, TLC is often used for monitoring chemicla reactions and for the qualitative analysis of reaction products. A small spot of solution containing the sample is applied to a plate, about 1 cm from the base. The plate is then dipped into a suitable solvent and placed in a sealed container. The solvent moves up the plate by capillary action and meets the sample mixture, which is dissolved and is carried up the plate by solvent. Different compounds of the sample mixture travel at different rates due to difference in solubility in solvents and due to difference in their attraction to the stationary phase. Finally put the dried plate in an iodine chamber or under the UV light to identify the spots.

2.5. Purification of Compounds

2.5.A. Recrystallization

It is a procedure for purifying compounds [1]. A typical situation is that a desired compound X is contaminated by a small amount of compound Y. A chemist can prepare a saturated of the mixture X+Y in a warm solvent and subsequently lower the temperature. For most compounds, the solubility decreases with decreasing temperature. If X is not soluble in the solvent at lower temperatures, and Y is soluble at lower temperatures, then X will precipitate as the temperature decreases, while Y stays in solution. The precipitate now has a much higher purity than the original mixture. The level of purity can then be checked by taking a melting point range of the solid and comparing it to an accepted melting point range if one exists. The cost of this purification method is the inevitable loss of the part of compound X that stays in solution. A typical yield might be 80%. Successful recrystallization depends on finding the right solvent. This is a combination of prediction and trial/error. The solvent must be soluble with X+Y at higher temperatures, and must be insoluble with either X or Y at lower temperatures to force the product to either precipitate out (while the impurity stays in solution), or stay in solution (while the impurity precipitates out). This separates the desired product from the impurity.

2.5.B. Column Chromatography

It is used to obtain pure chemical compounds from a mixture of compounds on a scale from micrograms up to kilograms using large industrial columns [1]. The classicalpreparative chromatography column is a glass tube with a diameter from 5 to 50 mm and a height of 50 cm to 1 m with a tap at the bottom. A slurry is prepared of the eluent with the stationary phase powder (usually silica gel or alumina) and then carefully poured into the column. Care must be taken to avoid air bubbles. A solution of the organic material is pipetted on top of the stationary phase. This layer is usually topped with a small layer of sand or with cotton or glass wool to protect the shape of the organic layer from the velocity of newly added eluent. Eluent is slowly passed through the column to advance the organic material. Often a spherical eluent reservoir or an eluent-filled and stoppered separating funeel is put on top of the column. The individual components are retained by the stationary phase differently and separate from each other while they are running at different speeds through the column with the eluent. At the end of the column they elute one at a time. During the entire chromatography process the eluent is collected in a series of fractions. The composition of the eluent flow can be monitored and each fraction is analyzed for dissolved compounds.

2.6. Functionalisation of Polypyrrole

2.6.A. Chemical Synthesis

General method of synthesis of functionalization of polypyrrole involves the oxidation of pyrrole monomer in distilled water, methanol-water (1:1) system. Calculated amount of ferrocene/iron porphyrin/iron phthalocyanine is added into it in the presence of anhydrous $FeCl_3$. The ratio of monomer, pyrrole to oxidant, $FeCl_3$ is kept constant in all cases (1:1 mol ratio). The reactions were carried out only at room temperature with constant magnetic stirring for 4 h. The resultant functionalized polymer was first washed well with water and finally once with methanol and kept for drying at 60^0C overnight. The details of stiochiometry and reaction time for each individual polymer are discussed separately in the experimental section of each chapter.

2.6.B. Electrochemical Synthesis

The electrochemical deposition was carried out in a single compartment cell with three electrodes system as shown in Fig. 2.1. The deposition of functionalized polypyrrole films were allowed to grow on Pt electrode and $FeCl_3$ activated gold coated PET film interdigited electrodes. CH electrochemical analyzer (USA) unit of model CH1604B connected to a computer, is used for the electrochemical polymerization. Initially, gold was deposited on clean thick PET (100 μm) transparencies using Hind HiVac, Vacuum coating unit (model 12A4D) using thermal evaporation method. The gold-coated substrates were then cut into 2 cm × 1.5 cm size and subsequently, interdigited electrode pattern was made on these substrates. Two copper leads were connected to one end of the two separated electrodes with silver paste to give electrical contact pad for external connections.

We have adopted various film deposition techniques like chronoamperometry, potentiodynamic growth etc. for the functionalisation of PPy films on the electrode surfaces. All the experiments were performed using saturated calomel electrode (SCE) as a standard reference electrode. The SCE was connected through the salt bridge containing agar-agar/KCl mixture to the electrolytic solution. The platinum (Pt) foil and gold coated interdigited PET film were used as counter and working electrodes respectively. The electrolyte solution contained normally 0.1 M solution of the monomer to be polymerized in an appropriate solvent, a suitable electrolyte and a desired amount of doping agent/oxidisable species was used.

Electrochemically functionalized PPy films were deposited on working electrode with the application of suitable potential [2]. Since, the functionalisation of polypyrrole was carried out in different conditions such as solvent, oxidizing agent, applied voltage and deposition time etc., the details of deposition in each case has been described in corresponding chapter separately.

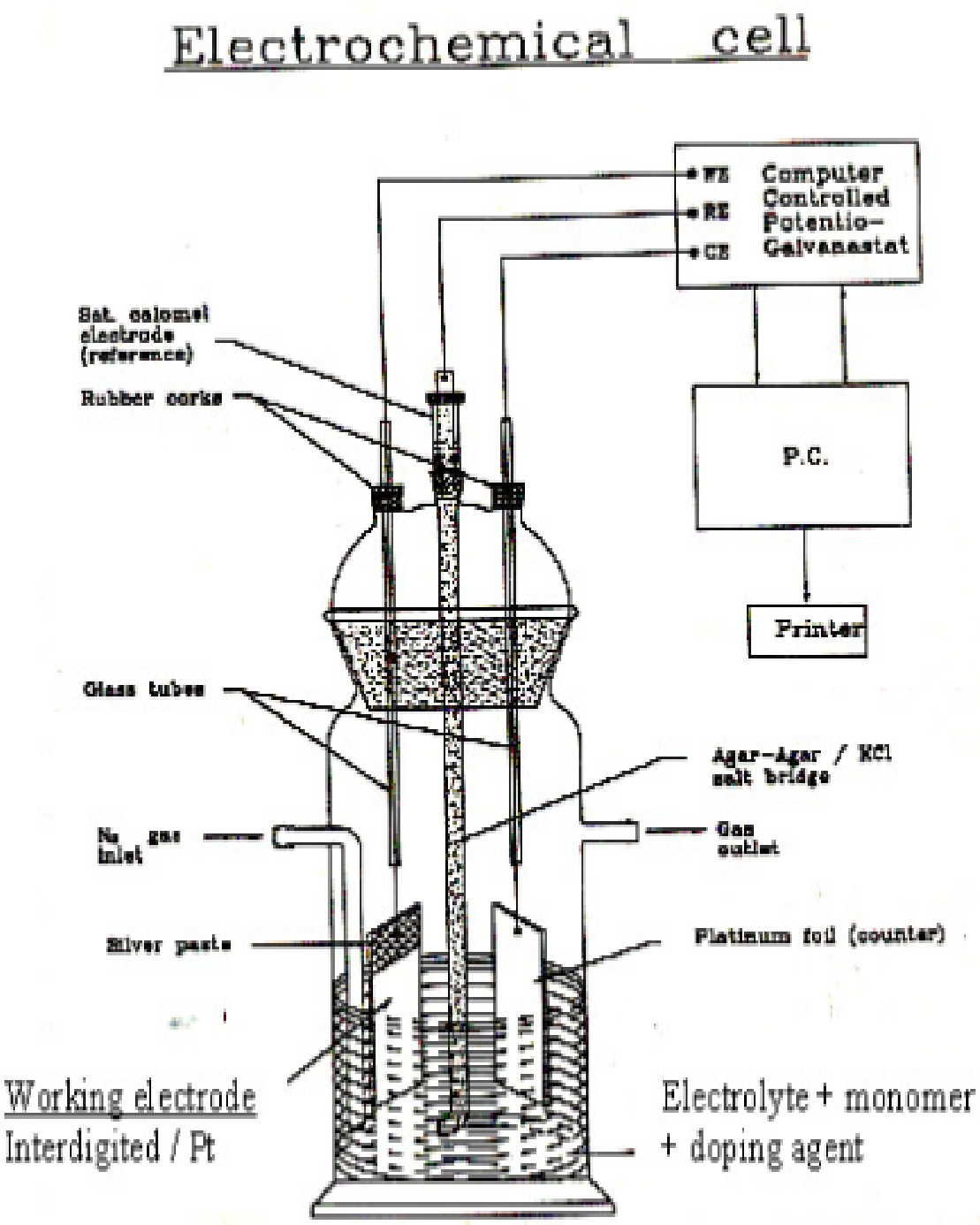

Figure 2.1. Single cell electrochemical deposition unit.

2.7. In situ Monitoring of the Polymerisation Reaction

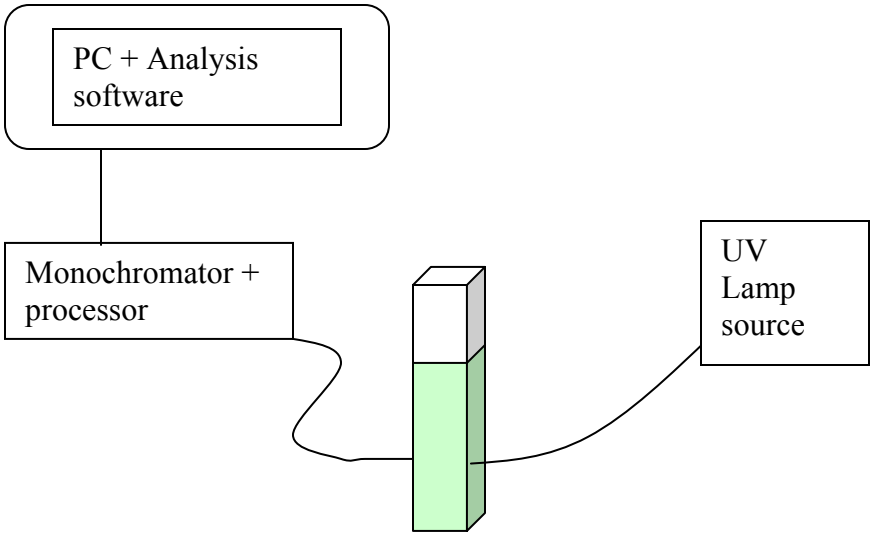

The reaction mixture was placed in the liquid cell (quartz or PMMA for aqueous) and the UV vis spectra scanned from 300nm to 900 nm and stored on the PC. Scanning time and time gap between the start of the scan was 1 min. In another case, the reaction was carried out externally in a glass beaker and samples drawn by micro pipette every min, diluted to 80% and placed in the sample holder for recording the spectra. Thus the evolution new peaks, increase/decrease of peaks corresponding to reactants etc. could be monitored continuously as the polymerisation reaction progressed.

In some cases the first filtrate obtained after the completion of the reaction was analyzed by the UV-Vis. spectroscopy so as to obtain the concentration of the unreacted component. The spectrometer was calibrated with standard solutions for quantification using Beer Lamberts law:

$$O.D. = \alpha \, . \, C \, . \, L$$

Where α is molar extinction coefficient, C the concentration and L the optical path length.

2.8. Copolymer Synthesis

The detailed procedure for synthesis of novel comonomer, ferrocenyl derivatised pyrrole and its interfacial copolymerization with pyrrole is presented in a separate chapter (see chapter IV). Characterizations and applications were also given elaborately in this section.

2.9. Characterization Techniques

2.9.A. UV-Vis. Spectroscopy (UV-Vis.)

The creation of mid-gap state in the conducting polymers due to doping process forms some charge transfer complexes can be studied by UV–visible spectroscopy [3]. The polymerization process was also monitored continuously using spectro-electrochemical unit with fiber optics while the reaction being carried out in the 10 mm path length disposable cell (model USB 2000, Ocean Optics, USA) connected to a computer. The spectra were scanned from 300 nm to 1000 nm and recorded every minute (the spectrometer can record the scans in micro seconds). The UV-Vis. spectra of he powdered samples were recorded by dissolving it in conventional solvents such as NMP. It is used for recording UV-Vis. spectra of colored complexes and organic compounds so as to know the electronic transitions and shifts of peaks during substitution.

2.9.B. Fourier Transform Infrared Spectroscopy (FTIR)

This is a wonderful spectroscopic tool to characterize the functional groups in the organic and organometallic compounds. Infrared (IR) studies [4] were carried out in order to confirm not only the incorporation of dopant species into polypyrrole but also the characteristic frequencies of the parent conducting polymers. The powdered samples were mulled with dry potassium bromide crystals and the pellets were mounted in IR cell. The spectra were recorded in the transmission mode using FTIR spectrometer [Perkin Elmer–Spectrum GX instrument]. The characteristic absorption bands obtained were tabulated and compared with known literature data.

2.9.C. Wide Angle X-ray Diffraction (WXRD)

Wide-angle X-RAY Diffraction (WXRD) studies [5] were done in order to analyze the structures of synthesized polypyrrole and modified PPy with various functional groups. The incorporation of these functional moieties into polypyrrole is expected to show some structural changes. The various polymeric compositions were investigated by WAXD, using a powder X-ray diffractometer (Rigaku Geigerflex refractometer) using CuKα source and β Ni filter. All the scans were recorded in the 2θ region of 5-50° at a scan rate of 4° per minute. For the amorphous polymeric materials, the average inter chain distance

(R) can be estimated from the position of the broad peak seen in the XRD plot by using the relation;

$$R = \{(5/8)\,\lambda / \sin\theta\}.$$

Where, R is the average interchain separation, λ is the wavelength (1.542 Å) of the X–ray used and θ is the diffraction angle.

For the crystalline phase, the *d*- values can be calculated using Brags equation:

$$n\lambda = 2d \sin\theta$$

$$d = (n\lambda / 2 \sin\theta) \quad ; \text{where } n = 1.$$

2.9.D. Thermogravimetric Analysis (TGA)

TGA [6] of virgin polypyrrole, functionalized polypyrroles and pure dopants were recorded over a temperature range of 50ºC to 600ºC with 10^0C per minute in nitrogen atmosphere using a Perkin Elmer Thermogravimetric analyzer, TGA to determine the weight loss at different temperatures. These studies were also used to find the onset degradation temperature of the polymers. The weight loss in functionalized polymer was compared with the original one in order to estimate the fractional component of the polymer at a fixed high temperature so that the thermal stability can be estimated.

2.9.E. Energy Dispersive X-ray Analysis (EDAX)

Energy Dispersive X-ray Analysis [EDAX] was carried out to find out the doping levels for various polymers [7]. From these studies various ratios like Fe, S, O, C, N, Cl, etc. can be find out. The iron content in the polymers functionalized with ferrocene, phthalocyanine and porphyrin was carried out using this technique. The measurements were carried out on EDAX microanalysis, Phoenix (U.S.A.).

2.9.F. Graphite Furnace Atomic Absorption Spectrometry (GFAAS)

Briefly, the technique is based on the fact that free atoms will absorb light at frequencies or wavelengths characteristic of the element of interest (hence the name atomic absorption spectrometry). Here, we are interested to looking the presence of iron and confirms the presence of ferrocene, iron phthalocyanine and iron porphyrin in PPy. GFAAS has done with GBC, AvantaΣ instrument. Within certain limits, the amount of

light absorbed can be linearly correlated to the concentration of analyte present. Free atoms of most elements can be produced from samples by the application of high temperatures. In GFAAS, samples are deposited in a small graphite or pyrolytic carbon coated graphite tube, which can then be heated to vaporize and atomize the analyte. The atoms absorb ultraviolet or visible light and make transitions to higher electronic energy levels.

2.9.G. Differential Scanning Calorimetry (DSC)

Differential Scanning Calorimetric studies on ferrocenyl derivatised pyrrole and its copolymer with pyrrole were carried out using DSC Q10 (TA instruments, USA). DSC gives an idea about the primary and secondary transition with change in temperature [8]. It gives the exothermic and endothermic changes occurring over a particular temperature range. DSC was recorded from ⁻50ºC to 200ºC for comonomer as well as the copolymers to understand the shift in T_g due to the incorporation of ferrocenyl derivative. The heating rate was kept constant at 40ºC per minute. DSC was recorded for both heating and cooling cycles. Endothermic changes like melting were recorded during heating cycle, and exothermic changes like crystallization were recorded during cooling. The melting point (T_m) as well as temperature of crystallization (T_c) and corresponding endothermic (ΔH_m) and exothermic (ΔH_c) changes in heat capacity was recorded and analyzed.

2.9.H. Proton Nuclear Magnetic Resonance Spectroscopy (^{1}H NMR)

Proton NMR is the application of nuclear magnetic resonance in NMR spectroscopy with respect to hydrogen [9]. Simple NMR spectra are recorded in solution and solvent protons should not interfere with the compound proton. Therefore a large range of deuterated solvents exist especially for NMR such as deuterated chloroform $CDCl_3$ and deuterated dimethyl sulphoxide $(CD_3)_2SO$ etc. Spectra are usually recorded against tetramethyl silane as the internal standard, set as zero. Proton NMR spectra are characterized by chemical shifts in the range +12 to ⁻4 ppm and by spin-spin coupling between protons. The integration curve for each proton reflects the abundance of the individual protons. Together with ^{13}C NMR, proton NMR is a powerful tool in structure elucidation in chemical compounds. We have well characterized all the compounds in multi stage synthesis process for comonomer, which are well matched with the reported

1H NMR spectra of the respective compounds. NMR spectra of the compounds were recorded in Bruker 200 MHz, 400 MHz and 500 MHz.

2.9.I. Micro Analysis (Elemental Analysis)

Elemental analysis is a process where a sample of some material (e.g., chemical compounds) is analyzed for its elemental composition (C, H, N, halogens, S etc.) [10] and sometimes isotopic composition. Here, our interest was estimating the % compositions of C, H and N in the compounds obtained in the multi stage comonomer synthesis. All were estimated and well in accordance with the theoretical values. The analysis was done with Lementar Vario EL instrument and Flash EA, 1112 series instruments.

2.9.J. Melting point Determination (m.p.)

Melting point of compounds of each stages of the multi stage comonomer synthesis was determined to know the purity, decomposition temperature and exact m.p. of the compounds. m.p. of the known compounds were compared with the reported data. The m.p. apparatus used for this purpose is Buchi B-540 melting point apparatus.

2.9.K. Single Crystal XRD

Single crystal XRD of the compound was analyzed in Bruker AXS smart apex diffractometer. It is a technique in crystallography in which the pattern produced by the diffraction of X-rays through the closely spaced lattice of atoms in a crystal is recorded and then analyzed to reveal the nature of that lattice [11]. This generally leads to an understanding of the material and molecular structure of a substance. The electrons that surround the atoms, rather than the atomic nuclei themselves, are the entities, which physically interact with the incoming X-ray photons. This technique is widely used in chemistry and other fields to determine the structures of an immense variety of molecules, including organic, inorganic, organo metallic compounds etc. X-ray diffraction is commonly carried out using single crystals of a material. Single crystal XRD is used to determine lattice structures as well as chemical formulas, bond lengths and angles. We have analyzed the molecular structure of a novel comonomer, *trans*–1–{4[2–(1–ferrocenyl)vinyl]phenyl}pyrrole using this technique.

2.9.L. Transmission Electron Microscopy (TEM)

By carefully selecting the orientation of the sample, it is possible not just to determine the position of defects but also to determine the type of defect present [12]. Defects that produce only displacement of atoms that do not tilt the crystal to the Bragg angle (i.e. displacements parallel to the crystal plane) will not produce strong contrast. TEM images were taken for the novel comonomer, *trans*–1–{4[2–(1–ferrocenyl)vinyl]phenyl}pyrrole synthesized and understood the shape of crystals. TEM has performed with JOEL, model 1200 ES instrument.

2.9.M. Cyclic Voltammetry (CV)

In CV, the potential is measured between the reference electrode and the working electrode and the current is measured between the working electrode and the counter electrode. This data is then plotted as current (I) v/s. potential (E). As the waveform shows, the forward scan produces a current peak for any analytes that can be reduced through the range of the potential scan. The current will increase as the potential reaches the reduction potential of the analyte, but then falls off as the concentration of the analyte is depleted close to the electrode surface. As the applied potential is reversed, it will reach a potential that will reoxidize the product formed in the first reduction reaction, and produce a current of reverse polarity from the forward scan. This oxidation peak will usually have a similar shape to the reduction peak. As a result, information about the redox potential and electrochemical reaction rates of the compounds is obtained.

Cyclic voltammetry experiments were frequently used to obtain information on the mechanism of polymer growth as well as redox behaviour and mode of electronic conduction [13]. In addition to this, in the present investigations, in order to study the effect of the functional groups incorporated into polypyrrole and the properties of conducting polymers were carried out in various electrolyte/solvent systems in CH electrochemical analyzer (USA) unit of model CH1604B. These estimations were carried out in a same electrolytic cell, which was used for electrochemical deposition of the polymers.

2.10. Electrical Measurements

The room temperature conductivity measurements and temperature dependence of conductivity was determined by placing the pellet or the film in a suitably designed apparatus as shown in Fig. 2.2. The apparatus consists of a sample holder, which was enclosed in an electromagnetic shielded cell, which in turn was mounted inside a glass jacket which could be sealed and connected to a rotary vacuum pump. A small heater was mounted close to the film or pellet and using a suitable control device controlled its temperature (rate of rise). A digital temperature indicator connected to a thermocouple placed near the sample measured the temperature inside the cell. The temperature was varied from 40^0C to about 120^0C for the doped samples and up to 150^0C for undoped samples at a rate of 3^0C per minute. The change in the resistivity with temperature was noted using an electrometer (Keithley 6514 model) and its conductivity was estimated using the formula:

$$\rho = RA / l \quad \text{----------(2.1)}$$

$$\sigma = 1 / \rho \quad \text{----------(2.2)}$$

Where ρ is its resistivity, A is the cross sectional area, l is the thickness, R is the sample resistance and σ is conductivity. The conductivity was recorded as a function of temperature. In order to estimate the activation energy, (ΔE) for conduction following equation was used:

$$\sigma = \sigma_o \exp. (\Delta E / kT) \text{ or } \text{----------(2.3)}$$

$$\text{Log } \sigma = \Delta E / kT + \log \sigma_o \quad \text{----------(2.4)}$$

Where k is the Boltzman constant. The slope of the plot of σ versus 1/T can be calculated as follows:

$$\text{Slope} = \frac{\log \sigma_2 - \log \sigma_1}{1/T_1 - 1/T_2} = \Delta E / k \quad \text{----------(2.5)}$$

The above equation can be rewritten in a convenient form by substituting the proper values for the constants and converting from natural logarithms to base 10 as:

$$\Delta E = \text{Slope} \times k \quad \text{----------(2.6)}$$

$$[k = 1.96 \times 10^{-4} \text{ eV}].$$

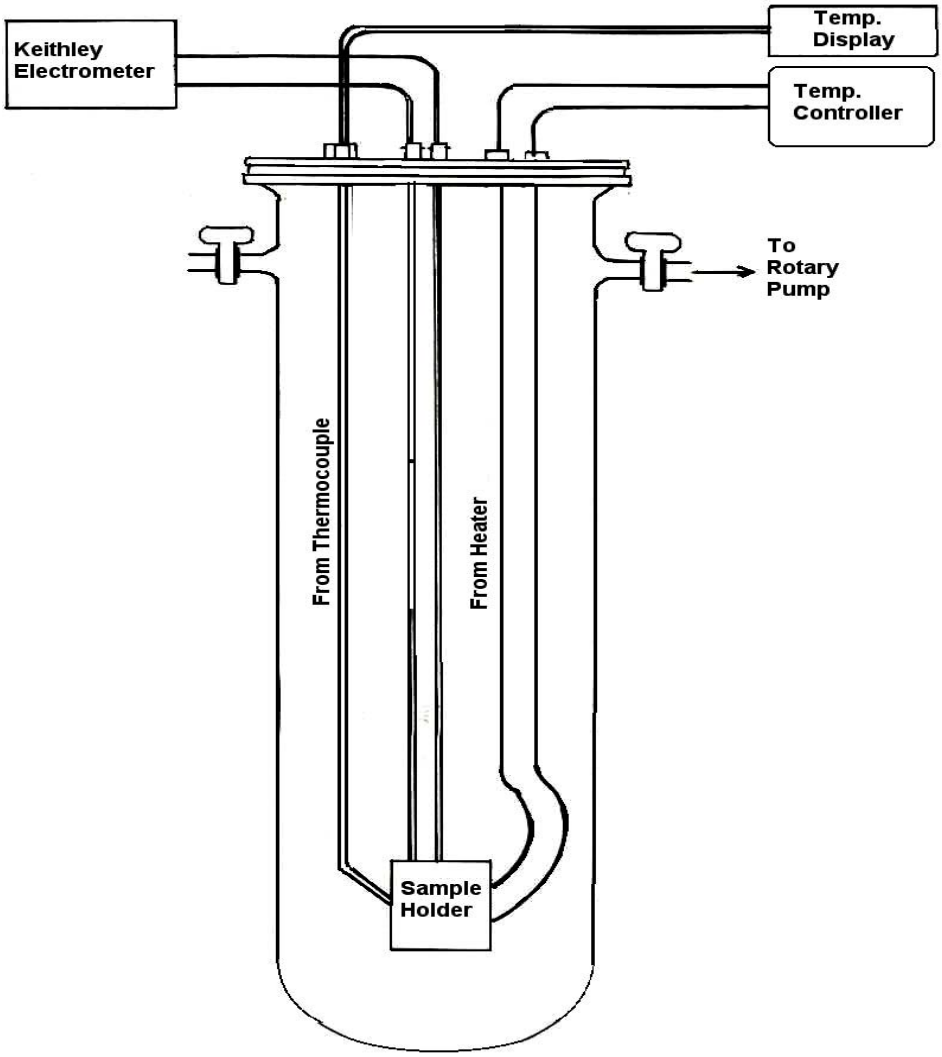

Fig. 2.2. Apparatus used for studying the temperature dependent conductivity of conducting polymers

2.11. Fabrication of Sensor with Functionalised PPy

Sensing elements with functionalized PPy active polymer films were prepared by first depositing gold films on 100 μm polyester film to form interdigited electrodes. The interelectrode distance was 0.5 mm and effective length was 10 mm. Polyethylene oxide was dissolved in methanol with addition of 10% $CuCl_2$ and stirred continuously to form homogenous solution. The modified polypyrrole powder samples (33 mg each) prepared in the above manner were then dispersed in the solution and stirred for 10 h to form uniform slurry. This type of dispersion is more amenable to coating the interdigited

electrode configuration and has been used for the purpose of sensing is reported in the literature [14, 15]. Two drops of this slurry were placed on the gold coated substrates and the solvent evaporated so as to form the test sensor in surface cell configuration (Fig. 2.3.).

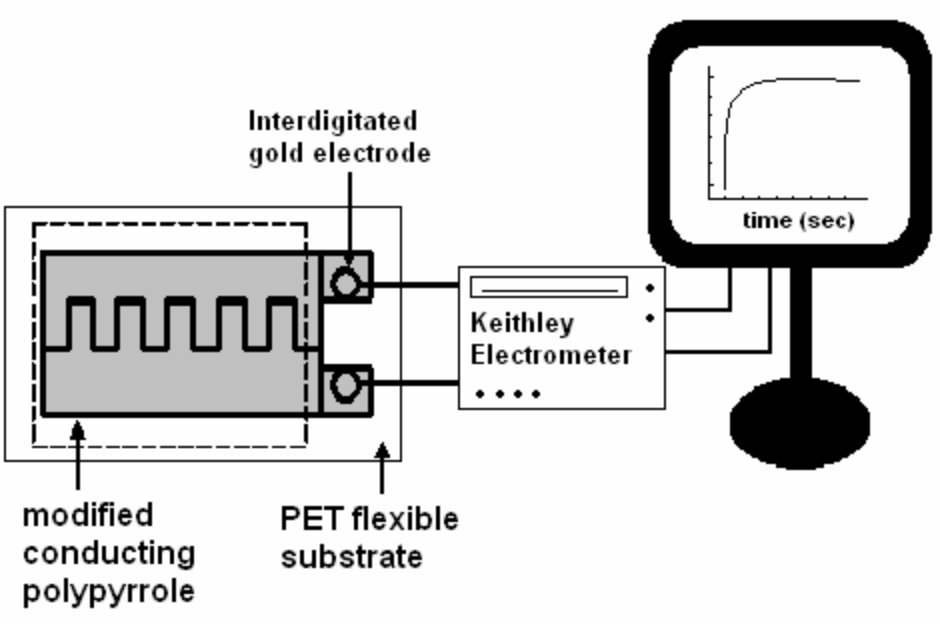

Fig. 2.3. Modified conducting polymer sensor material coated on gold coated interdigited electrode on PET transparency film (surface cell configuration), connected to Keithley electrometer and computer for online measurement.

In the case of electrochemically deposited films, the interdigited electrode deposited substrates were pretreated in 1M $FeCl_3$ for few hours so as to create active sites for binding the polypyrrole between the two electrodes. This procedure was followed according to the Patent [16]. By treating the surface, full coverage of the electrodes and the inter-electrode area was obtained after the ECP. These sensors were directly used for testing the sensitivity.

2.12. Sensitivity Measurements

For the sensitivity measurement study, a standard gas calibration bottle was used as shown in Fig. 2.4. The test cells prepared with modified polypyrrole samples were soldered on to a glass epoxy board fixture which could be inserted in the port of a calibration bottle (supplied by Drager, Germany) used for calibrating carbon monoxide

sensors. This bottle contains ampoules with calibrated concentration of the CO gas, which are broken internally. The sensor terminals were connected to digital Keithley electrometer interfaced to computer with Test Point software so as to monitor the sample conductivity continuously with fast sampling speed of ten points per second. The change of resistance was measured online from the time of exposing the material to CO gas. The measurements were continued up to 10 minutes. The sensitivity factor (% sensitivity) was calculated using the formula,

$$S = (\Delta R/R_0) \text{ X } 100$$

Where, ΔR is the change of resistance during exposure to CO gas. R_0 is the actual resistance of the material after making a slurry with PEO/$CuCl_2$ complex and coated on the intedigited electrode. Radhakrishnan et al. were worked extensively on these systems [17, 18].

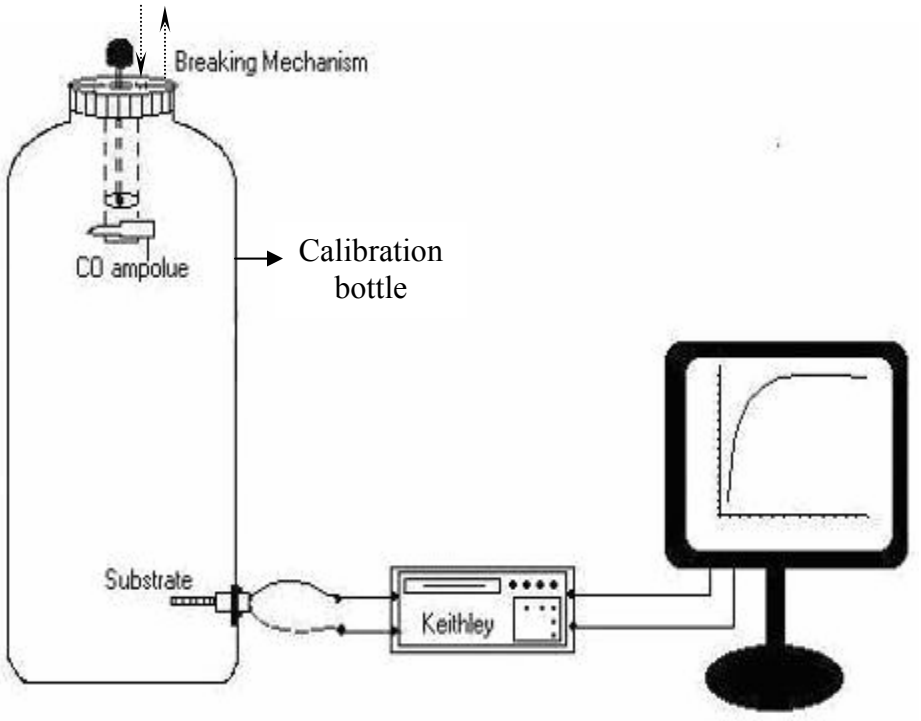

Fig. 2.4. Schematic representation of online measurement of CO gas sensitivity.

2.13. References

[1] W. L. F. Armarego, D. D. Perrin, Purification of laboratory chemicals, 4th ed., Butterworth-Heinemann, Oxford, London.

[2] S. Radhakrishnan, P. R. Somani, Chem. Phys. Lett. 292 (1998) 218.

[3] F. Hahn, B. Beden, M. J. Croissant, C. Lamy, Electrochim. Acta 31 (1986) 335.

[4] J. F. Rabek, "Experimental Methods in Polymer Chemistry" John Wiley and Sons, New York (1980).

[5] L. E. Alexander, "X-ray diffraction methods in Polymer Science" Wiley-Intersci., John Wiley and Sons, Inc. (1969).

[6] T. Hatakeyama, F. Y. Quinn, "Fundamentals & Applications of Polymer Science" John Wiley and Sons, Japan (1974).

[7] H. Miinstedt, Polymer 27 (1986) 899.

[8] Thermal characterization of polymeric materials, Academic press: London, 1981.

[9] R. M. Silvertein, G. C. Bassler, Spectroscopic identification of organic compounds, John Wiley and sons Inc., New York, 1967.

[10] J. P. Dixon, "Experimental Methods in Microanalysis" Pergamon Press, London. (1985)

[11] Synthesis, crystal growth and characterisation, Ed., Krishan Lal, North Holland Publishing company, Amsterdam, (1982).

[12] D. B. Williams, C. B. carter, Transmission electron microscopy: A text book for material science; Plenum press: New York, Vol. 1, 1996.

[13] G. G, Wallace, G. M. Spinks, L. A. P. Kane-Maguire, P. T. Teasdale, Conductive electroactive polymers intelligent material systems, CRC press, Florida, 2003.

[14] S. D. Deshpande, S. Radhakrishnan, Mat. Lett. 48(3) (2001) 144.

[15] S. Radhakrishnan, S. D. Deshpande, Sensors 2 (2002) 185.

[16] S. Radhakrishnan and S. D. Deshpande, Ind. Patent.Appl. (104/DEL/2001)

[17] S. Radhakrishnan, S. D. Deshpande, Sensors 2 (2002) 185.

[18] S. Unde, J. Ganu, S. Radhakrishnan, Adv. Mater. Optics and Electronics 6 (1996) 151.

CHAPTER III

FERROCENE–POLYPYRROLE SYSTEM

3.1 Introduction

The conducting polymeric materials are usually chemically functionalised [1] or incorporated with appropriate counter ions to enhance the properties [2, 3]. The redox activity of conducting polypyrrole-ferrocene derivative has been investigated by a few authors in the past [4–8]. Very few reports are available regarding gas sensor using ferrocene (Fc) moieties with organic polymeric materials [9, 10]. The conducting polymers are good candidates for the development of chemical or electrochemical sensors for many reasons: (i) ease of fabrication, (ii) low cost, (iii) easy to interface with electronic devices such as MEMS (iv) possibility of using the same polymer with different modifications so as to have selectivity to different gases or a signature in electronic nose. Ferrocene finds many applications in various fields such as DNA sensor [11, 12], ion detectors [13, 14], glucose biosensors [15, 16], photovoltaic cells [17] etc.

The incorporation of ferrocene into polypyrrole is an attractive possibility because oxidation of Fc may produce more charge transfer interactions with PPy units. It is well known that Fc or Fc^+ group dramatically alters the redox properties [18–20] of the polymer. The detection of carbon monoxide using such polymers is not extensively studied. Conventionally, carbon monoxide (CO) has been detected mostly by catalytic methods in which the material is held at high temperature and the changes in the temperature due to the reaction being monitored with a help of thermistor/pellistor [21–23]. MOSFET type gas sensor with tin oxide substrates coated on silicon chips is also a similar kind of work reported in the literature [24]. Alternatively, solid polymer electrolyte with proton conducting membrane has also been employed for detecting CO [25–27] by measuring the voltage generated in fuel cell mode. However, it would be advantageous to fabricate a dry sensor with simpler design such as chemi-resistor using sensitive material having electronic conduction rather than ionic processes so as to obtain faster response. In such a case, the electronic conductors would have to be functionalized in order to increase their sensitivity to gases at room temperature. This study was focused mainly on the effect of incorporation of ferrocene moieties into polypyrrole on its electrical conductivity and CO gas response. Ferrocene moieties acts as co-dopant in addition to Cl^- counter ions. The codopant, ferrocene was incorporated by insitu polymerization technique.

The present chapter describes the preparation of polypyrrole (PPy) and polypyrrole incorporated ferrocene (PPy-Fc) materials. The chemical synthesis method using anhydrous $FeCl_3$ as oxidising agent and the characterisation techniques have been discussed in chapter 2. The application of chemically synthesised PPy-Fc materials for chemical gas sensor is described in this chapter.

3.2. Experimental

3.2.A. Synthesis of Ferrocene Modified Polypyrrole

Ferrocene (Sigma Aldrich, high purity grade) was incorporated in polypyrrole (PPy) during the oxidative polymerization reaction of pyrrole using $FeCl_3$ as the initiator and doping agent [28, 29]. Ferrocene being as such not soluble in water, $FeCl_3$ was added first and then desired amount of Fc was added followed by the monomer. The pyrrole (Py) to $FeCl_3$ concentration was maintained 1:1 mol ratio in all cases while the Fc concentration was varied from 0 to 25 mol% Fc with respect to pyrrole. The aqueous route synthesis of PPy with $FeCl_3$ is reported elsewhere [30, 31]. In a typical reaction containing 25 mol% Fc in distilled water, following procedure was followed: 1.62 g $FeCl_3$ was dissolved in 100 ml distilled water and 470 mg ferrocene was added to it and kept overnight under dark to get it completely dissolved. The reaction was started with the addition of 0.7 ml pyrrole with stirring. The reaction was continued for 4 h in a stoppered bottle. The reacted mixture after 4 hours was added to 500 ml of distilled water for precipitation of modified PPy with incorporated species and kept for 24 h to completely precipitate the product. This was then filtered (filtrate is having green color-characteristic color of ferrocenium ions in dilute solutions), dried by heating and ground to fine powder. The first filtrate was collected and UV-Vis. spectroscopy of the same was recorded. In a similar set of experiments, varying amounts of Fc were added to the reaction mixture ranging from 1.56 to 25 mol percent with respect to pyrrole monomer, the other conditions being same as above. The polymers were dried at room temperature for 48 h and then they were preserved in the vacuum desiccator. The yield of the functionalised polymeric materials is tabulated in Table 3.1.

No.	Ferrocene added (mol%)	Yield (g)	% yield
1.	25	0.165	23.2
2.	8.33	0.19	27.9
3.	4.16	0.215	30.6
4.	2.78	0.226	32.6
5.	2.08	0.242	36.11
6.	1.56	0.275	41.04
7.	0 (Py)	0.29	43.1

Table 3.1. Summary of the % yield of Fc modified PPy obtained.

3.2.B. Real time UV-Vis. Spectrochemical Monitoring of Polymerisation Reaction

The real time UV-Vis. specrtroscopy of the polymerization reaction of polypyrrole along with the incorporation of Fc into PPy was recorded. Very dilute solutions were quantitatively prepared and used for this measurement in a disposable UV-Vis. cuvette and continuously monitored the reaction with respect to time. The reaction kinetics of PPy formation and doping in the presence of Fc is also calculated. The reaction procedure as follows:

1:36 mol ratio Fc:Py reaction: The reaction was carried out in aquestion syetm with slight amount of methanol to ensure the solubility of ferrocene. Fresh solutions of 26 mg ferrocene in 40 ml distilled water + 10 ml methanol solvent mixture, 70 µl pyrrole in 10 ml distilled water and 0.81 g anhydrous ferric chloride in 50 ml distilled water were made separately. 200 µl of the above prepared $FeCl_3$ solution was added carefully into 1 ml distilled water + 0.5 ml methanol mixed solvent system taken previously in a disposable UV-Vis. cuvette and then 200 µl of above prepared ferrocene solution was added subsequently into it. Both these solutions were mixed thoroughly and the online monitoring of the spectra was started with the addition of 200 µl above prepared pyrrole solution with distilled water, then the reaction mixture was mixed thoroughly before starting the polymerization reaction. Similarly polypyrrole synthesis reaction was also

carried out quantitatively and spectra were recorded. The spectra were analyzed and discussed in detailed in section 3.3.1.B.

3.3. Results and Discussions

3.3.A. Characterizations

3.3.A.a. UV-Vis. Spectroscopy

UV-Vis. spectroscopy technique was used to estimate the actual amount of ferrocene incorporated into polypyrrole and to know the electronic transitions of the polymer. The estimation of actual concentration of Fc inside polypyrrole is tabulated in Table 3.2. It has done by recording the spectrum at the beginning of the reaction and after completion of the reaction. It is observed that the color of the filtrate after the reaction varies from green to reddish in color depending on the concentration of ferrocenium ions (Fc^+) in the solution, which is formed by the oxidation with ferric chloride. The intensity of characteristic λ_{max} of Fc^+ obtained at 615 nm region goes down after completion of the reaction for all compositions from their original λ_{max} value.

mol% of ferrocene added	Absorbance at 615nm		Difference in OD	(%) Fc added	Actual con. of ferrocene incorporated (mol%)
	Before reaction	After reaction			
25	2.23	0.74	1.49	67	16.75
12.5	1.11	0.59	0.52	47.3	5.91
8	0.73	0.61	0.12	16.5	1.32
4.2	0.4	0.34	0.04	10	0.42

Table 3.2. The actual concentration of ferrocene incorporated during chemical reaction calculated by UV-Vis. spectroscopy method.

Pyrrole polymerization, 1:36 mol ratio of Fc:Py functionalisation reaction was carried out and the reaction was monitored by real time UV-Vis. spectrochemical method. PPy synthesis and its chemical modification with ferrocene (1:36) were shown in Figures 3.1.A. and 3.1.B. respectively. It is clear from the spectra that a prominent absorption peak at 415 nm region is due to the iron *d-d* electronic transition. A modified polypyrrole

film deposition starts on the inside walls of the cuvette as time progresses. It is explained that the increase in absorbance at 800–900 nm λ_{max} region with polymerization and modification of PPy during the reaction is the formation of conducting material. The presence of Fc^+ initiates the oligomeric formation, which is seen in spectrum Fig. 3.1.B. The oligomeric peak [32] evolves within 15 minutes of the reaction and observed through out the reaction period. This is because the functionalisation reaction is sluggish after 2 h of the reaction and moreover the reaction medium contains slight quantity of methanol to ensure the complete dissolution of ferrocene.

The rate of the reaction was calculated from the time dependent polymerization reaction (from the rate of formation of modified PPy). The OD of the polymer formation (product conversion, C) was ploted against time {[C] vs. t} is shown in Fig. 3.2. (λ_{max} at 800 nm region is considered). The time taken (t) to form the polymer [$(OD_t\text{-}OD_0)$ / OD_{max}] is calculated from the above graph and ploted in the log-log scale (Fig. 3.3.). The slope of the straight line obtained gives directly the rate of the reaction. Eventually there is no big difference in rate of polymerization in the presence of Fc. It is found that the rate of PPy synthesis is little higher than the Fc functionalisation reaction. This is mainly because Fc in the reaction system takes up $FeCl_3$ to form Fc^+. So, the total amount of $FeCl_3$ actually present in the system is not available for the PPy synthesis in the presence of ferrocene. The rate of the reaction for PPy is 4.52×10^{-3} and 4.24×10^{-3} for 1:36 Fc:Py reaction. The rise of absorbance in the wavelength region 800–900 nm is the evidence of formation of conducting material. This is a confirmation of the formation of bipolaronic band [33].

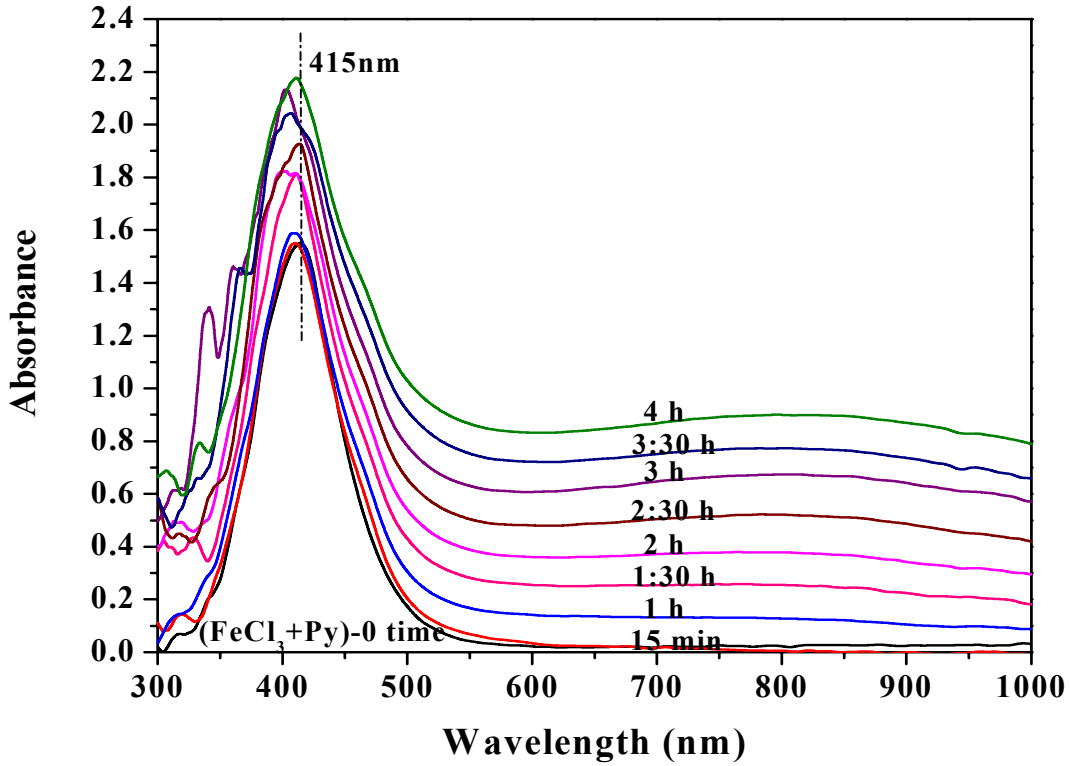

Fig. 3.1.A. Real time UV-Vis. spectroscopic monitoring of PPy synthesis.

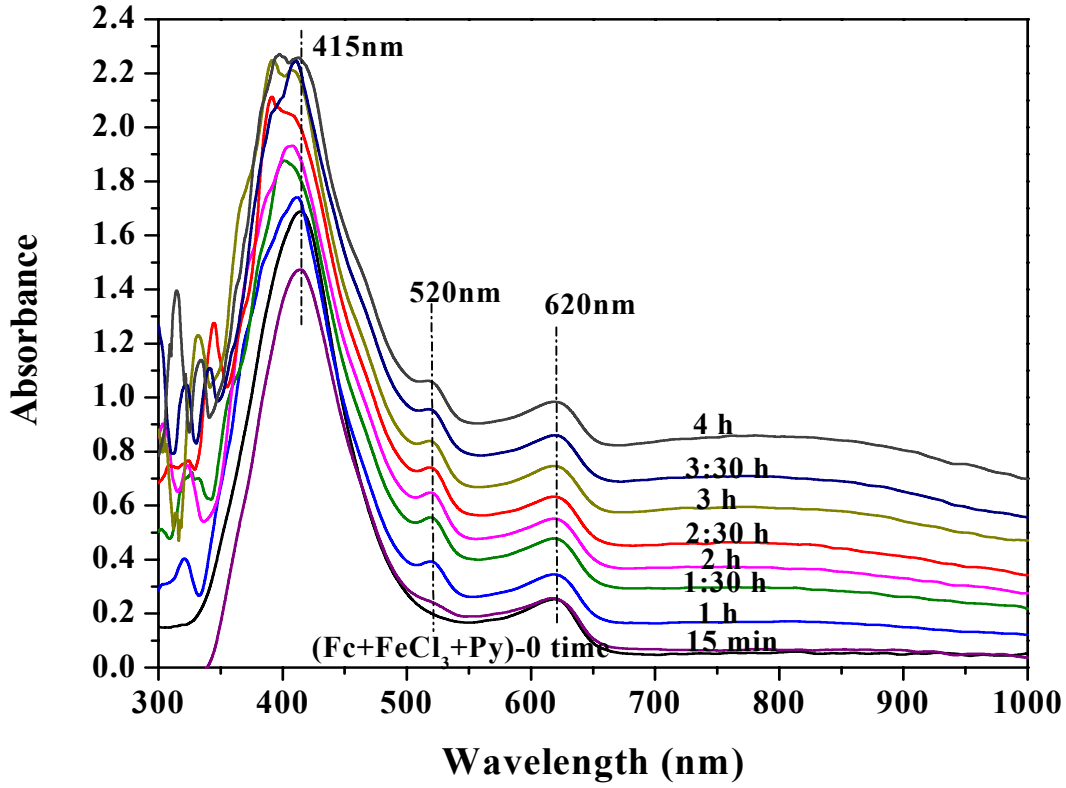

Fig. 3.1.B. Real time UV-Vis. spectroscopic monitoring of 1:36 mol ratio of Fc-Py polymerisation reaction.

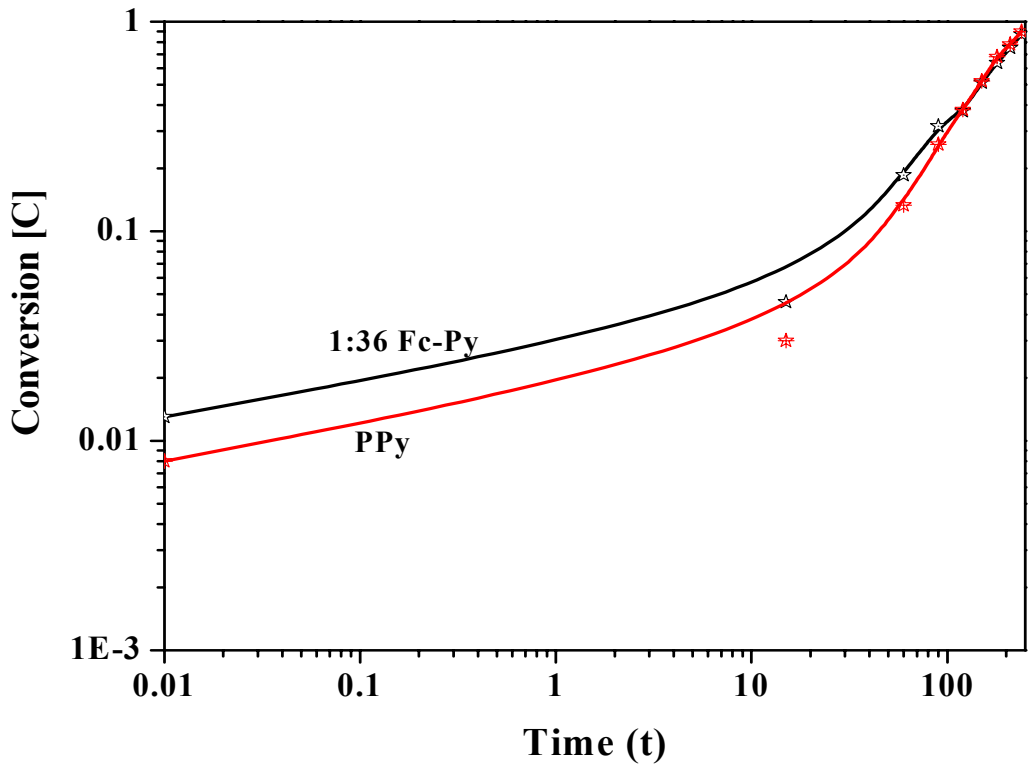

Fig. 3.2. Polymer conversion [C] at λ_{max} 800 nm at regular intervals of time.

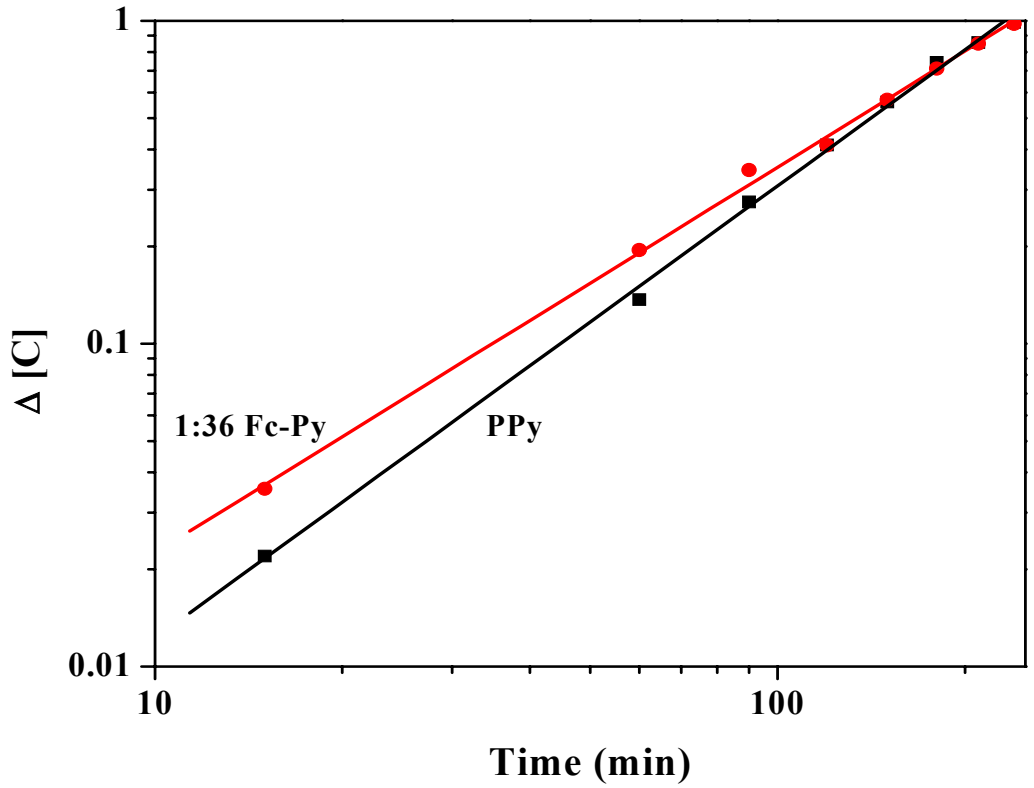

Fig. 3.3. Rate of PPy formation and PPy-Fc modified reactions.

1 mg of the various compositions of Fc-PPy samples grinded and well sonicated with 10 ml NMP for 2 h. It was filtered and UV-Vis. spectra of the dissolved portion was recorded is given in Fig. 3.4. The λ_{max} obtained at the bipolaronic region for the polymeric powders is tabulated in Table 3.3. The λ_{max} of the samples decreases with increasing concentration of ferrocene in the sample. Shift in λ_{max} values indicates effective modification of PPy and possibly more conducting PPy with less concentration of Fc.

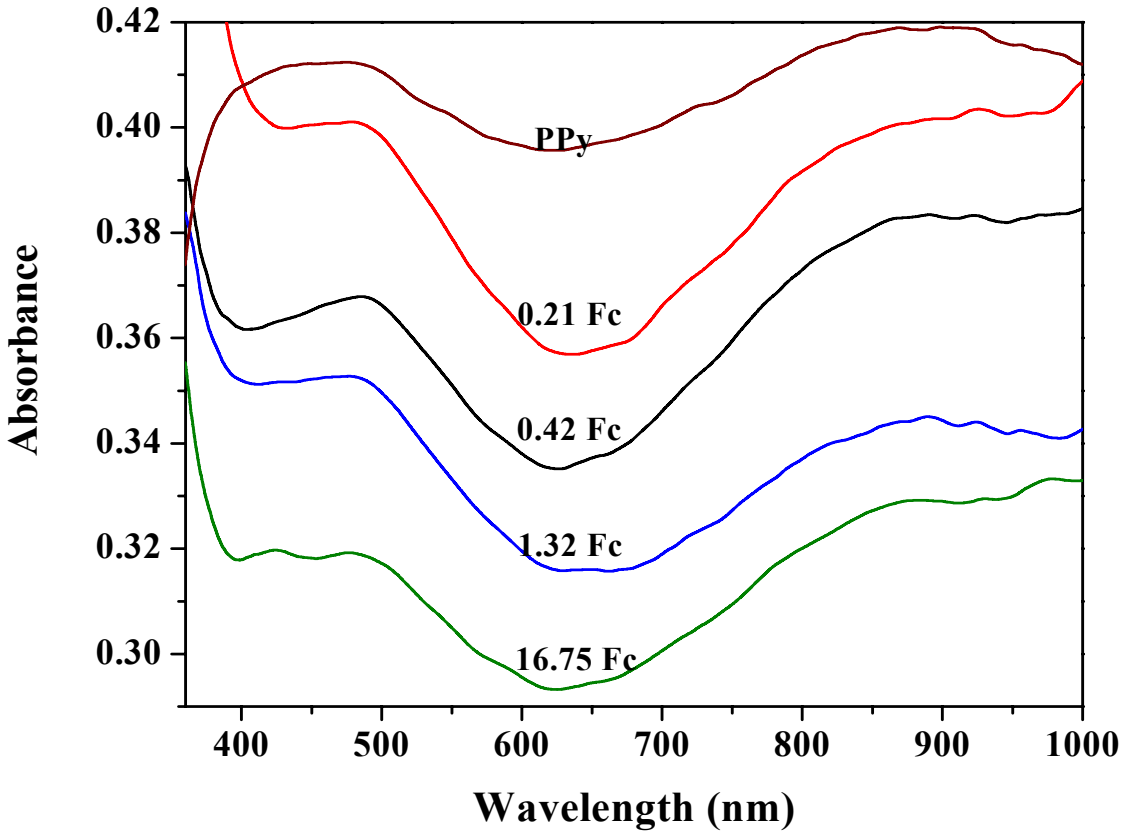

Fig. 3.4. UV-Vis. spectra of polypyrrole and polypyrrole modified with ferrocene (mol%) in different compositions.

Compositions (mol% of Fc incorporated)	λ_{max} (bipolaronic region)
0.21	882
0.42	874
1.32	869
16.75	866
PPy	886

Table 3.3. Wavelength of maximum absorption for PPy at bipolaronic regions.

3.3.A.b. FTIR Spectroscopy

The functionalization of pyrrole with ferrocene was confirmed with FTIR analysis of these polymers. The FTIR spectrum for the solid samples of pure Fc, Fc modified polypyrrole and polypyrrole in KBr pellete form are compared in Fig. 3.5.A., 3.5.B. and 3.5.C. respectively. The percentage transmission peaks observed and their possible assignments are tabulated in Table 3.4. The vibrational frequency values obtained for the PPy and ferrocene characteristic modes are well matched with the reported values of PPy [34, 35] and vibrational frequencies of Fc [36, 37] respectively. The peaks at 1108 cm^{-1}, 999 cm^{-1} and 811cm^{-1} arising from the out of plane vibration of cyclopentadiene and 476 cm^{-}1 peak is due to antisymmetric ring metal stretching vibration, which is characteristic of ferrocene molecules are clear evidence of the presence of ferrocene in the polymer. The major polypyrrole peaks appear at 1192 cm^{-1}, 1047 cm^{-1}, 929 cm^{-1} and 788 cm^{-1}. The peaks at 1697 cm^{-1}, 1550 cm^{-1} and 1192 cm^{-1} of pyrrole are also present in ferrocene – polypyrrole samples. Additionally, the 1464, 1305, 1192, 1094, 1049, 968, 925 and 788 cm^{-1} bands are also seen which are characteristic bands of polypyrrole.

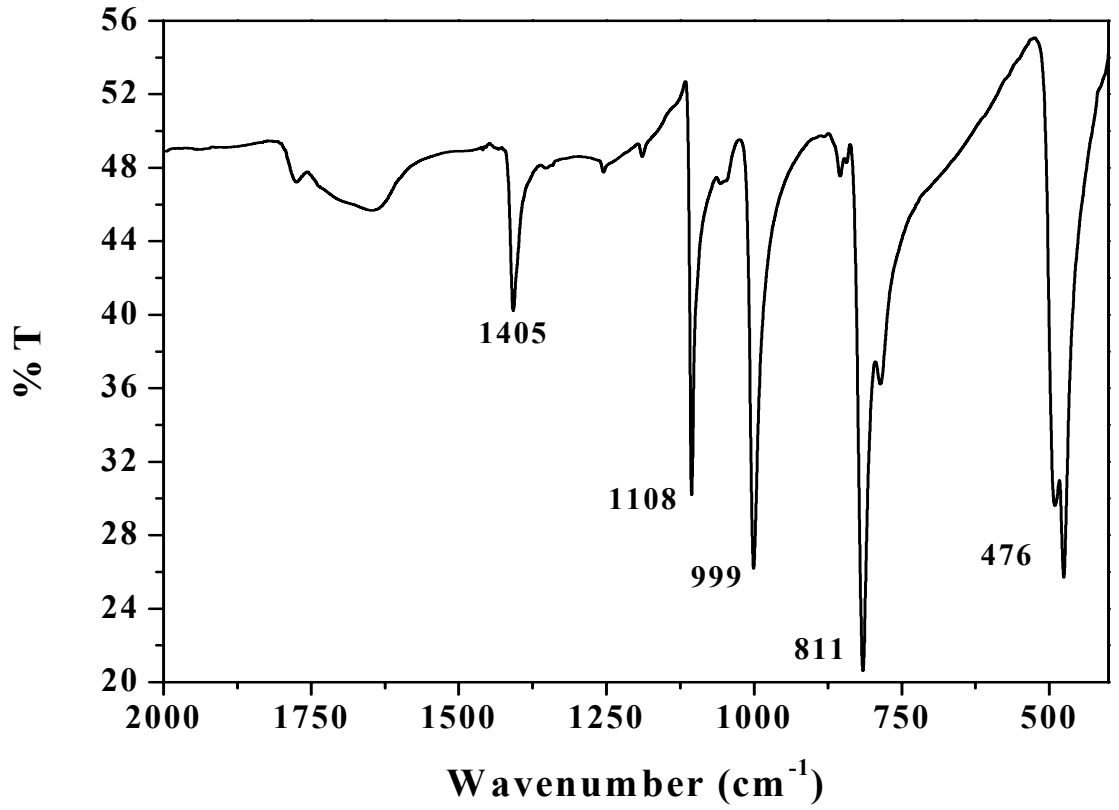

Fig. 3.5.A. FTIR spectrum of pure ferrocene.

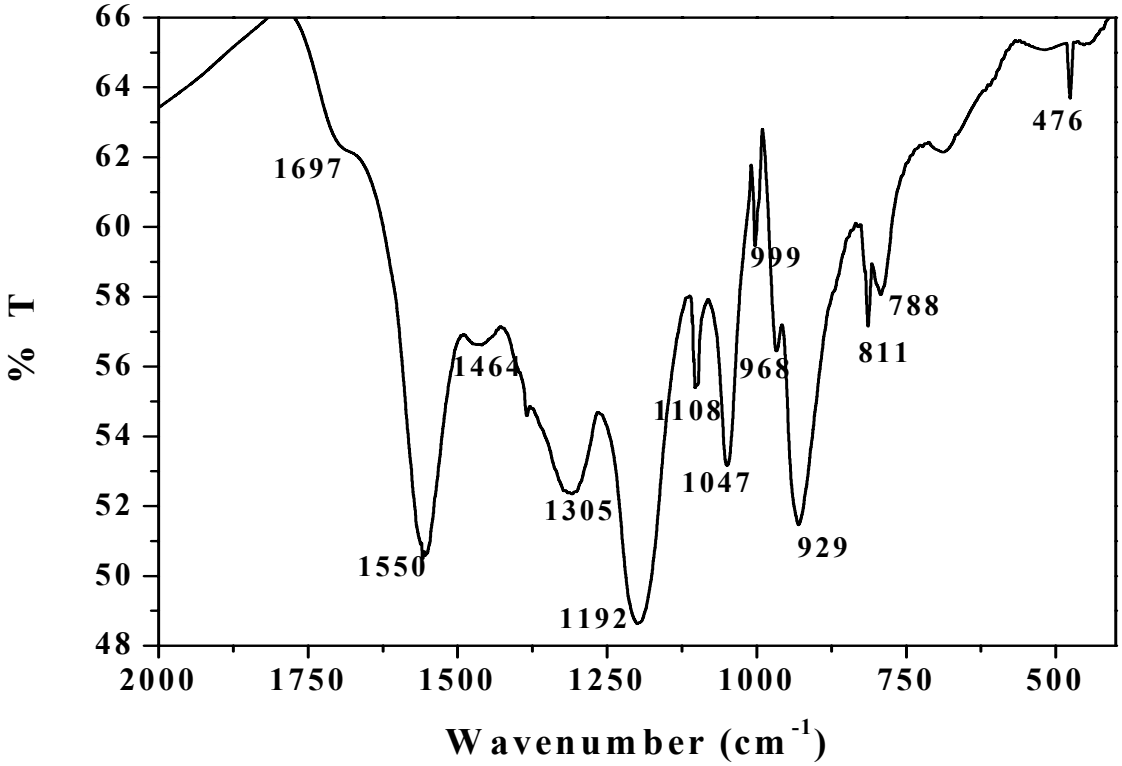

Fig. 3.5.B. FTIR spectrum of PPy-Fc material.

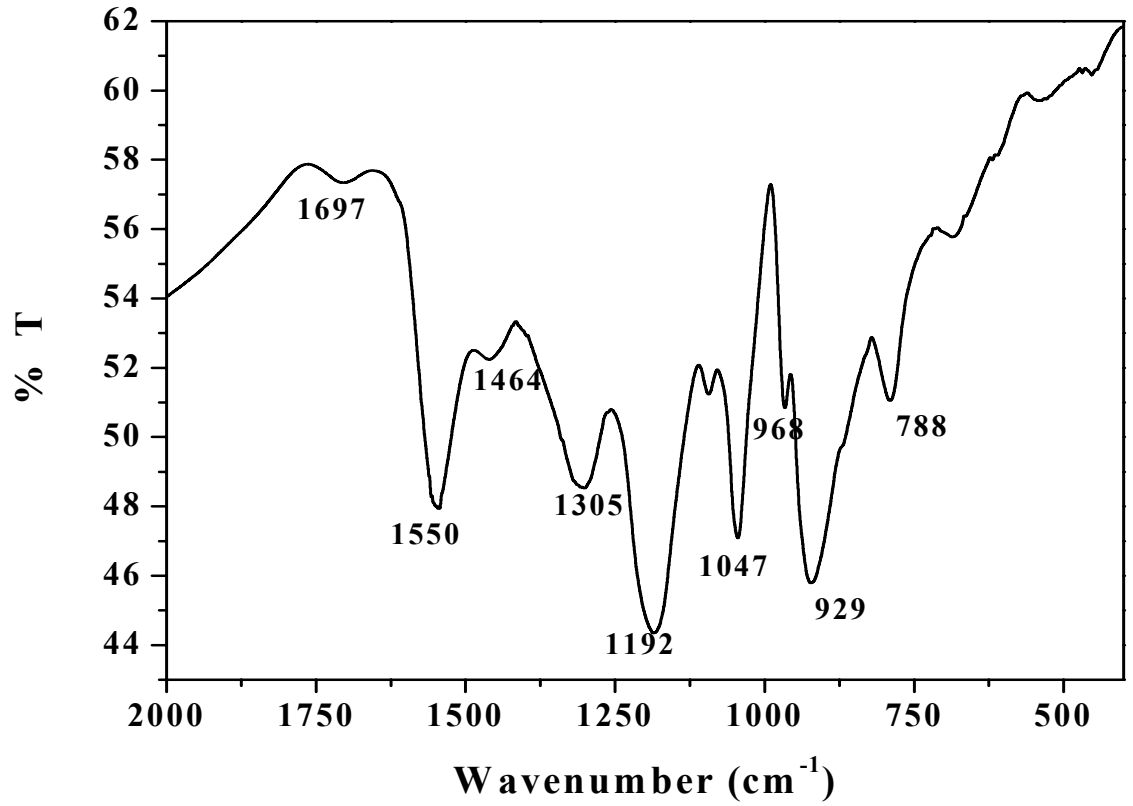

Fig. 3.5.C. FTIR spectrum of pure polypyrrole.

Material	υ_{max} (cm^{-1})	**Peak assignments**
Fc	1405	C-C stretching of cyclopentadienyl ring
	1108	Characteristic of a bis(π–cyclopentadienyl) metal compound with an unsubstituted ring (C–C stretching)
	999	–CH in plane deformation of cyclopentadienyl ring
	811	Out of plane –CH deformation of cyclopentadienyl ring
	476	Characteristic of ferrocene antisymmetric ring metal stretching vibration
PPy	1697, 1550	C=C / C–C stretch
	1464	Ring breathing with contributions from C=C / C–C and C–N
	1305	Aromatic C-N stretching
	1192	Ring breathing

	1049	C–H in plane bend
	968	Terminal rings are away from the influence of dopant or α–β linked units
	929	C–H bend
	788	Ring deformation centered at β-carbon atom
PPy-Fc	1697, 1550, 1464, 1305, 1192, 1047, 968, 929, and 788	Polypyrrole
	1108, 999, 811, 476	Ferrocene

Table 3.4. FT-IR vibrational peak assignments of PPy–Fc material.

3.3.A.c. X-ray Diffraction Studies

Ferrocene crystallizes in needle shaped forms elongated along [110] with monoclinic lattice with lattice parameters of a=10.50 Å, b=7.63 Å, c=5.95 Å, β=121^{0}C [38]. The major 2θ values observed at 15.23, 17.47 and 19. On the other hand ferrocene incorporated PPy do not show any long range order. All these samples are amorphous in nature. There is a very slight shift of the amorphous halo broad peak to lower 2θ region indicating the increase in the average interchain distance due to the presence of ferrocene molecules.

The interchain distance (R) could be calculated from the XRD of the PPy and 1 wt.% PPy-Fc which is in amorpous state. R was calculated by the following equation:

$$R = \frac{5}{8}\left[\frac{\lambda}{\sin\theta}\right]$$

The interchain distance for both pure PPy and 1 wt.% PPy-Fc is 4.14 and 4.53 respecdtively.

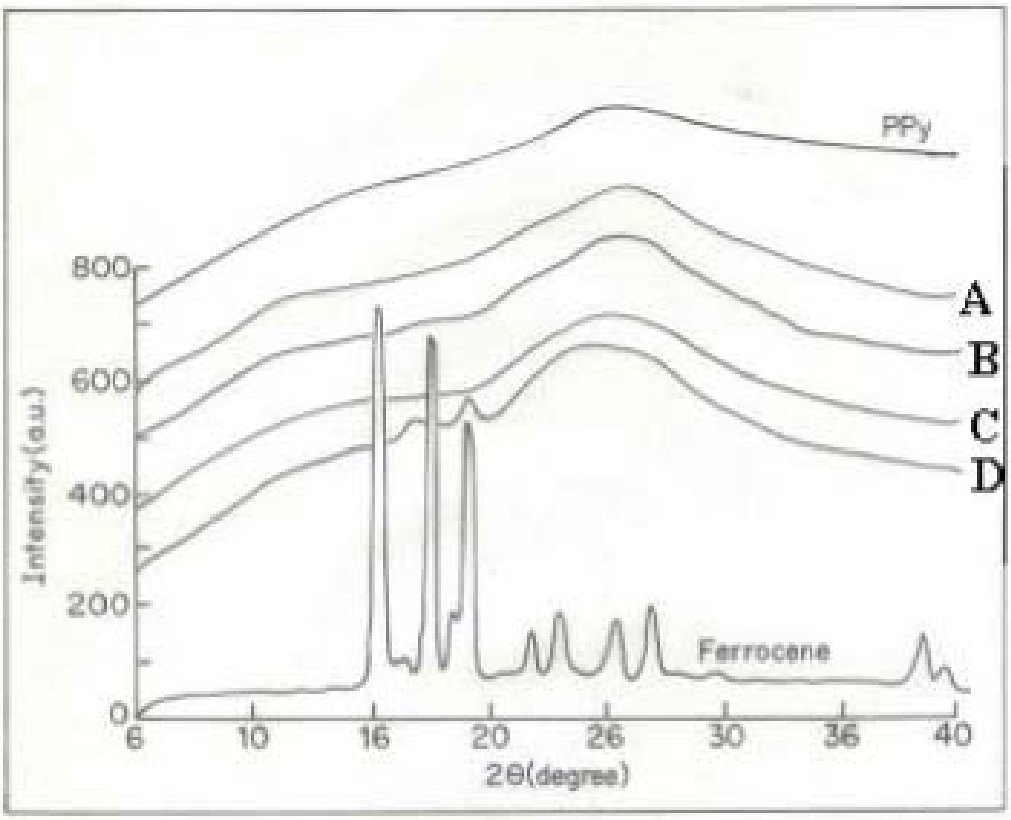

Fig. 3.6. X-ray diffraction patterns of PPy, Ferrocene and Fc-PPy samples: A) 0.28 B) 0.42 C) 1.32 D) 16.75 mol% Fc.

3.3.A.d. Graphite Furnace Atomic Absorption Spectroscopy

This technique (see section 2.5.6.) was used as an elemental detection mainly for the detection of trace quantities of transition metals. This data describes the incorporation of ferrocene into polypyrrole, in which the presence of iron was detected and tabulated in Table 3.5.

Composition (mol% of Fc)	Wt.% of Fe
16.75	1.485
5.91	0.498
1.32	0.119
0.28	0.0255
0.16	0.015
PPy	0.0

Table 3.5. GFAAS data for PPy-Fc samples.

Here, it is seen that polypyrrole doesn't contain any trace amount of iron, which indicates that the iron of $FeCl_3$ used as an oxidant was fully washed out from the polypyrrole and there is a proposional increase of iron content is observed with higher loading of ferrocene. 1.485 wt.% of Fe is detected with 16.5 mol% Fc doped sample and 0.015 wt.% for 0.16 mol% Fc doped polypyrrole sample.

3.3.A.e. EDAX Studies

EDAX (see section 2.5.5.) analysis used mainly to detect iron for the incorporation of ferrocene into polypyrrole. It is observed that there is a consistent and proportional increase in the iron content with increasing concentration of ferrocene. It is a clear indication of the incorporation of secondary dopant, ferrocene, as well as its influence on changing composition of elements at various concentrations. The EDAX data for various compositions were analyzed and shown in Fig. 3.7. Both GFAAS and EDAX data are in agreement in case of amount of iron content in the polymer.

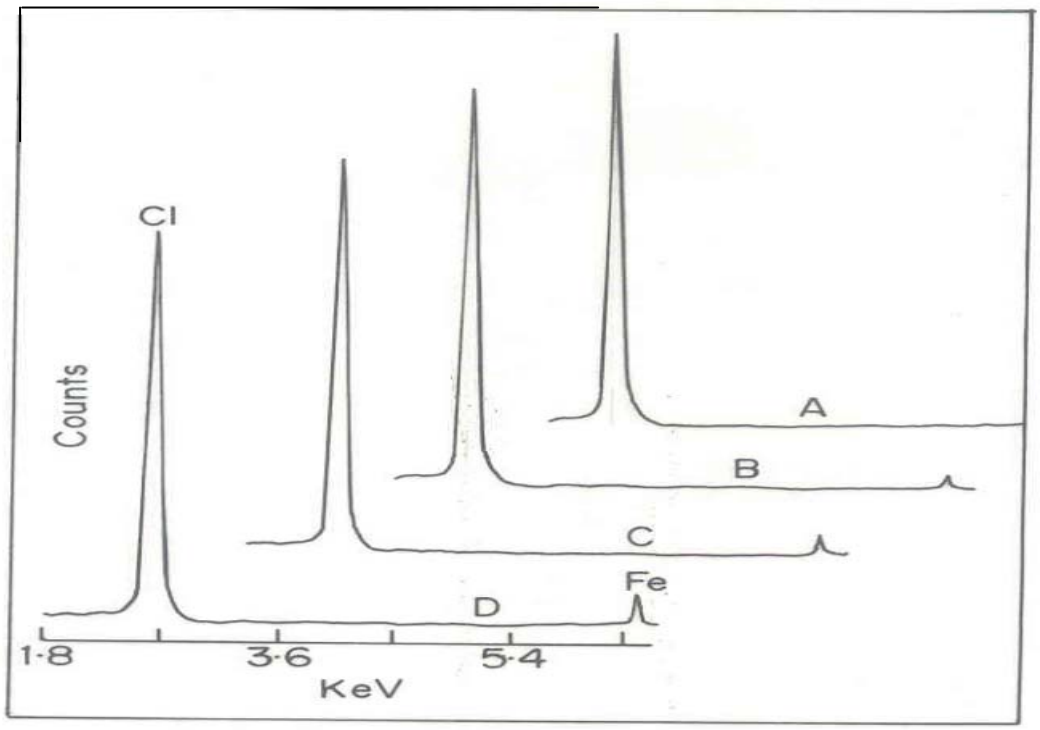

Fig. 3.7. EDAX data for Fc doped PPy samples; A) PPy, B) 1.32 mol% Fc, C) 5.91 mol% Fc, D) 16.75 mol% Fc.

3.3.A.f. TGA Studies

This is another supporting characterization technique to know the presence/influence of dopants on polymer from the thermal stability data obtained from the thermogravimetric pattern of percentage weight loss against temperature plot. The degradation of ferrocene starts at 90^0C and so, the percentage weight loss at 60^0C and 140^0C (before and after degradation of Fc) is calculated and tabulated the originally obtained and expected weight loss in Table 3.6. Here, it is clearly seen that the originally obtained weight loss is almost similar to the expected weight loss except 16.75 mol% PPy-Fc composition. In this particular case, the expected weight loss is 6.147% and experimentally obtained is 4.723%. This indicates that the excess ferrocene stabilizes the PPy. The thermal analysis plot is shown in Fig. 3.8.

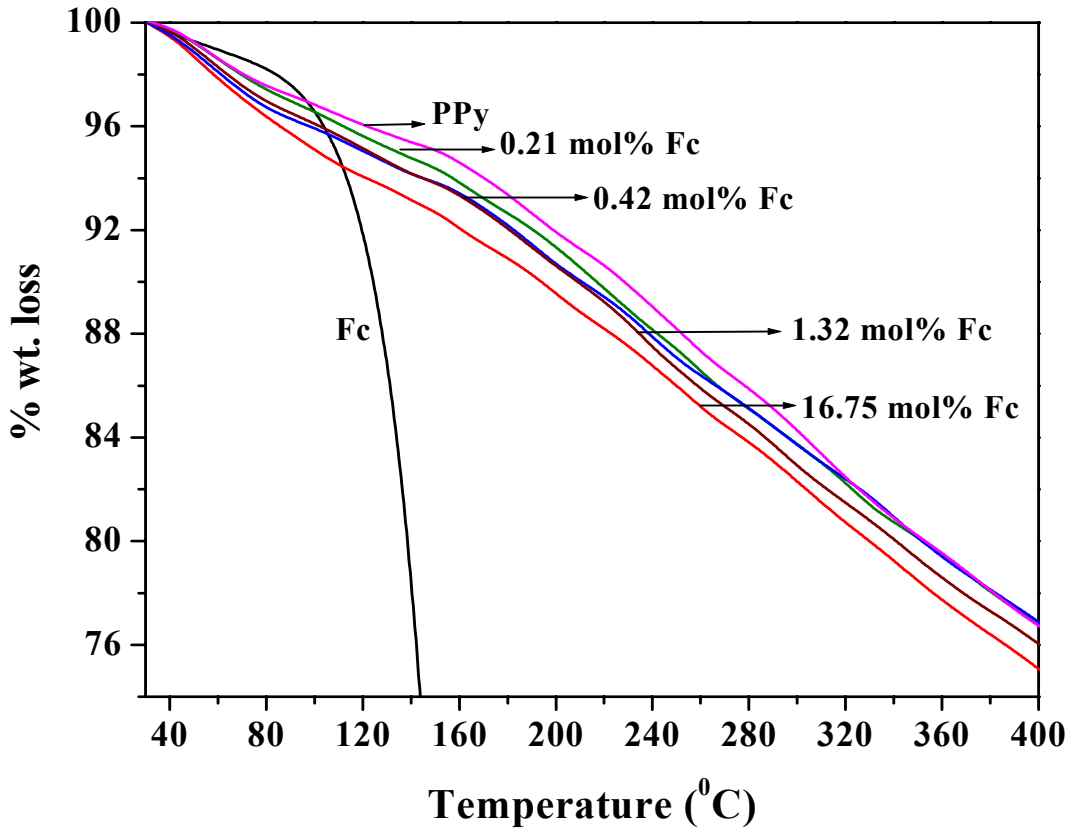

Fig. 3.8. Thermogravimetric pattern of Fc, PPy and Fc doped PPy samples.

Fc content (mol%)	% wt. loss at 60^0C	% wt. loss at 140^0C	Actual wt. loss (%)	Expected wt. loss (%)
0 (PPy)	1.35	4.62	3.27	3.27
0.21	1.34	5.01	3.67	3.306
0.42	1.88	5.59	3.71	3.342
1.32	2.01	5.78	3.77	3.5
16.75	2.1	6.923	4.823	6.147
100	1.4	21.47	20.43	20.43

Table 3.6. Percentage weight loss of the materials at the time of degradation of ferrocene.

3.3.B. Electrical Property Measurements

The effect of electrical conductivity at room temperature (σ) with the addition of ferrocene was studied and results obtained were shown in Fig. 3.9. It is seen that the room temperature conductivity drops down to 10^{-5} S/cm range with the addition of ferrocene moieties into polypyrrole. As can be seen from the figure that the room temperature conductivity decreases with increasing concentration of ferrocene (8.12 X 10^{-5} S/cm for 0.21 mol% Fc-PPy and 8.1 X 10^{-6} for 16.75 mol% Fc-PPy sample). The room temperature conductivity for pure polypyrrole synthesised through aqueous route is 4.88 X 10^{-2} S/cm.

The electrical conductivity in these materials is associated with number of free charge carriers and their mobility. The number of free charge carriers increases with the increasing doping level in the conducting polymer. The observed increase in resistivity with Fc concentration may happen because of different reasons: i) during the incorporation of Ferrocene, due to the presence of $FeCl_3$, it is converted to ferrocenium ion which essentially captures / reduces the dopant ion. This leads to lower doping level and hence decrease in creation of hole charge carriers ii) the position of ferrocene is supposed to be in between the polymeric chains, which hampers the charge transport between the adjacent chains or effectively decreases mobility and finally iii) the ferrocenium ions lead to additional impurity level in the PPy band gap which act as traps for the holes leading to decrease in the carrier concentration.

The electrical conductivity (σ), of PPy-Fc polymeric samples was measured in its pellet form. Pellets were made at a pressure of 5 tonnes using a hydraulic press. It is observed that the electrical conductivity of the Fc doped PPy materials are increased with increase of temperature. The results of the variation in electrical conductivity as a function of temperature are shown in Fig. 3.10.

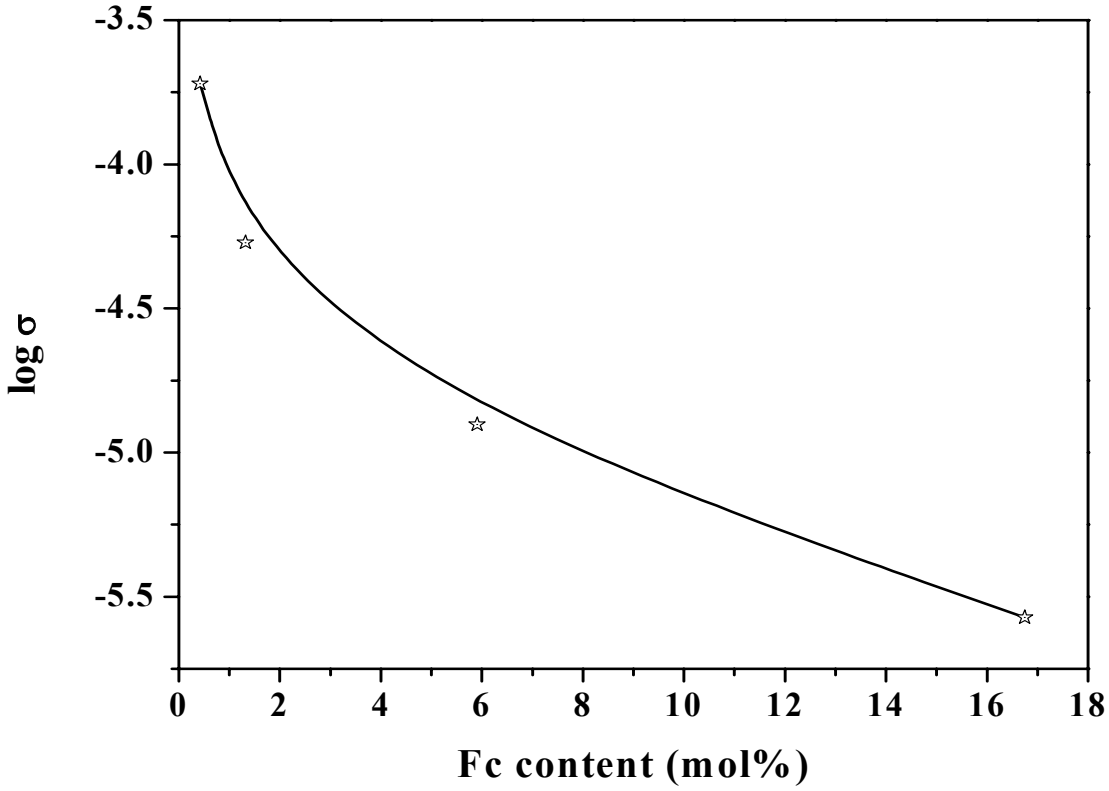

Fig. 3.9. log σ vs. mol percentages of ferrocene in polypyrrole.

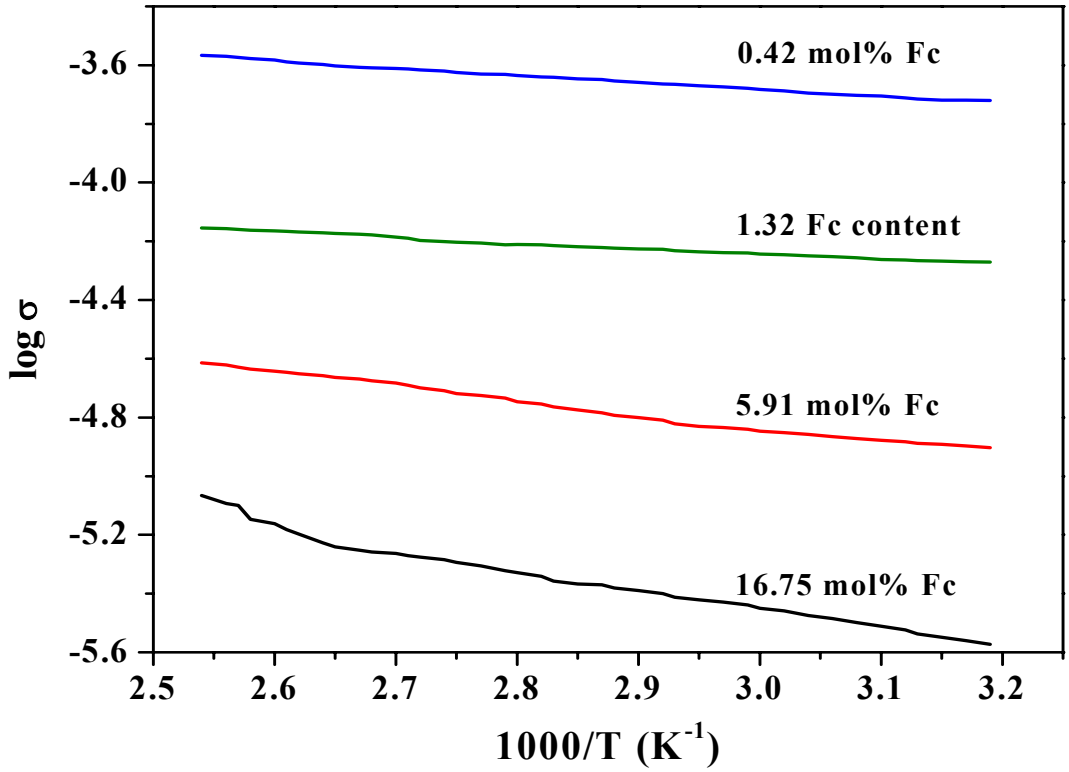

Fig. 3.10. Temperature dependent conductivity of PPy-Fc materials.

The activation energy (Ea) for the polypyrrole and PPy-Fc polymeric materials was calculated using the plot of log conductivity versus 1/T. The results obtained for activation energy for different compositions was analysed and tabulated in Table 3.7. The activation energy for pure polypyrrole sample is 0.033 eV, whereas, the Fc doped samples showing in the range of 0.047 eV to 0.11 eV. The thermal activation energy in this case is mainly due to hindrance to the mobility of carriers (interchain hopping process) and also creation of impurity state, which traps the holes. The decrease in the activation energy is associated with increase in electrical conductivity.

Fc content (mol%)	Ea (eV)
0	0.033
0.42	0.0476
1.32	0.0715
5.91	0.0941
16.75	0.11

Table 3.7. Activation energy against mol% of Fc content in PPy.

3.3.C. Carbon Monoxide Gas Sensitivity Measurements

The PPy powders doped with different concentrations of Fc is used to coat on interdigited electrode for the CO gas sensitivity measurements, which is described in section 2.10.

The sensor samples were tested for response to 300 ppm CO gas (allowable limit) [39, 40] by monitoring the resistance continuously for the interdigitated surface cells. The resistance was in the range of 5.0 to 100 KΩ depending on the composition and concentration of the dopant. The resistance increased rapidly within 100 s after exposure to a 300 ppm CO gas mixture with air. Figures 3.11.A. and 3.11.B. show a typical response curve obtained for PPy containing 1.32 mol% Fc and the response of various composition of Fc-PPy. The response factor ($\Delta R/R_0$), where (ΔR) is the change in resistance while R_0 is the original resistance value, was estimated for all samples after exposure to CO repeatedly. The response factor increased from 0.6% to 28% at a certain

composition as indicated in Fig. 3.12. and above the critical concentration of ferrocene, the response factor again dropped to a lower value. The speed of response determined from the t_{50} value, i.e. the time required to attain 50% of the maximum change, was low (96 s) for a certain composition of PPy-Fc (1.32 mol% Fc) and depended very much on the composition. These various sensor characteristic parameters for different compositions are given in Table 3.8.

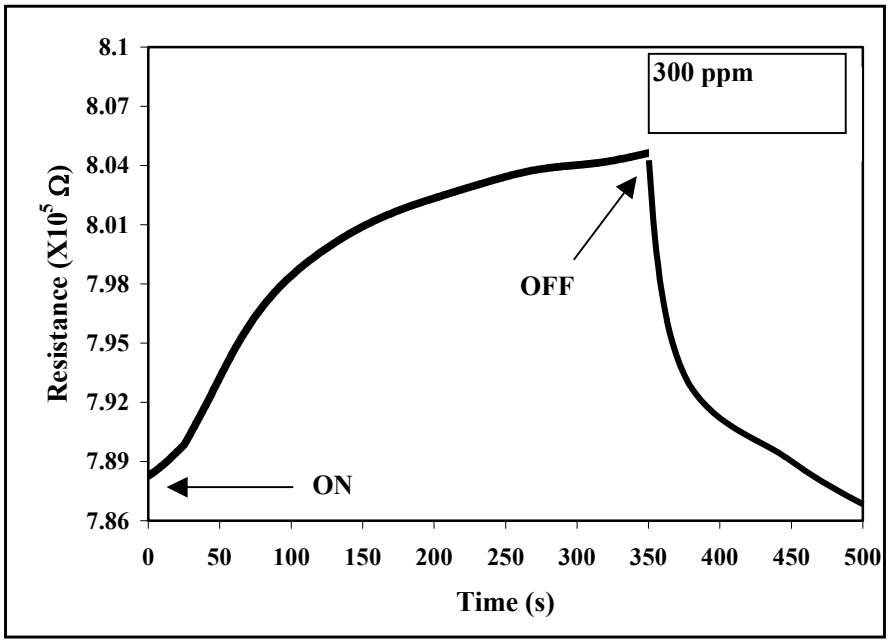

Fig. 3.11.A. The response characteristic of 1.32 mol% Fc containing PPy sample.

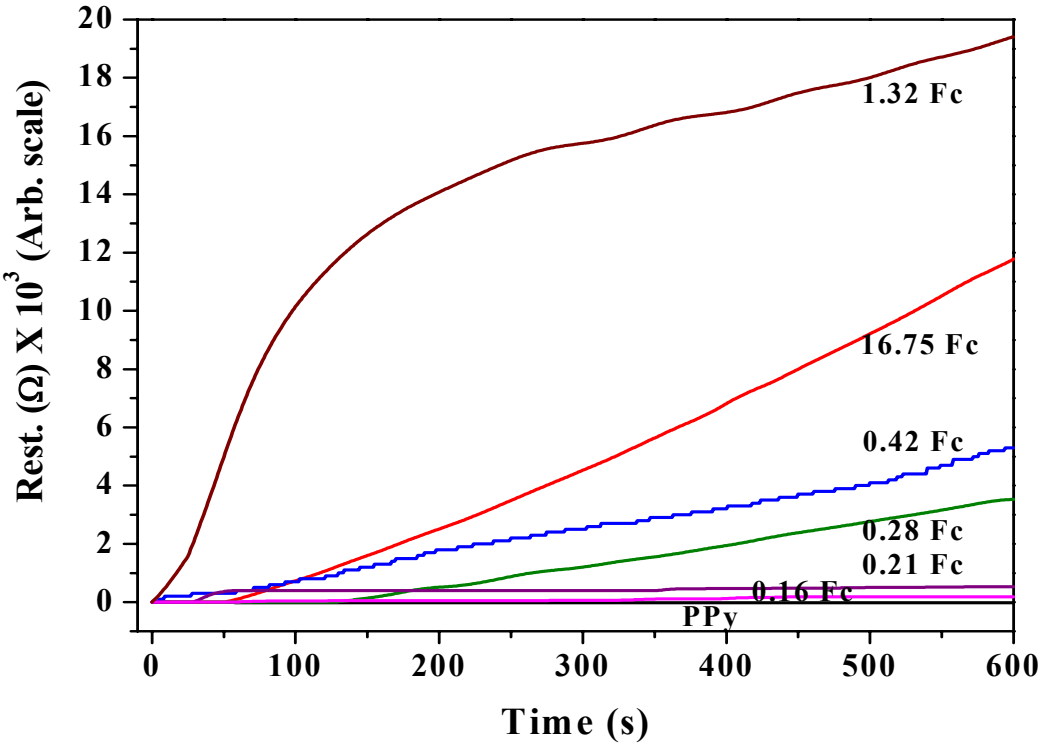

Fig. 3.11.B. CO response characteristics of various concentrations of PPy-Fc materials.

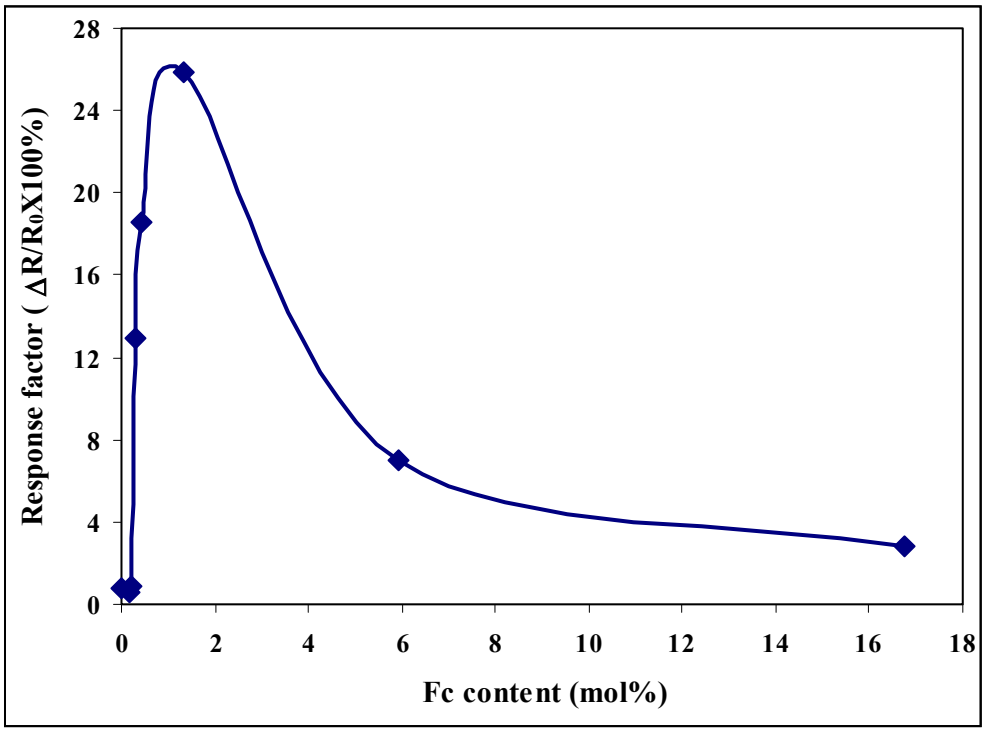

Fig. 3.12. Response factor with respect to composition of PPy containing ferrocene to 300 ppm CO.

Ferrocene content (mol%)	$(\Delta R/R_0)$ %	Sample resistance R_0 (Ω)	Response time t_{50} (s)
16.75	2.84	788383	348
5.91	6.99	28157	348
1.32	25.8	70698	96
0.42	18.6	80730	340
0.28	12.9	41092	342
0.21	0.9	6690	336
0.16	0.6	3340	351
0 mol Fc (100% PPy)	0.76	2615	936

Table 3.8. Effect of composition on the response factor and response time of ferrocene modified PPy to 300 ppm carbon monoxide.

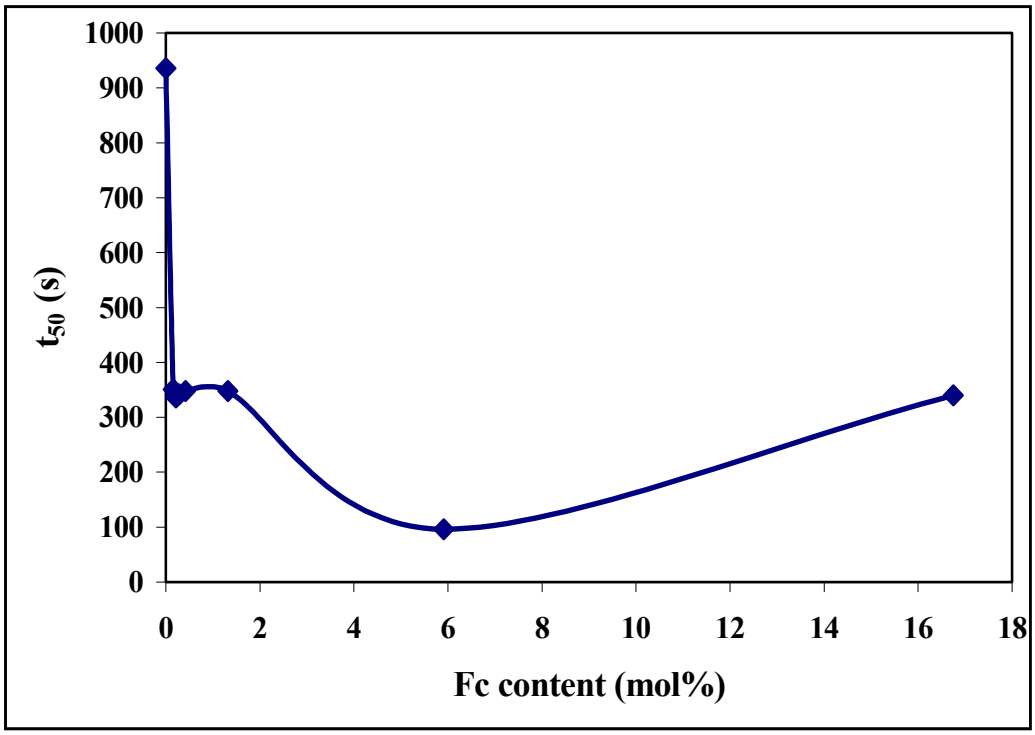

Fig. 3.13. Compositional dependence of response time (t_{50}) for PPy with ferrocene to 300 ppm CO.

Fig. 3.13. indicates the variation of speed of response with composition for PPy-Fc films. Here, a high response factor as well as a fast response at room temperature has been observed for a certain concentration of the functional additive, which demonstrates its applicability to these sensors.

In order to understand the underlying processes in the sensing mechanism, one has to look into various types of possible interactions between the conducting polyyrrole, ferrocene and CO molecules. The interaction between the lone pair on the nitrogen of pyrrole with the electron withdrawing nature of the CO molecule (as indicated in Fig. 3.14.A) will lead to the formation of polarons as suggested by some authors for polyaniline [40, 41]. This will give rise to an increase in conductivity rather than its decrease (increase in resistance) as observed in the present case. Lightly doped PPy without ferrocene, sometimes shows an increase in conductivity when exposed to carbon monoxide. However, since in the present case, an increase of resistance has been observed in most of the samples, one has to look for an alternative process for sensing property. It should be noted that the incorporation of ferrocene in polypyrole increases its electrical resistivity as such without exposure to gases i.e. the R_0 value (see Table 3.8 and Fig.3.9). Since polypyrrole was synthesized in the presence of ferric chloride together with ferrocene, it would be expected to form a ferrocenium ion and/or a donor acceptor complex with $FeCl_3$, which will essentially lead to less doping of polypyrrole. The fact that the bipolaronic absorption band in the UV-Vis spectra shifts towards lower λ_{max} in the presence of ferrocene also supports this argument. It is also known that carbon monoxide preferentially interacts with iron complexes [42 - 44], which in the present case is ferrocene and not the nitrogen atoms of polypyrrole (see Fig. 3.14. B). Thus exposure to CO will only lead to a further decrease in conductivity or increase of resistivity as observed in this case [45]. Further, it does not appear to be a permanent change in the material because the electrical resistance of the sample is seen to recover after the chamber is purged with air/oxygen. Also, these sensors are totally dry and there is no ionic conductivity or electrochemical reaction needed for the sensing action, which is advantageous for the fast response characteristics.

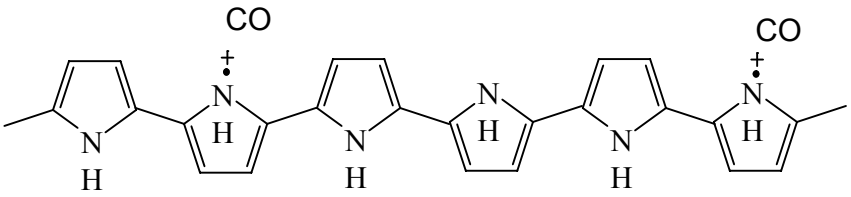

Fig. 3.14.A. Interaction of CO gas molecules with virgin PPy.

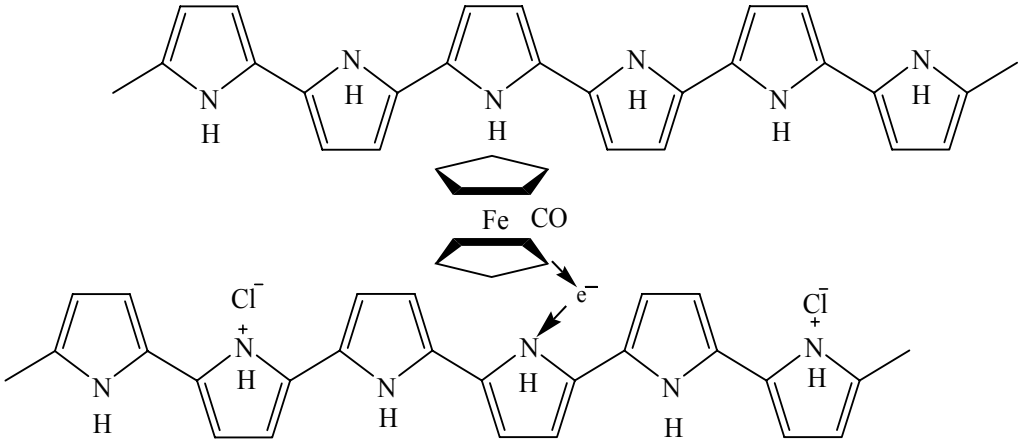

Fig. 3.14.B. Interaction of CO gas molecules with Fc doped PPy samples.

3.4. Conclusions

The chemical incorporation of ferrocene into polypyrrole has been successfully carried out during insitu polymerisation reaction of polypyrrole. The amount of ferrocene incorporated into the PPy is estimated by UV-Vis. optical spectroscopy method and different compositions were characterised thoroughly using various techniques. All these results indicate the incorporation of Fc moieties in the interchain spaces of the PPy. The structure of the ferrocene doped polymer was derived based on the results of XRD. The polymers obtained have shown lower conductivity values (RT conductivity in the range of 10^{-5} S/cm) as compared to PPy synthesized under same conditions.

The chemically doped PPy with ferrocene compounds were found to be fairly sensitive to CO gas. The magnitude of the change of resistance during exposure to 300 ppm CO gas is about three times of initial magnitude for 1.32 mol% Fc containing PPy material. The response signal obtained in all cases shows an increase of resistance with in a short period of time. There is an optimum composition at which the maximum response is obtained at 300 ppm CO gas. It should be particularly noted that this response signals occurred at RT and ordinary atmospheric conditions in a short period of time. Not only the response, but also the recovery is quick and immediate when the gas calibration bottle is flushed with dry air. Typical sensors made in a surface cell configuration can be used in dry state at room temperature and it has fast response characteristics since the sensing process involves only electronic charge transport and interactions with the conjugated electronic states rather than ionic, electrochemical or catalytic reactions which are observed for conventional carbon monoxide sensors.

3.5. References

[1] P. Godillot, H. K. Youssou, P. Srivastava, A. El Kassmi, F. Garnier, Synth. Met. 83 (1996) 117.

[2] C. Lee, M-H. Lee, Y. K. Kang, B. S. Moon, S. B. Rhee, Synth. Met. 55–57 (1993), 1119.

[3] G. Bidan, M. A. Niel, Synth. Met. 85 (1997) 1387.

[4] L. M. Goldenberg, M. R. Bryce, M. C. Petty, J. Mater. Chem. 9 (1999) 1957.

[5] J. G. Eaves, R. Mirrazaei, D. Parker, H. S. Munro, J. Chem. Soc. Perkin Trans II 1989, 373.

[6] J. C. Moutet, E Saint-Aman, M. Ungureanu, T. Visan, J. Electroanal. Chem. 79 (1996) 410.

[7] H. Korri-Youssou, B. Makrouf, Synth. Met. 119 (2001) 265.

[8] J. Chen, A. K. Burrell, G. E. Collis, D. L. Officer, G. F. Swiegers, C. O. Too, G. G. Wallace, Electrochim. Acta 47 (2002) 2715.

[9] C. Kim, E. Park, C. K. Song, B. W. Koo, Synth. Met. 123 (2001) 493.

[10] R. Mohd, I. E. Loren, M. Shadaram, Proceedings of SPIE-The International Society for Optical Engineering, 4036 (Chemical and Biological Sensing), 123.

[11] C. J. Yu, Y. Wan, H. Yowanto, J. Li, C. Tao, M. D. James, C. L. Tan, G. F. Blackburn, T.J. Meade, J. Am. Chem. Soc. 123 (2001) 11155.

[12] H. K. Youssoufi, A. Yassar, Biomacromolecules 2 (2001) 58.

[13] L. S. Diane, K. S. David, Polyhedron 22 (2003) 763.

[14] O. B. Sutcliffe, A. Chesney, M. R. Bryce, J. Organomet. Chem. 637–639 (2001) 134.

[15] M. P. G. Armada, J. Losada, I. Cuadrado, B. Alonso, B. Gonzalez, E.R. Oliva, C. M. Casado, Sens. and Actuat. B 88 (2003) 190.

[16] P. C. Pandey, S. Upadhyay, N. K. Shukla, S. Sharma, Biosens. Bioelectron.18 (2003) 1257.

[17] N. R. Armstrong, C. Carter, C. Donley, A. Simmonds , P. Lee, M. Brumbach, B. Kippelen, B. Domercq , S. Yoo, Thin Solid Films 445 (2003) 342.

[18] S. J. Higgins, C. L. Jones, S. M. Francis, Synth. Met. 98 (1999) 211.

[19] K. Naka, T. Uemura, Y. Chujo, Macromolecules 33 (2000) 6965.

[20] Y. Zhu, M. O. Wolf, J. Am. Chem. Soc. 122 (2000) 10121.

[21] H. Meixner, J. Gerblinger, U. Lampe, M. Fleischer, Sens. Actuators B 23 (1995) 119

[22] M. Di Guilio, G. Micocci, R. Rella, P. Siciliano, A. Tepore, Sens. Actuators B 23 (1995) 193.

[23] V. Casey, J. Cleary, G. D. Arcy, J. B. McMonagle, Sens. Actuators B 96 (2003) 114.

[24] U. Storm, O. Bartels, J. Binder, Sens. Actuators B 77 (2001) 529.

[25] E. Bakker, M. Telting-Diaz, Anal. Chem. 74 (2002) 2781.

[26] O. J. Prohaska, A. B. Laconti, J. D. Giner, M. Manoukian, U.S. Pat. Appl. Publ. US 2003121781 A1 3 Jul, 2003, 10 pp., Cont.-in-part of U.S. Ser. No. 444,334.

[27] A. Yasuda, T. Shimidzu, React. Funct. Polymers 41 (1999) 235.

[28] S. Rapi, V. Bocchi, G. P. Gardini, Synth. Met. 24 (1988) 217.

[29] S. Radhakrishnan, S. P. Khedkar, Synth. Met. 79 (1996) 219.

[30] S. Machinda, S. Miyata, Synth. Met. 31 (1989) 311.

[31] S. P. Armes, Synth. Met. 20 (1987) 365.

[32] M. Han, Y. Chu, D. Han, Y. Liu, J. Colloid Interf. Sci. 296 (2006) 110.

[33] B. Tion, G. Zerbi, J. Chem. Phys. 92 (1990) 3892.

[34] R. G. Davidson, T. G. Turner, Synth. Met. 72 (1995) 121.

[35] J. Lei, W. Liang, C. R. Martin, Synth. Met. 48 (1992) 301.

[36] P. Sohlir, J. Kuszmann, J. Mol. Structure 3 (1969) 359.

[37] G. N. Kamau, T. M. Saccucci, G. Gounili, A. E. F. Nassar, J. F. Rusling, Anal. Chem. 66 (1994) 994.

[38] J. D. Dunitz, L. E. Orgel, Nature (1953) 121.

[39] R. C. Frederick, Analyst 56 (1931) 561.

[40] N. I. Sax, Industrial pollution, Ed., Van Nostrand Reinhold Company, (Ch. 22) 1974, pp. 596.

[41] T. Hanawa, H. Yoneyana, Synth. Met. 30 (1989) 341.

[42] G. Harsanyi, Polymer films in sensor applications, Technomic publishing Co., Lancaster, 1995, pp. 211–214.

[43] K. H. Lee, M. L. Kennedy, M. Buchalova, D. R. Benson, Tetrahedron 56 (2000) 9725.

[44] G. Neri, A. Bonavita, S. Galvagno, L. Caputi, D. Pacile, R. Marsico, L. Papagno, Sens. Actuators B 80 (2001) 222.

[45] S. Radhakrishnan, Santhosh Paul, Sens. Actuators B (in print) (2007).

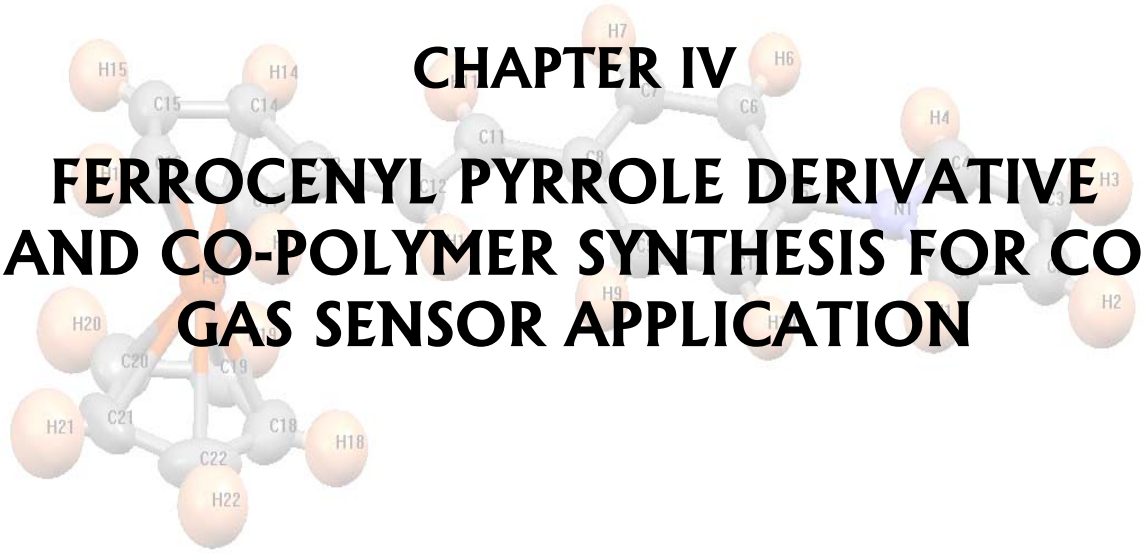

CHAPTER IV

FERROCENYL PYRROLE DERIVATIVE AND CO-POLYMER SYNTHESIS FOR CO GAS SENSOR APPLICATION

4.1. Introduction

A detailed study of chemical incorporation ferrocene into polypyrrole, characterization of the modified PPy powder and its CO sensor application were described in the previous chapter. It was observed the conductivity of PPy decreases by direct incorporation of Fc during chemical polymerization. It was hence thought that if Fc is derivatized pyrrole so that it can be attached to the main chain it may lead to better conductivity and performance. Also, the possibility of its inclusion in PPy by electrochemical polymerization would be worth looking into. This chapter illustrates the synthesis of ferrocenyl derivatives for the electrochemical incorporation as well as copolymerization with pyrrole and its effect on CO gas.

Derivatising the conducting polymer [1], doping and copolymer formation [2] or homopolymer synthesis are some of the effective ways of improving the specific properties and applications of conducting polymers. A new class of organometallic macromolecules containing skeletal ferrocenyl moieties attached with p-phenylene vinylene on the cyclopentadienyl ring was N-arylated with heterocyclic compound like pyrrole via efficient CuI catalyzed reaction. The ferrocenyl pyrrole derivative is a novel comonomer, which has been copolymerized with pyrrole for gas sensor application. There has been considerable interest in exploiting metal co-ordinating macrocycles [3, 4] and metallocene [5, 6] compounds such as phthalocyanines, porphyrin, ferrocenes and doped conductive polymers [7, 8] for gas sensors [9–12], which are mainly associated with detection of organic solvent vapors, ammonia, chlorine and other similar hazardous gases. The electrical, optical, and electrochemical properties of these materials can vary enormously as a result of the functional groups [13–15]. As we see in chapter 3, the incorporation of ferrocene derivative into polypyrrole is an attractive possibility because oxidation of Fc may produce more charge transfer interactions with PPy units. It is well known that Fc or Fc^+ group dramatically alters the redox properties [16–19] of the polymer. This chapter describes a new redox active macromolecular systems containing ferrocenyl moiety, which proved to be very good reversible redox reactions especially in the development of chemical sensors [20, 21]. The method which we have employed here for the N-arylation of heterocycles are the general one like indoles, pyridines, pyrroles, azoles etc. were reported elsewhere [22, 23]. In this chapter, we propose a new random

copolymer with a novel comonomer (*trans*-1-{4[2-(1-ferrocenyl)vinyl]phenyl}pyrrole) with pyrrole by chemical oxidation polymerization with special interest on carbon monoxide detection in ppm level.

The comonomer synthesis is a five stage process and subsequently it was copolymerized both by chemical as well as electrochemical methods. The detailed procedures for the synthesis, characterization and application are as follows:

4.2. Synthesis of Ferrocenyl Methyl Trimethylammonium Iodide

The total scheme for comonomer synthesis can be split into two: i) synthesis and characterization of ferrocenyl methyl trimethyl ammonium iodide and doping of this ferrocenyl derivative into polypyrrole for CO gas sensor measurements. The scheme of synthesis is given below (Scheme 1). ii) comonomer synthesis and its copolymerisation with pyrrole monomer and CO gas sensitivity studies in detail.

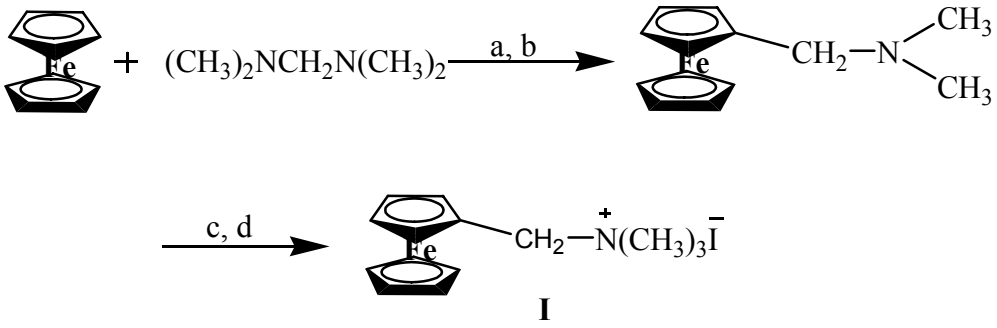

a = H_3PO_4 b = CH_3COOH c = CH_3I d = CH_3OH

Scheme 1

The synthesis of compound **I** starts with the preparation of ferrocenyl methyl dimethyl amine from ferrocene. It was methylated using iodomethane in methanol to get brown yellow crystals of ferrocenyl methyl trimethylammonium iodide (**I**).

4.3. Experimental Procedure

The reaction has been performed according to the reported literature procedure [24–28]. In a typical experiment, 46.4 g (0.25 mol) ferrocene (Fc) was added to a well stirred solution of 43.2 g (0.422 mol) bis(dimethylamino) methane and 43.2 g of ortho

phosphoric acid in 400 ml glacial acetic acid in a 2-1 three necked round bottom flask equipped with a condenser, a nitrogen inlet and a mechanical stirrer. The resulting suspension was heated on a steam bath under a slow stream of nitrogen for 5 h. The reaction mixture, a dark amber solution, was allowed to cool to room temperature and was diluted with 550 ml water. The unreacted ferrocene was removed by extracting the solution with three 325 ml portions of ether. The aqueous solution was then cooled in ice water and made alkaline by the addition of 245 g sodium hydroxide pellets. The tertiary amine separates from the alkaline solution as oil suspension. The mixture was extracted with three 500 ml portions of ether. The organic solution was washed with water and dried over anhydrous sodium sulphate. Crude dimethylamino methyl ferrocene obtained as a dark-red mobile liquid when the solvent was removed at the water pump.

To a gently swirled solution of the crude amine in methanol (54 ml) was added 54 ml of methyl iodide (123 g, 0.87 mol). The solution was heated on a steam bath for 5 minutes and cooled to room temperature and then 800 ml ether was added to the same. The methaiodide, which separates initially as oil crystallizes out slowly as an orange powder. The solid was collected in a Buchner funnel, washed with ether and dried at 20–50 mm pressure for several hours at RT. The product obtained was pure enough to carry out further reactions. The yield of the reaction is 75 g (76%), m.p. 190^0C (decomposed).

4.4. Results and Discussions for Ferrocenyl Methyl Trimethylammonium Iodide

4.4.A. Characterization

4.4.A.a. ^{1}H NMR Spectroscopy

Proton NMR is one of the powerful tools to get the structure of organic/organometallic compounds (explained under section 2.5.8.). The spectral detail of the compound is summarized below:

^{1}H NMR (200 MHz, D_2O) δ: 4.54 (t, 2H, Cp), 4.46 (t, 2H, Cp), 4.42 (s, 2H, (CH_2), 4.31 (s, 5H, Cp), 2.97 (s, 9H, –CH_3).

The compound **I** is soluble in D_2O and the spectrum was recorded in 200 MHz instrument. Iron dicyclopentadienyl compound gives three peaks at δ, 4.54; attributed to the two hydrogens at immediate vicinity of substituted carbon of one cyclopentadienyl ring. δ, 4.46 is also another triplet arises due to the effect of two hydrogens near to the

substituted carbon on the other two homogenous –CH of the substituted ring. A singlet peak seen at 4.31 is due to the effect of 5 H's of unsubstitued cyclopentadienyl ring. The other two singlet peaks obtained at δ, 4.42 and 2.97 is attributed to the $–CH_2$ group attached to one cyclopentadienyl ring and 9 H's of three $-CH_3$ groups attached to nitrogen under the same chemical environment. All these details lead to confirm the structure of the compound **I** with the help of other characterization tools. The ^{1}H NMR spectrum of **I** is given in Fig. 4.1.

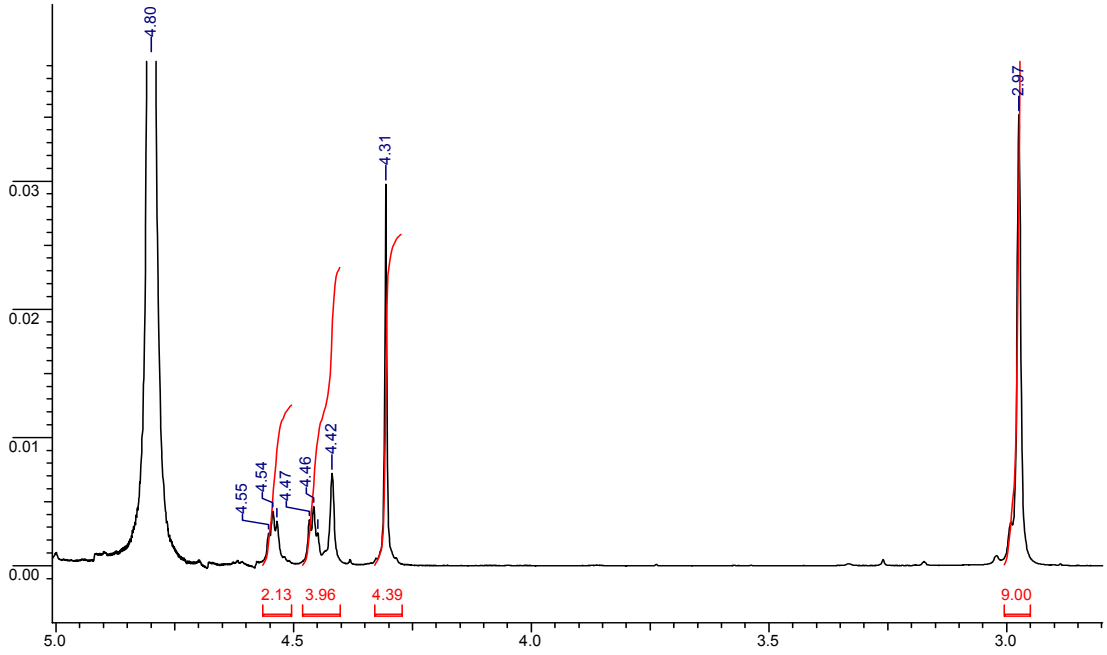

Fig. 4.1. ^{1}H NMR spectrum of ferrocenyl methyl trimethylammonium iodide in D_2O.

4.4.A.b. FTIR Spectroscopy

FTIR spectrum gives very good supporting evidence for the functional groups present in the compound (details under section 2.5.2.). The spectral details were given in brief and peak assignments are given in Table 4.1.

FTIR (KBr): υ_{max} 2936 cm^{-1} (N–CH_3), 1471 cm^{-1} (–CH_2) and 1102, 992, 820, 490 cm^{-1} (Fc).

Table 4.1. The characteristic peak assignment of FTIR spectrum of compound **I**

υ_{max} (cm^{-1})	**Peak assignments**
3042	C-H stretching of cyclopentadienyl ring
2936	Aliphatic $–NCH_3$
1472	$–CH_2$ deformation
1405	C-C stretching of cyclopentadienyl ring
1381	$-CH_3$ or $-CH_2$ deformation
1245	C-N stretching
1104	Characteristic of a bis(π–cyclopentadienyl) metal compound with an unsubstituted ring (C–C stretching)
992	–CH in plane deformation of cyclopentadienyl ring
880	$–CH_2–N–CH_3$
820	Out of plane –CH deformation of cyclopentadienyl ring
490	Characteristic of ferrocene antisymmetric ring metal stretching vibration.

The FTIR spectrum of compound **I** is shown in Fig. 4.2.

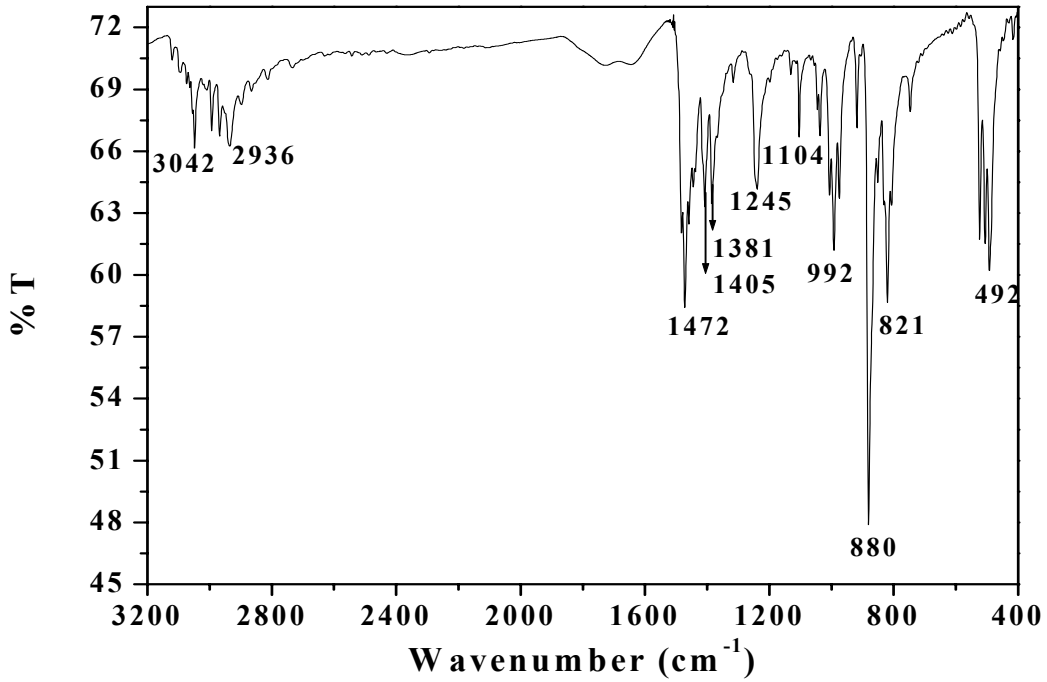

Fig. 4.2. FTIR spectrum of ferrocenyl methyl trimethylammonium iodide (KBr).

4.4.A.c. UV-Vis. Spectroscopy

UV-Vis. spectroscopy (see section under 2.5.1.) was recorded by dissolving 1 mg of compound **I** in 5 ml DCM. UV-Vis. spectroscopy gives characteristic electronic excitations like *d-d* transition of metal ion Fe^{+2} and cyclopentadienyl ring of ferrocene present in the compound. It is observed only one broad peak at 435 nm region is assigned to the *d-d* transition of metal ion present. A week band observed at 340 nm region comes from cyclopentadienyl ring. The UV-Vis. spectrum is compared in Fig. 4.17.

4.4.A.d. Microanalysis

The percentage composition of elements calculated theoretically was in well agreement with the observed results. The results are given below:

Anal. Calcd for $C_{14}H_{20}NFeI$: C, 43.3; H, 5.4; N, 3.6; Fe, 14.4%. Found: C, 43.1; H, 5.3; N, 3.88; Fe 14.78%.

4.4.B. Electrochemical Incorporation of Compound I into Polypyrrole

Polypyrrole was deposited as thin films on gold coated inter-digited electrodes with PET backing substrate by electrochemical technique. The procedure followed was a standard reported one which has been described in number of papers [35]. Pyrrole monomer (0.1 M) was dissolved in acetonitrile to which 0.1 M tetrabutyl ammonium perchlorate (TBAP) was added. The working electrodes were gold coated substrates prepared by vacuum deposition, which were pretreated with to etch the surface and create binding sites for PPy using proprietary method [36, 37]. The two connecting leads were shorted so that the whole substrate acted as single working electrode. The counter electrode is platinum foil with SCE as reference electrode. The functionalisation of PPy was done with ferrocenyl derivative as follows: 20 mg compound **I** (1 mmol), which was synthesized by above procedure, was dissolved in the same electrolyte containing 0.1 M TBAP, and 0.1 M pyrrole and films were deposited by chrono-amperometric method at a potential of 0.9 V for 5 min. These films were rinsed, dried and used for the detection of CO gas directly.

Potentiodynamic growth of PPy (2 mmol) and PPy doped with compound **I** (1 mmol) in acetonitrile containing 0.1 M TBAP as supporting electrolyte at a scan rate of 50 mV s^{-1}

between +1 V to -1 V is shown in Figures 4.3. and 4.4. respectively. The cyclic voltammograms obtained during potentiodynamic growth, display the expected increase in current with increasing number of potential cycles, which is consistent with electrochemically polymerized conducting polymers [41, 42]. After the completion of deposition, the films were rinsed and then studied by cyclic voltammetry in 0.1 M TBAP containing acetonitirle. The typical cyclic voltammograms obtained for PPy alone and PPy doped with ferrocenyl methyl trimethylammonium iodide films on Pt electrodes are compared in Figures 4.5. and 4.6., respectively. It is evident that PPy shows the characteristic oxidation and reduction peaks at 200 mV and 50 mV, which have been reported by number of authors in the past [43, 44]. On the otherhand, PPy doped with compound **I** reveals an additional peak in the cyclic voltammogram occurring at 900 mV with corresponding reduction at 230 mV, which can be associated with the redox behavior of ferrocene moieties present in it. These peaks are also observed in the CVs recorded during deposition of the films when the ferrocene derivative is added to the electrolyte. PPy alone exhibits the doping and dedoping behavior with ClO_4^- as the dopant but the compound **I** doped PPy gives additional peaks corresponding to the redox behavior of ferrocene. In Fig. 4.6. A and B corresponds to polypyrrole oxidation and reduction peaks and C and D corresponds to ferrocenyl moieties. Thus, not only the presence of the co-dopant in PPy film but also its activity in the electrochemical / external reactions gets confirmed from these observations.

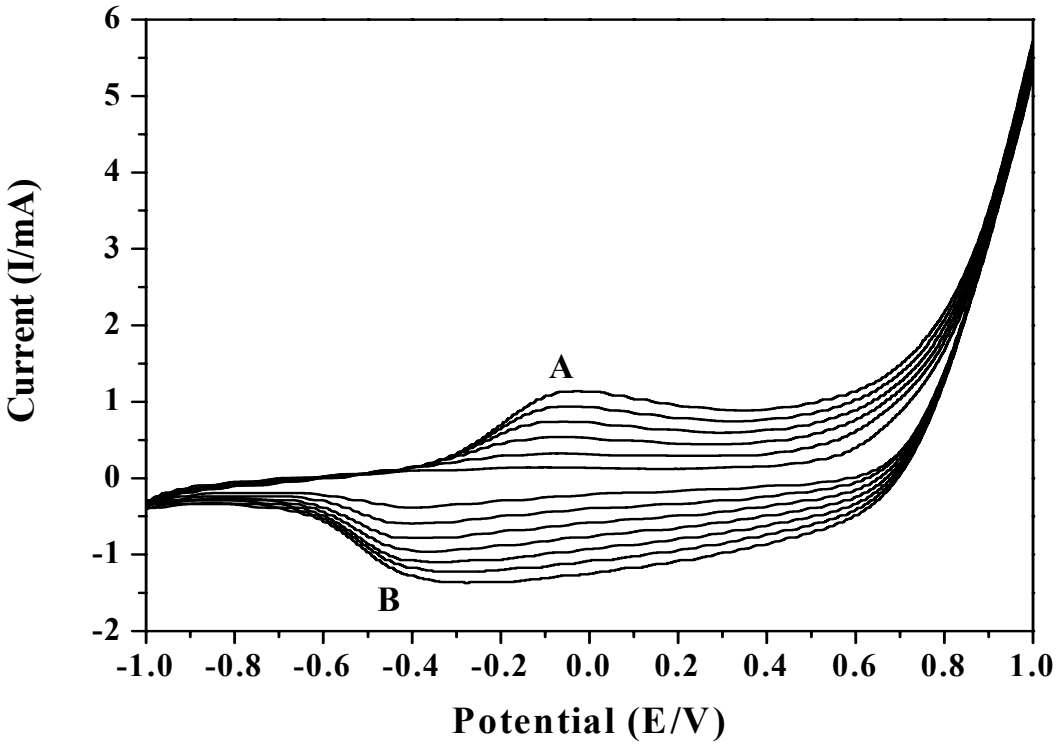

Fig. 4.3. Potentiodynamic curves for pyrrole polymerization in 0.1 M TBAP dissolved in acetonitrile. Scan rate: 50 mV/s.

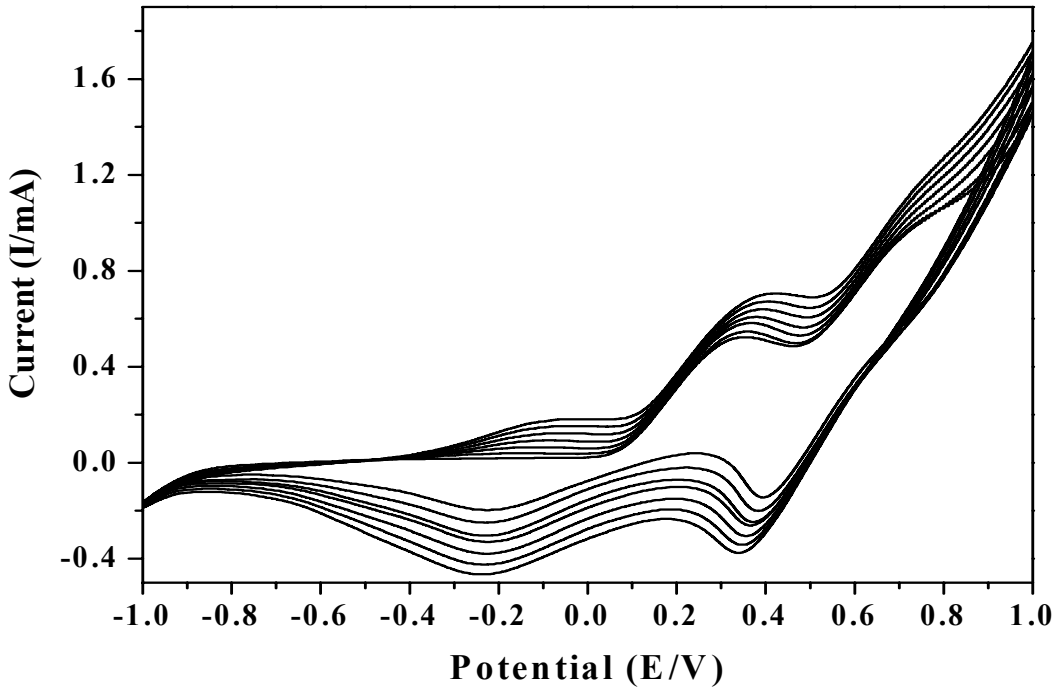

Fig. 4.4. Potentiodynamic curves for pyrrole polymerization in 0.1 M TBAP dissolved in acetonitrile with the addition of 2 mmol compound **I** derivative in the electrolyte. Scan rate: 50 mV/s.

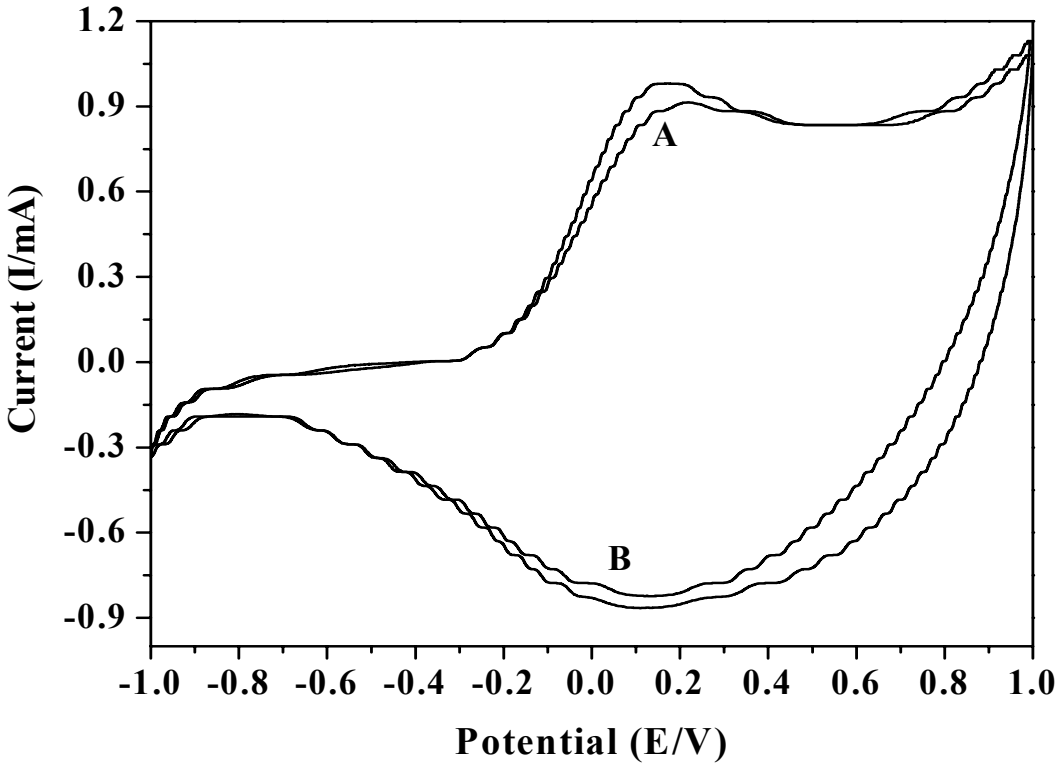

Fig. 4.5. Cyclic voltammograms of the polypyrrole film alone in 0.1 M TBAP electrolyte in acetonitrile. Scan rate: 50 mV/s.

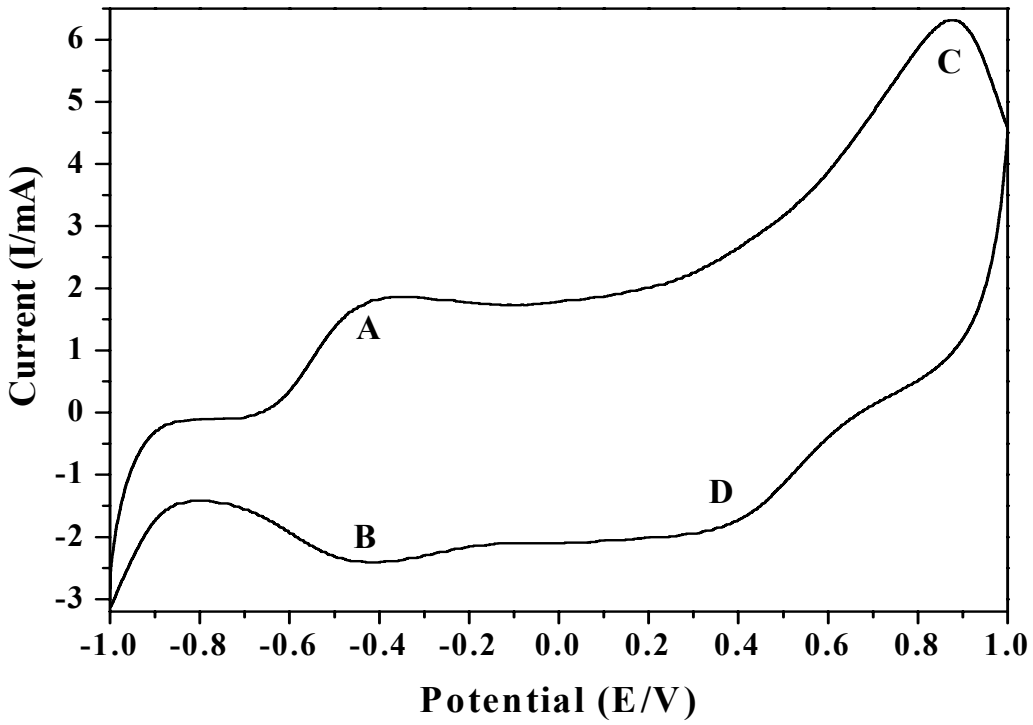

Fig. 4.6. Cyclic voltammograms of the polypyrrole film doped with Ferrocene-iodide derivative in 1 M $NaNO_3$ electrolyte in DI water. Scan rate: 50 mV/s.

4.4.C. Carbon Monoxide Gas Sensitivity Measurements

The surface cells prepared with PPy films containing various levels of compound **I** as co-dopant were tested for their sensitivity to 300 ppm carbon monoxide gas. Fig. 4.7. shows the response curve obtained in these cases.

It is clear from Fig. 4.7. that PPy deposited electrochemically with ClO_4^- as dopant alone is not at all sensitive to carbon monoxide gas, where as when ferrocene derivative is incorporated in PPy, there is a sudden increase of resistance observed immediately after exposure to CO gas. Further, the change in sample resistance at constant CO level depends on the concentration of the co-dopant present in PPy. The response factor [$(\Delta R / R_0)$ X 100] for these electrochemically deposited films of PPy with compound **I** is seen to depend critically on the co-dopant concentration. It is found to be highest (12%) for PPy films with 4 mol% of the dopant while it is practically 0.0 for PPy alone. The response factor (%) vs. composition plot is shown in Fig. 4.8. The initial resistance offered by the electrochemically deposited PPy films containing ferrocenyl derivative of concentrations 1, 4 and 10 mol% is 7.85, 9.2 and 17.3 Ω respectively.

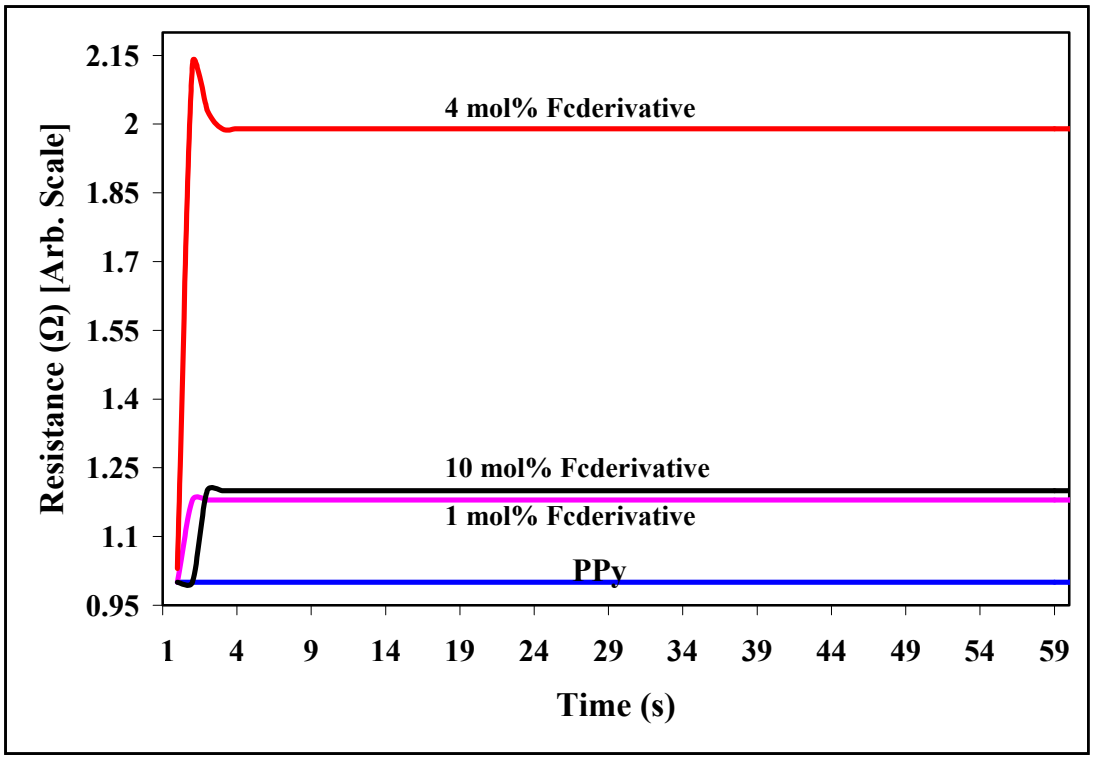

Fig. 4.7. Response curves for the surface cell containing PPy films doped with different concentrations of ferrocenyl derivative, compound **I** exposed to 300 ppm CO.

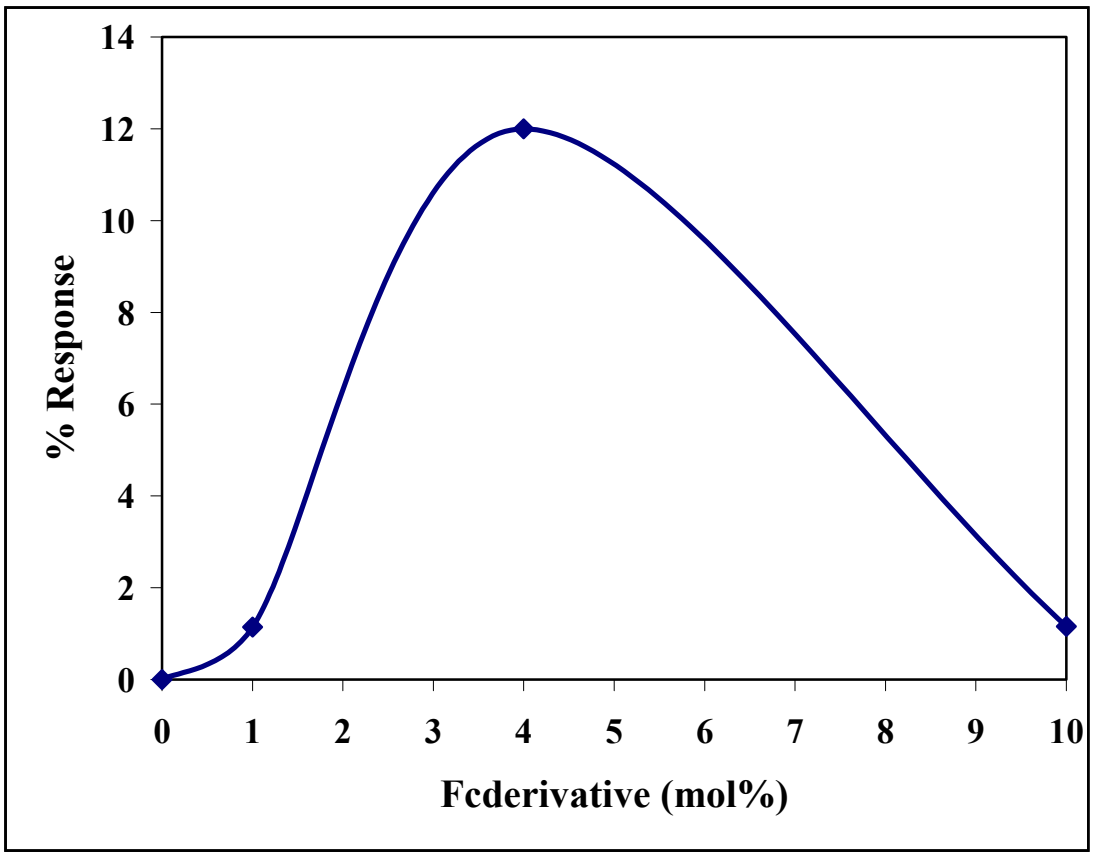

Fig. 4.8. Response factor with respect to composition of PPy containing compound **I** exposed to 300 ppm carbon monoxide.

The speed of response determined from the t_{50} value is quite low (0.43 s) in composition of 4 mol% compound **I** with PPy is presented in Fig. 4.9. This may be understood in terms of the number of available sites for interaction when the co-dopant is present with respect to the amount of CO that can be adsorbed by the PPy film. Since CO concentration has been maintained the same while testing all the films, there will be an optimum concentration of the compound **I** at which maximum change will be observed. For higher concentrations of the co-dopant, there will be excess of the material giving shielding effect and lower sensitivity. It is interesting to mention here that the sensing mechanism in the present case of modified PPy is quite different than that reported for polyaniline and its composites [45, 46] where CO interacts with the -NH groups to withdraw the lone pair electron and create a mobile positive charge / polaron giving rise to increase in conductivity (or decrease in resistance). On the other hand, decrease in

conductivity (increase of resistance) after exposure to CO gas, which depends on the concentration of ferrocene derivative. Hence, it is reasonable to state that in the present work, CO interaction with ferrocene is more dominating compared with its interaction with pyrrole moieties.

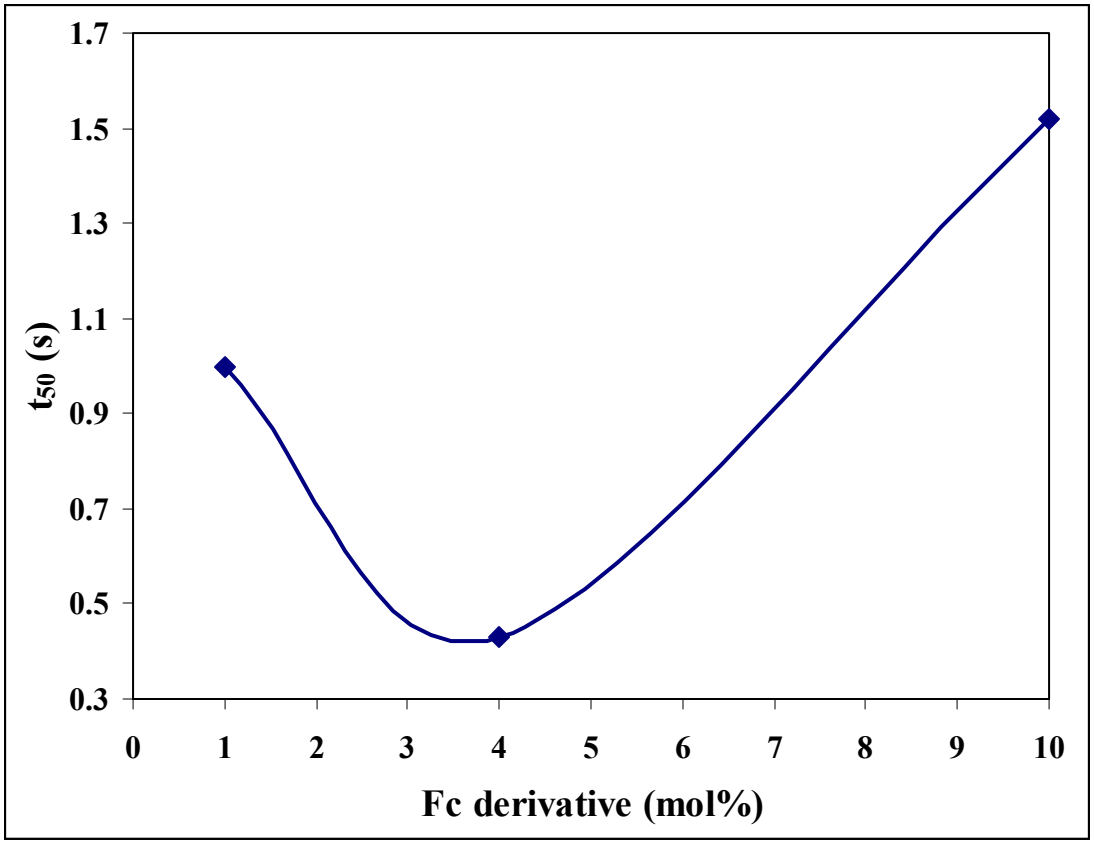

Fig. 4.9. Compositional dependence of response time (t_{50}) for PPy with compound **I** exposed to 300 ppm carbon monoxide.

The compositional dependence of change of resistance for the initial 3 minutes were also ploted (dR/dt) and found that 19.8 Ω/min. is the highest for 4 mol% concentration of compound **I** with PPy. It is shown in Fig. 4.10.

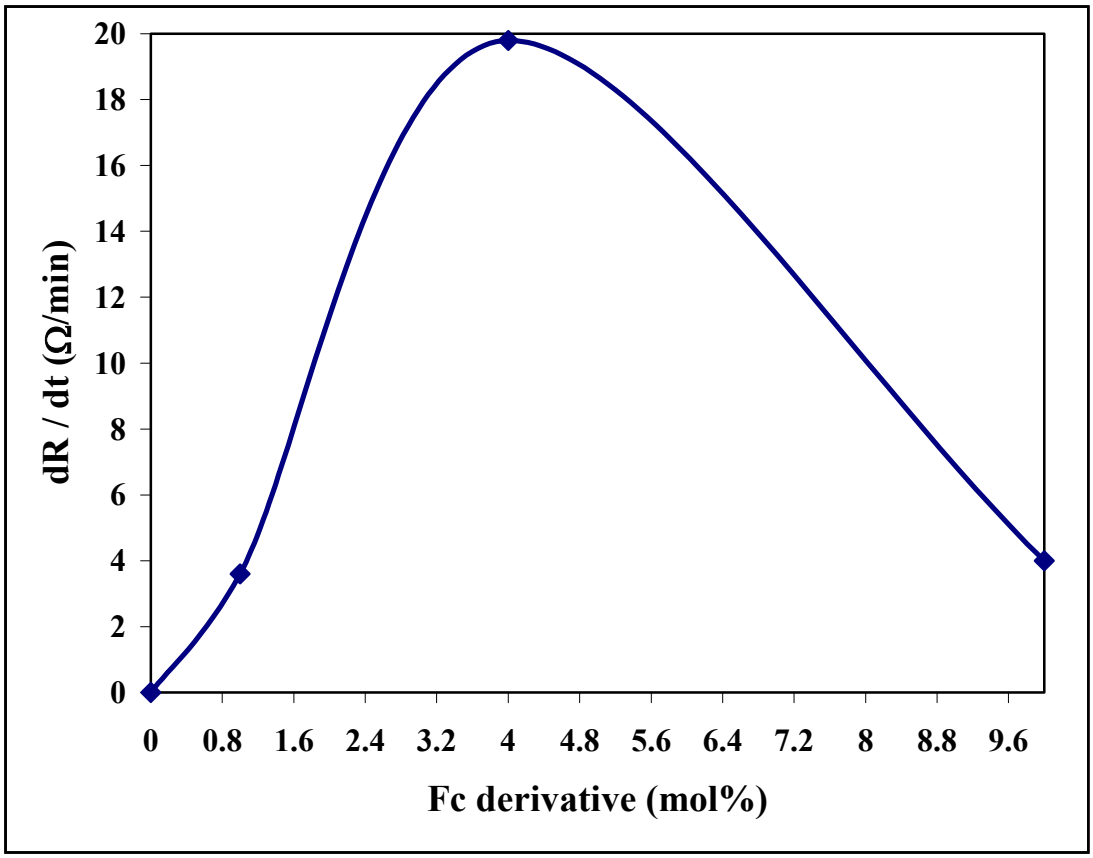

Fig. 4.10. Change of resistance for the initial 3 min. of the samples.

4.5. Ferrocenyl Derivatised Comonomer Synthesis

The comonomer synthesis was continued with the previous compound, ferrocenyl trimethylamino iodide. Ferrocenyl methyl triphenyl phosphonium iodide salt was synthesised by reacting **I** with triphenyl phosphine in ethanol for 16 h refluxion. The recrystallites from ethanol gives compound **II**. The synthesis of *trans*-1-ferrocenyl-2-(4-bromophenyl)ethylene (**III**) employs Witting olefination. It involves the reaction of compound **II** with n-BuLi/hexane in dry THF and then the addition of p-bromo benzaldehyde/dry THF reacted for 16 h at room temperature and finally purified by column chromatography gives deep reddish brown crystallites solid. The final product (**IV**) was synthesized using CuI catalysed reaction in the presence of *trans*-1,2-diammino cyclohexane as a ligand in 1,4-dioxane solvent. The column chromatography separates and purifies the compound in deep reddish brown crystals. The whole reaction steps are shown in Scheme 2.

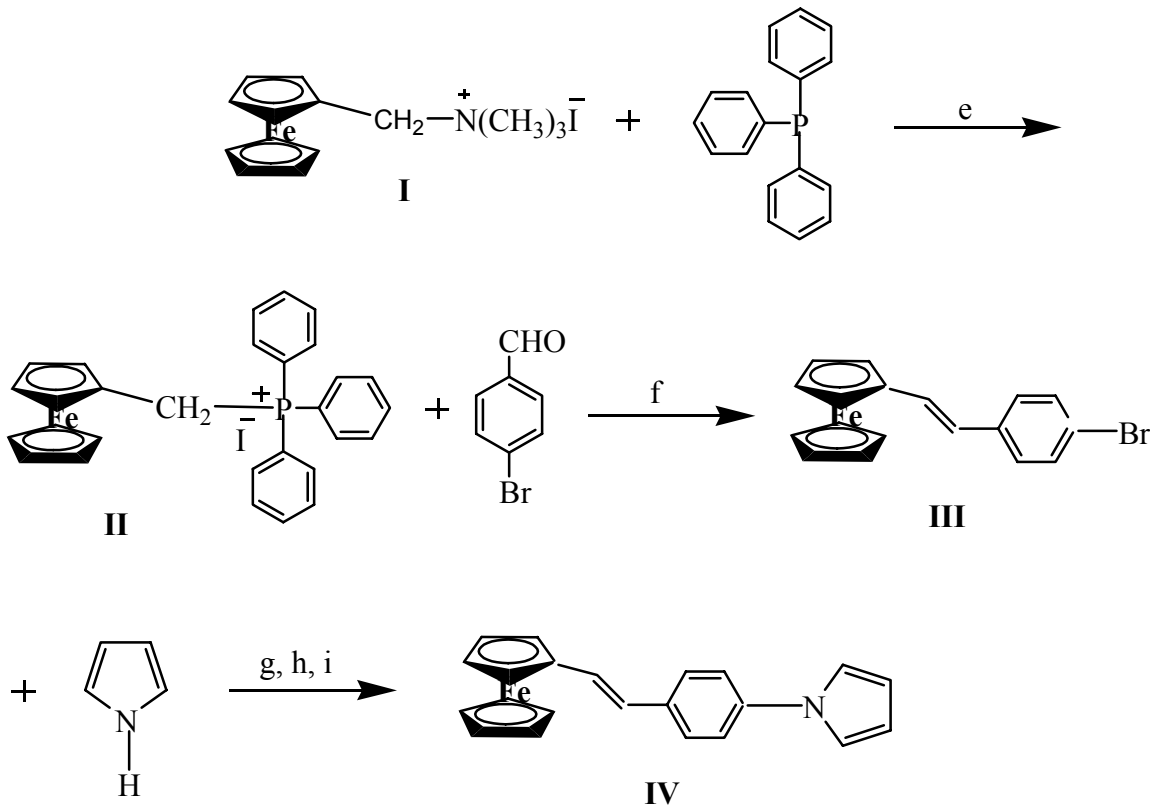

e = CH_3CH_2OH g = CuI, h = K_3PO_4

f = nBuLi/THF i = Dioxane

Scheme 2

4.5.A. Ferrocenyl Methyl Triphenyl Phosphonium Iodide

The following procedure is followed for the synthesis of ferrocenyl methyl triphenyl phosphonium iodide [29, 30].

10.25 g of compound **I** was taken in a 500 ml three necked RB flask along with 13.1 g triphenyl phosphine (TPP) and 300 ml dry ethanol was added into it. It was refluxed for 16 h and the clear solution obtained was allowed to cool and poured into 400 ml ether. The brown yellow ppt formed was filtered and washed thoroughly with ether. The crude compound was further decolorized by treating with charcoal in ethanol at refulx condition afforded 13 g of compound **II**, (83%), m.p. 231–235^{0}C (decomposed).

4.5.B. *trans*-1-ferrocenyl-2-(4-bromophenyl)ethylene

Synthesis of compound **IV** employs a Wittig olefination [31, 32] as follows:

A solution of 5.88 g (10 mmol) pure $FcCH_2P^+Ph_3I^-$ in 60 ml dry THF (explained in section 2.6.4.) was cooled to $^{-}78^0$C. 6 ml (10 mmol) n-BuLi/hexane was introduced drop by drop into the reaction system. It was stirred at 0^0C (ice bath) for 2 h. A solution of 1.85 g (10 mmol) *p*-BrPhCHO/in dry THF was added into the system drop by drop at 0^0C, and the resulting mixture was stirred in an ice bath for another 4 h and then at RT for 16 h. The reaction was quenched by the addition of 20 ml 20% aqu. HCl and then extracted the product with ethyl acetate. The ethyl acetate layer was washed with distilled water, followed by drying over anhydrous sodium sulfate. Pure trans isomer was separated by column chromatography (see section 2.8.2.) gave 2.8 g (76% yield) of pure **III** as a deep reddish brown crystalline solid: m.p. 195^0C.

4.5.C. *trans*-1-{4[2-(1-ferrocenyl) vinyl]phenyl}pyrrole

The reaction scheme explained a ligand assisted CuI catalysed C-N coupling reaction reported generally for N-heterocyclics and para substituted halogenated aromatics [33, 34]:

A 25 ml 2-necked flask was evacuated and back filled with nitrogen. 25 mg (0.02 mmol, 1 mol%) CuI was taken in a RB flask along with 850 mg (4.3 mmol) K_3PO_4, followed by 200 µl dodecane and 180 µl (2.6 mmol) pyrrole with stirring. Then 734 mg (2 mmol) compound **III** was added into it, followed by 30 µl (0.25 mmol, 12.5 mol%) *trans*-cyclohexane diammine and 4 ml dioxane. The reaction system was heated upto 110^0C using an oil bath. The reaction was allowed to take place for 30 h continuously and then cooled to ambient temperature, diluted with 5 ml ethyl acetate and filtered through a plug of silica gel. The compound was separated and purified by column chromatography gave 650 mg (92% yield) as deep reddish brown fine crystalline solid: m.p. 210–213^0C.

4.6. Copolymer Synthesis

The copolymer synthesis with pyrrole is explained under section 1.4. We have carried out the copolymerization reaction by both chemical as well as electrochemical route. These are explained in subsequent sections.

4.6.A. Chemical Copolymerization

The compound **IV** is having an easily oxidisable group, pyrrole, attached at the end of a ferrocenyl derivative. So, it is expected that this compound should be capable of forming copolymer with pyrrole in different proportions. The copolymer reaction procedure is as follows:

82.04 µl pyrrole (24 mmol) was added into 50 ml DCM solution containing 35.3 mg (2 mmol) *trans*-1-{4[2-(1-ferrocenyl)vinyl]phenyl}pyrrole (1 mol **IV**:12 mol pyrrole) monomer and stirred well. 150 mg (24 mmol) anhydrous $FeCl_3$ was added into it with continuous stirring. The interfacial co-polymer formed as a black precipitate with the addition of small amount of distilled water. It is observed that the color of the solution was turned from reddish brown to pale yellow after the reaction. 3.33 mol% and 1 mol% of comonomer (**IV**) is polymerized with pyrrole as above. Pure polypyrrole was also synthesized under the same route and keeping the same conditions.

4.6.B. Electrochemical Copolymerization

The electrochemical copolymerization of comonomer, compound **IV**, was carried out in dichloromethane DCM/TBAP system**.** The copolymer films were deposited on interdigited electrodes, which were previously activated with 1 M $FeCl_3$ solution for 24 h. Both potentiodynamic as well as chronoamperometry methods were used to deposit the conducting film on platinum electrode and interdigited electrode. A typical procedure adopted for the electrochemical copolymerization is as follows:

Electrochemical co-polymer synthesis was done by potentiodynamic method with an applied potential between $^{-}1$ V to $^{+}1$ V and chronoamperometry at 0.9 V. The reaction was carried out with 1 mmol compound **IV** and 30 mmol Py (1:30 mol ratio) in 0.1 M TBAP/DCM with Pt electrodes and standard calomel reference electrode system. The concentration of pyrrole is increased every time by keeping the same concentration of **IV** and electrolyte (1:50, 1:80 and 1:100 mol ratio of **IV** to pyrrole).

4.7. Results and Discussions

Results and discussions for chemically copolymerized samples were given under 4.7.A and electrochemically polymerized samples under 4.7.B.

4.7.A. Characterizations

The compounds obtained from each stages of the monomer synthesis from compound **I** to compound **IV** were well characterized using ^{1}H NMR, FTIR spectroscopy, UV-Vis. spectroscopy, elemental analysis, m.p. determinations etc. Additional characterizations like Single crystal XRD, DSC and TGA were also carried out for the novel comonomer **IV**. Each of the characterization techniques carried out for various compounds were described in detail.

4.7.A.a. Ferrocenyl Methyl Triphenyl Phosphonium Iodide

4.7.A.a.i. ^{1}H NMR Spectroscopy

The spectral detail of the compound is summarized below:

^{1}H NMR (DMSO–D_6) δ: 7.59–7.91 (m, 15H, Ar), 4.9 (d, 2H, CH_2), 4.24 (s, 5H, Cp), 4.1 (t, 2H, Cp), 3.87 (t, 2H, Cp).

The compound is soluble in DMSO-D_6 and the spectrum was recorded in 200 MHz instrument. A multiplet is observed at δ 7.59–7.91 is characteristic of aromatic region and this is due to three phenyl rings attached to phosphorous under the same chemical environment. Integration of the same gives fifteen hydrogens confirms the above statement. A prominent singlet peak at δ, 4.24 is the 5 H's of unsubstituted cyclopenta dienyl ring. The other two triplets obtained at δ, 4.1 and 3.87 shows two H's each indicating the substituted cyclopentadienyl ring. The ^{1}H NMR spectrum of compound **II** is given in Fig. 4.11.

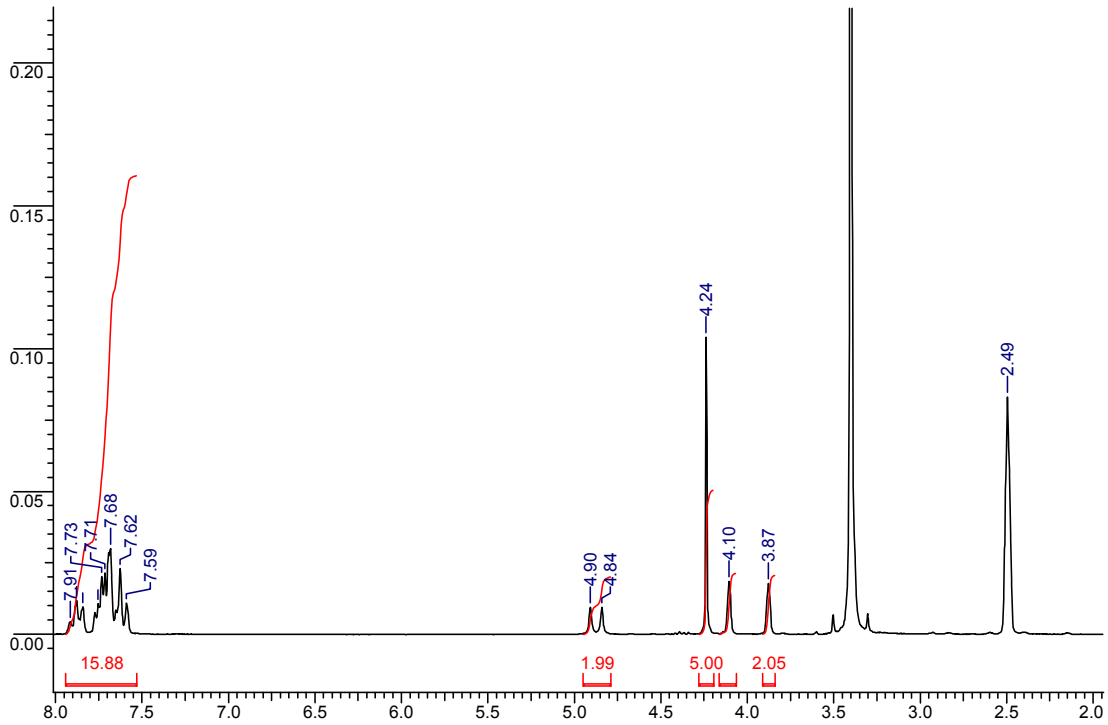

Fig. 4.11. ^{1}H NMR of ferrocenyl methyl triphenyl phosphonium iodide (DMSO-D_6).

4.7.A.a.ii. FTIR Spectroscopy

FTIR spectrum gives strong supporting evidence for the functional groups present in the compound. The spectral details are given in brief and peak assignments are given in Table 4.2. The FTIR spectrum of compound **II** is shown in Fig. 4.12.

FTIR (KBr): υ_{max} 3055 cm^{-1} (Ar-H), 2895 cm^{-1} (-CH_2), 1587 cm^{-1}, 1483 cm^{-1} (ArC=C), 1106 cm^{-1} (Fc), 1038 cm^{-1} (H-Ar), 996 cm^{-1} (Fc), 833 cm^{-1} (Fc), 749 cm^{-1} (mono sub. Ar), 692 cm^{-1} (Ar-H), 480 cm^{-1} (Fc).

Table 4.2. The characteristic peak assignment of FTIR spectrum of compound **II.**

υ_{max} (cm^{-1})	**Peak assignments**
3055, 3005	Aromatic hydrogen stretching frequency
2895, 2855	-CH stretching frequency from –CH_2 group
2361	Presence of phosphorous-carbon (P-phenyl)
1587, 1483, 1435	Aromatic –C=C– ring stretching frequencies
1106	Characteristic of a bis(π–cyclopentadienyl) metal compound with an unsubstituted ring (C–C stretching)

1038	–CH in plane bending frequency of aromatic ring.
996	–CH in plane deformation of cyclopentadienyl ring
833	Out of plane –CH deformation of cyclopentadienyl ring
749	Characteristic frequency of monosubstituted phenyl ring
692	Aromatic –CH out of plane vibration frequency
480	Characteristic of ferrocene antisymmetric ring metal stretching vibration.

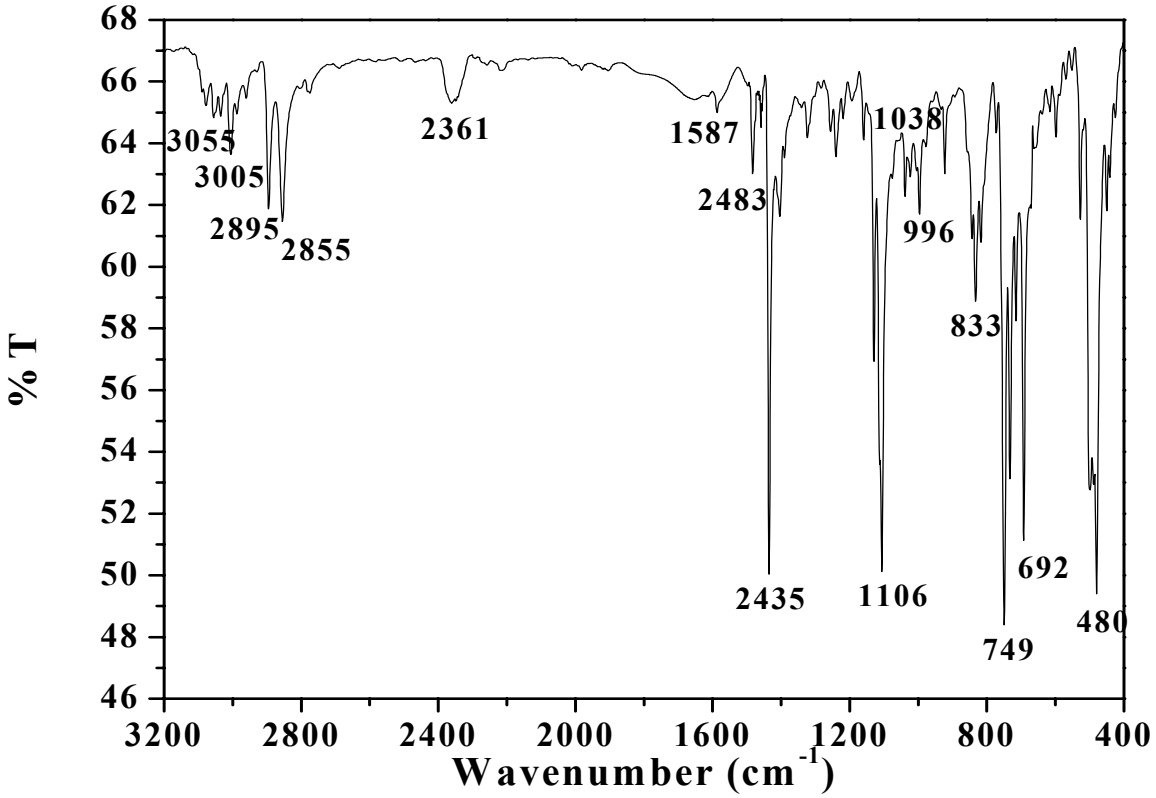

Fig. 4.12. FTIR spectrum of ferrocenylmethyltriphenylphosphonium iodide (KBr).

4.7.A.a.iii. UV-Vis. Spectroscopy

There are two λ_{max} is observed here, one prominent peak at 373 nm and another at 443 nm, which are attributed to the cyclopentadienyl ring and *d-d* transition of metal ion

respectively. Both these absorption bands are shifted to higher wavelength (red shift) side compared to compound **I**. The UV-Vis. spectrum is compared in Fig. 4.17.

4.7.A.a.iv. Microanalysis

The percentage composition of elements calculated theoretically was in well agreement with the observed results. The results were given below:

Anal. calcd for $C_{29}H_{26}PFeI$: C, 59; H, 4.4; Fe, 9.5%. Found: C, 58.71; H, 4.32; Fe, 9.31%.

4.7.A.b. *trans*-1-ferrocenyl-2-(4-bromophenyl)ethylene

4.7.A.b.i. ^{1}H NMR Spectroscopy

A brief description of ^{1}H NMR spectrum is given below:

^{1}H NMR ($CDCl_3$) δ: 7.45 (d, 2H, Ar), 7.3 (d, 2H, Ar), 6.91 (d, 2H, CH=), 6.66 (d, 2H, =CH), 4.45 (t, 2H, Cp), 4.3 (t, 2H, Cp), 4.14 (s, 5H, Cp).

The spectrum was recorded in 400 MHz instrument in $CDCl_3$ solvent. Two doublet peaks observed at δ, 7.45 and 7.3 in the aromatic region indicates these are due to phenyl protons of the identical chemical environments. Two more doublets were expected at δ, 6.91 and 6.66 is –CH=CH– protons. Triplets at δ, 4.45 and 4.3 attributed to the two hydrogens attached to the carbon at immediate vicinity of substituted carbon of one cyclopentadienyl ring and the other at next carbon respectively. Finally a prominent singlet peak at δ, 4.1 is the 5 H's of unsubstituted cyclopentadienyl ring. The ^{1}H NMR spectrum of compound **III** is shown in Fig. 4.13.

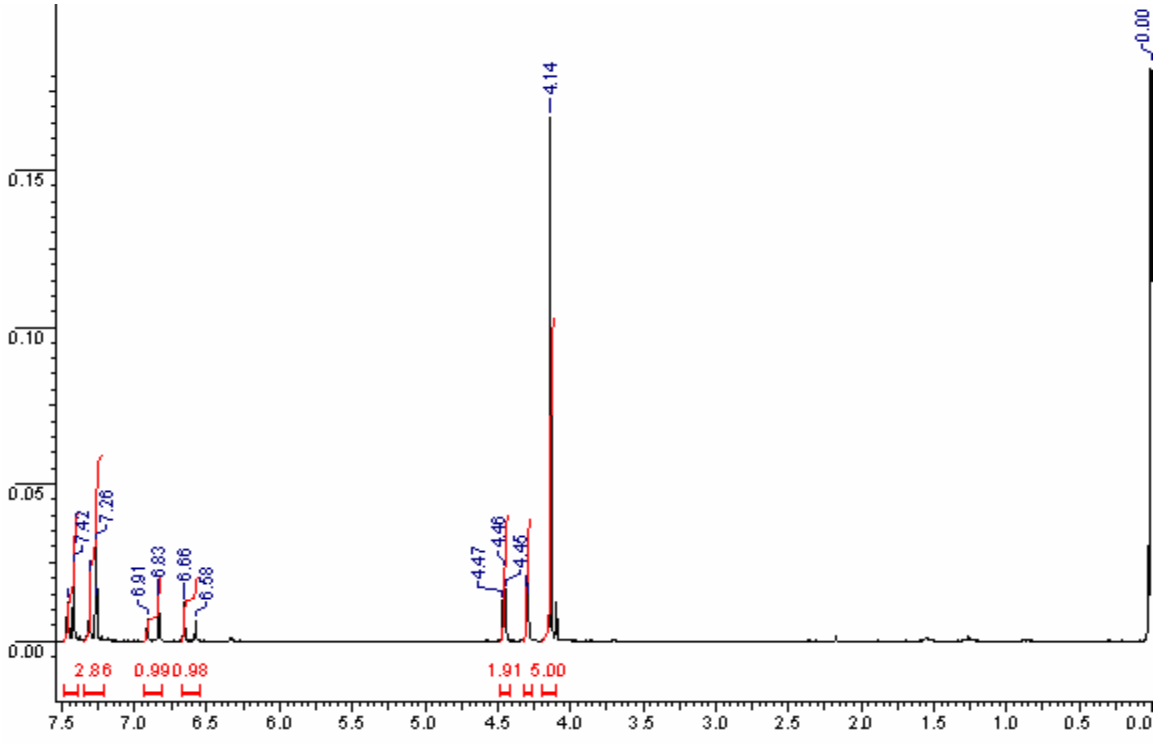

Fig. 4.13. ^{1}H NMR of *trans*-1-ferrocenyl-2-(4-bromophenyl)ethylene ($CDCl_3$).

4.7.A.b.ii. FTIR Spectroscopy

FTIR spectrum of compound **III** is a good evaluation for the functional groups of the compound. The peak assignments are given in Table 4.3. and The FTIR spectrum of compound **III** is shown in Fig. 4.14. A short conclusion of the spectrum is also given below:

FTIR (KBr): υ_{max} 3079 cm^{-1} (Ar-H), 1629 cm^{-1} (-C=C-), 1475 cm^{-1} (ArC=C), 1104 cm^{-1}, 1005 cm^{-1}, (Fc), 966 cm^{-1} (trans=C-H), 860 cm^{-1} (p-sub Ar), 810 cm^{-1} (Fc), 625 cm^{-1} (Ar-Br), 480 cm^{-1} (Fc).

Table 4.3. FTIR spectral data assignment of compound **III**

υ_{max} (cm^{-1})	Peak assignments
3079	Aromatic hydrogen stretching frequency
1629	Aryl substituted –C=C– out of plane blending
1475	Aromatic –C=C– ring stretching frequency
1104	Characteristic of a bis(π–cyclopentadienyl) metal compound

	with an unsubstituted ring (C–C stretching)
996	–CH in plane deformation of cyclopentadienyl ring
966	Trans-CH out of plane bending frequency
860	Aromatic 1,4-disubstitution (para) out of plane bending frequency
810	Out of plane –CH deformation of cyclopentadienyl ring
625	Aromatic bromine stretching frequency
480	Characteristic of ferrocene antisymmetric ring metal stretching vibration.

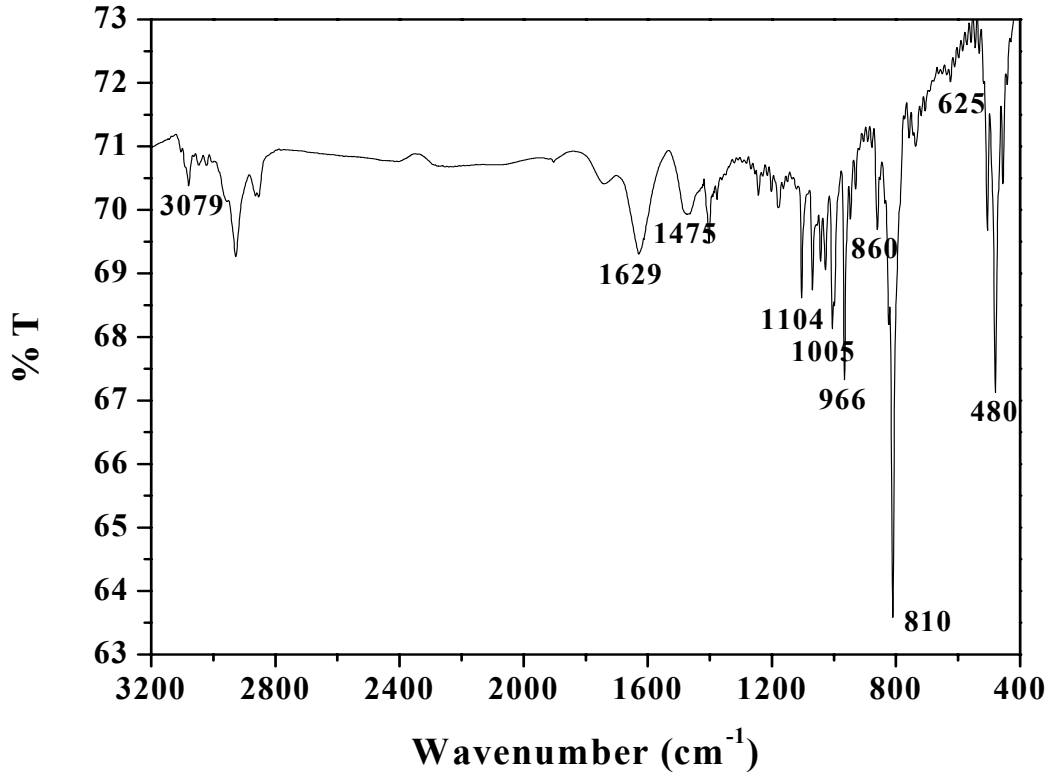

Fig. 4.14. FTIR spectrum of *trans*-1-ferrocenyl-2-(4-bromophenyl)ethylene (KBr).

4.7.A.b.iii. UV-Vis. Spectroscopy

The spectrum was recorded by dissolving 1 mg of compound **III** in 5 ml DCM is giving two λ_{max} at 385 nm and 460 nm region clearly indicating the *d-d* transition of Fe^{+2} metal ion and cyclopentadienyl ring of ferrocene. It is obvious that there is a shift in λ_{max} towards higher wavelength region (red shift as seen in the previous case) is an indication of increase of conjugation length. The UV-Vis. spectrum is compared in Fig. 4.17.

4.7.A.b.iv. Microanalysis

The C, H, N and Fe analysis gives good agreement in data between theoretical composition of elements in compound **III** and experimentally determined. The percentage composition calculated theoretically and experimentally is given below:

Anal. calcd for $C_{18}H_{15}FeBr$: C, 58.85; H, 4.1; Fe, 10.5%. Found: C, 58.6; H, 4.12; Fe, 10.21%.

4.7.A.b.v. Thermogravimetric Analysis

The TGA data gives the thermal stability of compound **III.** The onset of degradation is at 200^0C and then it degrades immediately. The percentage weight loss at 200^0C is 2.59, but at 300^0C is 70.23. The TGA data is compared in Fig. 4.18.

4.7.A.c. *trans*-1-{4[2-(1-ferrocenyl) vinyl]phenyl}pyrrole

4.7.A.c.i. ^{1}H NMR

The compound **IV** is not reported in the literature and so the spectral details are unknown. The spectrum recorded in 500 MHz instrument gives highly resolved and neat data of the expected compound in $CDCl_3$ solvent. The δ values of the compound **IV** are well interpretable and a short conclusion of the same is as follows:

^{1}H NMR ($CDCl_3$) δ: 7.46 (d, 2H, Ar), 7.33 (d, 2H, Ar), 7.1 (d, 2H, Py), 6.91 (d, 2H, CH=), 6.73 (d, 2H, =CH), 6.36 (d, 2H, Py), 4.47 (t, 2H, Cp), 4.30 (t, 2H, Cp), 4.15 (s, 5H, Cp).

There are six well resolved symmetrical doublet peaks observed for compound **IV**. The first two at δ, 7.46 and 7.33 are attributed to the identical protons in the aromatic phenyl ring. The N-substituted pyrrole is giving two doublets at δ, 7.1 and 6.36 is assigned to the two –CH groups near to heterocyclic nitrogen and the other for the protons next to it. Two more doublets were expected at δ, 6.91 and 6.73 is –CH=CH– protons. Two triplet peaks at δ, 4.47 and 4.3 are attributed to the two hydrogens attached to the carbon at immediate vicinity of substituted carbon of one cyclopentadienyl ring and the other at the hydrogens attached to the identical carbons next to it. Finally a prominent singlet peak at δ, 4.15 is the 5 H's of unsubstituted cyclopentadienyl ring. These spectral evidences

contribute to interpret the structure of the compound along with the help of other characterization tools. The ^{1}H NMR spectrum of **IV** is given in Fig. 4.15.

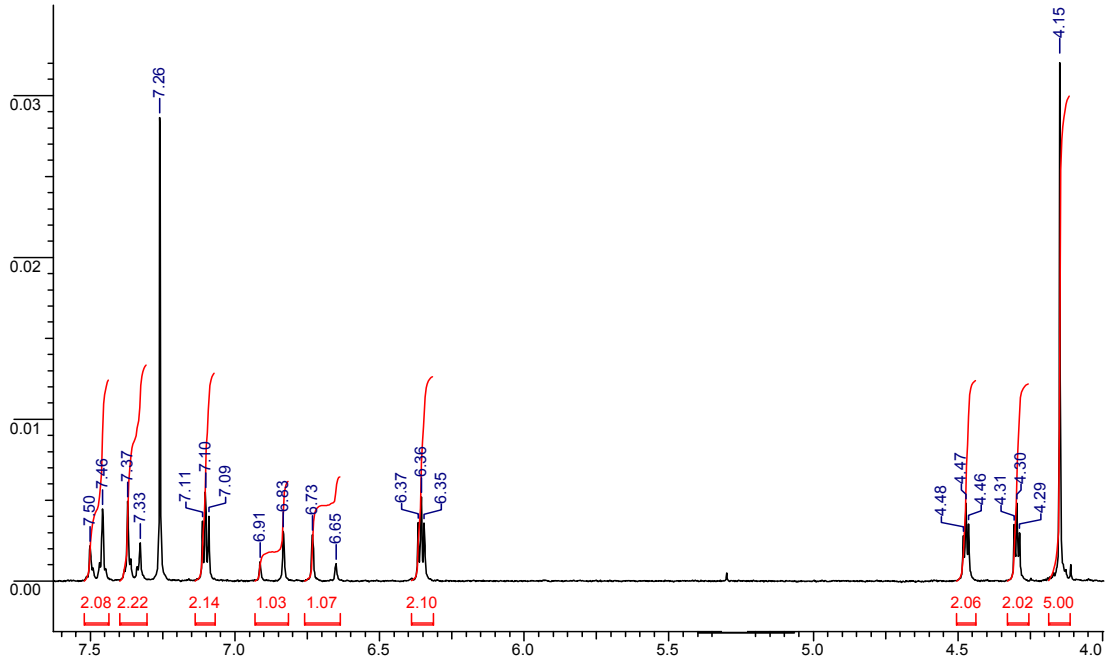

Fig. 4.15. ^{1}H NMR of *trans*-1-{4[2-(1-ferrocenyl) vinyl]phenyl}pyrrole ($CDCl_3$).

4.7.A.c.ii. FTIR Spectroscopy

FTIR spectroscopy was used for the structure elucidation of compound **IV** as a supporting characterization technique. The spectrum contributed the characteristic pyrrole vibrational frequencies, where pyrrole is attached to the previous compound (compound **III**). The spectral details with peak assignments are given in Table 4.4. FTIR spectrum of *trans*-1-{4[2-(1-ferrocenyl)vinyl]phenyl}pyrrole is shown in Fig. 4.16. A brief summary of peak evaluation as follows:

FTIR (KBr): υ_{max} 1630 cm^{-1} (–C=C–), 1527 cm^{-1} (Py), 1332 cm^{-1} (C-N), 1192 cm^{-1} (Py), 1104 cm^{-1} (Fc), 1047 cm^{-1} (Py), 1004 cm^{-1} (Fc), 960 cm^{-1} (trans =CH), 860 cm^{-1} (p-sub Ar), 814 cm^{-1} (Fc), 727 cm^{-1} (–HC=CH– of Py), 481 cm^{-1} (Fc).

Table 4.4. The FTIR spectral peak assignments of compound **IV.**

υ_{max} (cm^{-1})	**Peak assignments**
1630	Aryl substituted –C=C– out of plane bending frequency
1527	Belongs to pyrrole

1332	Aromatic –C–N– stretching frequency
1192	C-C stretch in pyrrole
1104	Characteristic of a bis(π–cyclopentadienyl) metal compound with an unsubstituted ring (C–C stretching)
1047	Assigned to pyrrole
1004	–CH in plane deformation of cyclopentadienyl ring
960	trans-CH out of plane bending frequency
860	Aromatic 1,4-disubstitution (para) out of plane bending frequency
814	Out of plane –CH deformation of cyclopentadienyl ring
727	-CH out of plane bending of aromatic or pyrrole ring
481	Characteristic of ferrocene antisymmetric ring metal stretching vibration.

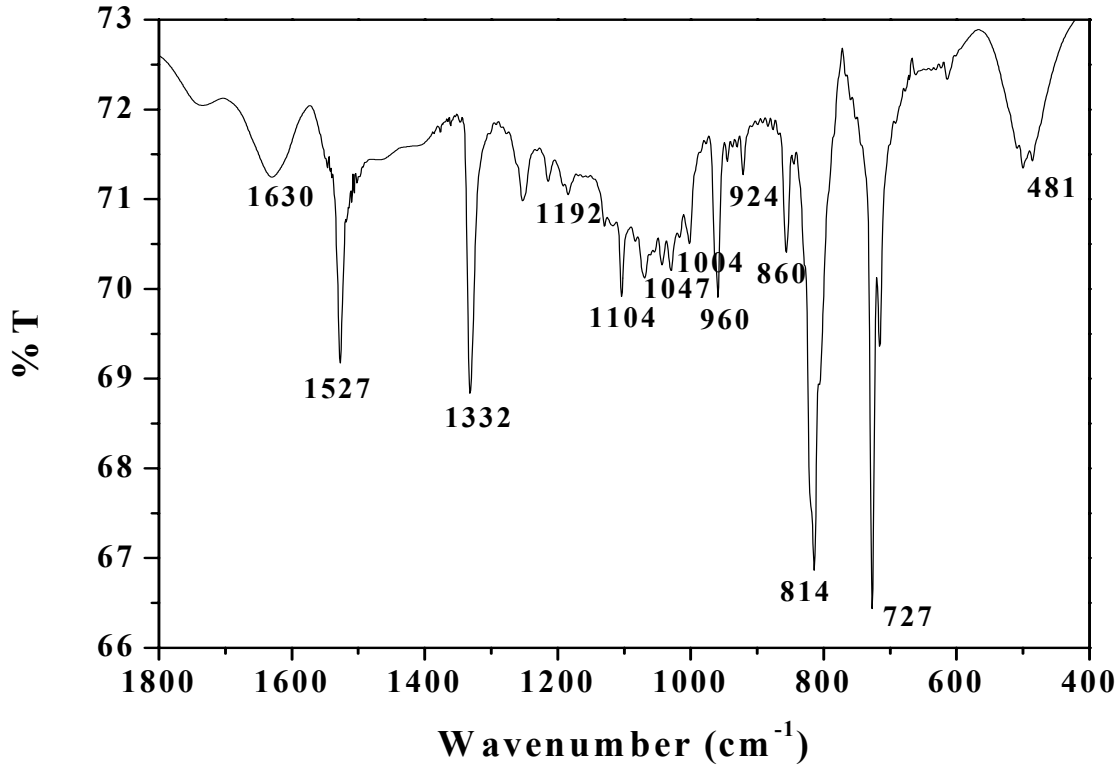

Fig. 4.16. FTIR spectrum of compound **IV.**

4.7.A.c.iii. UV-Vis. Spectroscopy

1 mg of compound **IV** was dissolved in 5 ml DCM and the spectrum was recorded. It is having two λ_{max} at 385 nm and 460 nm region clearly indicating the *d-d* transition of Fe^{+2} metal ion and cyclopentadienyl ring of ferrocene.

If we compare the spectra right from compound **I** to compound **IV**, the marked difference is the red shift in λ_{max}, prominence of cyclopentadienyl absorption band and increase of optical density. All these indicates that the conjugation length of the compound increases and subsequently the color of the compound intensifies with each step of synthesis and finally highest for compound **IV**. The UV-Vis. spectra of all compounds are done quantitatively and illustrated in Fig. 4.17. Solubilities of these compounds vary in DCM.

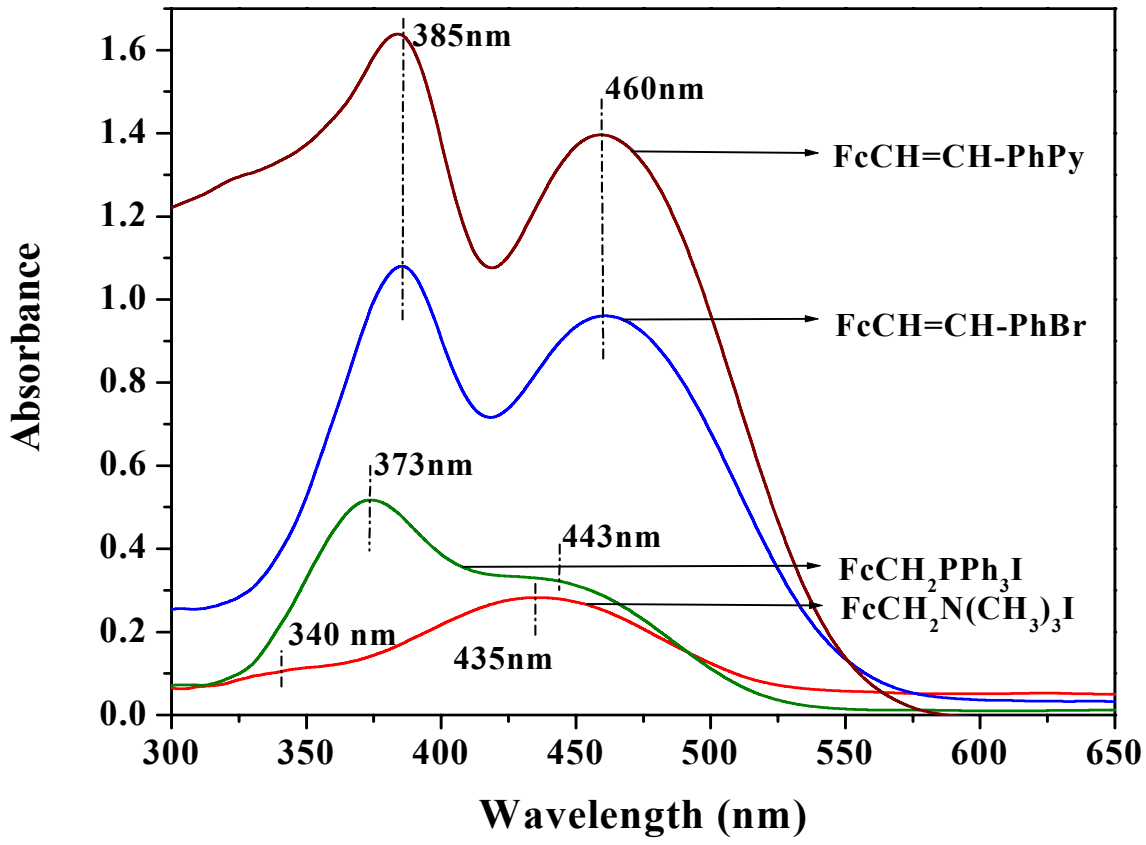

Fig. 4.17. Compiled UV-Vis. spectra of the multi stage synthesized compounds.

4.7.A.c.iv. Microanalysis

The percentage composition of elements (C, H, N and Fe) analysis data is well matched with the expected compound. Practically there is no difference between theoretically calculated % composition of elements and experimentally done results. The experimental results and analytically calculated results are shown below:

Anal. Calcd. for $C_{22}H_{19}FeN$: C, 74.78; H, 5.38; N, 3.96; Fe, 15.86%. Found: C, 74.6; H, 5.49; N, 4.0; Fe, 15.51%.

4.7.A.c.v. Thermogravimetric Analysis

The thermal stability of compound **IV** is obtained from TGA analysis. The onset of degradation is at 230^0C and then it degrades immediately. The percentage weight loss at 200^0C is 1.67, but at 300^0C is 35.61.

The percentage weight loss at 200^0C and 300^0C for compound **IV** is very less than compound **III** indicating the higher stability of compound **IV**. The TGA plots of compound **III** and compound **IV** is compared in Fig. 4.18.

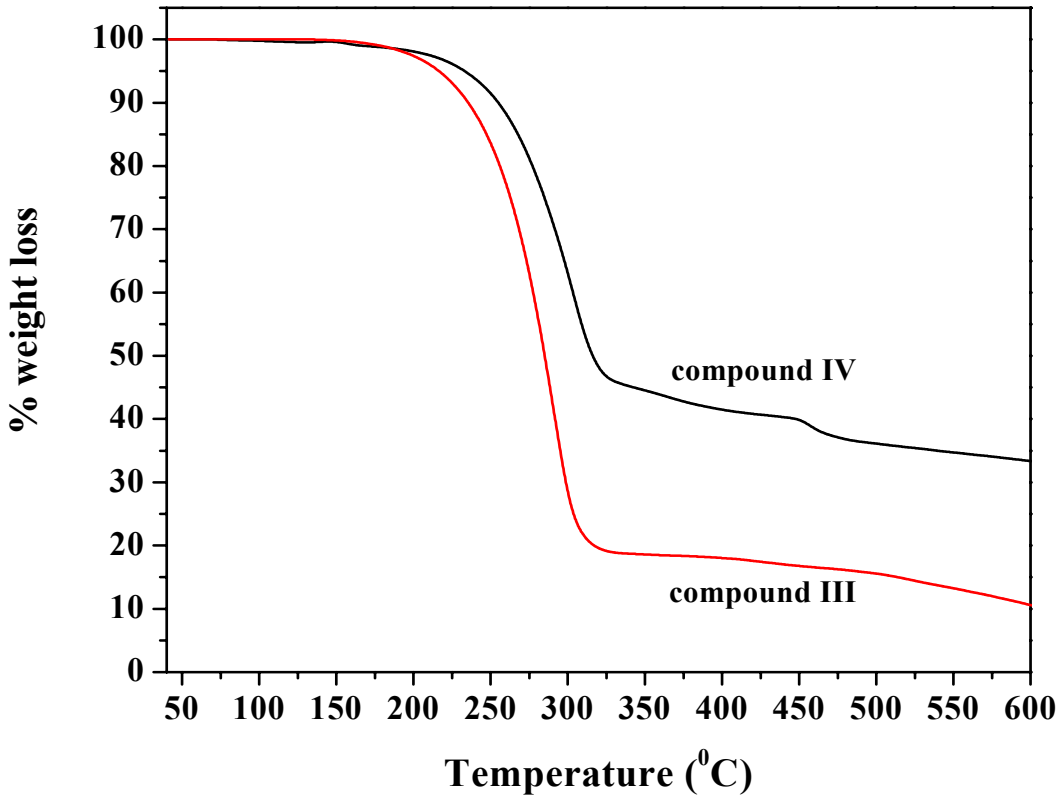

Fig. 4.18. TGA of compound **III** and compound **IV.**

4.7.A.c.vi. Differential Scanning Calorimetry

DSC of pure **IV** was carried out for one heating and cooling cycles between 50^0C to 220^0C at a heating rate of 10^0C per minute (see section 2.5.7.). Melting of the crystals starts at 210.28^0C and sharp melting (T_m) at 213.45^0C. The ΔH_m value is 75.92 J/g. Heat of crystallization is very sharp at 180.95^0C with ΔH_c value 87.25 J/g. the DSC of compound IV is shown in Fig. 4.19.

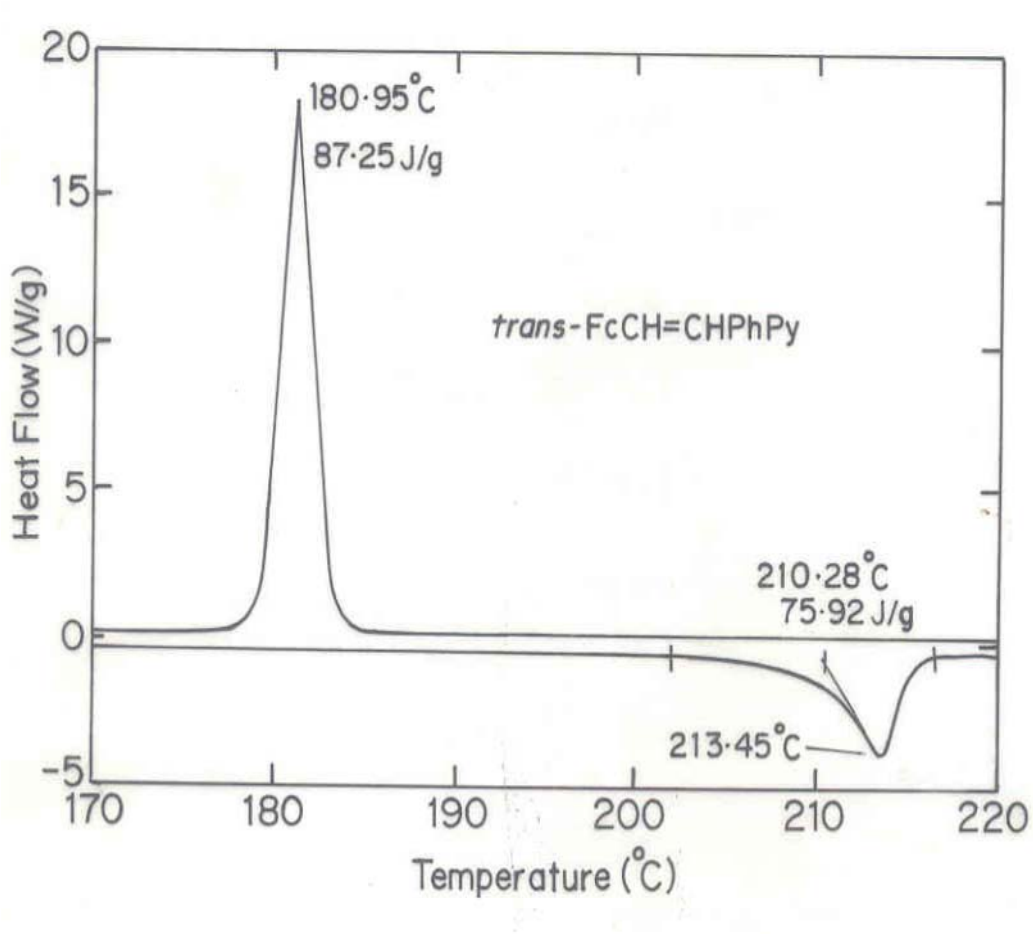

Fig. 4.19. DSC of compound **IV.**

4.7.A.c.vii. Transmission Electron Microscopy

TEM images of the pure crystals were taken to know the morphology, shape and orientation of tiny crystals. It is shown in Fig. 4.20.

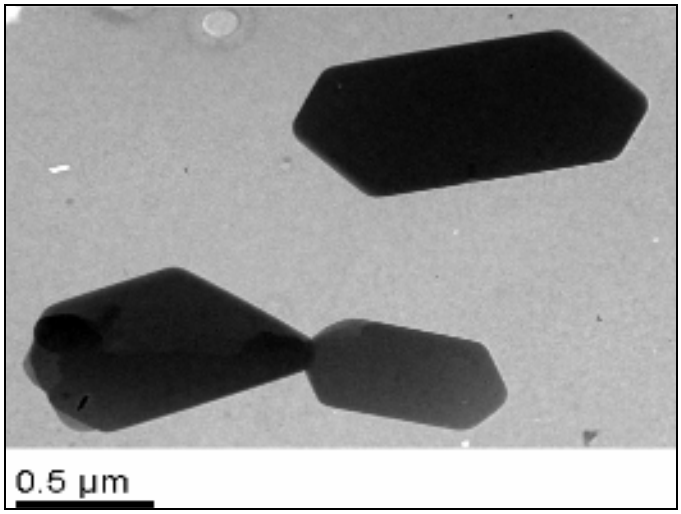

Fig. 4.20. TEM images of tiny crystals of compound **IV.**

4.7.A.c.viii. Single Crystal XRD

Single crystal of the compound **IV** gives the exact structure when it analysed with X-ray diffraction. From this technique, we came to know that the crystal belongs to monoclinic setting, its shape, size, space group, unit cell dimensions etc. are also available. The detailed descriptions from single crystal XRD is given in Table 4.5.

Table 4.5. Details of single crystal XRD data of compound **IV.**

Crystal data	
Chemical formula	$C_{22}H_{19}FeN$
Formula weight	353.23
Cell setting, space group	Monoclinic, *P*2(1)/*c*
Temperature (K)	293 (2)
Unit cell Dimensions	a = 7.5725 (6) Å; α = 90º b = 41.722 (3) Å; β = 90.407 (10) c = 10.6583 (8) Å; γ = 90º
Volume (Å^3)	3367.3 (4)
Z, Calculated density (Mg m^{-3})	8, 1.394
Radiation type	Mo *K*α
No. of reflections for cell parameters	4742
θ range (°)	2.47–23.85

Absorption coefficient (μ)	0.90 mm^{-1}
Crystal form, colour	Plate, deep red
Crystal size (mm)	0.48 × 0.20 × 0.05
Diffractometer	CCD Area Detector
Data collection method	ω and phi Scan
Absorption correction	Multi-scan (based on symmetry-related measurements)
Maximum and minimum transmission	0.673 and 0.957
Reflection collected / unique/ observed	24408, 5910, 4900
Goodness-of-fit on F^2	1.09
Final R indices [I >2σ(I)]	R1 = 0.044 wR2 = 0.101
Data / parameters	5910
No. of parameters	433
H-atom treatment	Constrained to parent site
Largest diff. Peak and hole (ρ_{max}, & ρ_{min})	0.30, –0.18 e $Å^{-3}$

The ORTEP diagram for the structure of compound **IV** obtained from single crystal XRD is given in Fig. 4.21.

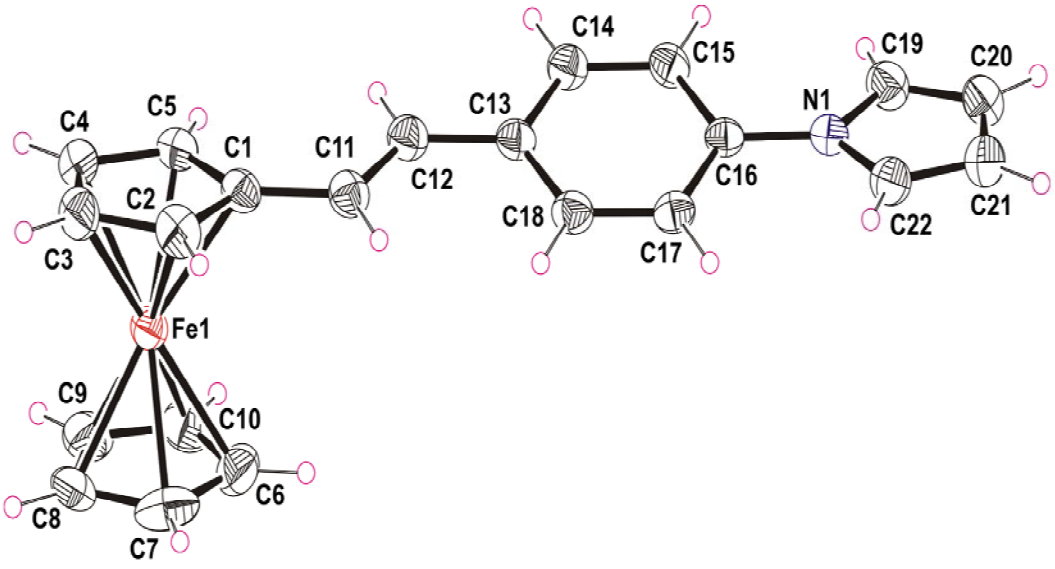

Fig. 4.21. ORTEP diagram of the structure of compound **IV** obtained from single crystal XRD.

4.7.B. Characterization of Chemically Synthesized Copolymer

4.7.B.a. UV-Vis. Spectroscopy

Online UV-Vis. spectra of the copolymer formation were carried out in a quartz UV cuvette as follows:

In the online spectroscopy measurement, the copolymerization reaction was continuously monitored at particular time intervals for 10 minutes. Dissolve 7 µl pyrrole in 10 ml DCM, 16 mg $FeCl_3$ in 10 ml DCM and 1.2 mg compound **IV** in 1 ml DCM separately. 600 µl each of the last two solutions were mixed thoroughly and the copolymerization reaction was monitored by recording the real time absorption spectra with the addition of 600 µl pyrrole solution into it. The copolymer formation starts with the addition of small amounts of water into it. The online UV-Vis. spectrum of copolymerization is shown in Fig. 4.22. The evolution of the absorption band at 750 nm associated with the bipolaronic band [38] indicated the formation of conducting copolymer of compound **IV**. The absorption band at 400 nm region is due to the oxidant ferric chloride present in the solution

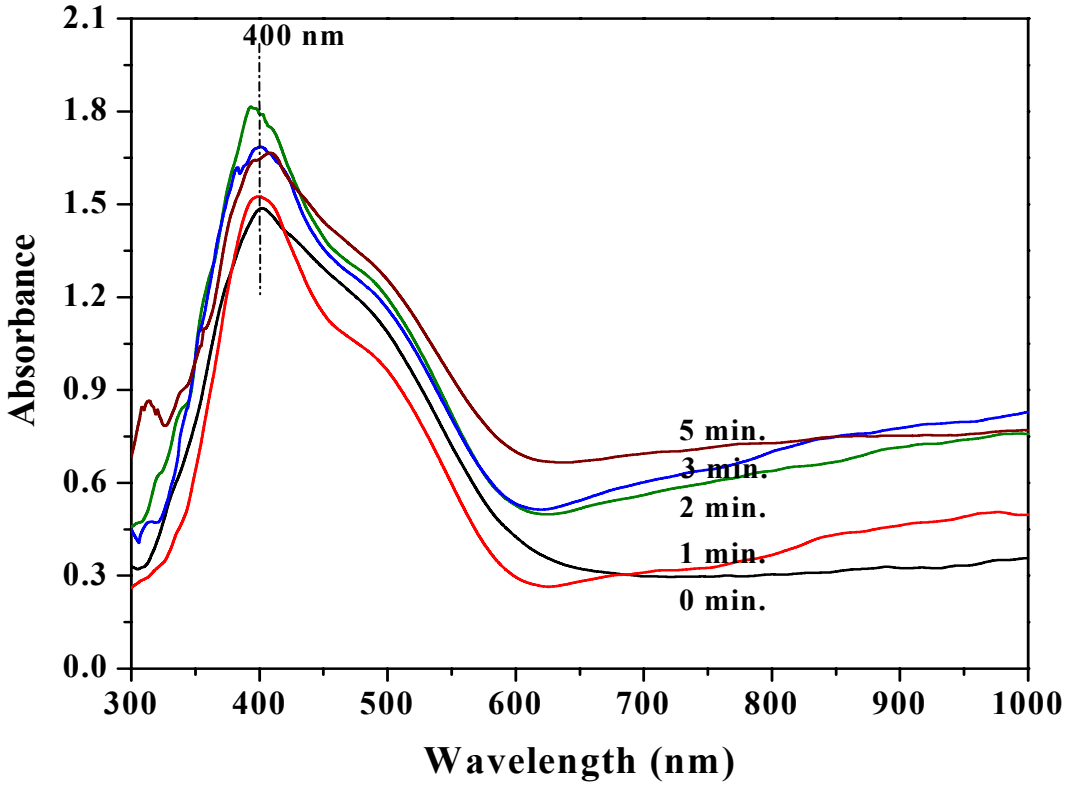

Fig. 4.22. The real time UV-Vis. spectra of copolymerization of compound **IV** and pyrrole.

It was estimated that the total amount of compound **IV** utilized for the formation of copolymer by UV-Vis. spectroscopy. The UV-Vis. spectrum of the reaction system before and after the completion of the reaction was recorded and analysed. The spectra were compared in Fig. 4.23.

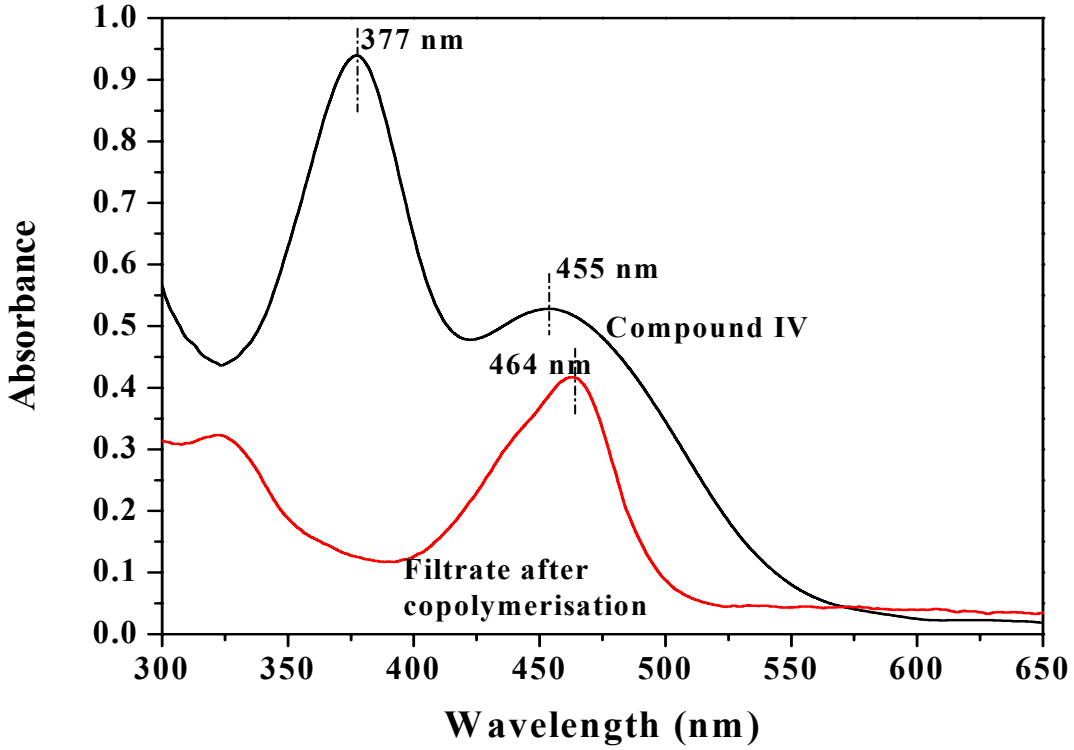

Fig. 4.23. UV-Vis. spectra of compound **IV** and filtrate after the copolymerization reaction.

The color of the system before starting the copolymerization reaction is dark reddish brown, which turned to pale yellow after the reaction. The absorption peaks obtained for pure compound **IV** is a *d-d* transition of iron at 377 nm and 455 nm of ferrocenyl conjugation, which vanishes after the completion of the reaction. An absorption peak at 464 nm is observed for the filtrate is due to the presence of some oligomeric pyrroles [39]. This spectral data clearly indicating the utilization of whole amount of compound **IV** for the formation of copolymer.

The UV-Vis. spectrum of the copolymer, compound **IV** and polypyrrole prepared by the interfacial copolymerisation is compared in Fig. 4.24. Quantitative amounts (1 mg) of the above materials were added into 5 ml NMP and sonicated for 2 h. The polymer solutions were then filtered and spectra were recorded.

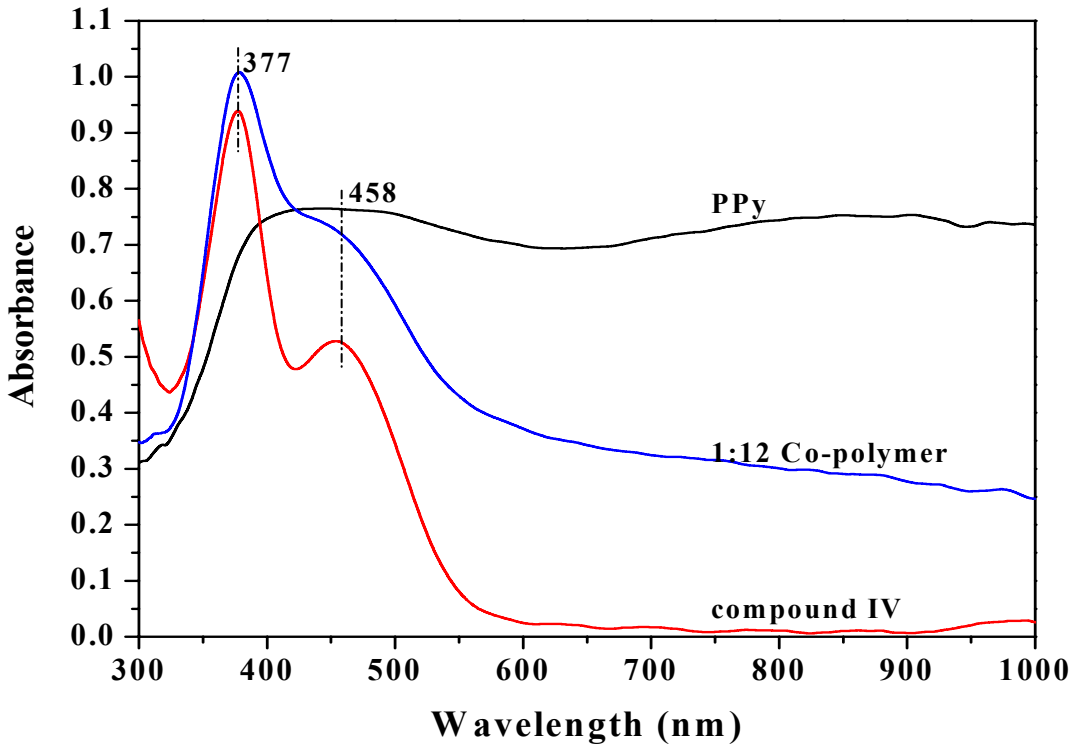

Fig. 4.24. Comparison of UV-Vis. spectra of copolymer, PPy and compound **IV** in NMP

4.7.B.b. FTIR Spectroscopy

FTIR spectra provide strong supporting evidence for the presence of compound **IV** and pyrrole. The spectral details with peak assignments were given in Table 4.6. FTIR spectrum of chemically synthesized copolymer is shown in Fig. 4.25.

υ_{max} (cm^{-1})	Peak assignments
1527	Belongs to polypyrrole C=C / C–C stretch
1332	Aromatic –C–N– stretching frequency
1104	Characteristic of a bis(π–cyclopentadienyl) metal compound with an unsubstituted ring (C–C stretching)
1041	Belongs to polypyrrole C–H in plane bend
1004	–CH in plane deformation of cyclopentadienyl ring
960	Trans-CH out of plane bending frequency
930	Polypyrrole peak C–H bend
860	Aromatic 1,4-disubstitution (para) out of plane bending frequency

814	Out of plane –CH deformation of cyclopentadienyl ring
796	Polypyrrole Ring deformation centered at β-carbon atom
727	Polypyrrole
480	Characteristic of ferrocene antisymmetric ring metal stretching vibration.

Table 4.6. FTIR spectrum of chemically synthesized copolymer.

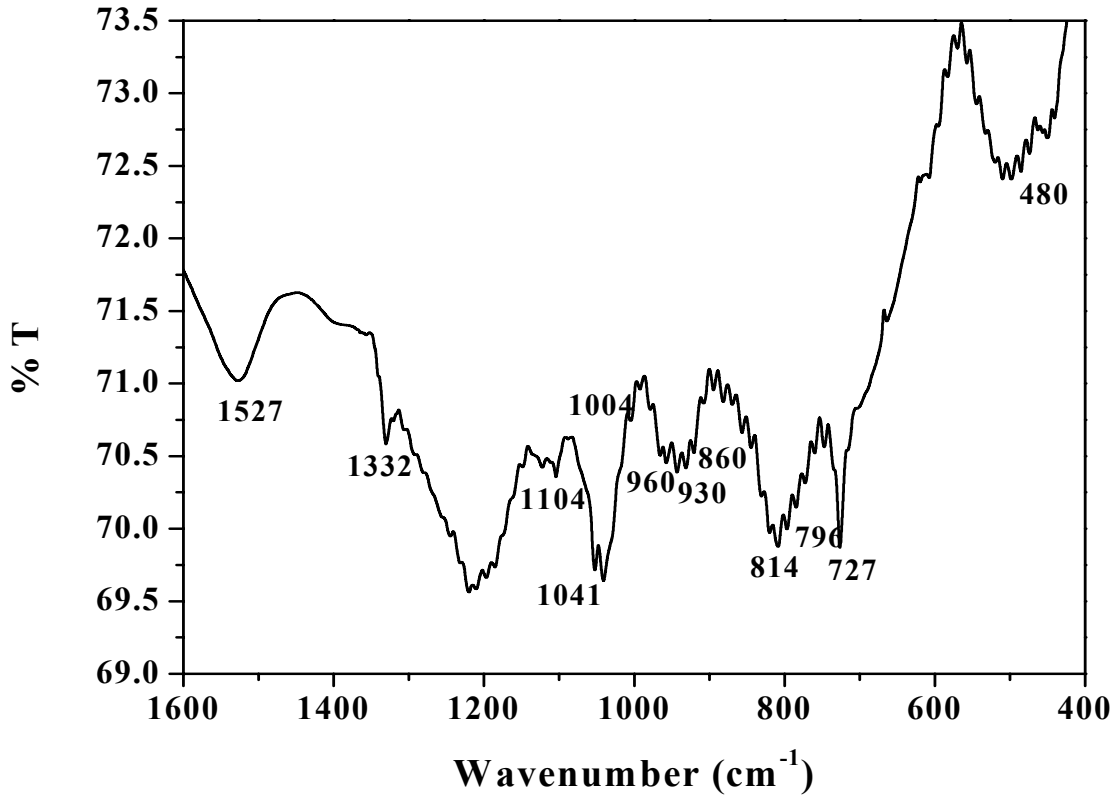

Fig. 4.25. FTIR spectrum (KBr) of copolymer.

4.7.B.c. Thermogravimetric Analysis

Thermal gravimetric pattern of copolymer, compound **IV** and PPy synthesized by interfacial polymerization technique in DCM/water solvent system is presented in Fig. 4.27. It is found that the thermal stability of PPy is improved with the presence of ferrocene derivative. The percentage weight loss before and after the major degradation

of **IV** calculated at 160^0C and 520^0C, the corresponding % weight loss calculated for copolymer and PPy is tabulated in Table 4.7. The expected weight loss and the experimentally obtained weight loss are in well agreement with each other. This indicates that the compound IV leaves PPy at this measured degradation temperature limits of ferrocenyl derivative.

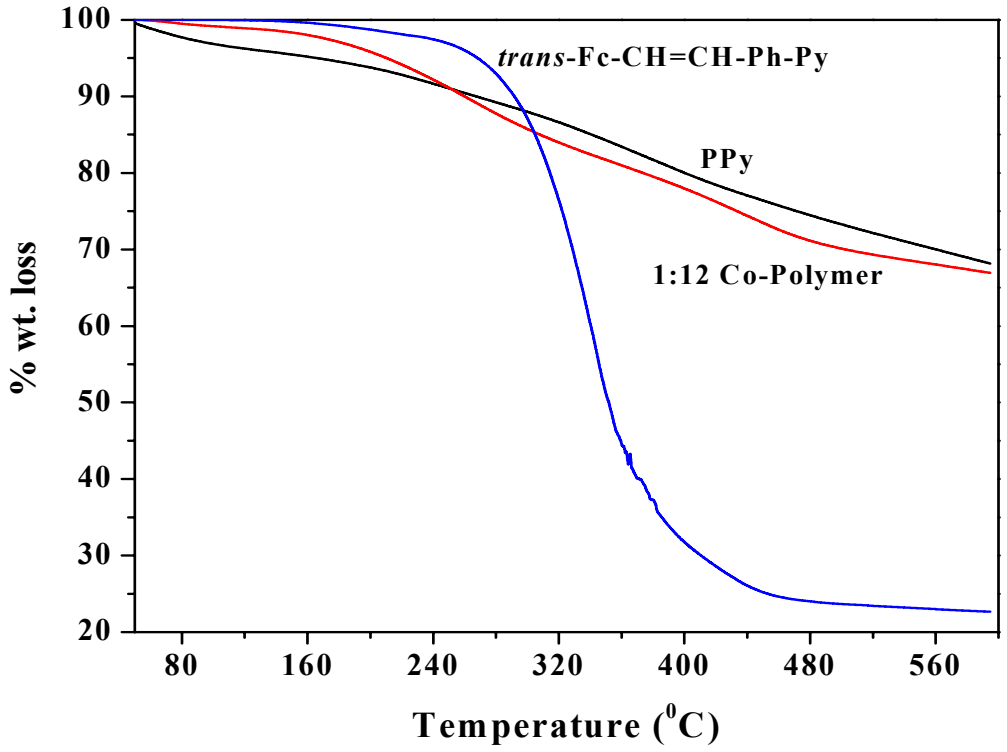

Fig. 4.26. Comparison of TGA of copolymer with polypyrrole and compound **IV.**

Material	% wt.loss at 160^0C	% wt. loss at 520^0C	Actual % weight loss	Expected % weight loss
Compound **IV**	0.42	76.69	76.27	76.27
Copolymer	2.17	29.86	27.69	27.595
Polypyrrole	4.78	27.93	23.15	23.15

Table 4.7. The % weight loss at degradation temperature of compound **IV**.

4.7.B.d. Differential Scanning Calorimetry

Figures 4.27.a, 4.27.b. and 4.27.c show the DSC of PPy prepared by interfacial copolymerization from DCM-water system, copolymer containing 1 and 8.33 mol% of ferrocenyl derivatised pyrrole respectively. DSC of copolymer of different compositions containing 8.33 and 1 mol% compound **IV** provides information of forming the copolymer. It is evident from the shift in T_g towards lower side with respect to increase in comonomer, **IV** concentration in the sample. The T_g of pure PPy prepared in DCM-water interfacial polymerization shifts from 134.6 to 54.01 and $^{-}10.18^{0}$C for copolymer containing 1 mol% and 8.33 mol% compound **IV**, respectively. This clearly indicates that the free volume increases with increasing concentration of compound **IV** in the copolymer. The clear shift in T_g with respect to compound **IV** in the material is an indication of the copolymer formation.

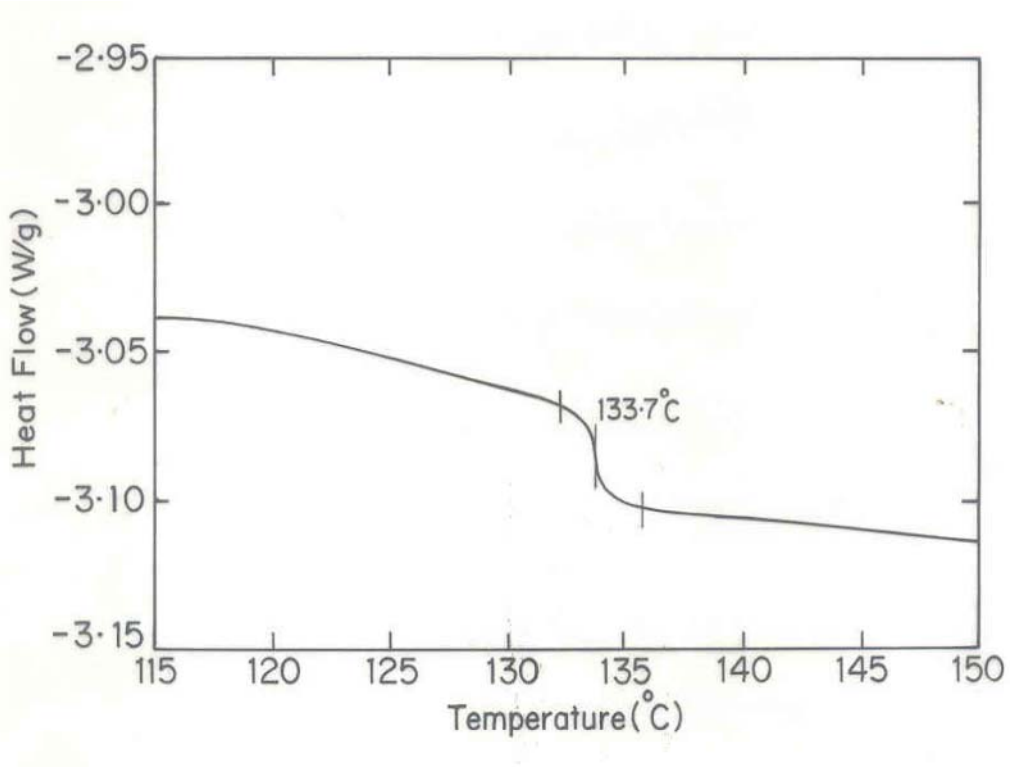

Fig. 4.27.a. DSC of PPy synthesized by interfacial polymerization (DCM-water system).

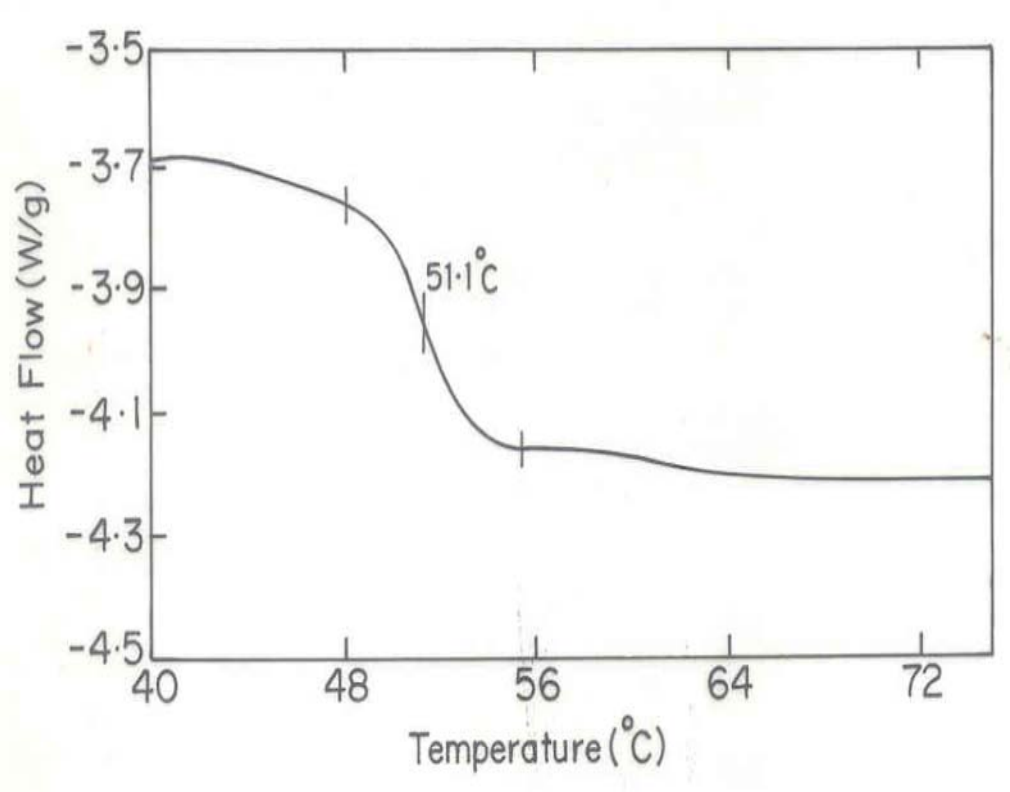

Fig. 4.27.b. DSC of copolymer containing 1 mol% ferrocenyl derivatised pyrrole.

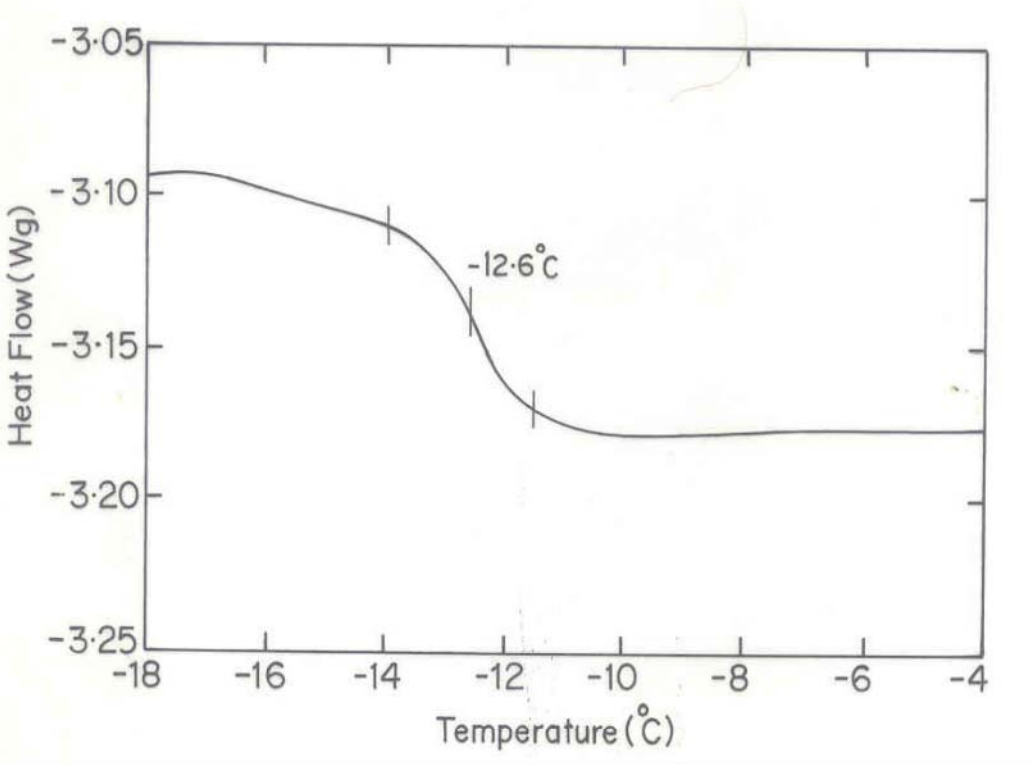

Fig. 4.27.c. DSC of copolymer containing 8.33 mol% ferrocenyl derivatised pyrrole.

All the above data conclude the probability of formation of a random copolymer of ferrocenyl derivatised pyrrole with pyrrole. The structure of random copolymer is expected to be as shown in Fig. 4.28.

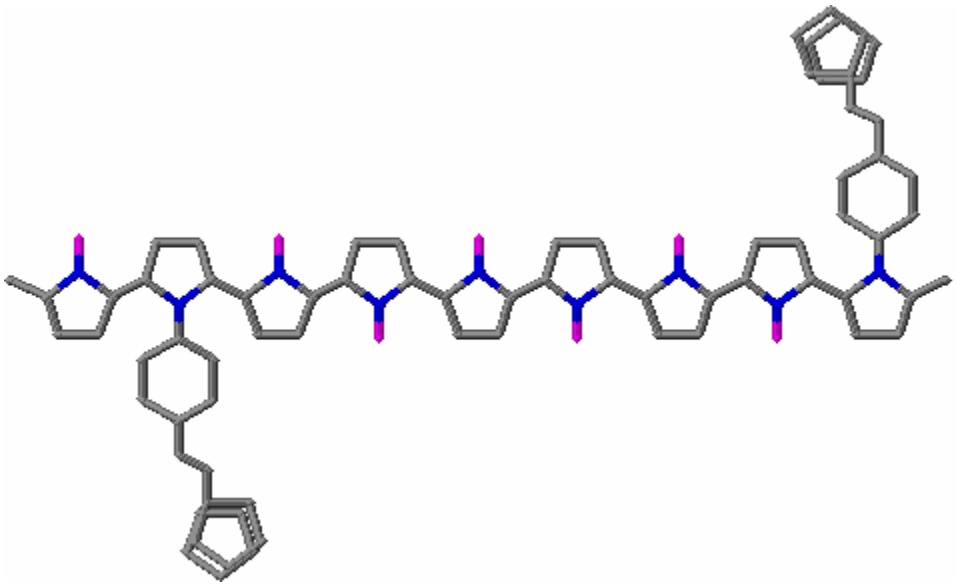

Fig. 4.28. Copolymer structure of compound **IV** with pyrrole.

4.7.C. CO Gas Sensitivity Measurements

The detailed experimental set up for CO gas sensitivity measurements is given under section 2.10.1.

The chemically copolymerised sample was used for the CO response experiments. It is observed that the highest change in resistance with 8.33 mol% of compound **IV** compared to other samples containing 3.33 mol% and 1 mol% compound **IV**. The resistance increased rapidly when the copolymer samples exposed to 300 ppm CO gas. Fig. 4.29. shows a typical response curve obtained for the copolymer samples.

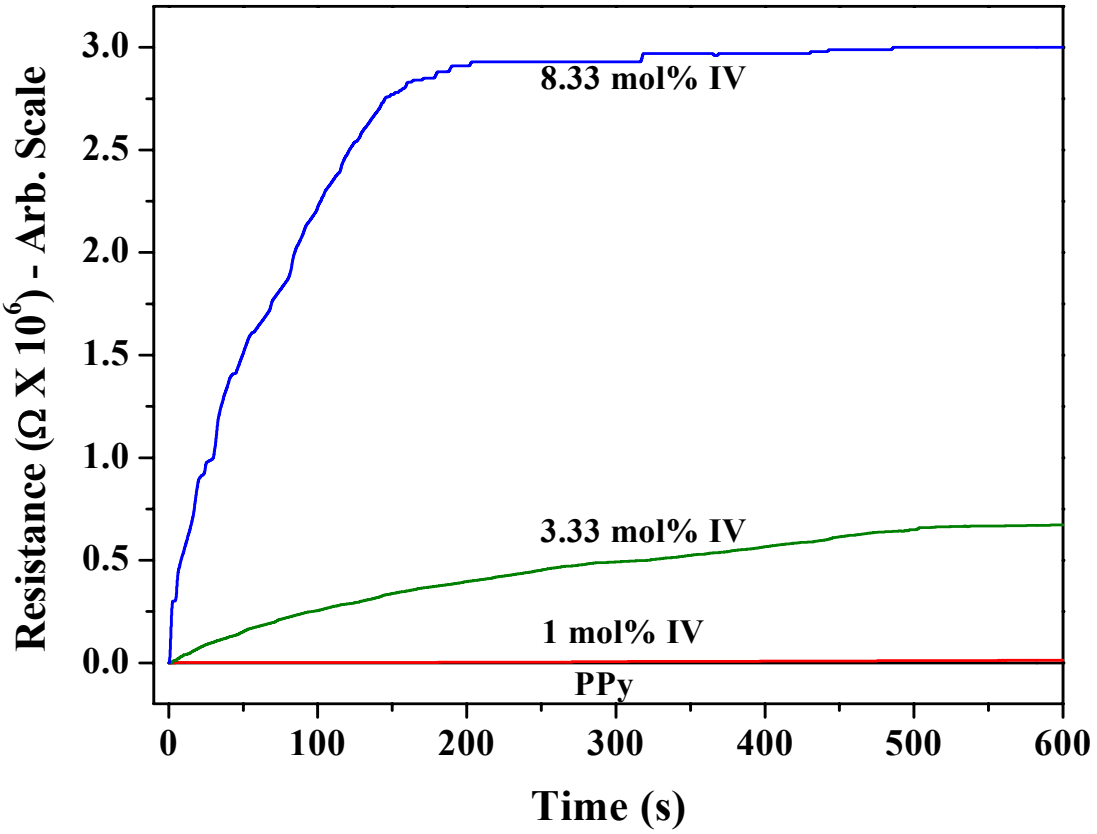

Fig. 4.29. The response signal of copolymer samples towards 300 ppm CO gas.

The response factor ($\Delta R/R_0$ X 100), is calculated as earlier for all samples after exposure to CO repeatedly. The response factor increased from 0.76% to 8.4% with increasing concentration of compound **IV**. The speed of response determined from the t_{50} value, is quite low (47 s) for copolymer containing 8.33 mol% **IV**. The maximum change of resistance occurred during exposure to CO gas is taking place within the initial 3 min, which is estimated from the CO response plot. So, the change of resistance (dR) for the initial 3 minutes (dt) is much relevant as far as the response of these materials are concerned. It was observed that there is a huge difference in change of resistance during the exposure of the materials towards 300 ppm CO gas. So, change of resistance (dR) for the initial 3 minutes (dt) is taken and dR/dt of the material is calculated. The various response characteristics of the copolymer samples are tabulated in Table 4.8.

Compound **IV** (mol%)	Sample Resistance R_0 (Ω)	$(\Delta R/R_0)$ %	Response time t_{50} (s)	dR/dt (Ω/min.)
8.33	48098757	8.4	47	957423
3.33	7998750	6.24	63	125973
1	246985	5.29	130	1000
0 (PPy)	2615	0.7	946	0.06

Table 4.8. The response characteristics of the copolymer materials.

In the present case, huge change in resistance as well as fast response at room temperature has been observed for higher concentration of the functional ferrocenyl derivatised pyrrole comonomer in the copolymer, which demonstrates the applicability of these sensors.

Virgin polypyrrole prepared with $FeCl_3$ route shows slight increase in conductivity when exposed to carbon monoxide gas. However, since all the samples in the present case, an increase of resistivity has been observed and so the sensing mechanism is entirely depends on the presence of ferrocenyl derivative to the back bone of the polymer and further charge transfer due to the interaction between CO and ferrocenyl derivative as seen with PPy-Fc in the previous chapter. So, the interaction of CO with the pyrrole nitrogen is not coming into picture as it happens with pure polypyrrole. When the material exposed to CO, it immediately comes to interact with iron atom of ferrocene and further electron contribution from the guest CO molecules to the ferrocene derivative establish an electronic pathway within the fully conjugated compound **IV.** Thus exposure to CO will only lead to further decrease in conductivity or increase of resistivity. Further, there does not appear to be permanent change in the material because the electrical resistance of the sample is seen to recover after the chamber is purged with air/oxygen. The reversibility of the sensor materials assured by subjecting them for repeated cycles within 1 min interval for the subsequent measurements. The diagrammatic representation of carbon monoxide interaction with copolymer and subsequent charge transfer from CO gas molecules to the copolymer is shown in Fig. 4.30.

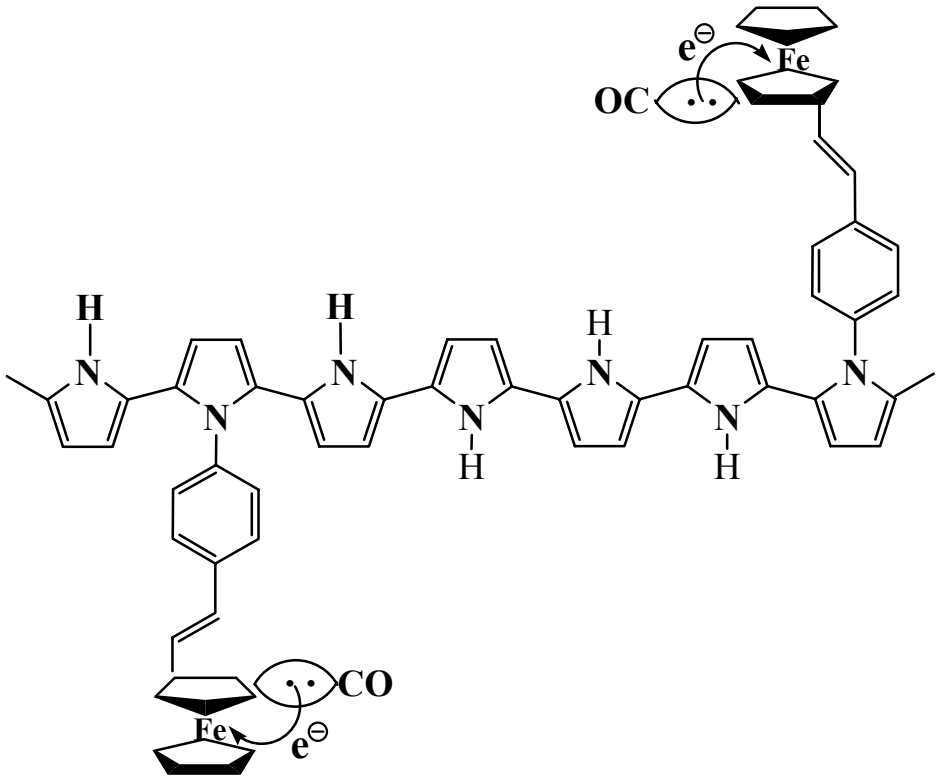

Fig. 4.30. Diagrammatic representation of CO-copolymer interaction and subsequent electron transfer process.

4.8. Electrochemical Copolymerisation

It was observed that an oxidation peak at 750 mV and the corresponding reduction peak at 210 mV for the CV of the compound **IV** obtained in 0.1 M TBAP in dichloromethane system with a scan rate of 50 mV/s. It is shown in Fig. 4.31. Potentiodynamic growth of copolymerization of compound **IV** (1 mmol) with pyrrole (30 mmol) in DCM containing 0.1 M TBAP as supporting electrolyte at a scan rate of 50 mV s^{-1} between $^{-}$1 V to +1 V is shown in Fig. 4.32. The cyclic voltammograms obtained during potentiodynamic growth, display the expected increase in current with increasing number of potential cycles which is consistent with electrochemically polymerized conducting polymers. After the completion of deposition, the films were rinsed and then studied by cyclic

voltammetry in 0.1 M TBAP containing acetonitrile. The typical cyclic voltammograms obtained for the copolymer film on Pt electrodes is given in Fig. 4.33. PPy oxidation and reduction peaks come at 200 mV and 50 mV respectively is evident from the previous experiment (see section 4.6.). On the other hand, the copolymer gives an additional peak in the cyclic voltammogram occurring at 410 mV with corresponding reduction at 160 mV which can be associated with the redox behavior of ferrocenyl back bone of the copolymer. Here, A & B represents ferrocenyl back bone in the copolymer and C & D for polypyrrole (Fig. 4.33.). These peaks are also observed in the CVs recorded during deposition of the copolymer films in TBAP/DCM system.

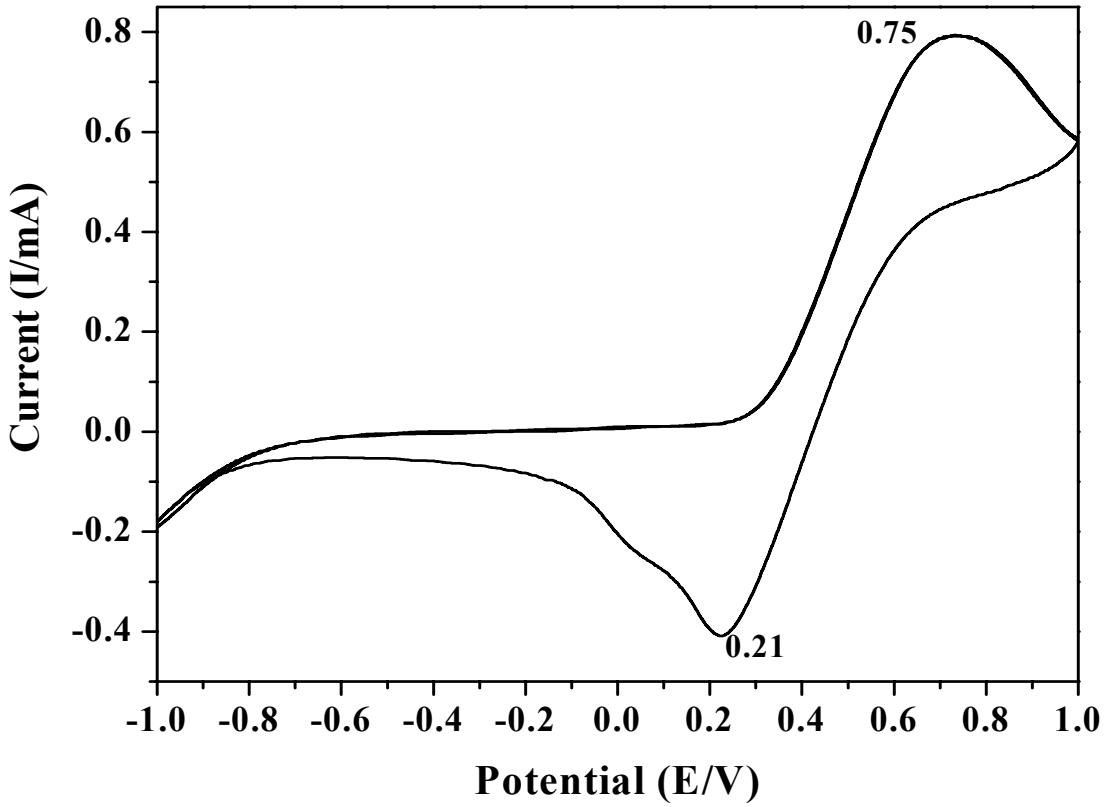

Fig. 4.31. CV of compound **IV** obtained in 0.1 M TBAP/DCM system. Scan rate: 50 mV/s.

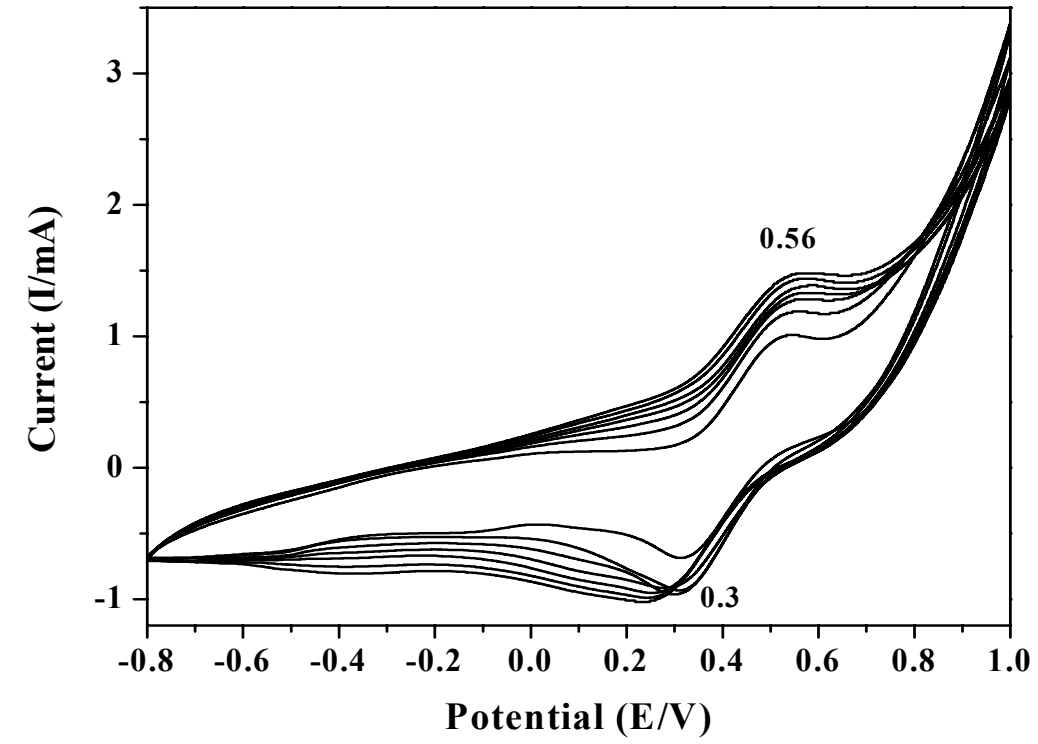

Fig. 4.32. Potentiodynamic deposition of copolymer film on Pt electrode. Scan rate: 50 mV/s.

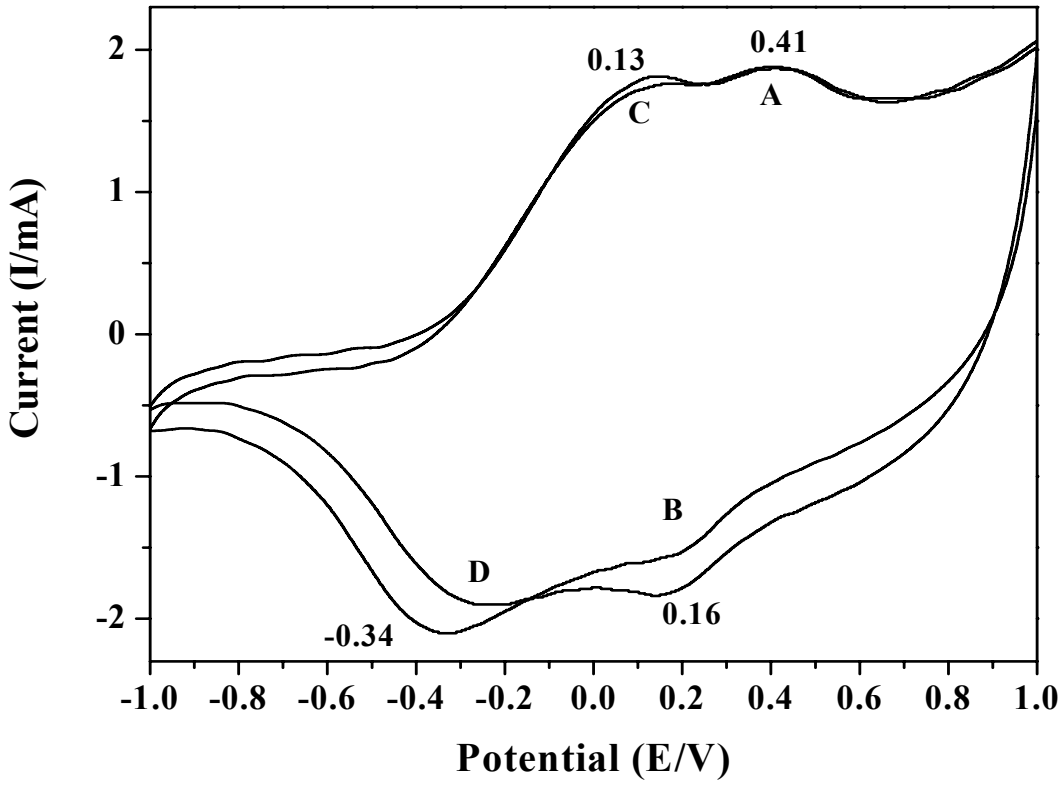

Fig. 4.33. CV of copolymer film deposited on Pt electrode with TBAP electrolyte in acetonitrile. Scan rate: 50 mV/s.

4.9. Conclusions

The present studies deal with the synthesis of a novel monomer, *trans*-1-{4[2-(1-ferrocenyl)vinyl]phenyl}pyrrole (**IV**) and the interfacial copolymerization with pyrrole in DCM/H_2O solvent using $FeCl_3$ as oxidant. The copolymer formation reaction is very fast in the presence of water. The coated copolymer on the interdigitated electrode configuration was used as a chemical sensor for detecting environmentally hazardous gases such as carbon monoxide (CO).

The novel comonomer synthesis is a multistep process, starts with derivatising ferrocene and finally p-phenylene vinylene on the cyclopentadienyl ring was N-arylated with pyrrole via efficient CuI catalyzed reaction. The compounds obtained in each step were well characterized with different techniques. The co-polymer was thoroughly characterized via FTIR, UV-Vis. spectroscopy, TGA, DSC etc. methods. It has been seen that the T_g of the polymer decreases as the concentration of the comonomer, **IV**, increases in the polypyrrole. The electrochemical synthesis and characterization of the copolymerization was also successfully carried out.

The gas sensitivity measurements show excellent response for these materials towards 300 ppm concentration of CO gas at room temperature. It is observed that there is a remarkable rise of resistance from the time of exposure of the material towards CO gas and then it saturates. The sensitivity is higher for the copolymer containing the higher concentration of **IV**, because of the guest gas (CO) is getting more interaction sites in the polymer and subsequently the charge transfer reaction is occurring and resistance shoots up. The response time, t_{50} obtained is short; response factor and response characteristics for the initial 3 minutes were also calculated for different compositions.

Compound **I** was electrochemically incorporated and characterized. It is narrated from the CO sensitivity of the electrochemically deposited films on interdigited electrode is that even at very low concentration of compound **I** (4 mol% with respect to pyrrole), CO gas is able to interact with the ferrocenyl moieties and subsequent change in resistance, which is rapid and consistent. The sensor parameters were calculated and plotted, which gives the insight of mechanism of CO interaction with ferrocenyl moieties and reason for rise of resistance.

4.10. References

[1] H. K. Youssoufi, B. Makrouf, Synth. Met. 119 (2001) 265.

[2] A. Naji, M. Cretin, M. Persin, J. Sarrazin, J. App. Poly. Sci. 91 (2004) 3947.

[3] S. Ching, C. M. Elliott, Langmuir 15 (1999) 1491.

[4] Q. Wang, L. Wang, L. Yu, J. Am. Chem. Soc. 120 (1998) 12860.

[5] S. Barlow, H. E. Bunting, C. Ringham, J. C. Green, G. U. Bublitz, S. G. Boxer, J. W. Perry, S. R. Marder, J. Am. Chem. Soc. 121 (1999) 3715.

[6] G. E. Southard, M. D. Curtis, Organometallics 20 (2001) 508.

[7] V. Casey, J. Cleary, G. D. Arcy, J. B. McMonagle, Sens. Actuators B 96 (2003) 114.

[8] U. Storm, O. Bartels, J. Binder, Sens. Actuators B 77 (2001) 529.

[9] A. C. Partridge, M. L. Jansen, W. M. Arnold, Mat. Sci. Eng. C 12 (2000) 37.

[10] S. Ampuero, J.O. Bosset, Sens. Actuators B 94 (2003) 1.

[11] G. Sberveglieri, Sens. Actuators B 23 (1995) 103.

[12] R. Cabala, V. Meister, K. Potje-Kamloth, J. Chem. Soc. Faraday Trans. 93 (1997), 131.

[13] L. S. Roman, M. R. Andersson, T. Yohannes, O. Inganas, Adv. Mater. 9 (1997) 1164.

[14] J. J. M. Halls, K. Pichler, R. H. Friend, S. C. Moratti, A. B. Holmes, Appl. Phys. Lett. 68 (1996) 3120.

[15] M. Kakimoto, H. Kashihara, T. Kashiwagi, T. Takiguchi, J. Ohshita, M. Ishikawa, Macromolecules 30 (1997) 7816.

[16] M. Kakimoto, H. Kashihara, T. Kashiwagi, T. Takiguchi, J. Ohshita, M. Ishikawa, Macromolecules 30 (1997) 7816.

[17] S. J. Higgins, C. L. Jones, S. M. Francis, Synth. Met. 98 (1999) 211.

[19] K. Naka, T. Uemura, Y. Chujo, Macromolecules 33 (2000) 6965.

[20] C. Kim, E. Park, C. K. Song, B. W. Koo, Synth. Met. 123 (2001) 493.

[21] C. G. D. Sykesud, P. A. Zhdan, D. J. Walton, L. S. Miller, C. A. Jasper, Thin Solid Films 1998, 325, 223.

[22] D. W. Old, M. C. Harris, S. L. Buchwald, Org. lett. 2 (2000) 1403.

[23] G. Mann, J. F. Hartwig, M. S. Driver, C. F. Rivas, J. Am. Che. Soc. 120 (1998) 827.

[24] C. R. Hauser, J. K. Lindsay, J. Org. Chem. 21 (1956) 382.

[25] D. Lednicer, C. R. Hauser, Org. Synth. 5 (1963) 434.

[26] J. K. Lindsay, C. R. Hauser, J. Org. Chem. 22 (1957) 355.

[27] D. Lednicer, C. R. Hauser, Org. Synth. 5 (1963) 434.

[28] P. J. Graham, R. V. Lindsey, G. W. Parchall, M. L. Peterson, G. M. Whitman, J. Am. Chem. Soc. 79 (1957) 3416.

[29] P. L. Pauson, W. E. Watts, J. Chem. Soc. (1963) 2990.

[30] K. L. Kott, R. J. McMohon, J. Org. Chem. 57 (1992) 3097.

[31] K. L. Kott, R. J. McMohon, J. Org. Chem. 57 (1992) 3097.

[32] J. C. Calabrese, L. T. Cheng, J. C. Green, S. R. Marder, W. J. Tam, J. Am. Chem. Soc. 113 (1991) 7227.

[33] A. Klapars, J. C. Antilla, X. Huang, S. L. Buchwald, J. Am. Chem. Soc. 123 (2001) 7727.

[34] F. Lang, D. Zewge, I. N. Houpis, R. P. Volante, Tetrahedron lett. 42 (2001) 3251.

[35] B. Scrosati, "Applications of Electroactive Polymers", Chapman Hall, London, 1995.

[36] S. Radhakrishnan, S. A. Patil, Indian Patent Appl. 102/DEL/2000.

[37] S. Radhakrishnan, S. D. Deshpande, Indian Patent Appl. 104/DEL/2001.

[38] B. Tion, G. Zerbi, J. Chem. Phys. 92 (1990) 3892.

[39] E. M. Genies, C. J.Tsintavis, J. electroanal. Chem. 239 (1988) 387.

[40] G. G.Wallace, G. M.Spinks, L. A. P. Kane-Maguire, P. R.Dale, CRC Pres London 2003, Ch.3.

[41] S. Radhakrishnan, S. Unde, J. Appl. Polym. Sci. 71 (1999) 2059.

[42] A. F. Talaie, G. G. Wallace, Synth. Met. 63 (1994) 83.

[43] N. Densakulprasert, L. Wannatong, D. Chotpattanont, P. Hiamtup, A. Sirivat, J. Schwank, Mater. Sci. Eng. B 117 (2005) 276.

[44] S. Watcharaphalakom, L. Ruangchuay, D. Chotapattanont, A. Sirivat, J. Schwank, Polymer Int. 54 (2005) 1126.

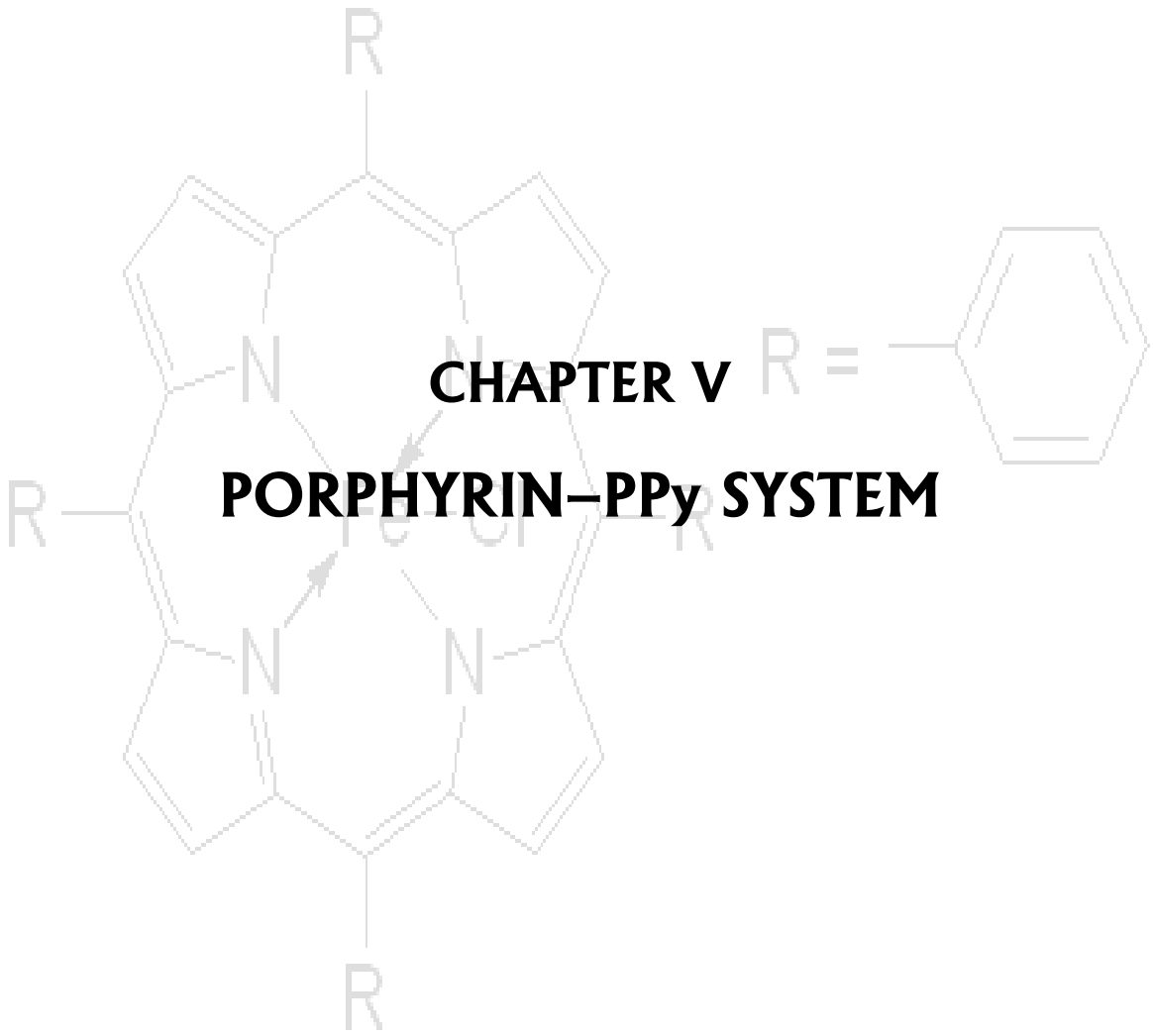

CHAPTER V

PORPHYRIN–PPy SYSTEM

5.1. Introduction

Incorporation of metalloporphyrins into polymer electrodes has been developed over the past years and these materials are aimed at being efficient electrocatalysts for chemical as well as for photochemical applications. The incorporation of porhyrin into polypyrrole has been documented in the literature [1–3]. However, there are only few reports available for the gas sensor application of porphyrin containing polypyrroles. Bediioui et. al have shown that pyrrole-based polymers containing porphyrin complexes appeared among one of the candidates for NO gas sensor [1, 4] applications. Metalloporphyrins have been electrochemically incorporated into polypyrrole films according to two ways: i) as counter-ions (or "doping" ions) during the electrochemical growth of the films in solutions containing pyrrole and anionic complexes as supporting electrolyte [5–7] and ii) by electro-oxidative polymerization of suitably designed pyrrole monosubstituted porphyrins [8–12]. Generally small inorganic anions can easily leave the PPy film during reduction while large polymeric anions are firmly fixed into the film. FeTPPCl having relatively large size probably may not be able to leave the PPy film. In principle, porphyrins with or without a metal ion in the center can be used as anionic dopants. It has been incorporated chemically during pyrrole polymerization reaction.

Attachment of transition-metal complexes to electrodes has been researched over the past years [l3] and preparation of modified electrodes by means of electrochemical polymerization of pyrrole and derivatives has been widely developed [14]. Conducting polypyrrole incorporated with porphyrins find many applications in the field of catalysis [15, 16], potentiometric sensor [17] etc. Even though the polymerization of these pyrrole-substituted complexes has produced interesting polymers aimed at catalyzing redox and organic reactions, these materials do not display generally the desired electronic conductivity of polypyrrole. Metal porphyrins dispersed in polyurethane have been used in ion selective electrodes since the selectivity of these detectors was controlled by the central metal atom. For example, with the central metal atom as In(III) gives good response to chloride, Ga(III) for fluoride and Co(III) for nitrate was obtained [18]. It is well known that carbon monoxide interacts with hemoglobin/heme and causes deterioration of their oxygen uptake/transfer activity [19]. Hence, that groups are

potential candidates for functionalisation of conducting polymer used for detection of carbon monoxide.

The present chapter describes the preparation of polypyrrole incorporated with porphyrin, viz. 5,10,15,20-tetraphenyl-21H,23H-porphineiron(III) chloride (FeTPPCl) and the performance of these materials for sensing carbon monoxide. Chemical as well as electrochemical route were used for the incorporation of these species into polypyrrole. The chemical synthesis method using anhydrous $FeCl_3$ as oxidising agents in water-methanol solvent system and their characterisation was discussed in Section A. The application of chemically synthesised PPy-FeTPPCl materials for chemical gas sensor is also discussed in this section. Section B describes the electrochemical method employed for the PPy-FeTPPCl film deposition in detail. The section B also deals with the characterisation of the films deposited on the Pt electrode using post cyclic voltammetry. The property measurements such as electrical conductivity and chemical sensitivity for these films were discussed in detail in the same section. Finally, the conclusions drawn from the present study on incorporation of phthalocyanine into polypyrrole matrix has been presented.

5.2. Experimental

5.2.A. Chemical Functionalisation of Polypyrrole with Iron Porphyrin

The typical reaction as follows: Iron porphyrin (FeTPPCl) of 10 mg (1% by weight of pyrrole) was dissolved in 50 ml methanol in a stoppered flask and stirred well with 1.62 g (0.1 M) anhydrous ferric chloride. 1 ml pyrrole (silica column purified) was added into the reaction system with continued stirring and 50 ml distilled water was slowly added into it. As soon as the addition of water progresses, the initial brown colour of the solution becomes progressively darker. The stirring continued for another two more hours at room temperature to ensure complete oxidation of pyrrole monomer into polymer and incorporation of FeTPPCl into polypyrrole, which eventually precipitated at the bottom of the flask. The black colored PPy-FeTPPCl precipitates were filtered through a Whattman filter paper, the first filtrate was collected and UV-Vis. spectroscopy of the same was recorded. It was washed well with distilled water and dried at 50^0C. In a similar set of experiments, varying amounts of FeTPPCl were added to the reaction mixture

ranging from 1 to 15 weight percent with respect to pyrrole monomer, the other conditions being same as above. The polymers were dried at room temperature for 48 h and then they were preserved in the vacuum desiccator.

5.2.A.a. Real Time Monitoring of Polymerisation Reaction

The online monitoring of pyrrole polymerization and incorporation of FeTPPCl into PPy reaction was recorded with respect to time (see section 2.5.1.). Very dilute solutions were quantitatively prepared and used for this measurement in a disposable UV-Vis. cuvette and continuously monitored the reaction and recorded the spectra at particular intervals of time. The reaction kinetics of PPy formation and incorporation of FeTPPCl into PPy is derived from real time UV-Vis. spectroscopy. The reaction procedure as follows:

1 wt.% of PPy-FeTPPCl reaction - 5 mg FeTPPCl was dissolved in 50 ml, 100 µl pyrrole dissolved in 10 ml and then 0.162 g anhydrous ferric chloride in 10 ml methanol. 200 µl of the above prepared FeTPPCl solution was added into 1.5 ml mixed solvent system of 1:1 distilled water/methanol, which was taken previously in a disposable UV-Vis. cuvette and the spectrum was recorded. 200 µl of above prepared $FeCl_3$ solution was well mixed with it. Then the online monitoring of the polymerization reaction started with the addition of 200 µl of above prepared pyrrole solution into it. A blank polypyrrole reaction (without FeTPPCl) was also carried out quantitatively in the same condition as above and monitored carefully. The spectra were recorded with a time interval of 30 min.

5.2.B. Electrochemical Functionalisation of PPy with FeTPPCl

PET transparencies were cleaned well and gold was deposited on it by vacuum deposition technique. Interdigited electrodes were made with these gold coated substrates and activated with 1 M $FeCl_3$ solution for 32 h and used for the electrochemical deposition of PPy-FeTPPCl films of different concentrations for CO sensing measurements. Platinum electrodes were also used as working electrodes for deposition of modified PPy films. The cyclic voltammetry of this modified film on Pt electrode was recorded and analysed.

The electrochemical synthesis procedure as follows: 0.34 g tetrabutyl ammonium perchlorate (0.1 M) was dissolved in 10 ml DCM and 7 mg (0.001 M) iron porphyrin was dissolved in it. Then 70 µl pyrrole (0.1 M) was added into it and the electrochemical deposition of PPy-FeTPPCl films were performed by chronoamperometry method at a

potential of 0.9 V on Pt electrodes and $FeCl_3$ activated interdigited electrodes. The film deposition was carried out for 5 minutes. Different concentrations of the solution were made each time by increasing the concentration of pyrrole and keeping the same concentration of FeTPPCl. Solutions of 1 mmol porphyrin with 0.14 M, 0.18 M and 0.2 M pyrrole were prepared separately and PPy-FeTPPCl films were deposited on the interdigited electrodes. All the reactions were carried out under the same conditions. The electrolytic cell comprised of a single compartment cell containing SCE (saturated calomel electrode), platinum foil as a counter electrode and gold coated PET interdigited substrates as a working electrode.

The modified PPy films deposited were then rinsed thoroughly in distilled water. The films were allowed to dry at room temperature for 24 hours, which were used for the CO sensitivity measurements. The cyclic voltammetric measurements were recorded in 0.1 M TBAP/CH_3CN system.

5.3. Results and Discussions

5.3.A. Characterizations

5.3.A.a. UV-Vis. Spectroscopy

The online monitoring of pyrrole polymerization and 1 wt.% FeTPPCl incorporation into PPy in water-methanol solvent system is shown in Figures 5.1.A. and 5.1.B. respectively. It is clear from the spectra that a prominent *d-d* transition at 400 nm in case of Py-FeTPPCl is due to transition metal, iron. It is observed that the black deposition of modified polymer starts coating on the inside walls of the cuvette as time progresses. There is an increase in absorbance at the λ_{max} region 800–900 nm with progress of polymerization and modification of PPy during the reaction. It is evident from the spectra that the reaction proceeds faster with the addition of FeTPPCl compared to PPy synthesis under the same conditions. Polypyrrole formation takes 4 h to complete the reaction where as 1 wt.% PPy-FeTPPCl system takes only 2.5 h to complete the modification of PPy. This tells the catalytic activity of FeTPPCl in converting pyrrole monomer into polypyrrole and incorporation by itself.

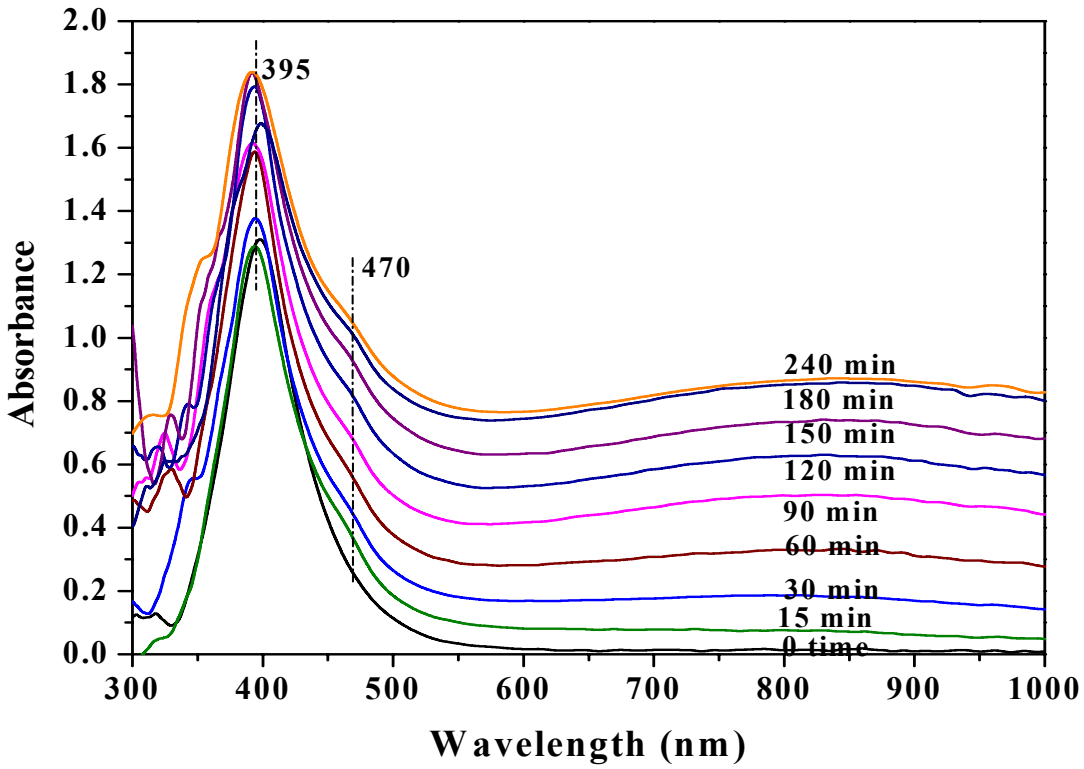

Fig. 5.1.A. Real time UV-Vis. spectroscopic monitoring of PPy synthesis in water-MeOH system.

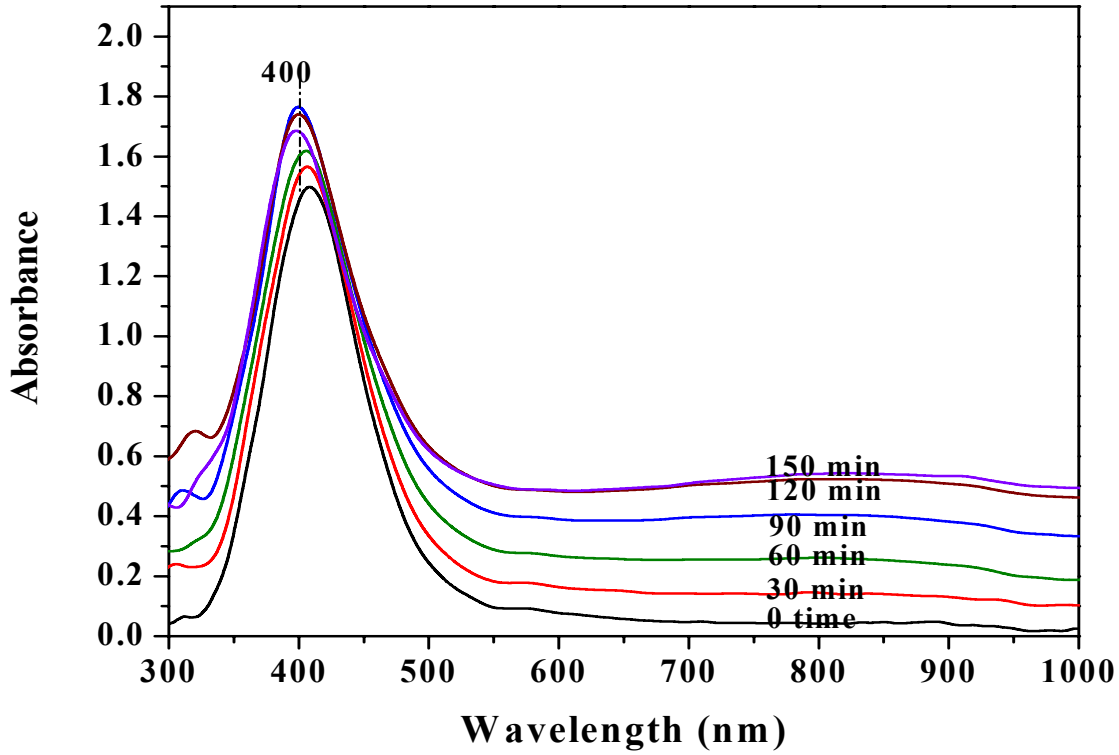

Fig. 5.1.B. Real time UV-Vis. spectroscopic monitoring of 1 wt.% FeTPPCl-Py system.

From the real time UV-Vis. spectra of PPy and 1 wt.% FeTPPCl systems, the oligomeric formation at λ_{max} 470 nm region is evident in PPy synthesis as a shoulder where as it is not obvious in the presence of FeTPPCl. This peak evolves within 15 minutes after the polymerization reaction starts in case of pure PPy synthesis. Polypyrrole synthesis in methanol solvent is sluggish than in aqueous system. This indicates that pyrrole oligomers are present in the PPy system and it is a slow process compared to the other case. These evidences strongly support the above statements.

The rate of the reaction was calculated from the time dependent polymerization reaction. The rate of PPy/modified PPy formation is considered. The conversion of the monomer to polymer at 800 nm region is considered for the rate determination. Both polymer conversion [C] is ploted against time (t) in log scale is shown in Fig. 5.2. The time taken to form the polymer is normalized on the y-axis [$(OD_t-OD_0) / OD_{max}$] and ploted against time (Fig. 5.3.). The slope of the above straight line plot (log-log scale) gives rate of the reaction. It is found that the rate of PPy synthesis is less than the system containing FeTPPCl. The rate of the reaction for PPy is 5.1 X 10^{-3} and 6.4 X 10^{-3} for 1 wt.% Py-FeTPPCl reaction. The rise of absorbance in the wavelength region 800–900 nm is the evidence of formation of conducting material. This is a confirmation of the formation of bipolaronic band [20].

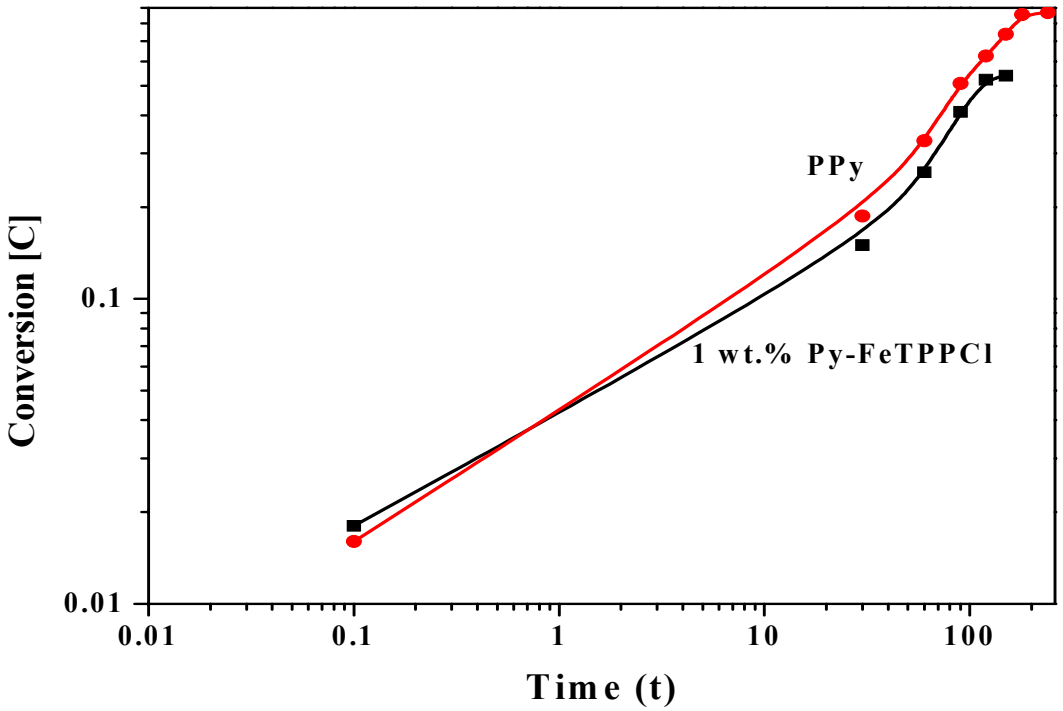

Fig. 5.2. A plot of conversion at λ_{max} 800 nm with respect to reaction time.

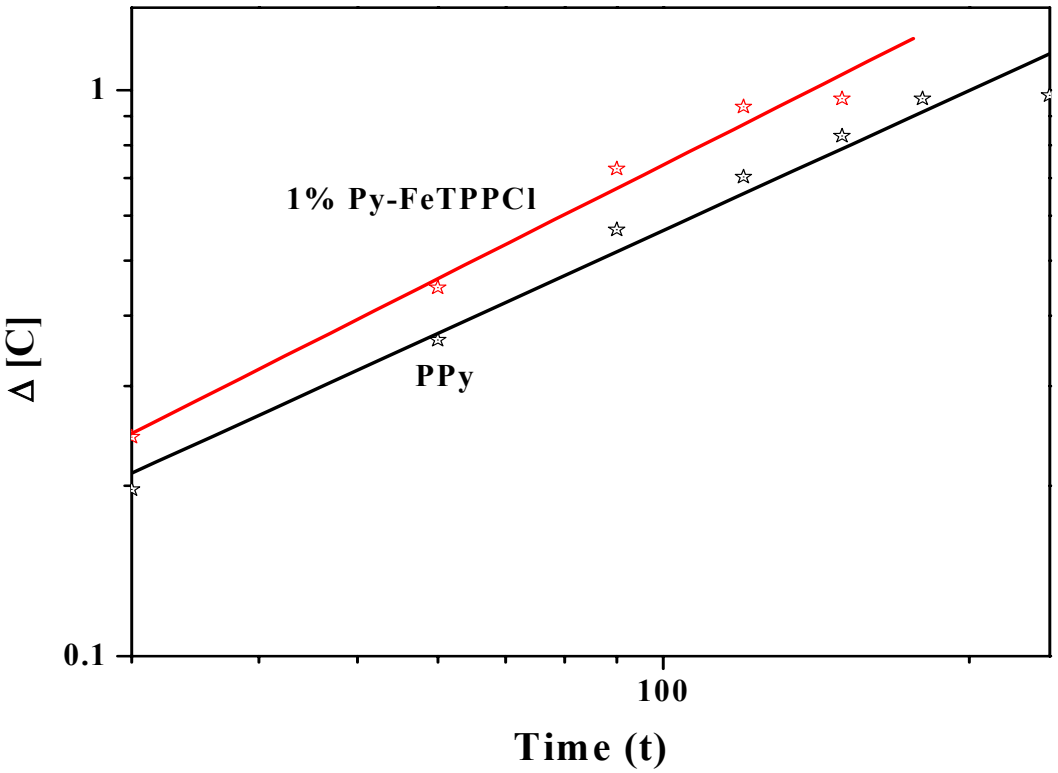

Fig. 5.3. Rate of the reaction from the slope of Δ[C] vs. time plot.

The quantitative analysis was done by estimating the amount of FeTPPCl incorporated into PPy using UV-Vis. spectroscopy technique. The spectrum was recorded before and after the reaction to know the exact amount of FeTPPCl incorporated into polypyrrole. It is observed that the color of the filtrate after the reaction was a very slight pale yellow where as the FeTPPCl solution before the reaction looked intense dark brown in color. The characteristic λ_{max} for FeTPPCl obtained at 410 nm region in methanol-water mixture vanished after the reaction and a new absorption band arises at 464 nm, is due to the small amount of pyrrole oligomer remaining unreacted in the solution [21]. The spectra of various compositions clearly show that λ_{max} of filtrates at 464 nm exhibits a gradual decrease in intensity with increasing concentration of FeTPPCl. This evidence suggests that FeTPPCl improves the conversion of pyrrole monomers into polymer which is also found from the yield of the reaction (see Table 5.1.). Fig. 5.4. depicts the spectra of the first filtrates recorded immediately after the reaction. Since there is no evidences for the presence of any peak for FeTPPCl (410 nm) in the filtrate, it is clear that the whole amount (1–15 wt.% with respect to pyrrole) of FeTPPCl added into the reaction system is getting incorporated into polypyrrole during chemical reaction.

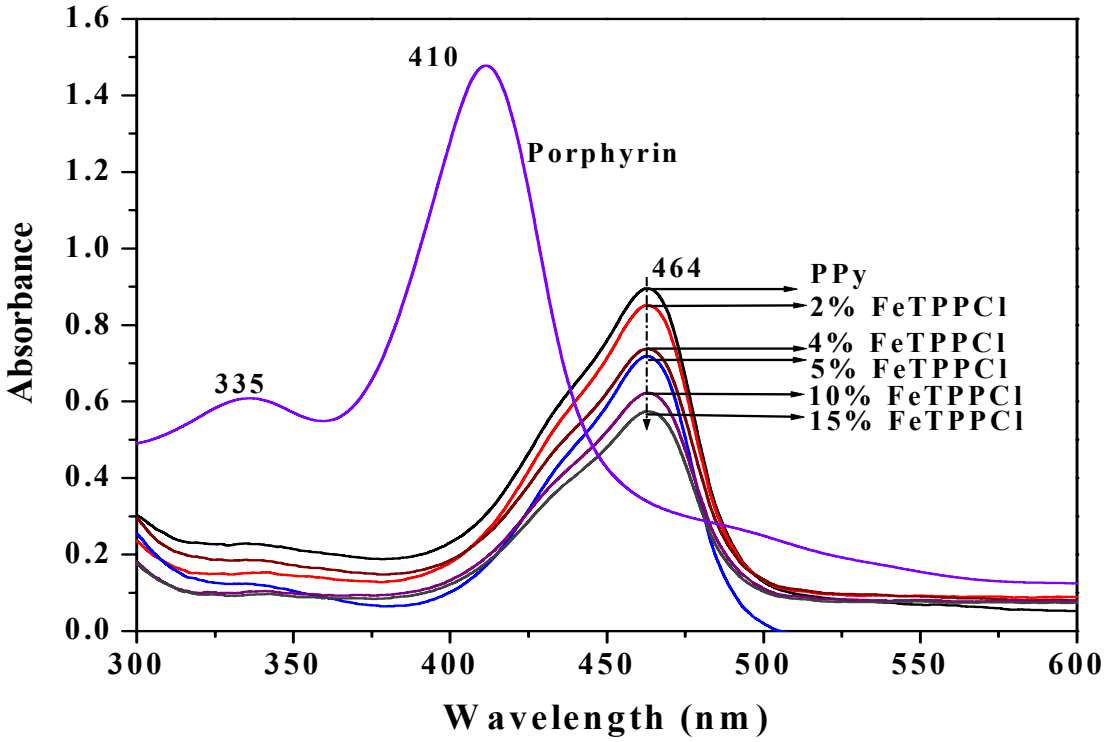

Fig. 5.4. UV-Vis. spectra of the filtrates after completion of the Py-FeTPPCl reaction in methanol-water mixture.

Quantity of the reactants taken				OD of the filtrate at 464 nm	Yield (g)
Pyrrole (ml) (0.0145 mol)	Anhydrous $FeCl_3$ (g)	Porphyrin			
		Wt.%w.r.t. Py	Mol w.r.t. Py		
1	1.62	0	-	0.897	0.197
1	1.62	2 (20 mg)	1.96×10^{-3}	0.851	0.247
1	1.62	4 (40 mg)	3.92×10^{-3}	0.739	0.267
1	1.62	5 (50 mg)	4.90×10^{-3}	0.722	0.276
1	1.62	10 (100 mg)	9.80×10^{-3}	0.622	0.309
1	1.62	15 (150 mg)	1.50×10^{-3}	0.576	0.363

Table 5.1. Summary of FeTPPCl modified reaction in terms of reactants taken, UV-Vis. of filtrate and yield of the product obtained.

1 mg of the various compositions of PPy modified powders were added into 10 ml NMP and sonicated for 4 h. It was filtered and UV-Vis. spectra of the dissolved portion was recorded is shown in Fig. 5.5. The λ_{max} obtained for the bipolaronic region of the polymeric samples is tabulated in Table 5.2. A blue shift is observed for porphyrin peak in the modified PPy samples at 450 nm region for all samples, indicating the effective modification of PPy with FeTPPCl. The shift is consistent towards lower wavelength side with increasing concentration of FeTPPCl in PPy. It may be noted that the second peaks of the FeTPPCl occurring at 570 nm appear quite prominent in NMP as well as when incorporated in PPy. This can arise from the interaction of FeTPPCl with nitrogen atoms of PPy (which are also present in NMP). It may be pointed out that these were not prominent with methanol as the solvent (see Fig. 5.4.), which suggests that the common factor of nitrogen interaction could lead to these additional peaks. The splitting of the triplet state and /or singlet to triplet exciton transition in porphyrin may be additionally taking place due to this interaction with nitrogen lone pair.

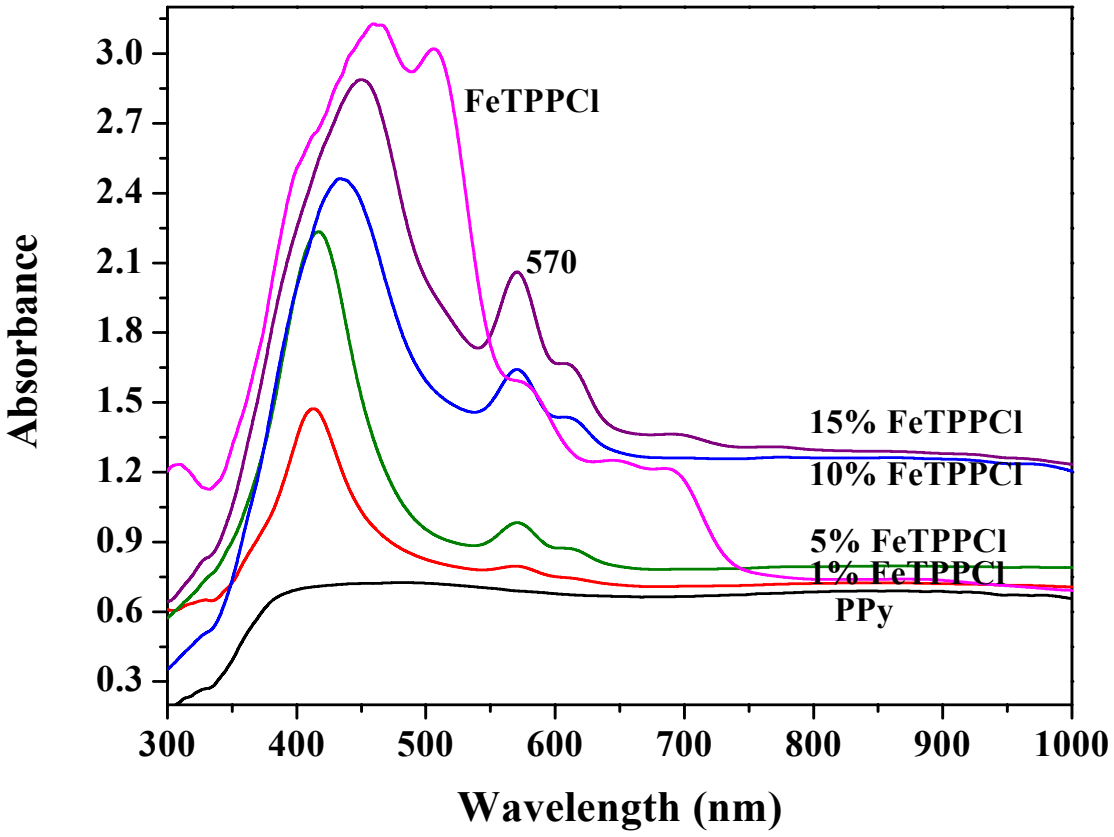

Fig. 5.5. UV-Vis. spectra of polypyrrole and polypyrrole doped with FeTPPCl in different compositions.

Compositions mol% of FeTPPCl w.r.t. Py	λ_{max} at bipolaronic region
0.0 (PPy)	883
0.09	879
0.473	874
0.946	868
1.42	860

Table 5.2. Wavelength of maximum absorption at the bipolaronic region for PPy and FeTPPCl doped PPy samples

5.3.A.b. FTIR Spectroscopy

The functionalization of pyrrole with porphyrin was confirmed with FTIR analysis of these polymers. The FTIR spectrum for the solid samples of polypyrrole (see section 3.3.1.A., Fig.3.1.C. and Table 3.3.), pure FeTPPCl and polypyrrole containing porphyrin in KBr pellet were recorded and compared in Fig. 5.6.A. and 5.6.B. respectively. The peaks corresponds to the wave number were noted down and their possible assignments are tabulated in Table 5.3. The values obtained for the PPy and FeTPPCl skeletal modes are well matched with the reported values of PPy [22, 23] and characteristic vibrational peaks of porphyrin [24] respectively.

The characteristic IR peaks of FeTPPCl is observed at 1600, 1439, 1203, 1339, 1175, 1072, 1004, 805, 750 and 703 cm^{-1}. Most of these peaks are aromatic C-H and C-C vibrations and seen in the porphyrin functionalized PPy samples also. The polymers exhibit IR bands at 1558, 1339, 1203, 1175, 1072, 1049, 1004, 930, 805 and 750 cm^{-1}. A strong peak at 1004 cm^{-1} is characteristic of all metalloporphyrins. Additionally, the 1464, 1305, 1094 and 968 cm^{-1} bands are also seen which are characteristic bands of polypyrrole.

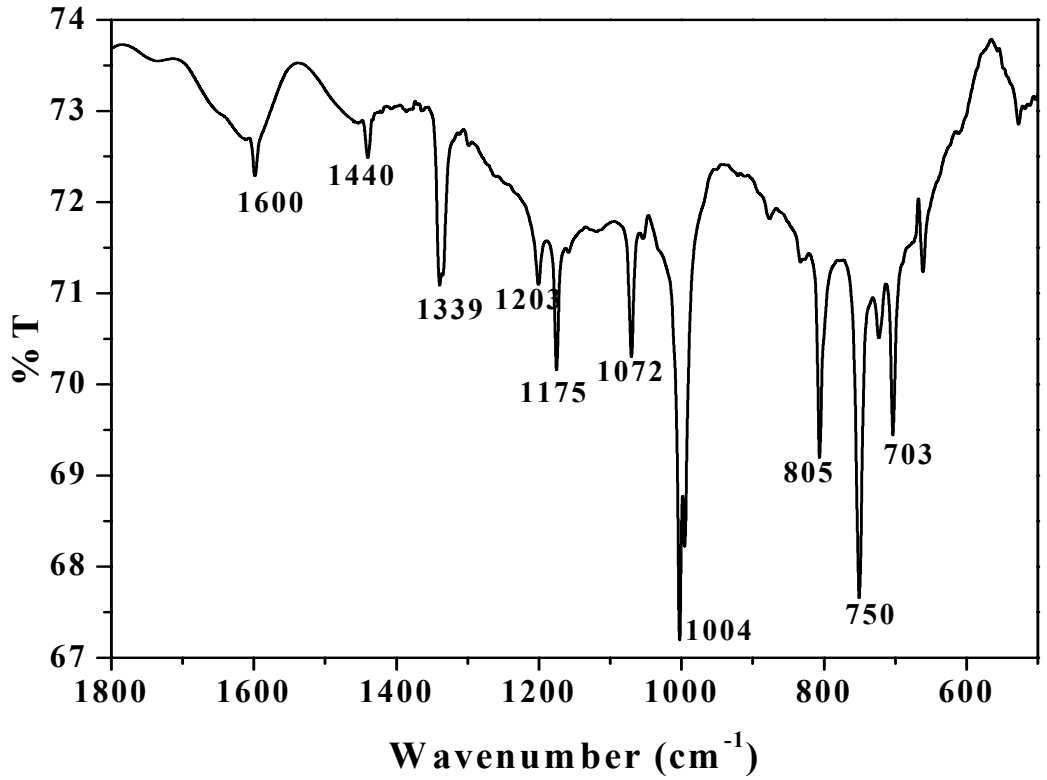

Fig. 5.6.A. FTIR spectrum of iron porphyrin (KBr).

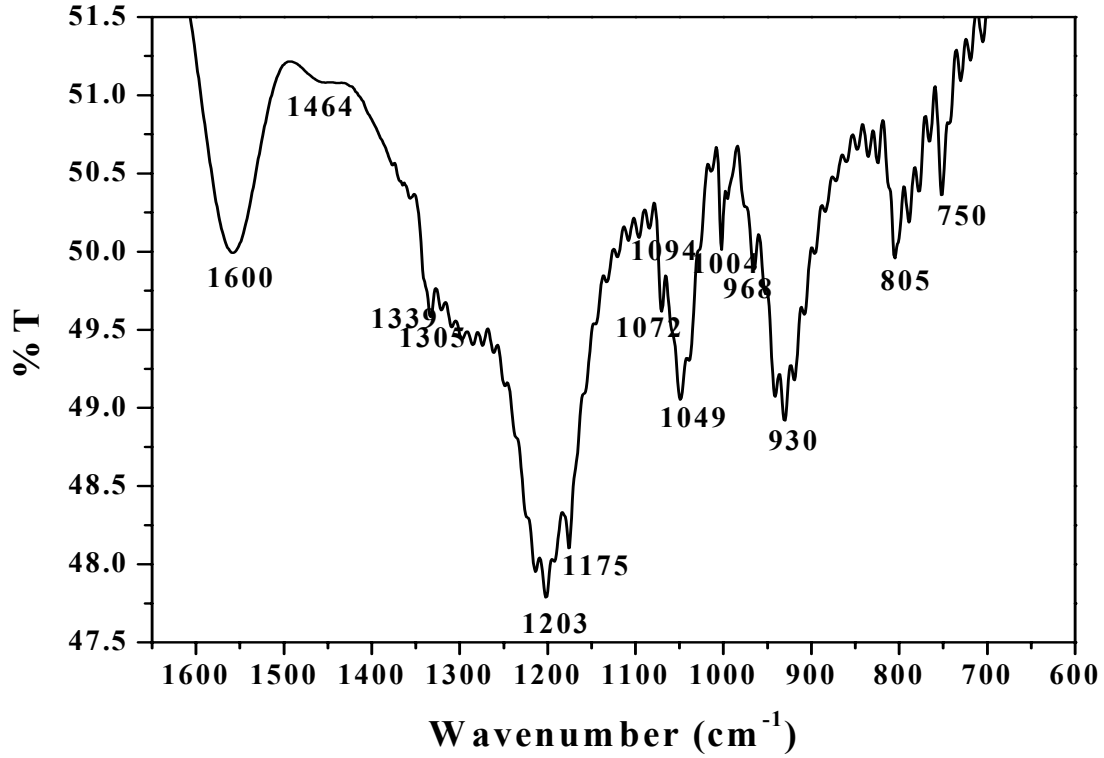

Fig. 5.6.B. FTIR spectrum of PPy-FeTPPCl material (KBr).

Material	υ_{max} (cm^{-1})	Peak assignments
FeTPPCl	1600	Conjugated C=C stretch
	1440	Methyl -CH Asymetric/symmetric bend
	1339, 1305	Aromatic -C-N stretch
	1203	Aromatic –CH in plane bend
	1175, 1072	–CN stretch
	805	-CH deformation of benzene
	1004	Characteristic peak of metalloporphyrin
	750	Monosubstituted phenyl –CH bend
	703	Monosubstituted phenyl ring
PPy-FeTPPCl	1464, 1339, 1305, 1094, 1049, 968, 930	Polypyrrole
	1600, 1203, 1175, 1072, 1004, 805, 750	FeTPPCl

Table 5.3. FTIR peak assignments of FeTPPCl incorporated PPy material.

5.3.A.c. X-ray Diffraction Studies

The XRD patterns obtained for the FeTPPCl modified PPy samples are indicted in Fig. 5.7. It is observed that PPy is mainly amorphous and after the incorporation of the FeTPPCl, it remains amorphous up to the concentration of 5%, above which a few well defined peaks appear in the XRD suggesting that there is some crystalline order. At higher concentrations of the FeTPPCl in PPy, quite a number of peaks are observed, which are tabulated in Table 5.4. The detailed analysis of these patterns was carried out using iterative technique. The FeTPPCl by itself crystallizes in tetragonal form with a = 14.56 Å and c = 9.4 Å [25]. The peaks observed for the pure FeTPPCl have been fully assigned to different reflections arising from this crystalline form (see Table 5.4.). On the other hand, after incorporation of the FeTPPCl in PPy matrix, the crystal structure appears to be modified because the peaks observed are not identical to original FeTPPCl. The peak positions as well as their relative intensities are different from the original

compound. The detailed analysis of new XRD pattern suggested that the crystalline structure had some similarity to original i.e. it was tetragonal but with lattice parameters of a = 16 Å and c= 9.64 Å. Also, the hkl indices are different in the polymer modified case than the pure compound. Thus, the PPy molecules interact with the FeTPPCl possibly at the four phenyl groups and expand the lattice slightly. It may be mentioned that the FeTPPCl structure is not fully planar, i.e. the phenyl groups are not placed in the same plane as the porphyrin central unit but are at angle of almost 90 degrees. The PPy molecules surrounding these give rise to twisting of these tetra phenyl groups and cause the difference in the structure developed. It is interesting to note that there is certain minimum quantity of the FeTPPCl required for the formation of ordered structure. At low concentrations, the molecules are in fully dispersed state and do not form aggregates.

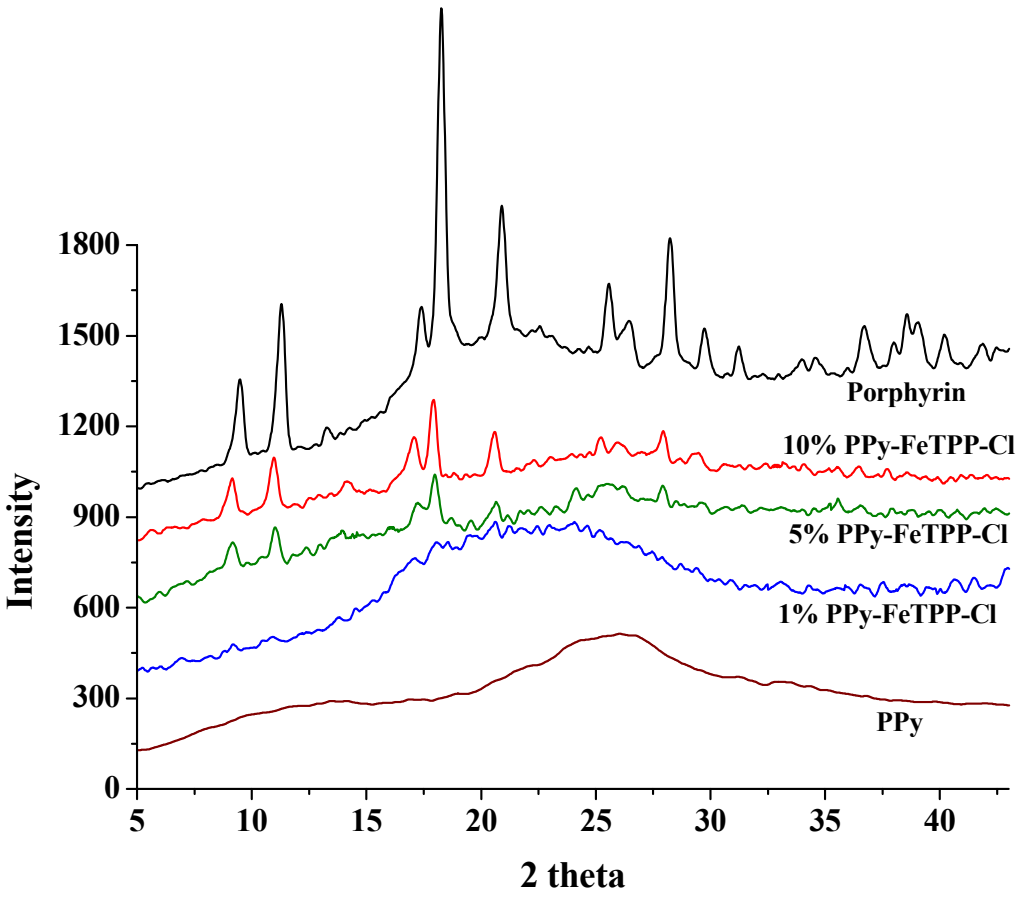

Fig. 5.7. X-ray diffraction patterns of PPy, FeTPPCl and FeTPPCl incorporated PPy materials.

FeTPPCl			PPy-FeTPPCl			
2θ	*d*-value	hkl	2θ	*d*-observed	*d*-calculated	hkl
9.42	9.4	001	9.18	9.64	9.64	001
11.24	7.87	101/011	10.98	8.06	8.06	200
17.39	5.14	220	17.10	5.18	5.09	310
18.298	4.84	300	17.91	4.94	4.91	310/221
20.97	4.24	112	20.52	4.33	4.44	112
25.597	3.5	410	25.33	3.52	3.53	331/102
26.49	3.35	401/302	25.98	3.43	3.38	421
28.29	3.16	003	27.9	3.21	3.21	003
29.83	2.96	500/113	29.33	3.04	3.09	113/402
31.24	2.85	402	—	—	—	—
36.7	2.44	600	—	—	—	—
38.54	2.33	004	—	—	—	—

Table 5.4. XRD analysis of FeTPPCl modified PPy.

The interchain distance (R) could be calculated from the XRD of the PPy and 1 wt.% PPy-FeTPPCl which is in amorpous state. R was calculated by the following equation:

$$R = \frac{5}{8}\left[\frac{\lambda}{\sin\theta}\right]$$

The interchain distance for both pure PPy and 1 wt.% PPy-FeTPPCl is tabulated in Table 5.5.

Material	2θ	R (Å)
PPy	26.92	4.14
PPy-FeTPPCl	19.988	5.555

Table 5.5. Inter chain separation of pure PPy and PPy-FeTPPCl materials.

5.3.A.d. Graphite Furnace Atomic Absorption Spectroscopy

This technique (see section 2.5.6.) was used as an elemental detection mainly for the detection of trace quantities of transition metals. This technique describes the incorporation of iron porphyrin into polypyrrole, in which the presence of iron was detected and tabulated in Table 5.6.

Composition	Wt. % of iron
15% PPy-FeTPPCl	0.393
10% PPy-FeTPPCl	0.293
5% PPy-FeTPPCl	0.166
1% PPy-FeTPPCl	0.0244
PPy	0

Table 5.6. GFAAS data for FeTPPCl incorporated polypyrrole materials.

The iron of the oxidant, $FeCl_3$ used for the synthesis of polypyrrole was completely washed out with distilled water, which is evident from GFAAS analysis. A propotional increase in iron content is observed with higher loading of FeTPPCl in PPy. Iron content of 0.0244 wt.% is detected for 1 wt.% of FeTPPCl incorporated PPy where as 0.393 wt.% of iron detected in 15 wt.% FeTPPCl incorporated polypyrrole.

5.3.A.e. EDAX Studies

The presence of iron in the functionalized polymer was done with EDAX (see section 2.5.5.) technique. It gives a proportional increase in iron content with increase in porphyrin concentration in the polymer. This analysis gives a clear indication of the incorporation of FeTPPCl as well as its influence on changing composition of elements at various concentrations. The EDAX data is shown in Fig. 5.8.

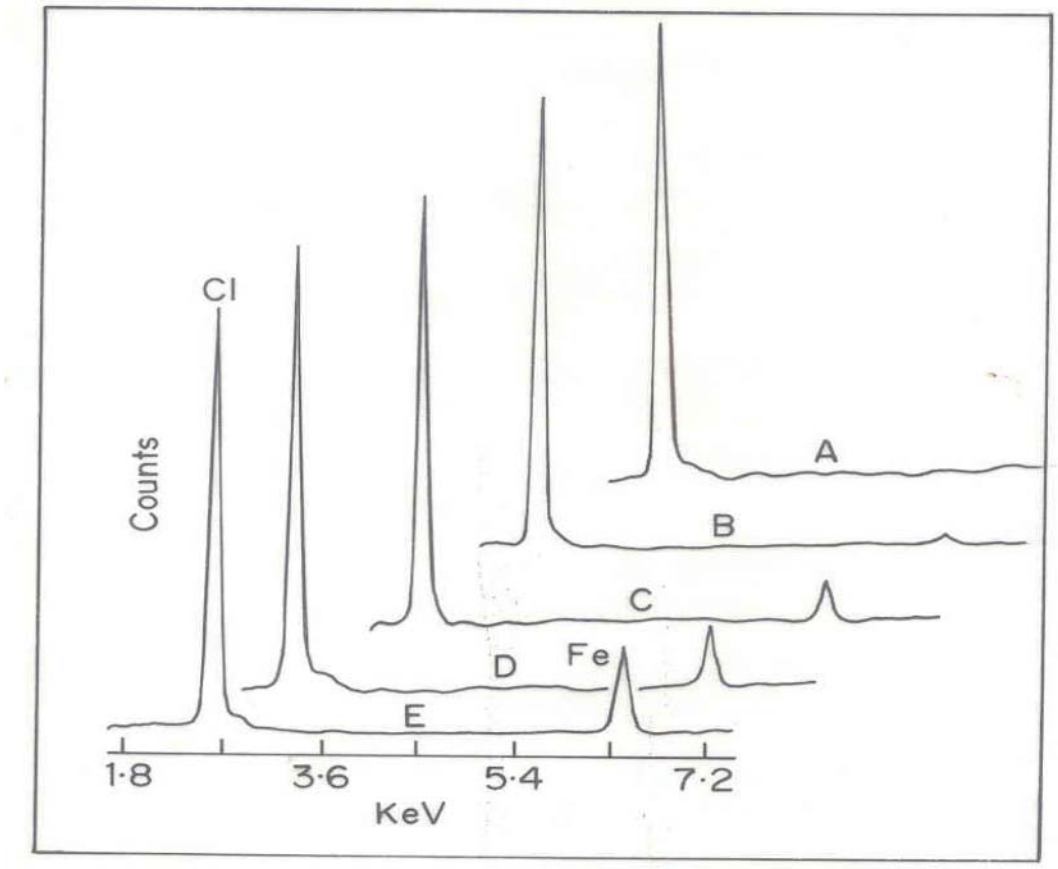

Table 5.8. EDAX data of FeTPPCl functionalised PPy materials: A) PPy, B) 1 wt.% PPy-FeTPPCl, C) 5 wt.% PPy-FeTPPCl, D) 10 wt.% PPy-FeTPPCl, E) 15 wt.% PPy-FeTPPCl.

5.3.A.f. TGA Studies

The percentage weight losses of the thermogram pattern of PPy-FeTPPCl samples obtained from thermogravimetric analysis is a good supporting evidence for the incorporated species and thermal stability of the modified materials. It clearly reveals the enhancement of thermal stability of modified PPy samples with increase in concentration of FeTPPCl in the polymer. It is shown in Fig. 5.9.

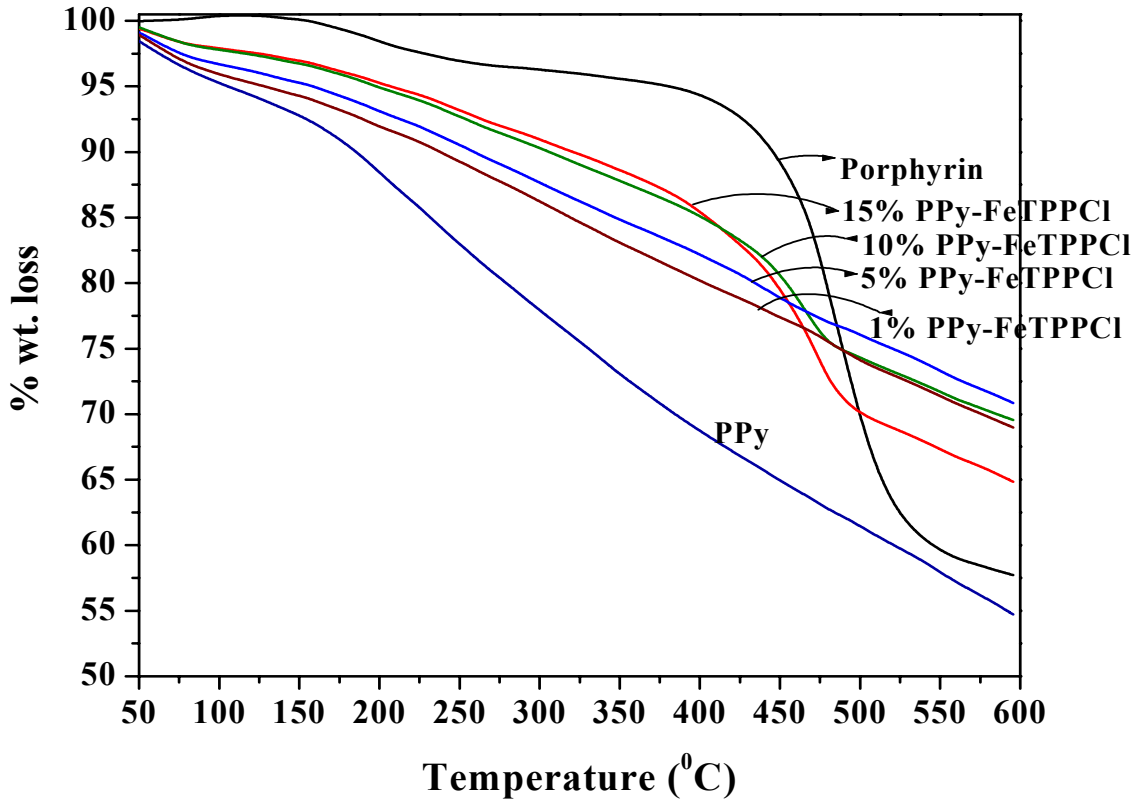

Fig. 5.9. Thermogravimetric pattern of FeTPPCl, PPy and PPy-FeTPPCl materials.

Iron porphyrin degrades in two stages, onset at 160^{0}C, which is assigned to the liberation of chlorine and the major second stage of weight loss observed at 410^{0}C due to the total degradation of porphyrin structure. The percentage weight losses calculated before and after degradation of porphyrin (ie. 350 and 600^{0}C) gives the stability obtained by the incorporation of porphyrin into the polymer. The thermogravimetric figure shows that the thermal stability of the modified PPy materials increases with FeTPPCl concentration upto 400^{0}C. As it is obvious from the Table 5.7. that the actual weight loss is always higher than the expected weight loss indicating the stability obtained by the PPy material due to he incorporation of FeTPPCl.

FeTPPCl content (mol%)	% wt. loss at 350^0C	% wt. loss at 600^0C	Actual wt. loss (%)	Expected wt. loss (%)
100	4.4	42.58	38.18	38.18
1.42	12.18	33.56	21.38	21.63
0.946	11.33	31.81	20.48	20.52
0.473	15.22	29.98	14.76	19.58
0.09	17.25	31.82	14.57	18.75
0 (PPy)	26.94	45.5	18.56	18.56

Table 5.7. Percentage weight loss of the materials at the time of degradation of FeTPPCl

5.3.B. Electrical Property Measurements

The electrical conductivity (σ), of PPy-FeTPPCl polymers were measured in its pellet form. Pellets were made at a pressure of 5 tonnes using a hydraulic press. The results of the variation in electrical conductivity as a function of temperature are shown in Fig. 5.10. The conductivity decreases with increasing concentration of porphyrin in the polymer. FeTPPCl hampers the charge transport between the chains and acts as an impurity level between the PPy band gap, which effectively works as a trap for charge carriers. The temperature dependent conductivity of the materials were measured and shown in Fig. 5.10. The activation energy required for each material is also calculated from the slope of the straight line obtained for log conductivity vs. I/T plot and the results were shown in Table 5.8.

FeTPPCl content (mol%)	σ (S/cm)	Ea (eV)
0 (PPy)	1.93×10^{-2}	0.0212
0.090	1.77×10^{-2}	0.0229
0.473	2.35×10^{-3}	0.0792
0.946	2.88×10^{-4}	0.1068
1.420	4.77×10^{-5}	0.1118

Table 5.8. Room temperature conductivity and activation energy with respect to FeTPPCl content in PPy.

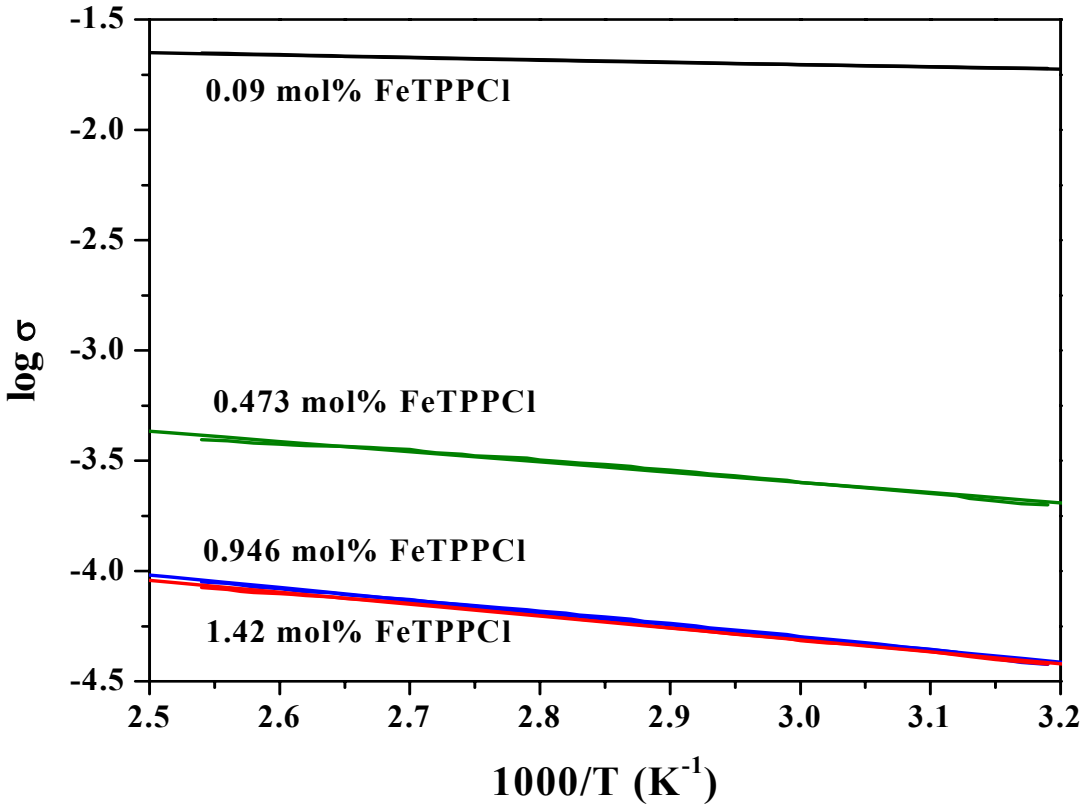

Fig. 5.10. Temperature dependent conductivity of PPy-FeTPPCl materials.

The activation energy for pure polypyrrole sample is 0.0212 eV, whereas, polypyrrole containing 1.42 mol% porphyrin material showed this value as 0.1118 eV. The increase in the activation energy is associated with decrease in electrical conductivity. These observations are in agreement with the results obtained in the UV-Vis spectroscopy i.e. the blue shift of the various bands which implies higher transition energy between ground state and the excited state.

5.3.C. Carbon Monoxide Gas Sensitivity Measurements

The interdigitated electrodes were coated using chemically modified PPy with FeTPPCl samples and CO gas response measurements were carried out as described earlier (see section 2.10.).

It is observed that PPy-FeTPPCl system shows increase in resistance during exposure to CO gas. The response depends on the composition of the material; 0.946 mol% PPy-FeTPPCl material shows the highest response of 12 times over the measured time of 10

minutes. The highest response factor obtained is 12 (calculated from $\Delta R/R_0$ X 100) for the same material; dR is the change of resistance after the exposure to CO gas and R_0, the initial resistance before exposure to CO gas. The materials were recovered (resistance of the materials were came back to its initial value) when flushed with excess air. It was confirmed by repeated response measurements within 1 min interval of time for the subsequent tests. The response characteristics of PPy-FeTPPCl samples were shown in Fig. 5.11. The initial resistance of the coated material on the interdigited electrode is given in Table 5.9.

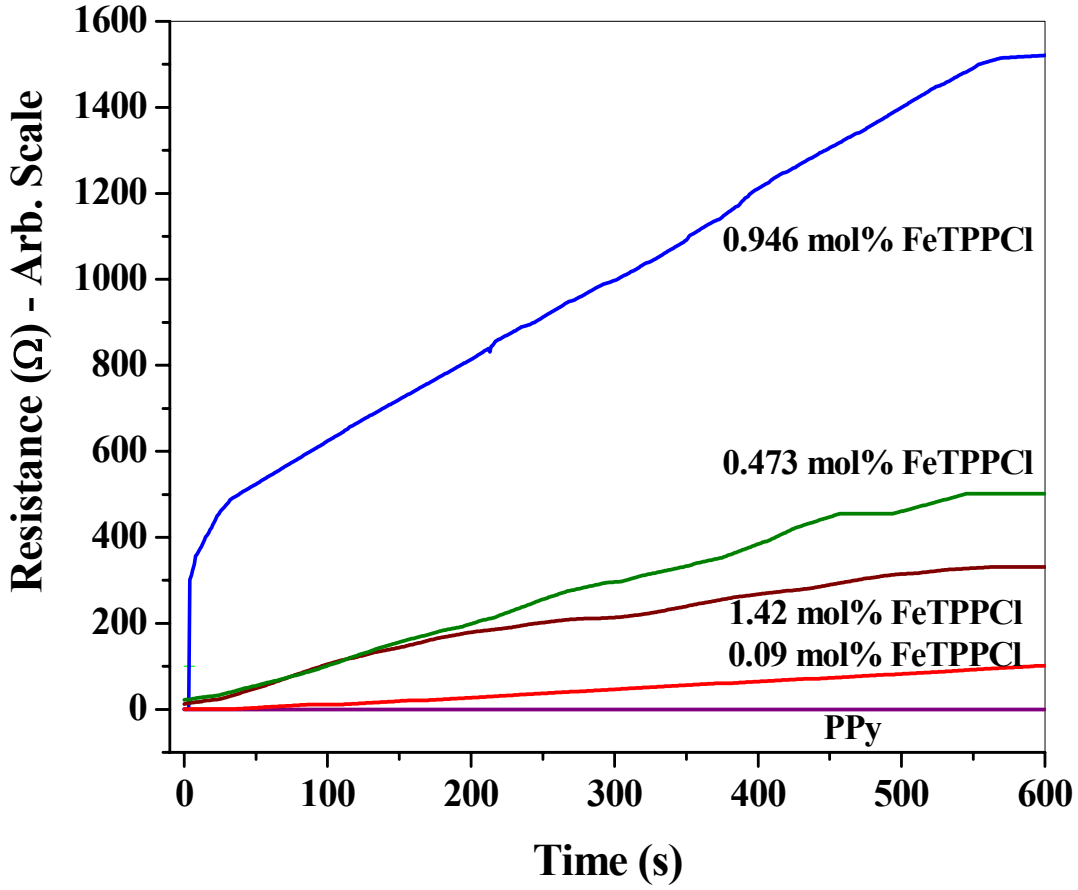

Fig. 5.11. 300 ppm CO gas response of PPy-FeTPPCl samples at RT.

FeTPPCl (mol%)	Resistance, R_0 (Ω)
0.09	2390
0.473	4840
0.946	14200
1.42	23803

Table 5.9. The initial resistance (R_0) of the PPy-FeTPPCl materials on interdigited electrode.

The possible sensing mechanism of these materials towards CO gas as follows:

It is noted here that the resistance of pure polypyrrole decreases slightly when interacting with CO, whereas, FeTPPCl incorporated samples give marked difference in increase of resistance. In case of pure polypyrrole, the hole charge carriers increases during interaction with CO gas, because of the readiness to donate the lone pair of electrons on the nitrogen atom of pyrrole units to incoming CO gas molecules. Hence, the resistance of semiconducting polypyrrole (PPy is p-type semiconductor) decreases slightly. This is a very slow process and only a slight variation in resistance is observed during the interaction with CO, but in case of modified PPy with FeTPPCl, the change of resistance is excellent and exactly opposite to polypyrrole. The sensing mechanism for the doped samples is different than that of pure polypyrrole because of the presence of functional units. Here, CO immediately interacts with iron (not with nitrogen of PPy) and contributes electrons to the vacant metal *d*-orbital of porphyrin and subsequently electronic charge transport takes place from FeTPPCl to polypyrrole. Then the effective hole charge carriers of PPy decreases, which raises the resistance of the material during exposure to CO gas. The importance of modifying PPy with iron porphyrin is to provide more interaction sites for the guest CO gas within the polymer other than nitrogen of pyrrole. It is believed that CO interacts very fast with iron of porphyrin and the interaction makes more opposite charges (electrons), which, gets transferred to the polymer chains and multiplies to give response signal. Obviously, the chances of CO interaction with iron porphyrin modified PPy is higher and repeated experiments show that only a physical interaction takes place between porphyrin and CO molecule [26]. The

repeatability of the sample was tested with in a time interval of 1 min for the subsequent tests. The interaction and electron transfer mechanism for PPy-FeTPPCl is shown in Fig. 5.12.

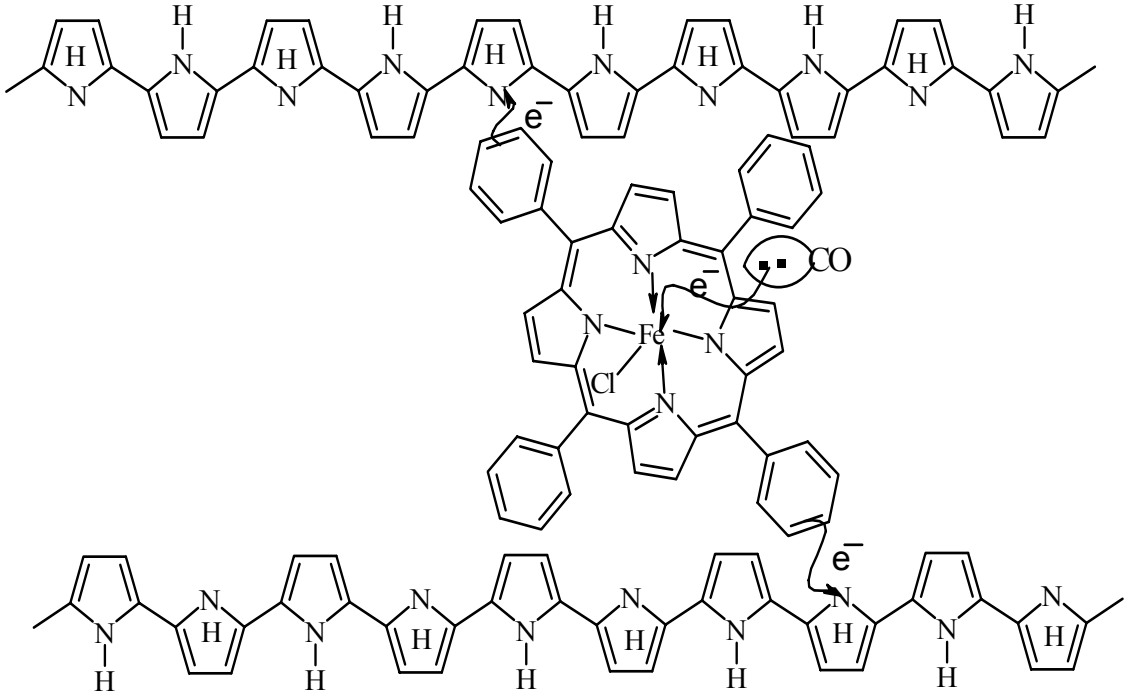

Fig. 5.12. The diagrammatic representation of CO interaction and subsequent electron charge transfer from porphyrin to polypyrrole.

The response factor (dR/R_0 X 100) versus weight percentage of FeTPPCl in PPy is shown in Fig. 5.13. Here, the polymer with 0.946 mol% FeTPPCl is more sensitive to CO than any other composition, which indicates that the response factor is compositional dependent. The response factor for 1.42 mol% of FeTPPCl in PPy sample is lower (4.22) than 0.946 mol% of FeTPPCl (12) which appears to give highest sensitivity. The maximum speed of response determined from the t_{50} value varies with compositions. The lowest response time obtained is 169 s for 0.946 mol% of FeTPPCl in PPy. The speed of response of FeTPPCl doped PPy materials were summarized in Fig. 5.14.

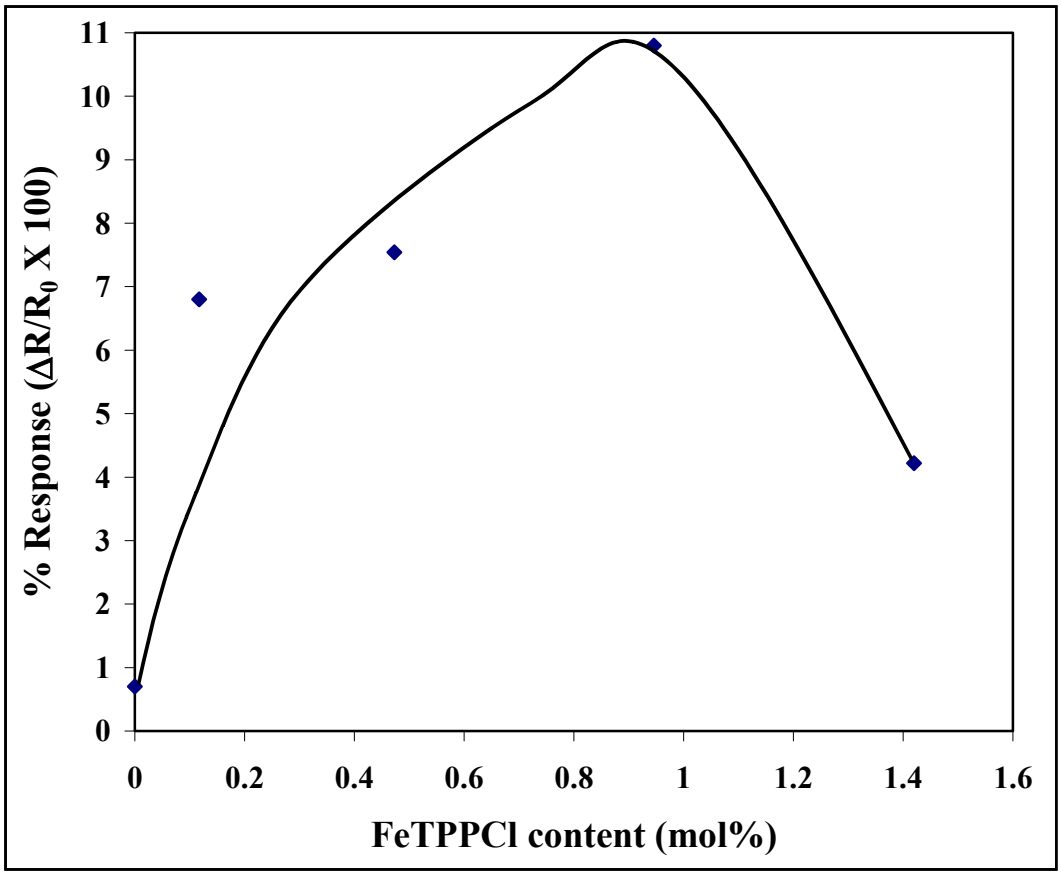

Fig. 5.13. A plot of response factor vs. concentration of FeTPPCl in PPy.

The change of resistance with respect to time (dR/dt) plot indicates that dR value is quite good for the measured period of time. dR is the change of resistance before and after exposure to 300 ppm CO gas and dt is the time taken to occur resistance change for initial 4 minutes. The first 4 min during CO gas exposure is relevant in this case because the maximum change of resistance occurred within that period. The highest change of resistance observed with exposure to CO is 193.75 Ω/min for 0.946 mol% of FeTPPCl in PPy. This is shown in Fig. 5.15. More interestingly, the measurements were carried out at room temperature and in the presence of atmospheric air. All other compositions having resistance change in the range 8–53 Ω/min. This clearly indicates that the sensitivity factor and speed of response to particular gas depends on the particular composition of FeTPPCl in PPy.

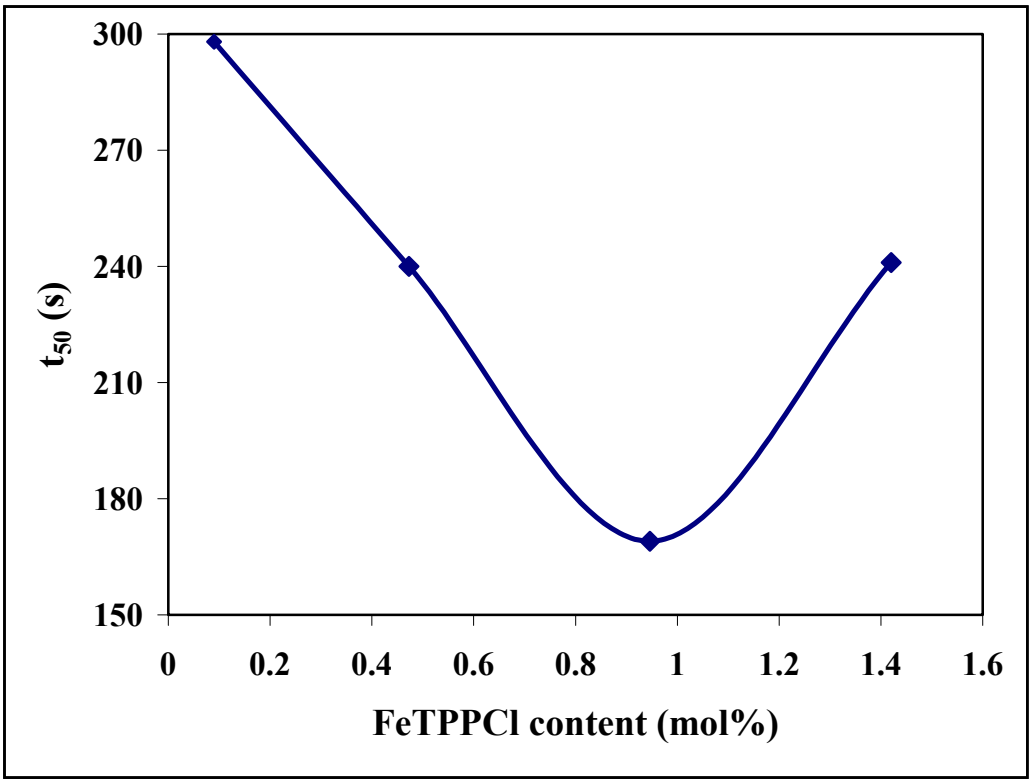

Fig. 5.14. The speed of response (t_{50}) of PPy-FeTPPCl towards 300 ppm CO gas.

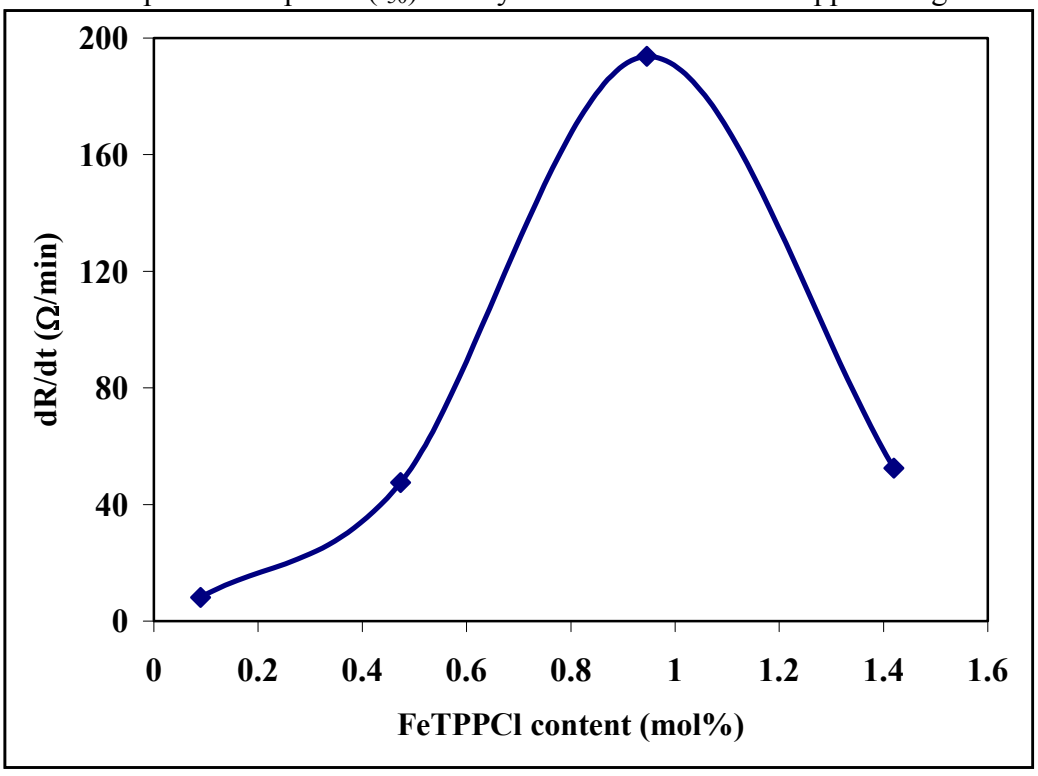

Fig. 5.15. Maximum change of resistance for the initial four minutes of the measurements of 300 ppm CO gas to PPy-FeTPPCl materials.

5.4. Electrochemical Incorporation of FeTPPCl into PPy

The same procedure described in section 4.4.2. is followed here to deposit porphyrin modified PPy films on interdigited electrodes. The thickness of the deposited films depends upon the time of deposition, which was maintained same in all cases. The modified PPy film was characterised by cyclic voltammetry technique. The films from the same set were used for 300 ppm CO gas sensitivity measurements.

The electrochemical system for the deposition of FeTPPCl with PPy films consists of 0.1 M TBAP electrolyte in dichloromethane solvent. The cyclic voltammogram of porphyrin solution in 0.1 M TBAP/DCM is shown in Fig. 5.16., which gives a peak at 0.812 V in the positive scan and another peak at 0.714 V in the negative scan indicating the oxidation and reduction states of iron respectively. Another reduction peak at -0.7 V is due to the porphyrin conjugated structure. The electrochemical reaction was carried out using standard calomel electrode at a scan rate of 0.05 V/s. The potential limit given was $^{+}1$ to $^{-}1$ V.

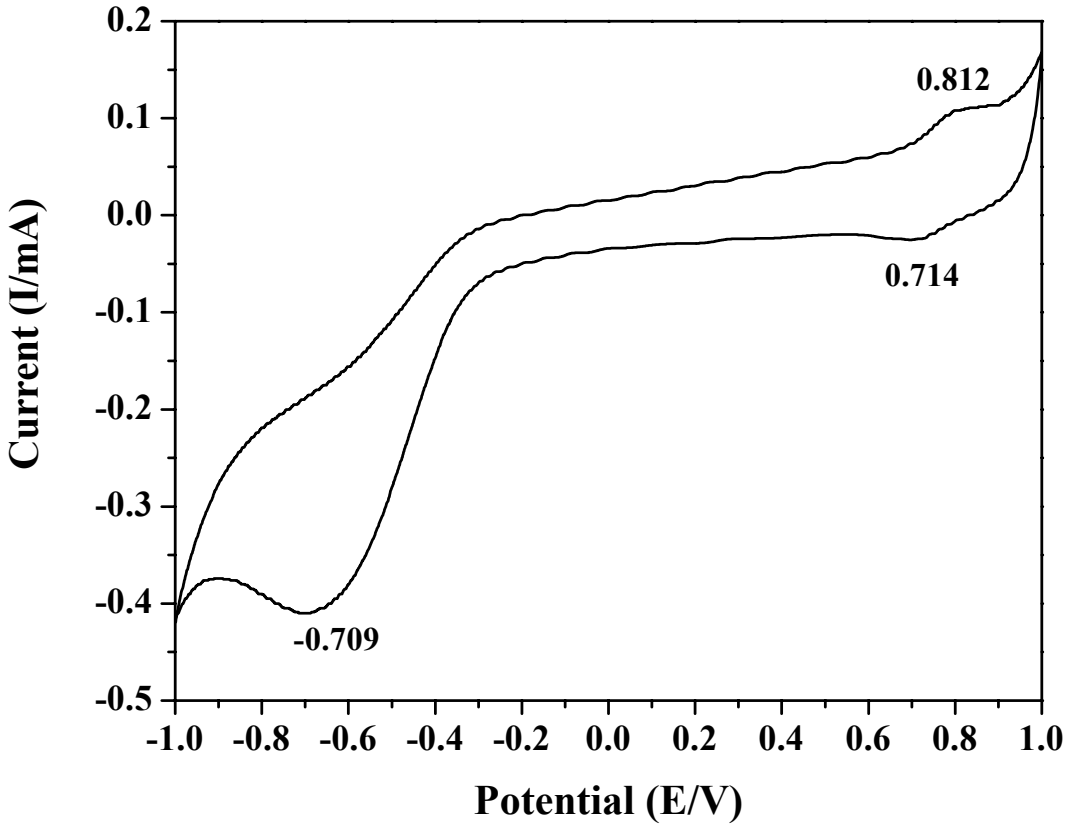

Fig. 5.16. The cyclic voltammogram of porphyrin/DCM solution. Electrolyte: 0.1 M TBAP, Scan rate: 50 mV/s.

The cyclic voltammograms of PPy-FeTPPCl films deposition on Pt plate working electrode was carried out within a potential limit of +1 to -1 V using a standard calomel electrode at a scan rate of 50 mV/s, clearly shows the redox system of porphyrin macrocycle reduction peak at -0.5 V, which is 0.2 V less compared to the peak obtained for pure porphyrin in DCM. Polypyrrole oxidation and reduction peaks are evident at 0.3 V and ¯0.15 V. The current consistently increases for each cycle of deposition is make sure that the material deposited is conducting. It is shown in Fig. 5.17.

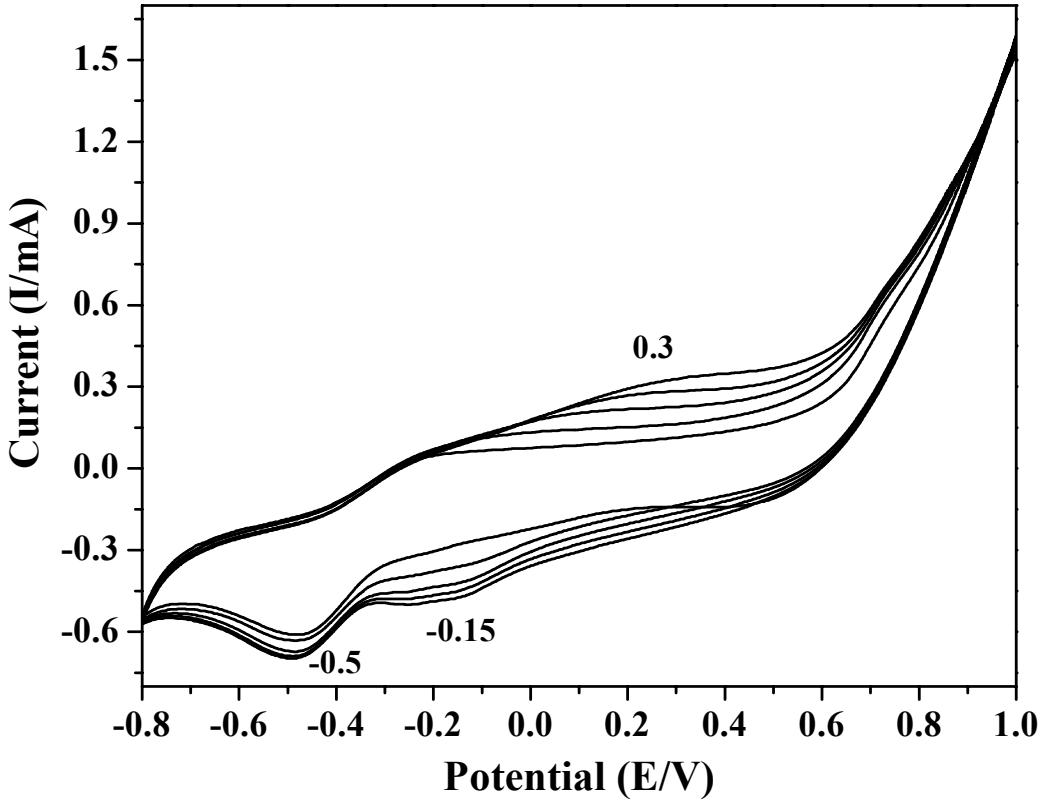

Fig. 5.17. The cyclic voltammogram of PPy-FeTPPCl deposition on Pt plate working electrode in 0.1 M TBAP/DCM system. Standard calomel electrode as reference electrode; scan rate is 50 mV/s.

The cyclic voltammetry of post polymerization films were carried out in 1 M $NaNO_3$ is a clear evidence of the incorporated porphyrin species in polypyrrole. It gives iron oxidation and reduction peaks at 0.78 V and 0.215 V, respectively. The reduction peak for porphyrin conjugated structure was suppressed due to the presence of polypyrrole reduction peak at ¯0.4 V. The electrolyte used was 1 M $NaNO_3$ in de ionised water with

standard calomel electrode. A scan rate of 50 mV/s. was given. Fig. 5.18. shows the cyclic voltammogram of the PPy-FeTPPCl film deposited on platinum electrode.

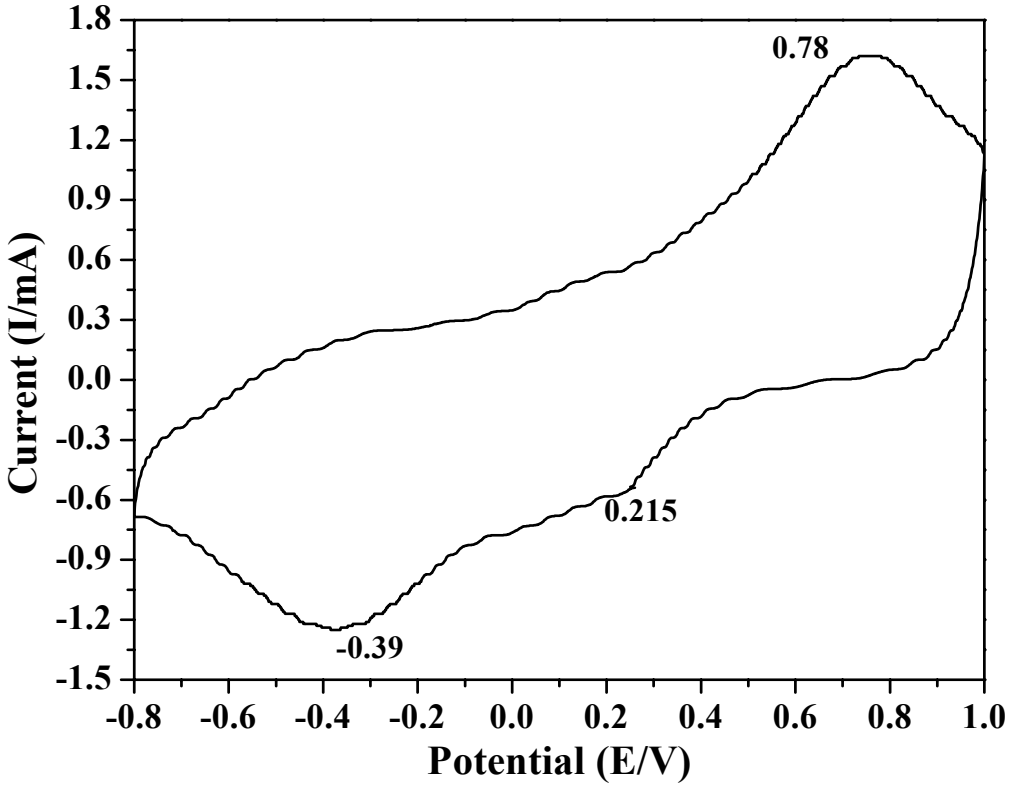

Fig. 5.18. Cyclic voltammogram of PPy-FeTPPCl film deposited on Pt electrode. Electrolyte: 1 M $NaNO_3$ in DI water, scan rate: 50 mV/s;Calomel electrode.

5.4.A. CO Gas Sensitivity Measurement of Electrochemically Modified PPy Films

The surface cells prepared with PPy-FeTPPCl films deposited electrochemically on interdigited electrode containing various concentration levels of FeTPPCl as a secondary incorporated species were tested for their response to 300 ppm carbon monoxide gas in a standard gas calibration bottle. Fig. 5.19 shows the response curve obtained in these cases. The initial resistance offered by the electrochemically deposited films on interdigited electrodes is tabulated in Table 5.10.

Table 5.10. Original resistance of the electrochemically deposited PPy-FeTPPCl films on gold deposited PET interdigited electrode.

FeTPPCl (mmol%)	Resistance, R_0 (Ω)
PPy	16.6
5	13.3
7	10.5
10	5.63

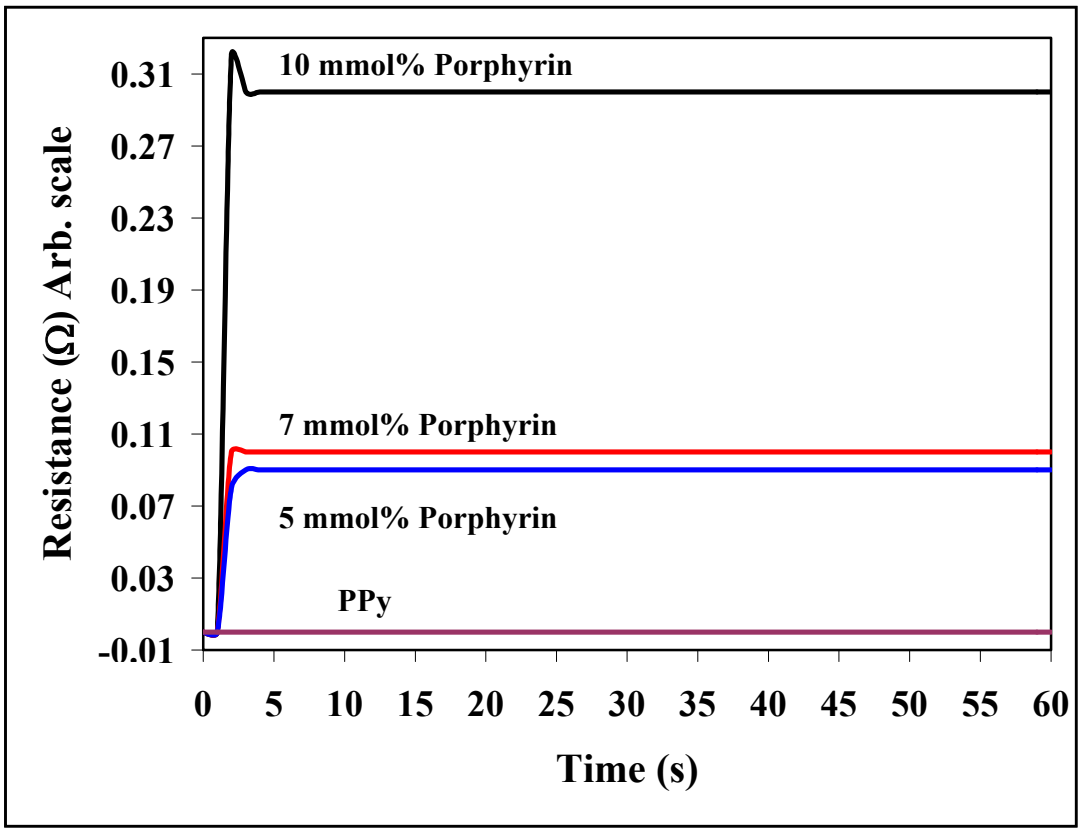

Fig. 5.19. Response curves for the surface cell containing PPy films doped with different concentrations of porphyrin, exposed to 300 ppm CO gas.

The less response for the electrochemically deposited films may be explained as the denser packed structure compared to chemically deposited films. So, the surface phenomenon is more prominent in case of electrochemically deposited films than the bulk phenomenon in chemically synthesized materials. The Fig. 5.19. indicates that the PPy deposited electrochemically with ClO_4^- as dopant alone is not at all sensitive to

carbon monoxide gas, where as, the electrochemically deposited films of PPy-FeTPPCl is giving a sudden response when exposed to CO gas. Further, the change in sample resistance at constant CO level depends on the concentration of the porphyrin moieties present in PPy. Here, it is seen that the sensitivity increases with increasing concentration of porphyrin. The response factor, [($\Delta R/R_0$) X 100], depend critically on the porphyrin concentration. It is found to be highest (4.16%) for 10 mmol% of porphyrin in PPy, while it is practically 0.0 for PPy alone. The response factor (%) vs. composition plot is shown in Fig. 5.20.

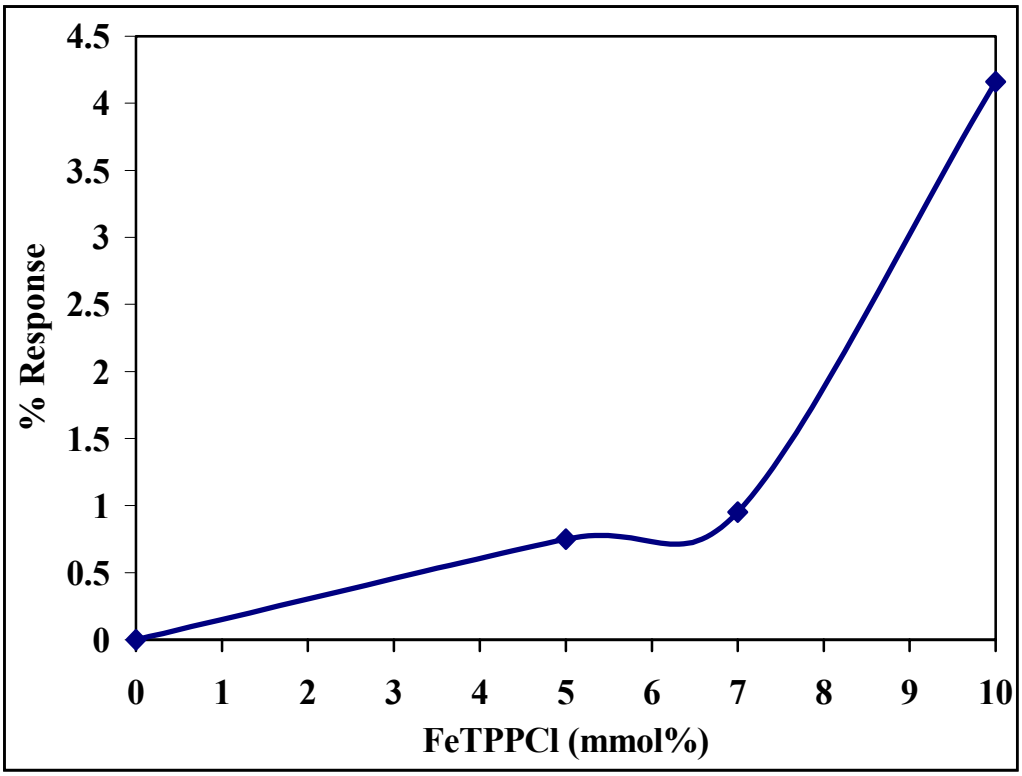

Fig. 5.20. The response factor with respect to composition of PPy containing porphyrin exposed to 300 ppm carbon monoxide gas.

The speed of response (Table 5.11.) determined from the t_{50} value is quite low (0.496 s) in composition of 10 mmol% of porphyrin in PPy film. This may be understood in terms of the number of available sites for interaction when FeTPPCl is present with respect to the amount of CO that can be adsorbed by the PPy film. It should be noted here that CO gas can be detected with even very low concentration of porphyrin in PPy. So, the change of resistance is not very high because of the low concentration of FeTPPCl. Since the material is a dye, there was no attempt made to increase the concentration of FeTPPCl in

the feed because of the high intensity color developed while dissolving it in the solvent. It is interesting to mention here that the sensing of these materials are not taking place due to the interaction with pyrrole nitrogen, but the interaction between guest CO gas and iron porphyrin. The opposite charge carriers (electrons) were generated due to the interaction with porphyrin and which subsequently transferred immediately to polypyrrole chains. This increases the resistance of the material (see Fig. 5.19.). Decrease in conductivity (increase of resistance) when exposed to CO gas, depends on the concentration of porphyrin in the polymer. Hence, CO interaction with FeTPPCl is dominating rather than with pyrrole moieties in the present samples.

FeTPPCl (mmol%)	t_{50} (s)
5	0.504
7	0.503
10	0.496

Table 5.11. The speed of response (t_{50}) of the FeTPPCl modified PPy films to CO gas.

In this case, the response is fast and so the initial 2 s is crucial for the detection of CO gas. The change of resistance (dR) over the initial 2 s (dt) is plotted against mmol% of FeTPPCl in PPy is shown in Fig. 5.21. It is found that 0.16 Ω/s is the highest for 10 mmol% of FeTPPCl concentration in PPy.

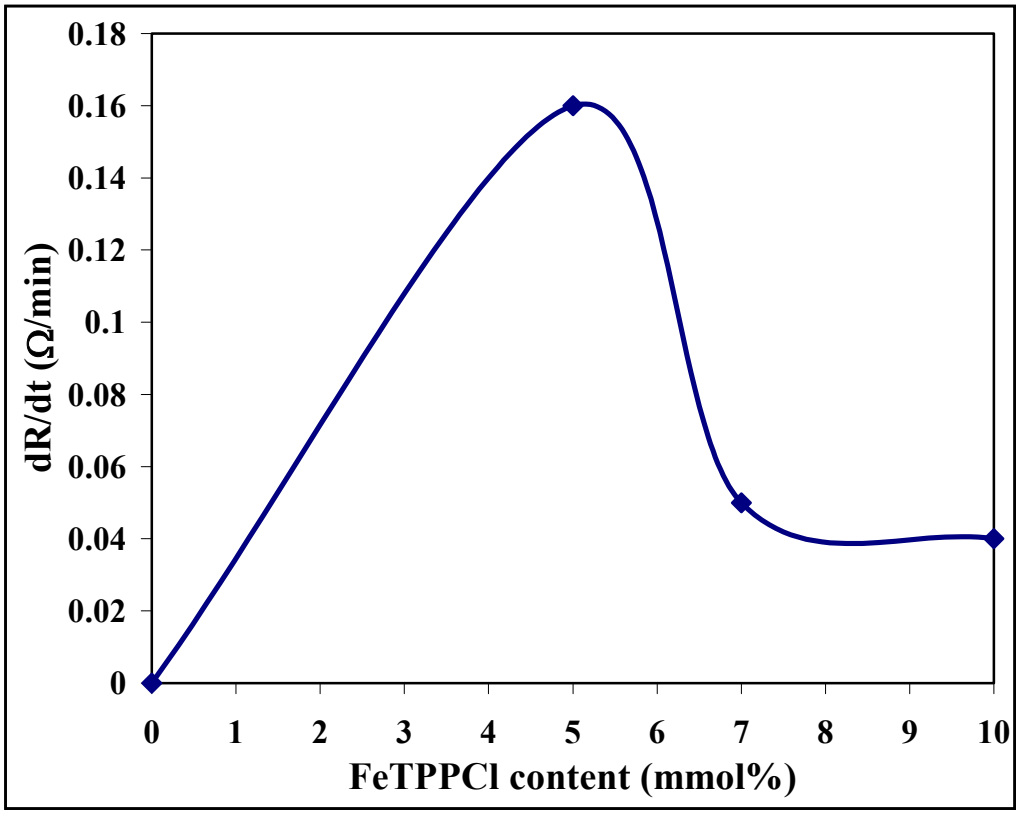

Fig. 5.21. Change of resistance for the initial 2 seconds of the PPy-FeTPPCl materials.

5.5. Conclusions

The incorporation of porphyrin into polypyrrole has been successfully carried out, using both chemical as well as electrochemical method. The conductivity of the different compositions of PPy-FeTPPCl materials prepared is falling in the semiconducting region. Various characterisation techniques like FTIR and UV-VIS spectroscopies were used to confirm the presence of porphyrin in the synthesized polymers. The chemically synthesized PPy shows mainly amorphous nature, which continues to remain after incorporation of FeTPPCl upto 5%. At higher concentration of the porphyrin there is evidence of new crystalline order in the PPy-FeTPPCl materials. TGA, GFAAS and EDAX studies clearly indicates the presence of porphyrin inside the polymer. The conductivity data shows that there is a decrease in conductivity with higher concentration of porphyrin. The temperature dependent conductivities gave activation energy values, which were found to be higher than original PPy which support the observations made in UV-Vis spectroscopy viz. the blue shift of the absorption bands. The net effect of

addition of pophyrin in the PPy polymeric chain is the enhancement of carbon monoxide sensitivity of the polypyrrole. The response factor and speed of response of the materials to CO gas was found to be favourable at certain concentration of FeTPPCl. At higher concentrations of the porphyrin molecules there is aggregate formation and crystalline order, which does not allow the CO gas to diffuse fully and interact with the functional groups. Thus, the sensitivity decreases at higher concentrations of the FeTPPCl due to aggregate formation. The best performance is obtained at a certain concentration of the functional additive.

The electrochemical activity of the PPy is enhanced by the incorporation of porphyrin into the PPy. Further, the carbon monoxide response of these materials was found to be good. The speed of response of the electrochemically synthesised materials is much faster than the chemically prepared samples; it takes only a second or even less as compared to several seconds in latter case. The sensing of CO gas for electrochemically prepared films is mainly due to surface phenomena – the film thickness being about a micron, the gas does not have to diffuse over long distance. Consequently, the number of reactive sites are also less in number as compared to particulate samples of chemically prepared PPy. Further, the only part of the quantity of FeTPPCl added to the electrolyte gets incorporated during ECP deposition. The number of the sensitive sites available in these cases is much less as compared to the chemically synthesized one and hence there is no peak in sensitivity with respect to concentration observed for ECP made samples. Nevertheless, the response characteristic of electrochemically deposited films to CO gas is a demonstration of the detection of CO gas in the presence of even low content of iron porphyrin inside polypyrrole. It may be said that the Fe-porphyrin acts as “sensitizer” for polypyrrole so that it can get activated after exposure to ppm levels of carbon monoxide.

5.6. References

[1] N. Diab, W. Schuhmann, Electrochim. Acta 47 (2001) 265.

[2] F. Bedioui, C. Bongars, J. Devynck, J. Electroanal. Chem. 207 (1986) 87.

[3] U. Johanson, M. Marandi, V. Sammelselg, J. Tamm, J. Electroanal. Chem. 575 (2005) 267.

[4] F. Bedioui**,** Y. Bouhier**,** C. Sorel, J. Dewynck, L. C. Guerente, A. Deronzier, J. C. Moutet, Electrochim. Acta, 38 (1993) 2485.

[5] K. Okabayashi, O. lkeda, H. Tamura, J. Chem. Soc. Chem. Commun. 684 (1983).

[6] O. Ikeda, O. Okabayashi, N. Yoshida, H. Tamura, J. electroanal. Chem. l91, 157 (1985).

[7] F. Bedioui, C. Bonaars, J. Devvnck, C. B. Charreton, C. Hinnen, J. Electroanal. Chem. 207 (1986) 87.

[8] A. Deronxier, J. M. Latour, J. electroanal. Chem. 224 (1987) 295.

[9] F. Bedioui, A. Merino, J. Devynck, C. E. Mestres, C. B. Charreton, J. electroanal. Chem. 239 (1988) 433.

[10] C. Annengaud, P. Moisy, F. Bedioui, J. Devynck, C. B. Charreton, J. Electroanal. Chem. 277 (1990) 197.

[11] A. Deronzier, R. Devaux, D. Limosin and J. M. Latour, J. Electroanal. Chem. 319 (1991) 347.

[12] G. Ramachandraiah, F. Bedioui, J. Devynck, M. Serrar, C. B. Charreton, J. Electroanal. Chem. 319 (1991) 395.

[13] R. W. Murray in A. J. Bard (Ed.), Electroanalytical Chemistry, Vol. 13, Marcel Dekker, New York, 1984, pp. 191-368.

[14] T. A. Skotheim (Ed.), Handbook of Conducting Polymers, Marcel Dekker, New York, 1986, Vols. 1 and 2.

[15] O. Ikeda, K. Okabayashi, H. Tamura, Chem. Lett. (1983) 1821.

[16] T. Skotheim, M. V. Rosenthal, C. A. Linkous J. Chem Soc. Chem. Commun. (1985) 612.

[17] C. Sun, J. Zhao, H. Xu, Y. Sun, X. Zhang, J. Shen, Talanta 46 (1998) 15.

[18] Ivan S. Silbor, "Anion sensing, Topics in current chemistry", Springer, 2005 p-102.

[19] R. C. Frederick, The Analyst 666 (1931) 561.

[20] B. Tion, G. Zerbi, J. Chem. Phys. 92 (1990) 3892.

[21] M. Han, Y. Chu, D. Han, Y. Liu, J. Colloid Interf. Sci. 296 (2006) 110.

[22] J. Lei, W. Liang, C. R. Martin, Synth. Met. 48 (1992) 301.

[23] R. G. Davidson, T. G. Turner, Synth. Met. 72 (1995) 121.

[24] D. W. Thomas, A. E. Martell, J. Am. Chem. Soc. 81 (1985) 5111.

[25] J. L. Hoard, G. H. Cohen, M. D. Glick, J. Am. Chem. Soc. 89 (1967) 1992.

[26] J. R. Hill, C. J. Ziegler, K. S. Suslick, D. D. Dlott, C. W. Della, M. D. Fayer, J. Phys. Chem. 100 (1996) 18023.

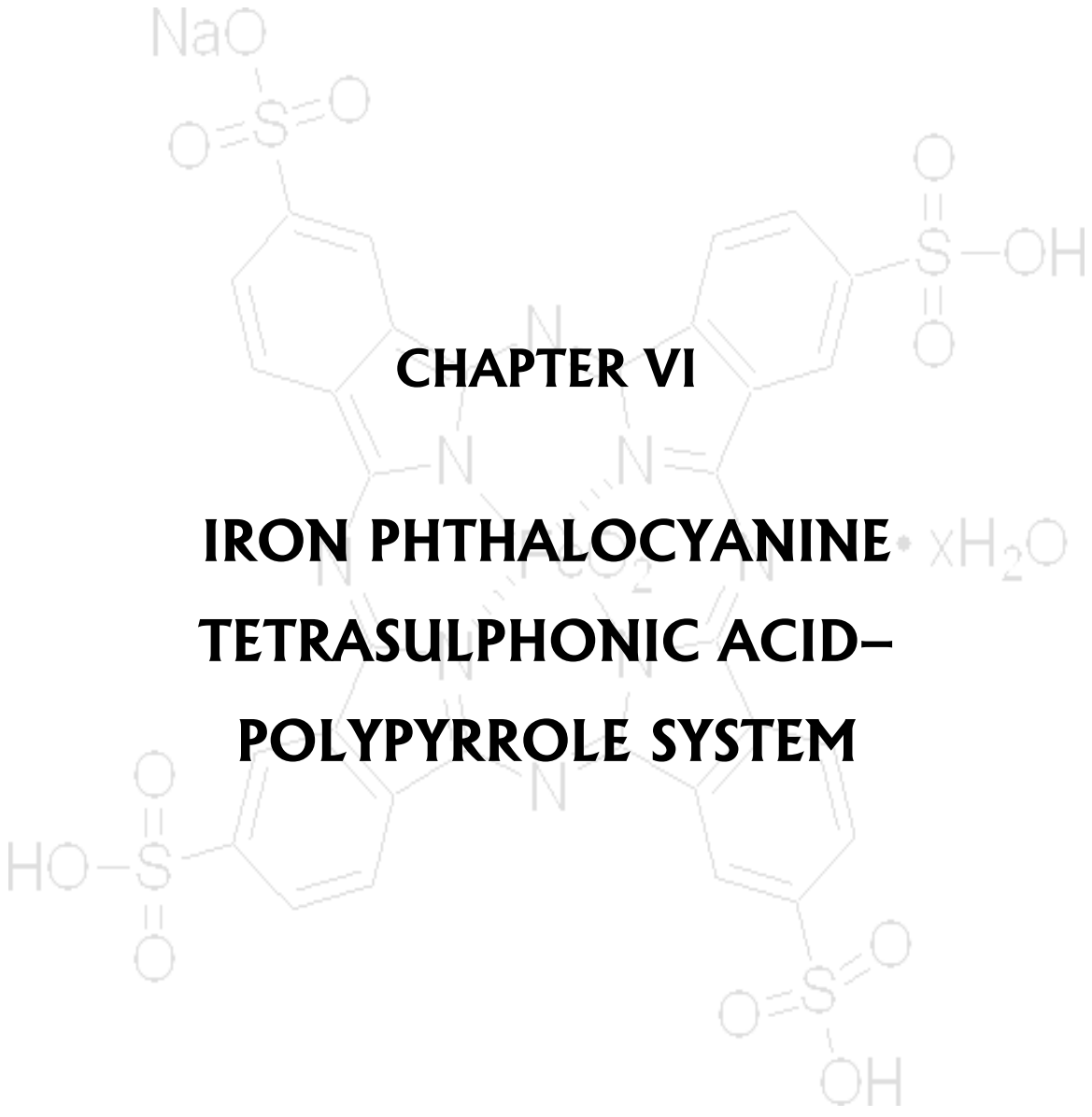

CHAPTER VI

IRON PHTHALOCYANINE TETRASULPHONIC ACID–POLYPYRROLE SYSTEM

6.1. Introduction

Macrocyclic phthalocyanine compounds have found many technological applications in microelectronics, gas sensing, modified electrodes for catalysis and as photoresponsive materials [1–3]. This wide range arises from their unique, specific properties such as semiconductivity, well-defined redox activity and high thermal stability etc. However, most non-substituted phthalocyanines are poorly soluble, and therefore film fabrication has relied on vapor deposition techniques. To overcome this difficulty, metallic phthalocyanines with appropriate chemical groups have been synthesized, in particular, incorporation of sulphonic acid groups to metallic phthalocyanine will make it soluble. Such a water soluble tetra sulphonated phthalocyanine is used to incorporate into polypyrrole. Using phthalocyanines in the form of thin films has some advantages, but for large scale applications especially in the form of micro electro machined devices (MEMs) or electronic nose as well as low cost disposable sensors, it is essential to fabricated the sensors by simpler method such as solution spinning, dipping, micro-drop coating etc. Also, the phthalocyanines without doping have fairly high electrical resistivity (> 10^7 Ohm-cm), though they are termed semiconductors. This gives rise to high sample resistance in surface cell mode requiring high input impedance detector circuits. On the other hand, inherently conducting polymers such as polypyrrole (PPy), polyaniline have low resistance values and also give some sensing response to different gases. It is essential to improve the performance of PPy as regards sensitivity, selectivity and speed of response for applications in practical sensors.

A great deal of interest has been generated to the electrochemical preparation of a number of polypyrroles, using a variety of ionic complexes and polyelectrolytes as the electrolytes. These polyelectrolyte or ionic complexes mainly serve as charge balancing dopant anions during electropolymerization. This has led to a new class of multicomponent materials with controllable electrical, mechanical, electrochemical, catalytic ion-binding and ion-releasing properties. Several polymeric composites were prepared using this strategy and those include preparation of PPy containing Ru-bipyridine complexes [4], naphthoquinone and benzoquinone groups [5], complexes with metallotetraphenyl-porphyrin [6] and phthalocyanine complexes [7] etc.

Metal phthalocyanine complexes have found many technological applications in microelectronics [8, 9], electronic tongue [10], gas sensing [11–15], modified electrodes for catalysis [16], oxygen reduction [17, 18], biosensors [19], photoresponsive materials [20] etc. The phtalocyanines based gas sensors are used for pollution control measuring low concentrations of pollutant gases in air, generated by motor vehicle or industrial emissions and for detection of nitrogen oxide in human body [21, 22]. This versatility of these materials arises from their unique, specific properties such as semiconductivity, well-defined redox activity and high thermal stability. Since, phthalocyanines are p-type semiconductors, the electron transfer from semiconductor to gas leads to an increase in their electrical conductivity [23–28]. However, in conventional gas sensors, which are constructed from inorganic semiconductors such as SnO_2, sufficiently high adsorption and desorption rates of gas at room temperature have not been achieved. The operating principle of the gas sensors is based on the change in conductivity due to the chemisorption/physisorption of gas molecules at the sensitive layer surface. Metal phthalocyanine films have been extensively used as chemical sensors by measuring changes in conductivity when a gas is adsorbed at the surface [29]. There are a few reports available in the literature for the incorporation of phthalocyanines into polypyrrole [30–32].

The present chapter focused mainly on the effect of incorporation of phthalocyanine into polypyrrole for the application of CO gas sensor. The codopant, iron(III) phthalocyanine tetrasulphonic acid monosodium salt (FePcTSA) was incorporated by insitu polymerization technique. There are two methods used to synthesize these materials namely: (i) Chemical and (ii) Electrochemical polymerisation. The detailed study of synthesis, characterisation, electrical properties and application as CO gas sensor are presented in detail.

6.2. Experimental

6.2.A. Chemical Functionalisation

The typical reaction as follows: To a well stirred solution of 10 mg (1% by wt. of pyrrole) FePcTSA with 1.62 g (0.1 M) anhydrous ferric chloride in 100 ml distilled water, 1 ml Py (silica column purified) was added with continued stirring. As soon as addition of pyrrole

progresses, the initial yellow-orange colour of the solution becomes progressively dark. After about an hour, the solution becomes colourless and black precipitates of modified polypyrrole were precipitated at the bottom of the reaction flask. The stirring continued for another three more hours at room temperature to ensure complete oxidation of pyrrole monomer into polymer and incorporation of FePcTSA into polypyrrole. It was filtered through a Whattman filter paper and the first filtrate was collected and UV-Vis. spectroscopy of the same was recorded. The residual black colored PPy doped with FePcTSA was washed well with distilled water and dried at 50^0C; yield is 362 mg. In a similar set of experiments, varying amounts of phthalocyanine [FePcTSA] were added to the reaction mixture ranging from 1 to 15 weight percent with respect to pyrrole monomer, the other conditions being same as above. The polymers were dried at room temperature for 48 h and then they were preserved in a vacuum desiccator.

6.2.A.a. Real Time Monitoring of Polymerisation Reaction

The real time UV-Vis. spectroscopy of the polymerization reaction of polypyrrole along with the incorporation of FePcTSA into PPy was recorded. Very dilute solutions were quantitatively prepared and used for this measurement in a disposable UV-Vis. cuvette and spectra were continuously monitored as a function of reaction time. A brief description of the reaction procedure as follows:

1 wt.% of Py-FePcTSA reaction – The following quantities of the reactants were dissolved in appropriate quantities of distilled water; 5 mg FePcTSA in 50 ml, 1 ml pyrrole in 100 ml and 0.81 g anhydrous ferric chloride in 50 ml. 100 µl FePcTSA of the above stock solution was added into 2 ml distilled water taken previously in a disposable UV-Vis. cuvette and spectrum of the same was recorded. It was mixed thoroughly with 100 µl of above prepared solution of $FeCl_3$. Then the online monitoring of the polymerization reaction was started with the addition of 100 µl of above prepared pyrrole solution into it. Polypyrrole synthesis in distilled water was also monitored under the same way. The spectra were recorded with respect to time and discussed under section 6.3.A.a.ii.

6.2.B. Electrochemical Functionalisation of PPy with FePcTSA

Initially, PET transparencies were gold deposited by thermal evaporation technique (in vacuum). Interdigited electrodes were made with these gold coated substrates and activated with 1 M $FeCl_3$ solution for 32 h and used for deposition of PPy-FePcTSA films for CO sensing measurements. Platinum electrodes were also used as working electrodes for deposition of modified PPy films.

A stock solution of 6 mg (0.2 mmol) FePcTSA in 25 ml was made. 70 µl pyrrole was added to 10 ml of above solution and chronoamperometry was performed immediately after the addition of 100 µl conc. H_2SO_4 as electrolyte. Chronoamperometry experiments were carried out at 0.85 V and current flowing through electrode was measured for 30 s. The stock solution was made to desired amounts of FePcTSA, say 0.18 mmol, 0.14 mmol, and 0.1 mmol with respect to pyrrole and the above reaction was carried out under the same conditions. The electrolytic cell comprised of a single compartment cell containing SCE (Saturated Calomel electrode), platinum foil as a counter electrode and gold coated PET interdigitated substrates as a working electrode.

The deposited films were then rinsed thoroughly in distilled water a number of times. The films were allowed to dry at room temperature for 24 hours. The cyclic voltammetric measurements were recorded in 0.1 M TBAP/CH_3CN system.

6.3. Results and Discussions

6.3.A. Characterization

6.3.A.a. UV-Vis. Spectroscopy

The quantitative analysis of the FePcTSA incorporated into PPy was done by UV-Vis. spectroscopy technique. This has been done by recording the spectrum before and after the reaction. It is observed that the color of the filtrate after the reaction is a slight pale yellow, where as the FePcTSA solution before the reaction looks intense blue (phthalocyanine dye color) in color. The characteristic λ_{max} of FePcTSA obtained at 640 nm region vanishes after the reaction and a new absorption band arises at 460 nm; this peak is reported as oligomeric formation of pyrrole [33].

The online monitoring of pyrrole polymerization and reaction between 1 wt.% FePcTSA-Py in aqueous system is shown in Figures 6.1.A. and 6.1.B., respectively. It is clear from

the spectra that a prominent *d-d* transition at 380 nm is due to transition metal, iron. It is observed that the polymer starts coating on inside walls of the cuvette as time progresses. The increase in absorbance at λ_{max} 800–900 nm region during polymerization process ensures semiconducting nature of the polymer. When the concentration of FePcTSA is more, the polymerization reaction completes faster. This is observed with saturation of OD from the Figures (see spectra 5.1.A., 5.1.B.). Polypyrrole formation takes 4 h to complete the reaction, where as 1 wt.% PPy-FePcTSA system takes only 2 h to complete the modification of PPy.

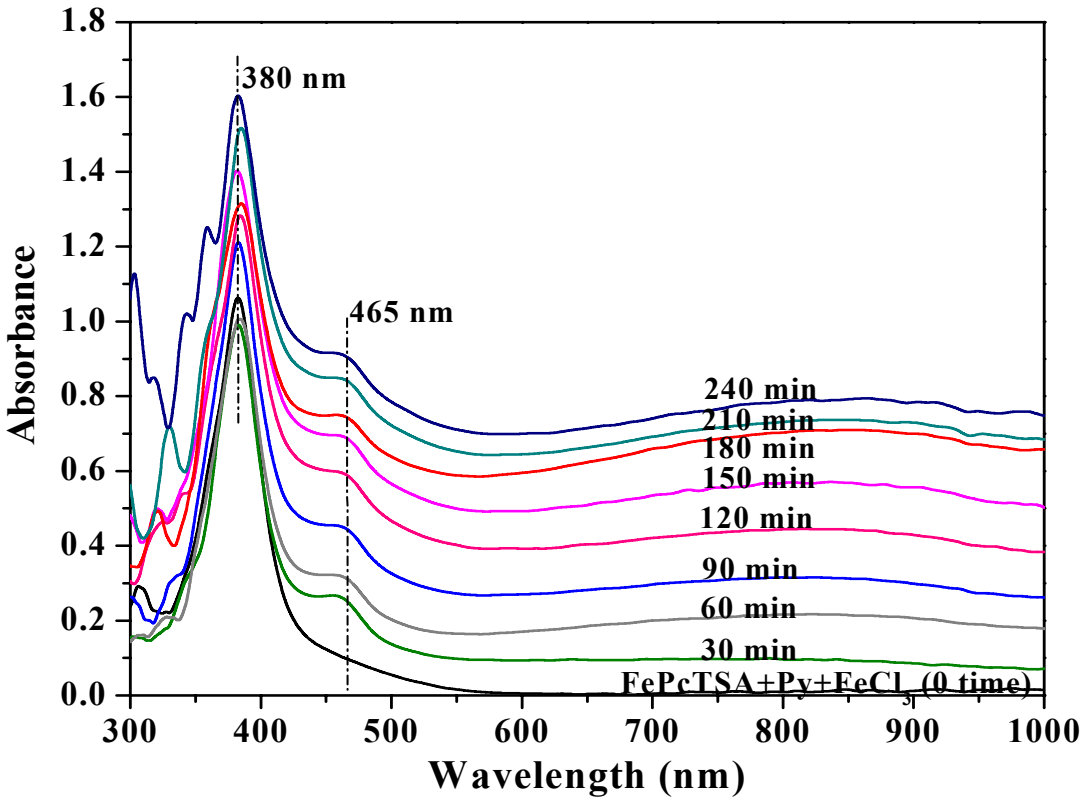

Fig. 6.1.A. Real time UV-Vis. spectroscopic monitoring of PPy synthesis in water.

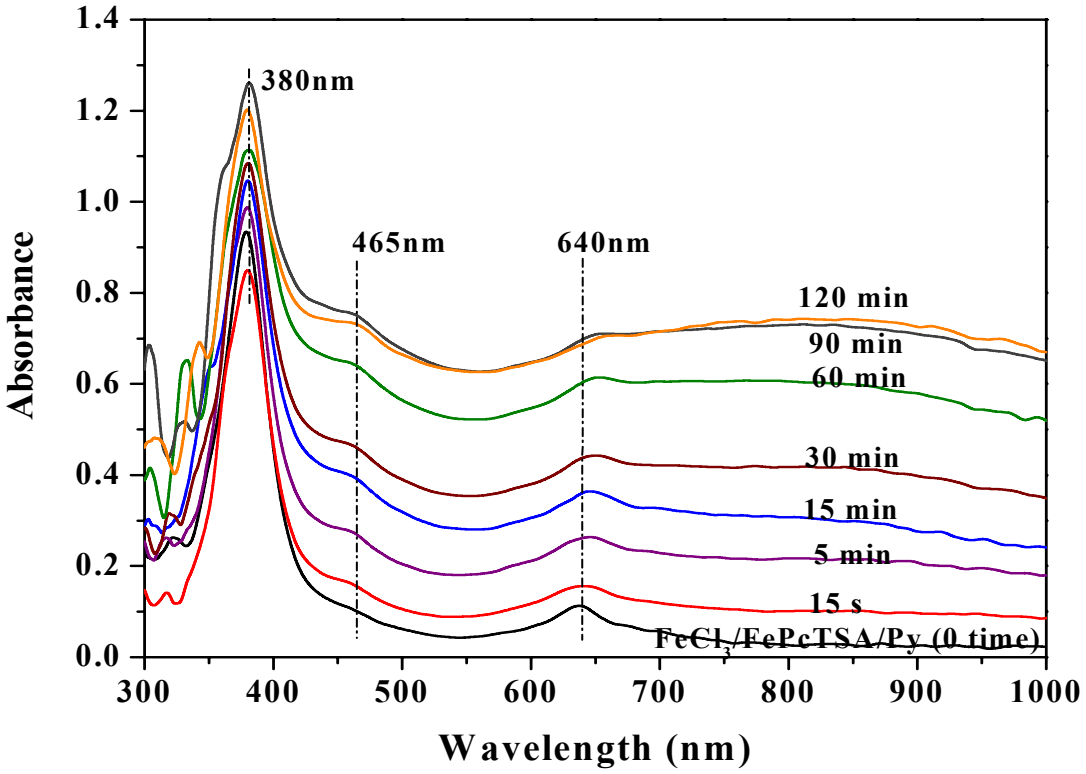

Fig. 6.1.B. Real time UV-Vis. spectroscopic monitoring of 1 wt.% FePcTSA-Py system.

From the real time UV-Vis. spectra of PPy and 1 wt.% Py-FePcTSA, the oligomeric formation is very much evident in PPy synthesis with a λ_{max} at 465 nm. This peak evolves within 5 minutes in case of pure PPy synthesis and 15 s taken for 1 wt.% Py-FePcTSA system. This suggests that more pyrrole oligomeric species are available in the PPy system and it is a slow process compared to the other case. The rise of absorbance in the wavelength region 800–900 nm is normally attributed to the formation of bipolaronic band [34].

The rate of the reaction was calculated from the time dependent polymerization reaction. The rate of PPy/modified PPy formation is considered. The OD at 800 nm gives the formation of polypyrrole [C], which is ploted against particular time is shown in Fig. 6.2. The conversion scale was normalized to get exact change in concentration, $[(OD_t-OD_0) / OD_{max}]$ and ploted against time (Fig. 6.3.). The slope of the above straight line plot (log-log scale) gives rate of the reaction. It is found that the rate of PPy synthesis is less than the system containing FePcTSA in the present case. The rate of the reaction for PPy is 4.37×10^{-3} and 9.26×10^{-3} for 1 wt.% Py:FePcTSA reaction.

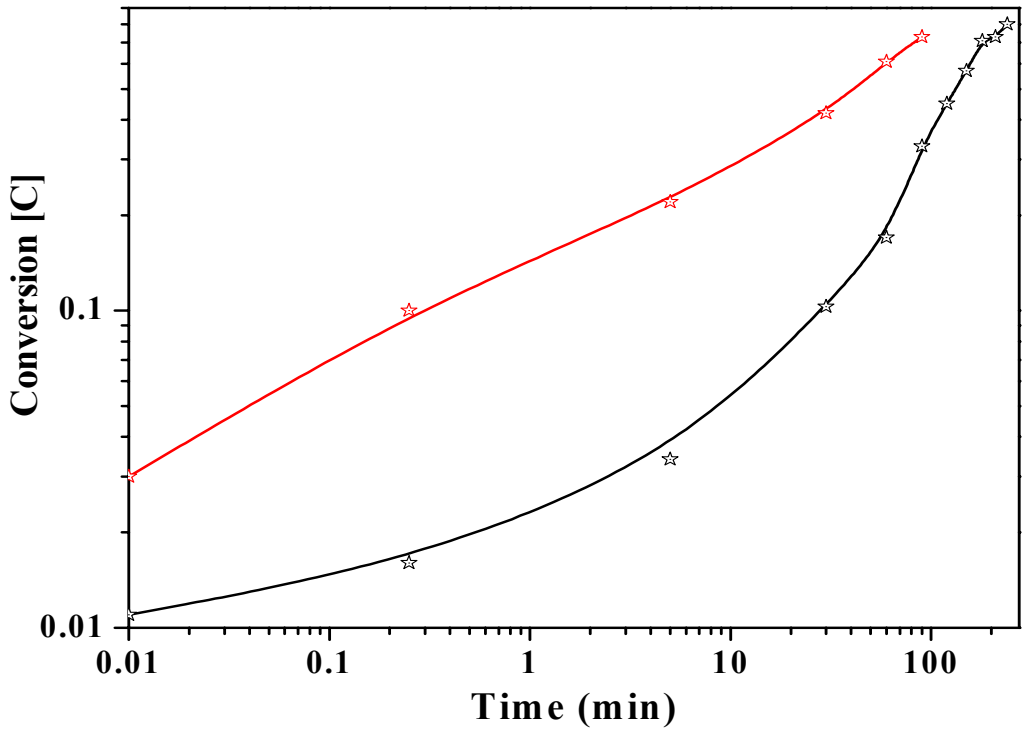

Fig. 6.2. Polymer conversion from monomer [C] at particular time, t.

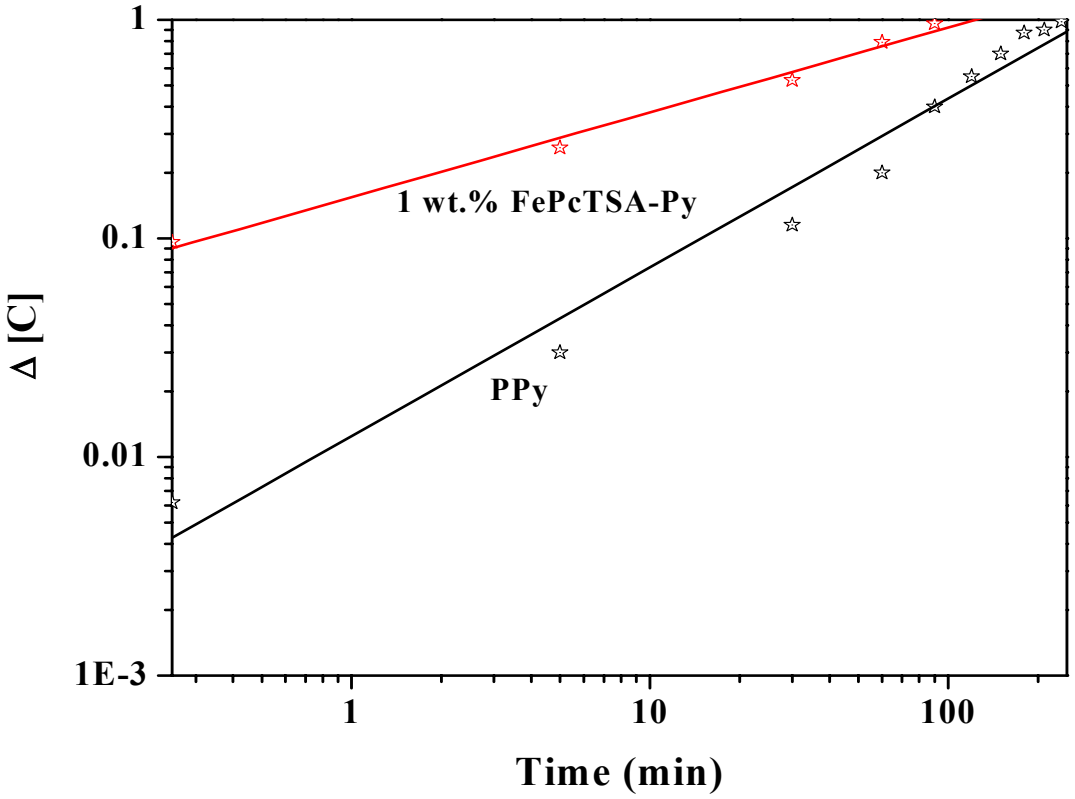

Fig. 6.3. Rate of the reaction from the slope of log [C] vs. log t plot.

The spectra of various compositions clearly show that the λ_{max} of filtrates at 460 nm exhibits a gradual decrease in intensity with increase of concentration of FePcTSA. This evidence concludes that the conversion of pyrrole monomer to polypyrrole is very efficient and fast in the presence of FePcTSA. The reaction yield presented in Table 6.1. provides strong support to this observation. The spectra of the filtrates were recorded and shown in Fig. 6.4. This indicates that the whole amount of various weight percentages (1–10 wt.% with respect to pyrrole) of FePcTSA added into the reaction system is getting doped with polypyrrole during chemical reaction.

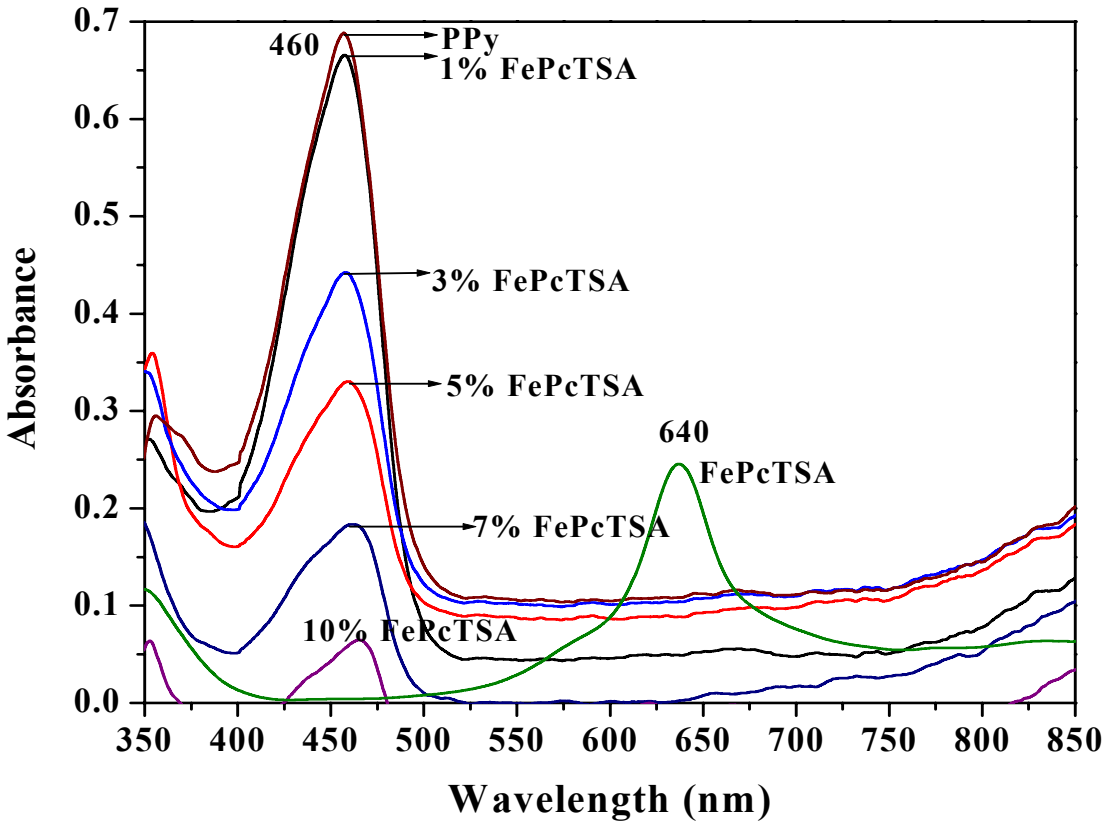

Fig. 6.4. UV-Vis. spectra of the filtrates after completion of polymerization reaction of PPy with FePcTSA.

Quantity of the reactants taken				OD for the filtrate at 460 nm	Yield (g)
Pyrrole (ml) (0.0145 mol)	Anh. $FeCl_3$ (g)	FePcTSA			
		wt.% w.r.t Py	mol w.r.t. Py		
1	1.62	0	Nil	0.689	0.289
1	1.62	1% (10 mg)	7.1×10^{-4}	0.681	0.362
1	1.62	2% (20 mg)	1.42×10^{-3}	0.665	0.373
1	1.62	3% (30 mg)	2.1×10^{-3}	0.439	0.411
1	1.62	4% (40 mg)	2.84×10^{-3}	0.325	0.435
1	1.62	5% (50 mg)	3.55×10^{-3}	0.182	0.453
1	1.62	10% (0.1 g)	4.26×10^{-3}	0.059	0.609

Table 6.1. Summary of FePcTSA modified reaction interms of reactants taken, λ_{max} of filtrates and yield of the product obtained.

1 mg of the various compositions of PPy modified powders were added into 10 ml NMP and sonicated for 4 h. It was filtered and UV-Vis. spectra of the dissolved portion was recorded is given in Fig. 6.5. The λ_{max} obtained for the bipolaronic region of PPy-FePcTSA is tabulated and given in Table 6.2. A red shift is observed for phthalocyanine peak in the modified PPy samples at 658 nm region (640 nm for pure FePcTSA) for 10 wt.% and 15 wt.% PPy-FePcTSA samples suggests an effective modification of PPy was taken place with the incorporation of FePcTSA. It also suggests that the possibility of phase separation of phthalocyanine when exceeds an optimum concentration. The spectra clearly show the increase of solubility with increasing content of phthalocyanine.

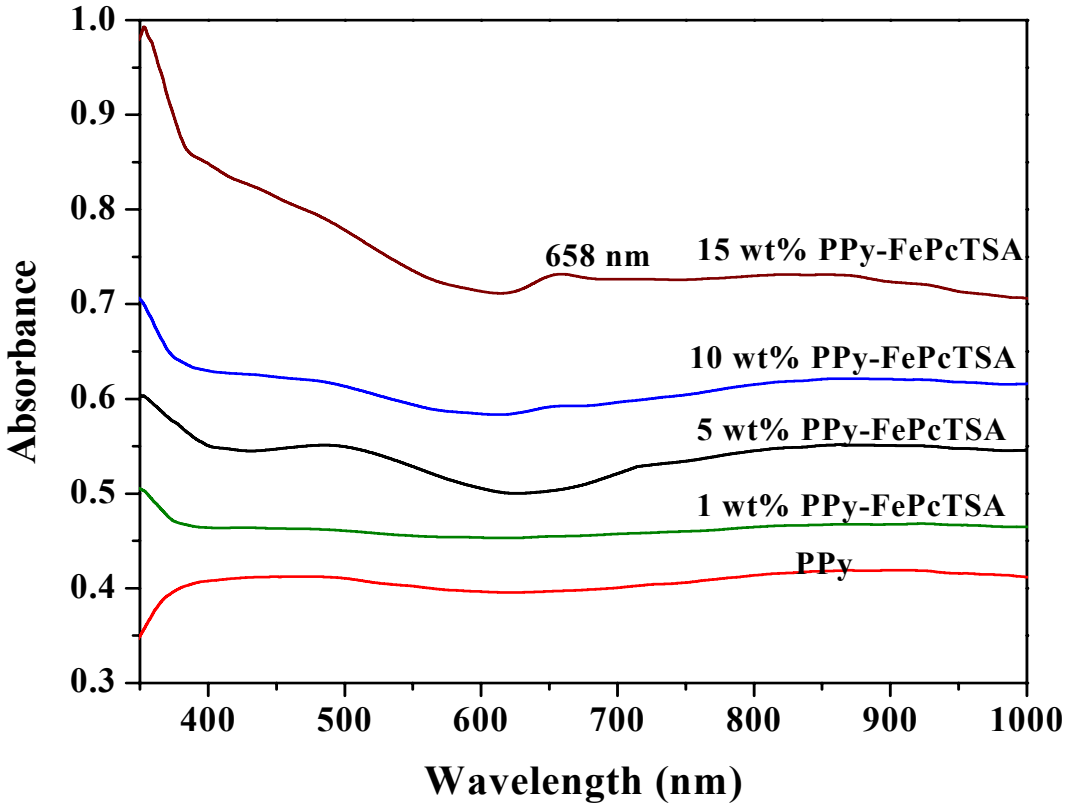

Fig. 6.5. UV-Vis. spectra of polypyrrole and polypyrrole doped with FePcTSA in different compositions.

Compositions Wt.% of FePcTSA w.r.t. Py	λ_{max} at bipolaronic region
1	888
5	889
10	870
15	860
PPy	886

Table 6.2. Wavelength of maximum absorption for PPy and PPy-FePcTSA materials.

6.3.A.b. FTIR Spectroscopy

The functionalization of pyrrole with phthalocyanine was confirmed with FT-IR analysis of these polymers. The FT-IR spectrum for the solid samples of pure FePcTSA and polypyrrole containing phthalocyanine in KBr are compared in Fig. 6.6.A. and 6.6.B. respectively (see section 3.3.A.ii. for PPy spectrum). The % transmission peaks observed and their possible assignments are tabulated in Table 6.3. The values obtained for the PPy and FePcTSA skeletal modes are well matched with the reported values of PPy [35] and characteristic vibrational peaks of FePcTSA, [36] respectively. Usually sulphonic acid groups give four major characteristic peaks in the region 1230–1030 cm^{-1} and 3450–3000 cm^{-1} [37]. The polymers exhibit IR bands at 3436, 1455, 1147, 1110, 1040, 746 and 700 cm^{-1}, which are assigned to the sulphonic acid groups and phthalocyanine skeletal motions. Additionally, the 1556, 1464, 1305, 1192, 1094, 968, 925, 788, 721, and 682 cm^{-1} bands are also seen which are characteristic bands of polypyrrole.

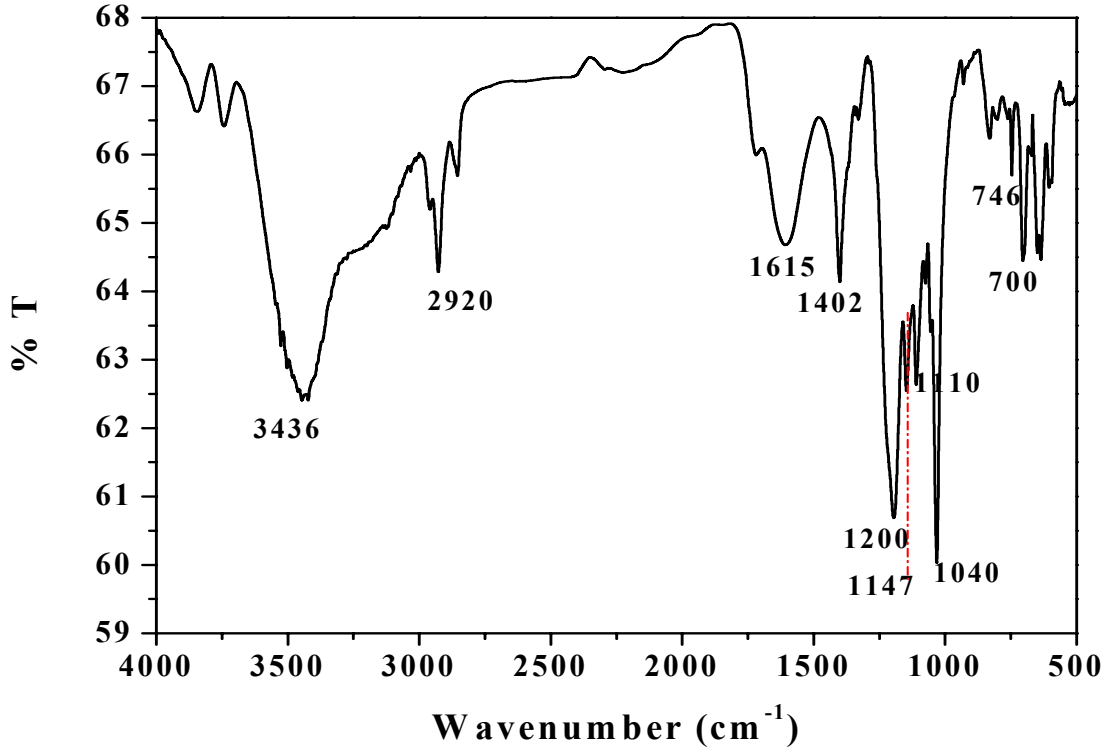

Fig. 6.6.A. FTIR spectrum of pure FePcTSA (KBr).

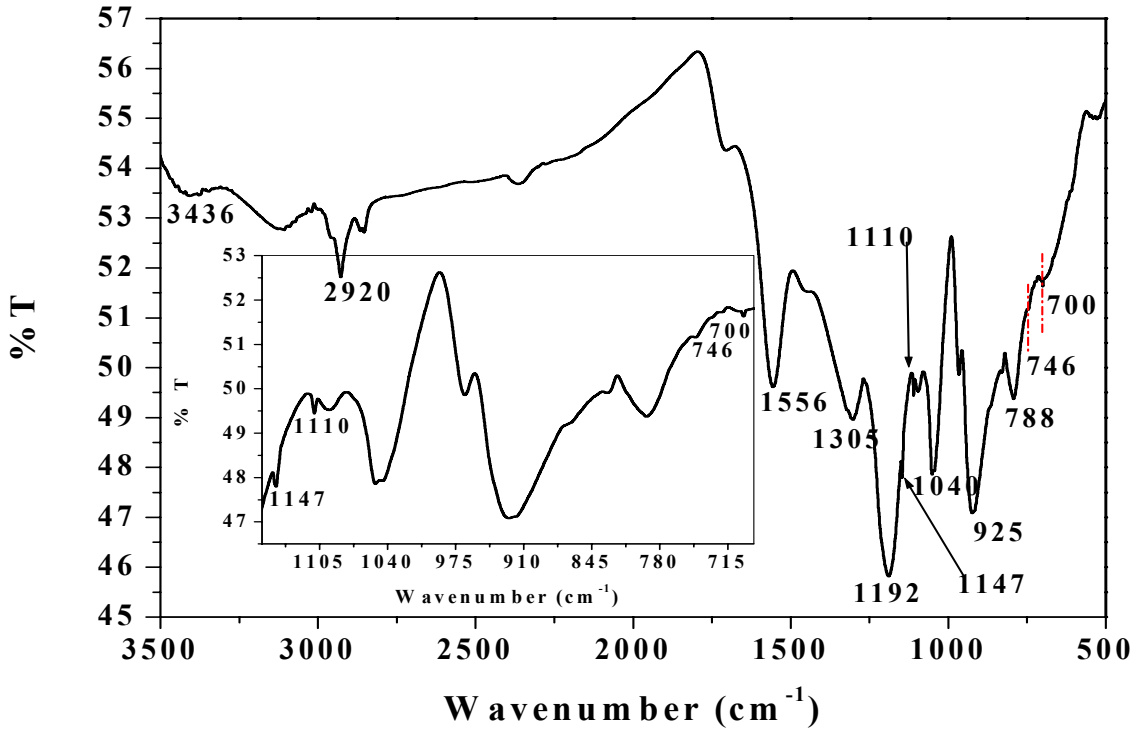

Fig. 6.6.B. FTIR spectrum of PPy-FePcTSA (KBr).

Sample	υ_{max} (cm^{-1})	Peak assignments
FePcTSA	3436	-S-Phenyl vibration
	2920	Methyne –CH stretch
	1615	Aromatic ring stretch
	1402	Organic sulphate
	1200	-CN stretch
	1147, 1110	$–SO_3H$
	1040	Sulphate ion
	746	-CH deformation of benzene
	700	Aromatic ring stretch
PPy-FePcTSA	3436, 2920, 1147, 1110, 1040, 746, 700	Phthalocyanine
	1556, 1305, 1192, 925, 788	Polypyrrole

Table 6.3. FTIR peak assignments of FePcTSA doped PPy material.

6.3.A.c. X-ray Diffraction Studies

The XRD patterns of the PPy and FePcTSA doped PPy did not exhibit any well defined peaks (see Fig. 6.7) indicating that these were mainly amorphous. It may be noted that FePcTSA by itself has good amount of crystalline nature and it exhibits well defined peaks at 9.69, 11.12, 19.88, 29.25, 30.54 and 36.98 degrees. In this case, no well defined ordered structure could be seen even at 15% of phthalocyanine in PPy as compared to the porphyrin incorporated PPy (see Chapter 5). This could be due to much larger molecular size together with the fact that solfonic groups give rise to dopant type interaction with the PPy chains which leads to better dispersion/distribution of molecules in the matrix preventing their crystallization.

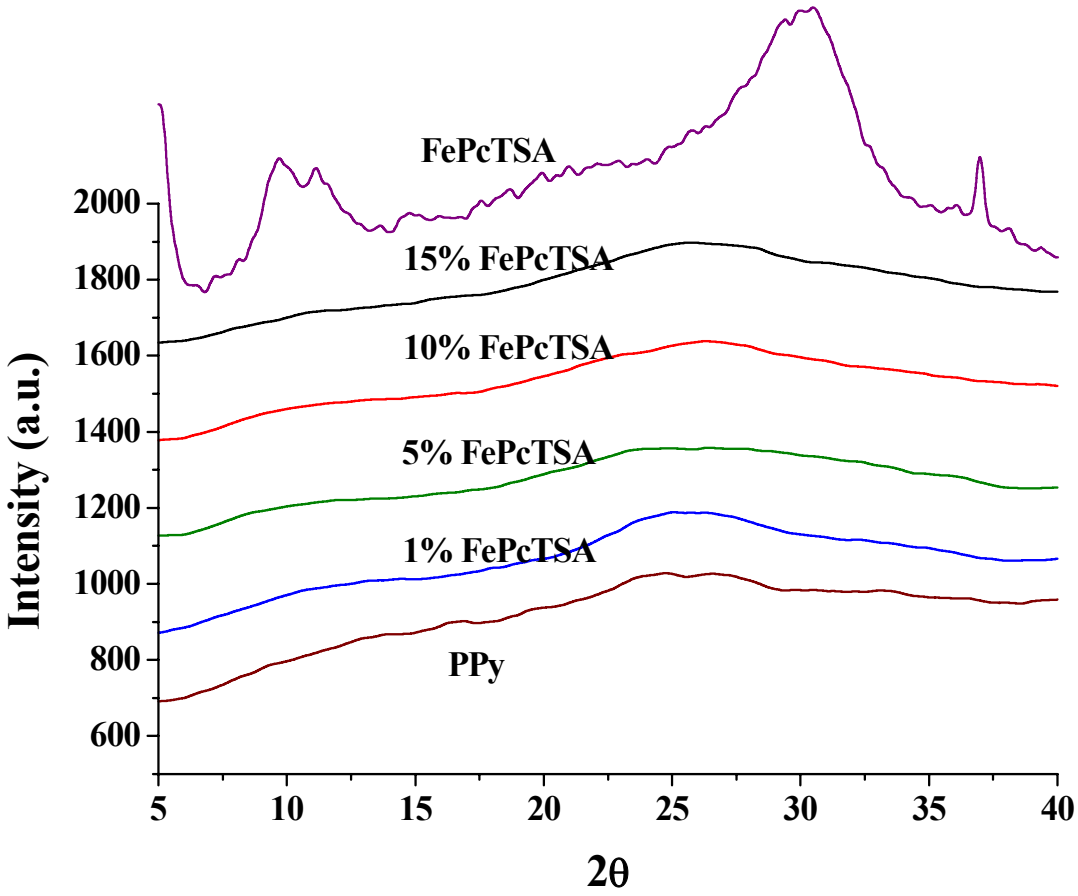

Fig. 6.7. X-ray diffraction patterns of PPy, FePcTSA and PPy-FePcTSA materials.

The interchain distance (R) could be calculated (as done previously: Ch.5) from the XRD of the PPy and 1 wt.% PPy-FePcTSA, which is in amorpous state. The interchain distance for both pure PPy and 1 wt.% PPy-FePcTSA is 4.14Å and 4.59Å respectively

6.3.A.d. Graphite Furnace Atomic Absorption Spectroscopy

This technique (see section 2.5.6.) was used as an elemental detection mainly used here for the determination of trace quantities of transition metal, iron. Presence of iron was detected and the results are tabulated in Table 6.4.

Composition	Wt.% of Fe in the sample
15 wt.% Pc	1.1177
10 wt.% Pc	0.7694
5 wt.% Pc	0.3481
1 wt.% Pc	0.0773
Polypyrrole	0.0

Table 6.4. GFAAS data for FePcTSA doped polypyrrole samples.

Here, it is seen that polypyrrole doesn't contain any trace amount of iron, which indicates that the iron of $FeCl_3$ used as an oxidant is fully washed out from the polypyrrole and there is a gradual increase of iron content is observed with higher loading of FePcTSA. 0.0773 wt.% of Fe is detected in 1 wt.% of FePcTSA doped PPy where as 1.1177 wt.% of iron detected for 15 wt.% FePcTSA doped polypyrrole.

6.3.A.e. EDAX Studies

EDAX (see section 2.5.5.) analyzed the quantity of the different elements present in the polymer. In the present work, this analysis was used for the detection of iron and sulphur of doped phthalocyanine. It is observed that the iron content as well as sulphur content increase proportionally with increasing amount of phthalocyanine in the polymer. This suggests the incorporation of dopant, phthalocyanine as well as its influence on elemental composition at various concentrations. The EDAX data is shown in Fig. 6.8.

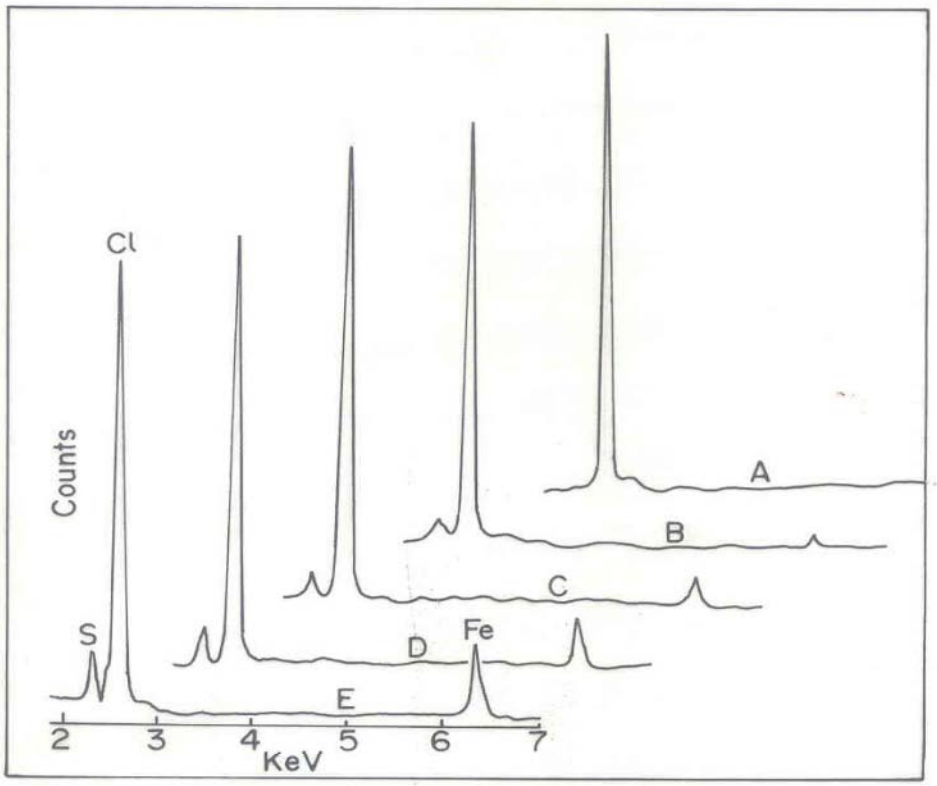

Fig. 6.8. EDAX data for iron and sulphur for PPy-FePcTSA materials; A) PPy, B) 1 wt.% FePcTSA, C) 5 wt.% FePcTSA, D) 10 wt.% FePcTSA, E) 15 wt.% FePcTSA.

6.3.A.f. TGA Studies

This is another supporting characterization technique to know the presence of dopants from the thermal stability data obtained from the thermogravimetric pattern of percentage weight loss against temperature plot. It clearly reveals the enhancement of thermal stability of modified PPy samples with increasing concentration of FePcTSA in the polymer. The TGA data obtained is shown in Fig. 6.9.

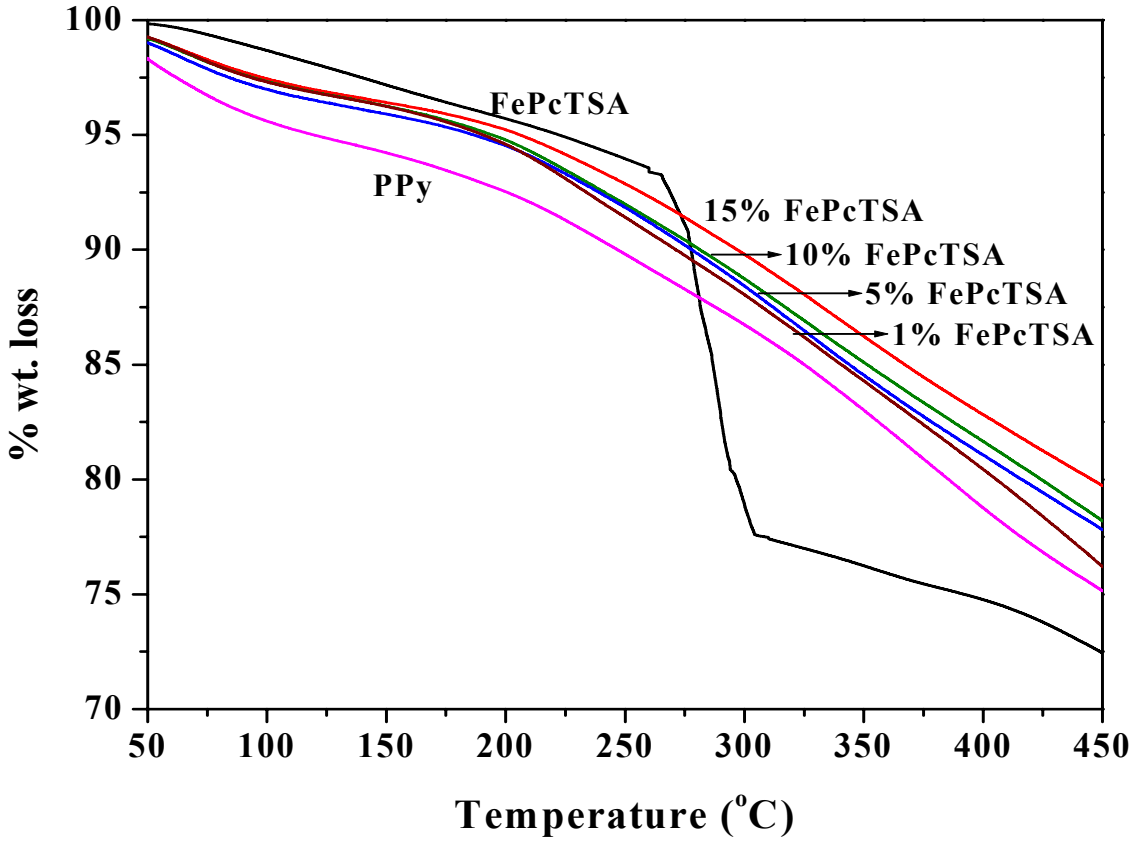

Fig. 6.9. Thermogravimetric pattern of FePcTSA, PPy and PPy-FePcTSA materials.

The degradation of FePcTSA is a two step process, onset at 260^0C, where sulphonic acid group is leaving and second stage of weight loss observed at 504^0C is the total degradation of phthalocyanine. The effect of phthalocyanine on the thermal stability of the material is studied by calculating the % weight loss before and after the major weight loss of phthalocyanine. The percentage weight loss were equally calculated for the other samples at this temperature and the obtained weight loss and weight loss expected is also calculated and tabulated in Table 6.5. It is seen from the calculated data that the expected weight loss is higher than the experimentally obtained data. This indicates that the presence of phthalocyanine inside the polymer has thermal stabilization effect.

FePcTSA content (%)	% wt. loss at 200^{0}C	% weight loss at 400^{0}C	Actual weight loss (%)	Expected % weight loss
100	4.25	25.28	21.03	21.03
15	4.74	17.12	12.38	14.77
10	5.13	18.21	13.08	14.39
5	5.33	18.59	13.26	14.06
1	5.52	19.08	13.56	13.73
0 (PPy)	7.49	21.15	13.66	13.66

Table 6.5. Percentage weight loss of the materials during the first stage of degradation of FePcTSA.

6.3.A.g. X-ray Photoelectron Spectroscopy

ESCA of pure polypyrrole and various concentrations of FePcTSA doped PPy powders were recorded and analysed (see Figures 6.10.A. and 6.10.B.). It gives typical core level spectra corresponding to C_{1s} and N_{1s} levels. Both C_{1s} and N_{1s} peaks have deconvoluted into three components and details are summarised in Tables 6.6.A. and 6.7.

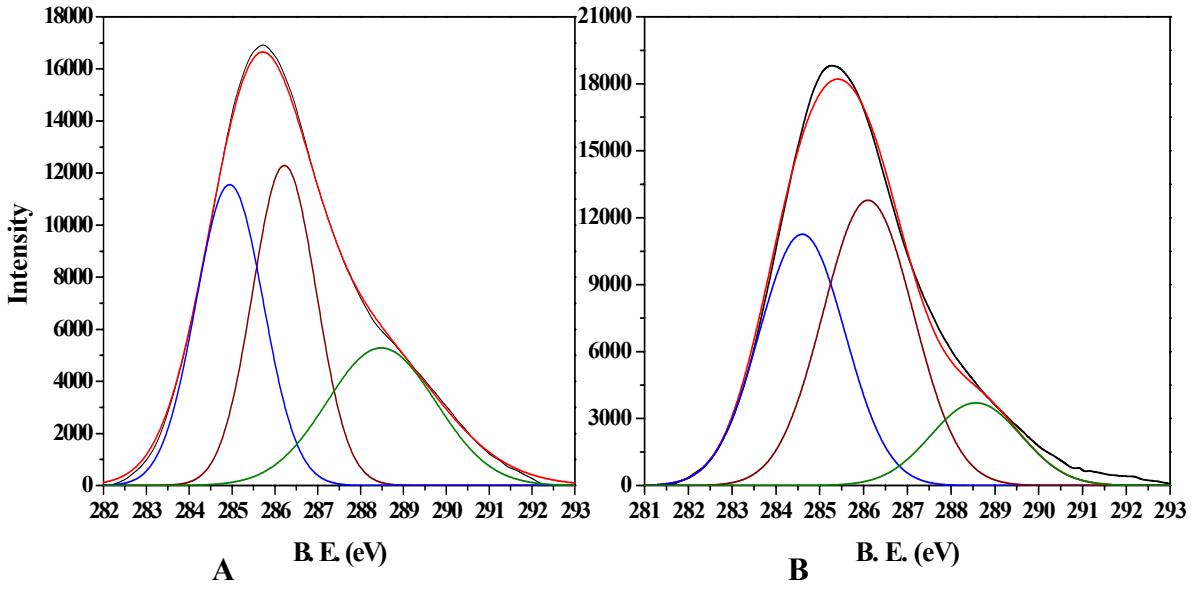

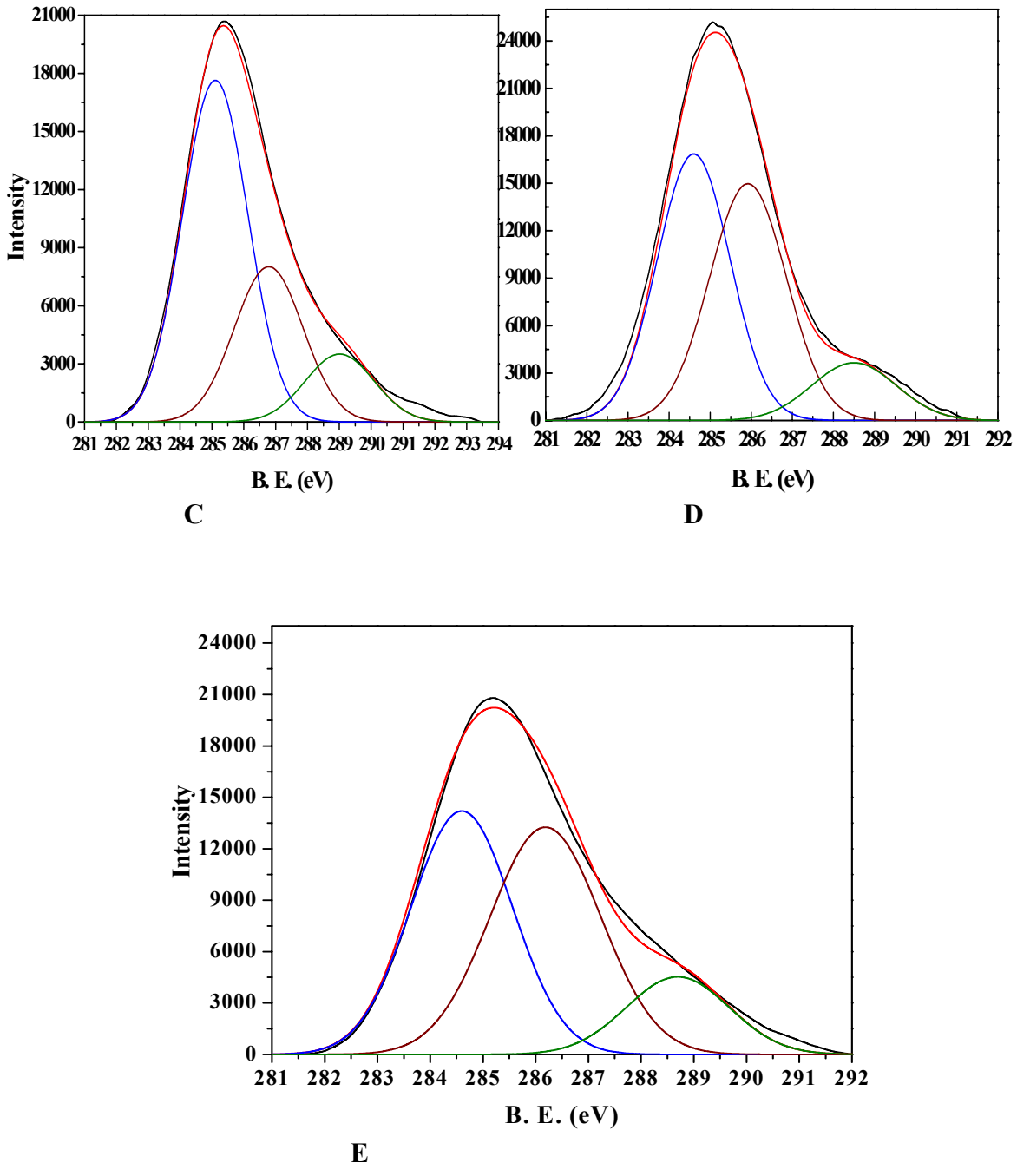

Fig. 6.10.A. C_{1s} core level spectrum A) PPy B) 1wt.% PPy-FePcTSA C) 5 wt.% PPy-FePcTSA, D) 10 wt.% PPy-FePcTSA and E) 15 wt.% PPy-FePcTSA material.

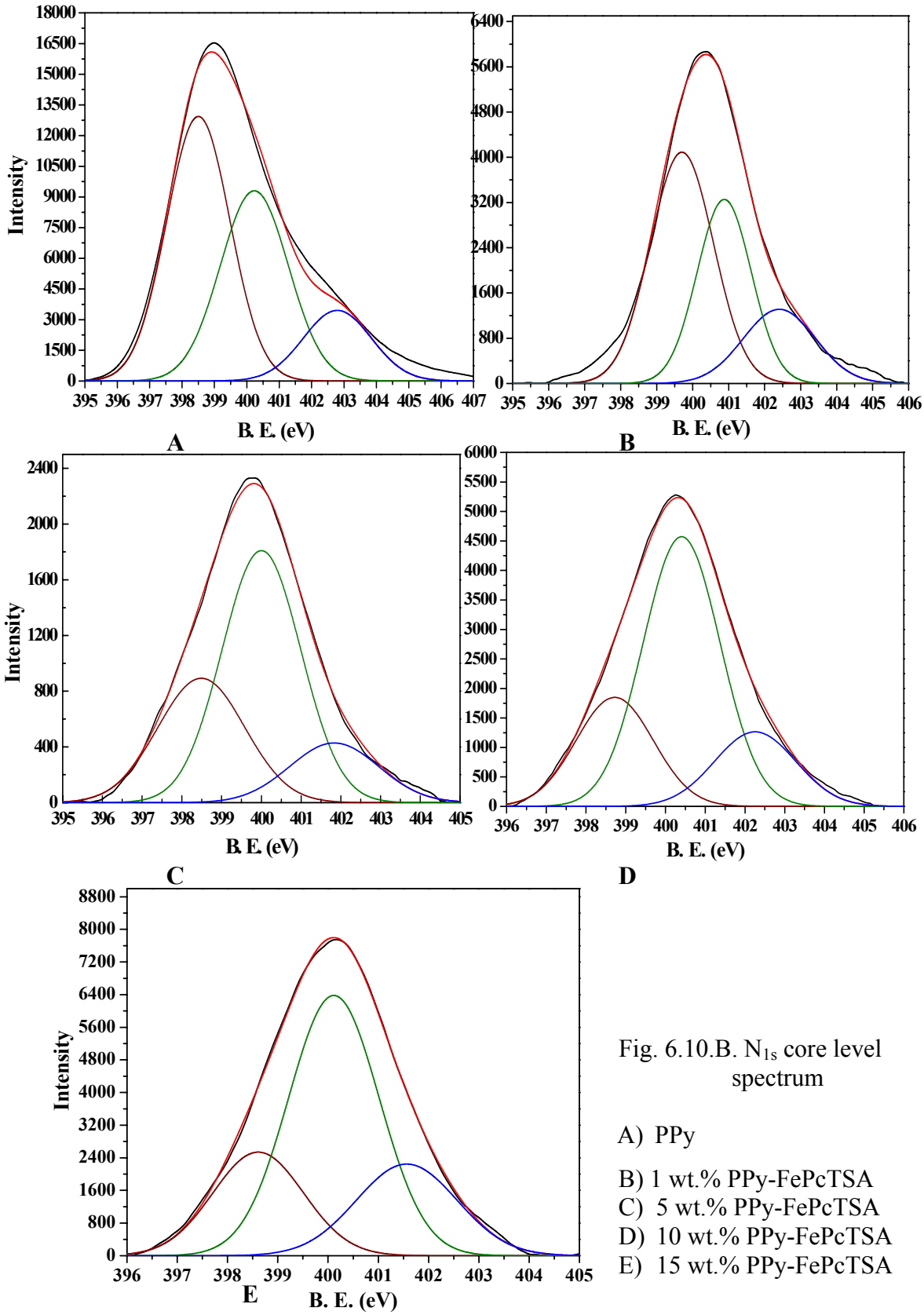

Fig. 6.10.B. N_{1s} core level spectrum

A) PPy

B) 1 wt.% PPy-FePcTSA
C) 5 wt.% PPy-FePcTSA
D) 10 wt.% PPy-FePcTSA
E) 15 wt.% PPy-FePcTSA

Material	Binding energy (eV)	FWHM (eV)	Charged C (%) $[(C_2+C_3) / (C_1+C_2+C_3)] \times 100$
PPy	C_1 = 284.6 C_2 = 286.2 C_3 = 288.1	1.5 1.4 2.5	63
1 wt.% PPy-FePcTSA	C_1 = 284.6 C_2 = 286.1 C_3 = 288.5	1.9 2 2	61
5 wt.% PPy-FePcTSA	C_1 = 284.6 C_2 = 285.9 C_3 = 288.5	1.7 1.8 2	54
10 wt.% PPy-FePcTSA	C_1 = 284.6 C_2 = 286.2 C_3 = 288.5	2 2.1 2.1	51
15 wt.% PPy-FePcTSA	C_1 = 284.6 C_2 = 286.1 C_3 = 288.7	1.92 2.1 1.95	57

Table 6.6. ESCA results for C1s level for PPy-FePcTSA materials.

Material	Binding energy (eV)	FWHM (eV)	Charged N (%) $[(N_2+N_3) / (N_1+N_2+N_3)] \times 100$
PPy	N_1 = 385.8 N_2 = 388.0 N_3 = 388.8	2.32 2.6 2.5	38
1 wt.% PPy-FePcTSA	N_1 = 399.7 N_2 = 400.8 N_3 = 402.4	1.75 2 1.5	51
5 wt.% PPy-FePcTSA	N_1 = 398.5 N_2 = 400.0 N_3 = 401.8	2.2 1.9 2.2	70
10 wt.% PPy-FePcTSA	N_1 = 398.7 N_2 = 400.4 N_3 = 402.2	1.9 1.9 2	75
15 wt.% PPy-FePcTSA	N_1 = 398.8 N_2 = 400.1 N_3 = 401.4	1 1 1	70

Table 6.7. ESCA results for N_{1s} level for PPy-FePcTSA materials.

From the ESCA plot, the area under each curve is calculated and the percentage charged carbons and nitrogens were calculated using the formula $[(C_2+C_3)/(C_1+C_2+C_3)]$ X 100 and $[(N_2+N_3)/(N_1+N_2+N_3)]$ X 100. From the data, it is observed that there is an increasing trend of percentage charged nitrogen species with the increase of FePcTSA in PPy. Where as, it shows a decrease for 15 wt.% PPy-FePcTSA material. This is a clear indication of phase separation of phthalocyanine after an optimum level (10 wt.%) takes place. Charged carbon data also follows the trend of increasing phase separation after 10 wt.% PPy-FePcTSA material.

6.3.B. Electrical Property Measurements

The effect of electrical conductivity with the addition of phthalocyanine was studied and it is found that the room temperature conductivity increases initially from 6.9 X 10^{-2} S/cm for 1 wt.% (0.073 mol%) PPy-FePcTSA upto 9.33 X 10^{-2} S/cm for 5 wt.% (0.365 mol%) of PPy-FePcTSA. Then it starts decreasing further to 1.13 X 10^{-2} S/cm for 15 wt.% (1.098 mol%) of PPy-FePcTSA material. The room temperature conductivity for pure polypyrrole synthesised through aqueous route is 4.88 X 10^{-2} S/cm. Here, the increase in conductivity may be associated with additional secondary doping effect. This effect has been described in detail for polyaniline doped with two protonic acids [38].

An initial increase in conductivity of polypyrrole is observed, when the phthalocyanine is incorporated into it. Due to the addition of phthalocyanine, the extent of secondary doping increases, giving higher number of delocalised electrons. The electrical conductivity in these materials is associated with not only the total carrier density but also mobility. The charge transport takes place not only along the chain (intra chain hopping) but also across the chains (inter chain transport). The latter is facilitated by the conjugated structure of phthalocyanine and the charges at four tetra sulfonic groups linking at different nitrogen moieties of different chains. Thus, more delocalisation of the charge carriers take place giving rise to higher conductivity.

The electrical conductivity (σ), of PPy-FePcTSA polymers was measured in its pellet form. Pellets were made at a pressure of 5 tonnes using a hydraulic press. The conductivity of the order of 10^{-2} S/cm was obtained. These materials give the temperature dependent conductivity with Arrhenius plots being linear, except for 15 wt.% PPy-

FePcTSA as shown in Fig. 6.11. It is observed that two activation energies may exist for this particular composition.

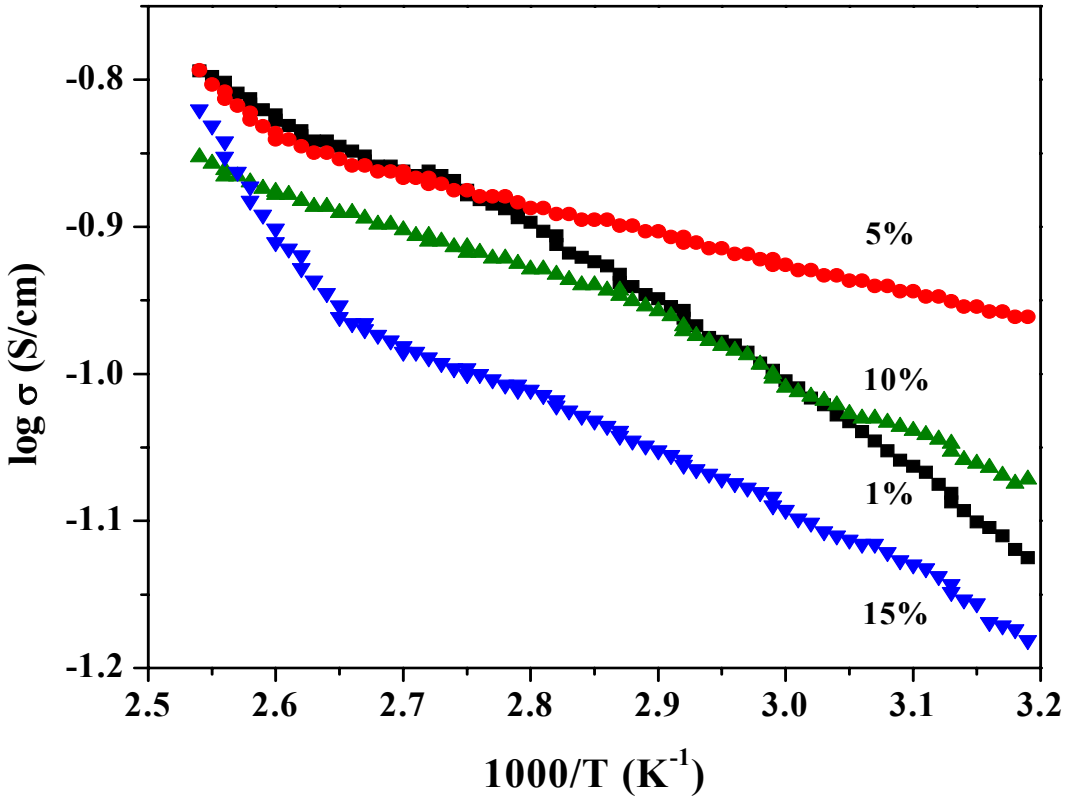

Fig. 6.11. Temperature dependent conductivity of PPy-FePcTSA samples.

The activation energy (ΔE) for the polypyrrole and PPy-FePcTSA polymers were calculated from the straight line plot of log conductivity versus 1/T. The results obtained for room temperature conductivity and activation energy with respect to FePcTSA content in PPy are analysed and tabulated in Table 6.8. The activation energy for pure polypyrrole sample is 0.031 eV, whereas, polypyrrole containing 5 wt.% phthalocyanine sample showed this value as 0.022 eV. It may be noted that the conductivity values as well as the thermal activation energy for conduction in these samples are much different than those obtained for ferrocene or Fe-porphyrin doped PPy (see chapters 3 and 5). In the present case the conductivity is high and not much affected by the incorporation of FePcTSA. The activation energy is low and infact it decreases slightly by the incorporation of FePcTSA. Since the phthalocyanine compound used in the present case contains the sulfonic acid groups, there is considerable secondary doping effect seen in

this case. Also, the inter chain transport of charge is facilitated due extensive interaction brought about by the sulfonic acid moieties appearing at different sites on PPy. At high concentration of FePcTSA, due to aggregate formation, the secondary doping effects are reduced and the conductivity is observed to decrease. It is observed that there are two activation energies possible for 15 wt.% (1.098 mol%) PPy-FePcTSA sample. This indicates that Ea = 0.061 eV is for the phthalocyanine incorporated into PPy matrix and Ea = 0.28 eV is for phase separated phthalocyanine which does not provide easy path for the charge transport. Here, the phase separated FePcTSA acts as trapping centre for charge carriers leading to higher activation energy and less conductivity.

FePcTSA content (mol%)	σ (S/cm)	Ea (eV)
0 (PPy)	4.88×10^{-2}	0.031
0.073	6.9×10^{-2}	0.028
0.365	9.33×10^{-2}	0.022
0.732	4.26×10^{-2}	0.039
1.098	1.13×10^{-2}	0.061, 0.28

Table 6.8. Room temperature conductivity and activation energy with respect to FePcTSA content in PPy.

6.3.C. Carbon Monoxide Gas Sensitivity Measurements

The room temperature resistance (R_0) of the PPy-FePcTSA material coated on the interdigited electrode is given in Table 6.9.

PPy-FePcTSA system shows very rapid change of resistance (unlike PPy-ferrocene and PPy-porphyrin systems) with the exposure to 300 ppm CO gas. PPy containing 0.946 mol% FePcTSA is giving a highest variation in resistance (700 Ω) in a short period of time, 0.51 s. The highest response factor obtained is 51.8 (calculated from $dR/R_0 \times 100$) for 0.732 mol% PPy-FePcTSA material; dR is the change of resistance after the exposure to CO gas and R_0, the initial resistance before exposure to CO gas. In all the cases, the response signal (resistance) rapidly increases when exposed to CO gas at RT in the ordinary air atmosphere. The recovery of the materials were ensured by repeated cycles

of experiments within a period of 10 min (resistance of the materials were came back to its initial value). A typical CO sensitivity signal for 21 ppm and 100 ppm CO gas is shown in Fig. 6.12. The response factor of 5 wt.% PPy-FePcTSA composition at different CO gas concentration is 25.74 for 21 ppm and 45.6 for 100 ppm. The CO response of various compositions of PPy-FePcTSA materials is shown in Fig. 6.13.

FePcTSA content (mol%)	Initial resistance, R_0 (Ω)
0.073	473
0.214	354
0.365	690
0.57	1061
0.732	1180
1.098	2060

Table 6.9. The initial resisatnce of the PPy-FePcTSA materials coated on the interdigited electrode.

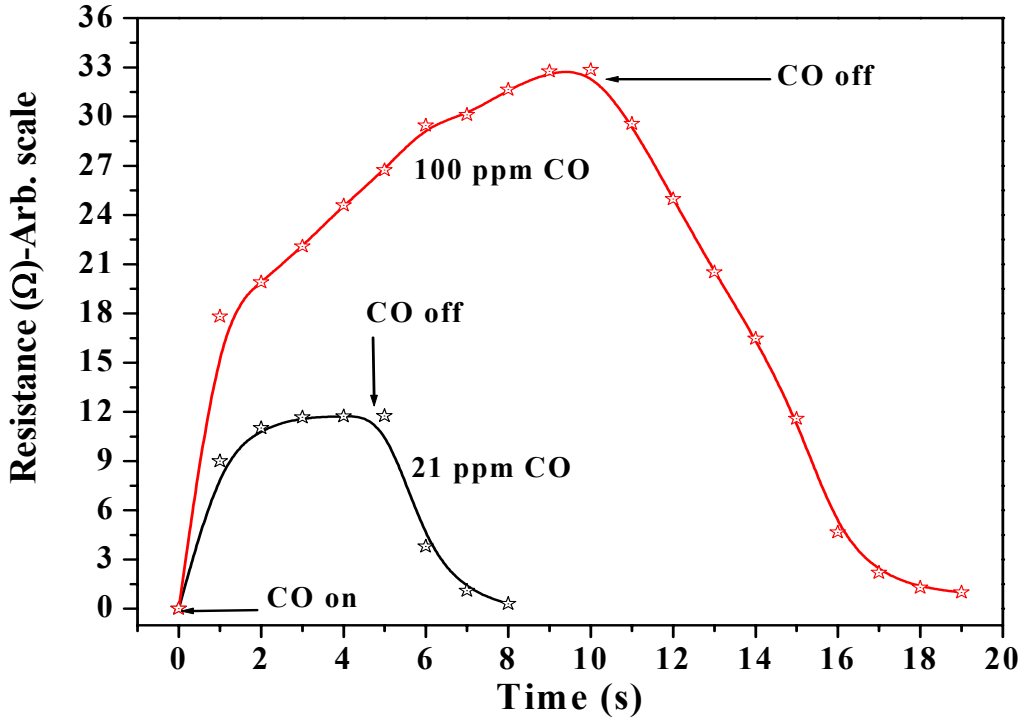

Fig. 6.12. Sensor characteristics when CO gas at 21 and 100 ppm exposed to 5 wt.% PPy-FePcTSA material.

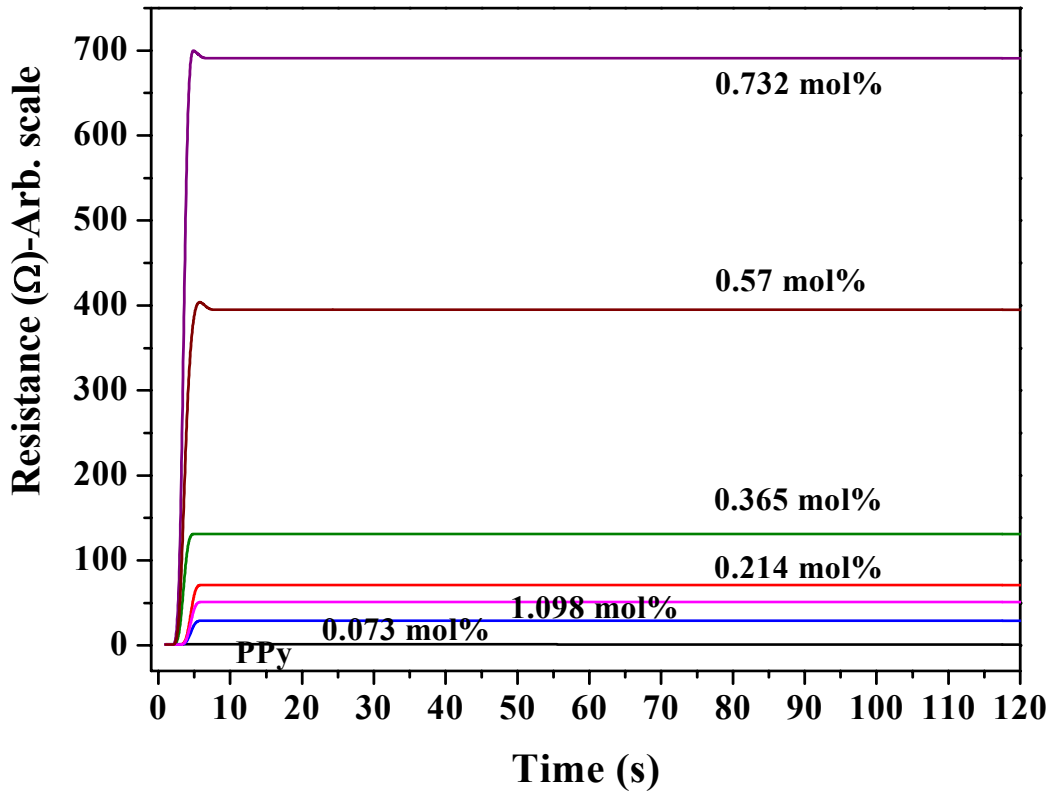

Fig. 6.13. 300 ppm CO gas response of PPy-FePcTSA materials at room temperature.

The CO interaction with PPy-FePcTSA materials and the change of resistance during exposure is expected to be similar as observed with ferrocene and porphyrin systems. Based on various characterization results, electrical property measurements and the response characteristics of the materials, the sensing mechanism of these materials towards CO gas is proposed as follows:

In case of PPy, there is interaction between CO and nitrogen of pyrrole taking place. It is extremely a slow process and change of resistance during exposure is negligible, but in case of modified PPy with FePcTSA, the change of resistance is remarkable and rapid (not like previous cases). Here, the resistance of the material increases from their base value within seconds and gets saturated immediately. The affinity of CO with iron complexes were proved in the previous chapters, systems like PPy-Fc, PPy-FePcTSA etc. It is believed that CO immediately comes closer to iron of phthalocyanine whenever the material is exposed to the guest gas and reduce Fe^{+3} to Fe^{+2}, which subsequently increase the number of electron charge carriers (the effective hole charge carriers diminishes), gets transferred to the polymer chains and multiplies faster. So, a fast response (rise of

resistance) expected in FePcTSA doped samples during the exposure. Phthalocyanine structure shows similarity with hemoglobin, which is 250–300 times prone to attack by CO than oxygen [39, 40]. It was ensured from the recovery graph that only a physical interaction is taking place between CO and FePcTSA (unlike CO-hemoglobin interaction). Obviously, the macrocyclic nature of phthalocyanine may give more interaction sites for CO gas to interact. A model structure for the expected CO interaction with FePcTSA doped polypyrrole and subsequent charge transport is shown in Fig. 6.14.

The response factor versus mol% of FePcTSA with respect to monomer pyrrole is shown in Fig. 6.15. It appears that percentage response strongly dependent on the composition. Thus PPy with 0.732 mol% FePcTSA showed highest response to CO gas than other compositions of lower or higher FePcTSA content. The response factor obtained for 1.42 mol% FePcTSA in PPy material is 0.9 indicates that if the concentration of FePcTSA increased beyond certain limit (0.732 mol% of FePcTSA is supposed to be the optimum limit), the gas response decreases.

The optimum concentration of phthalocyanine in PPy is required for the highest response of CO gas is 0.73 mole%. It is obvious from UV-Vis. Spectra of the PPy-FePcTSA powders in NMP that there is free phthalocyanine present in the polymer for 1.098 wt.% FePcTSA, the λ_{max} for phthalocyanine is observed at 658 nm region. The results obtained from temperature dependent conductivity measurements also confirms the possibility of phase separation of phthalocyanine with high concentration in the polymer. There is only a single activation energy exists for PPy-FePcTSA materials upto the concentration level of 10 wt.%, but two activation energy exists for 1.098 mol% PPy-FePcTSA material. Ea = 0.061 eV for PPy-FePcTSA and Ea = 0.28 eV for phase separated FePcTSA alone. Phase separation of phthalocyanine in 1.098% PPy-FePcTSA material is attributed to the main reason for the lowering of CO response, which happens after an optimum concentration of 0.732 mol% FePcTSA in PPy. Once the phase separation occurs, the free phthalocyanine acts as charge carrier traps and so the effective charge transfer process during interaction with CO gas gets hampered. Since the free phthalocyanine present, the effective number of charge carriers as well as the mobility will get affected. This makes 1.098 mol% PPy-FePcTSA material less sensitive to CO gas compared to any other composition.

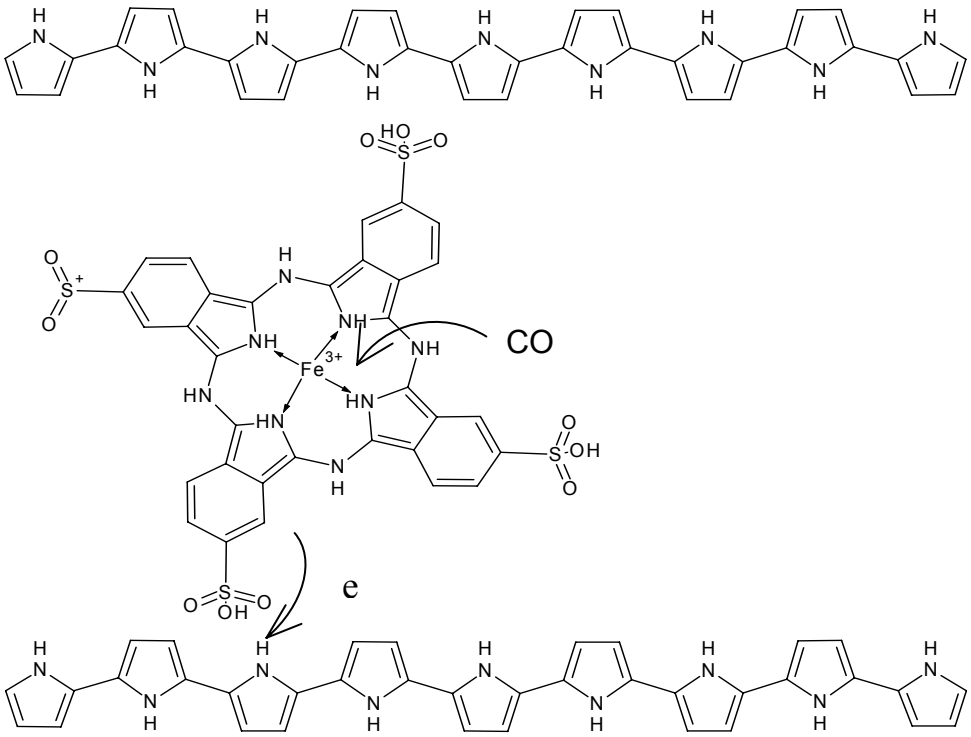

Fig. 6.14. A model structural representation for the CO interaction with FePcTSA and subsequent charge ransport process.

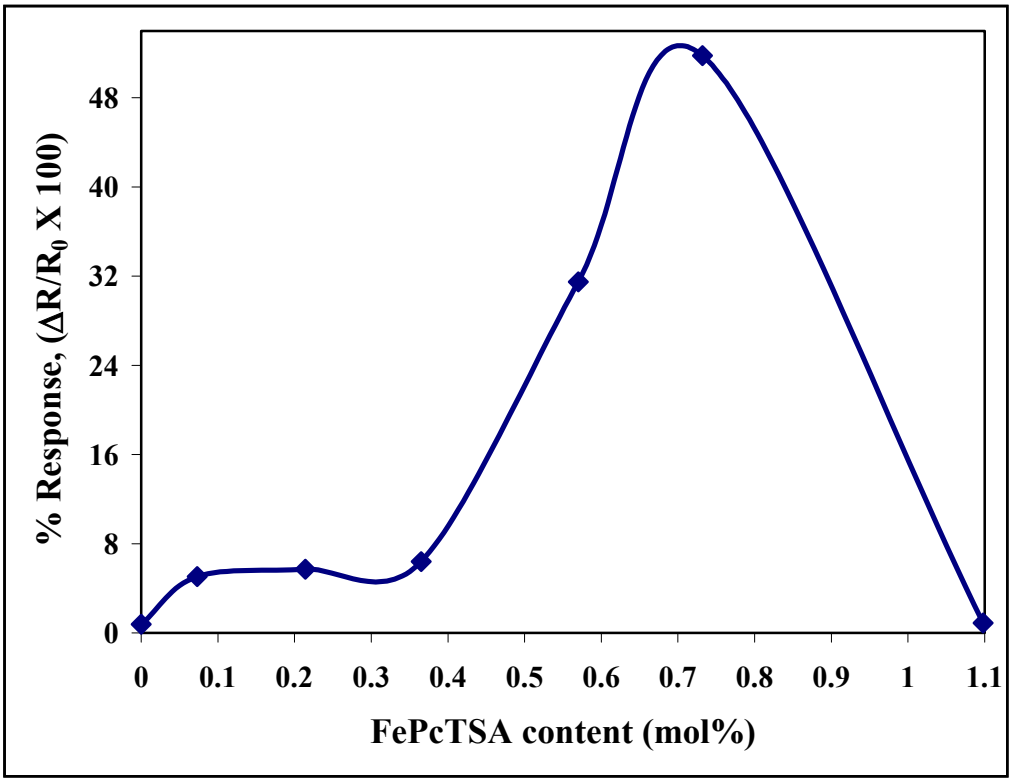

Fig. 6.15. A plot of response factor vs. FePcTSA content (mol%) in PPy.

The maximum speed of response determined from the t_{50} value obtained is 0.53 s for PPy containing 0.732 mol% FePcTSA. The rate of response of FePcTSA doped PPy materials are shown in Fig. 6.16.

Change of resistance with respect to time (dR/dt) is shown in Fig. 6.17, indicating that dR value is quite high at the measured time. dR is the change of resistance before and after exposure to 300 ppm CO gas and dt is the time taken to occur maximum change of resistance for the initial 2 seconds. The highest change of resistance observed with exposure to CO is 300.26 Ω/s for 0.732 mol% of FePcTSA in PPy. 300 Ω change in resistance is remarkable, more interestingly, it happens within a second and at RT, where as all other compositions (PPy-FePcTSA) having resistance change in the range 14–65 Ω/s. This clearly indicates that the response factor and speed of response to particular gas depends on the particular composition of FePcTSA in PPy.

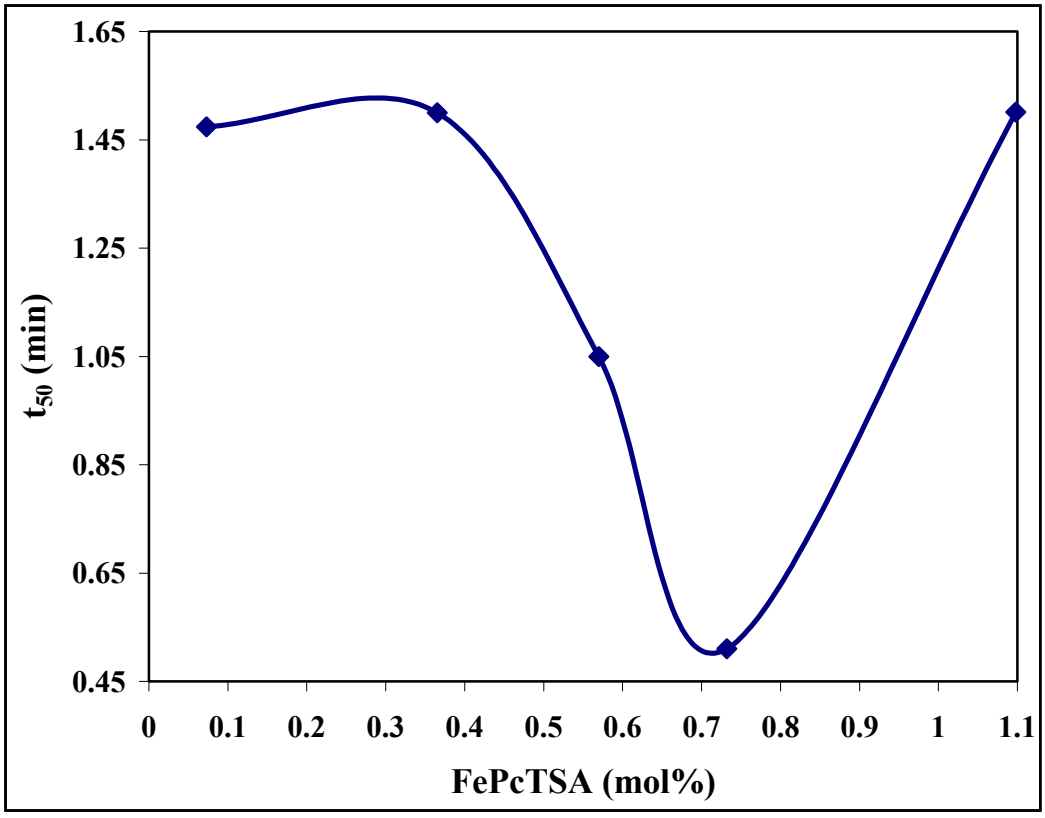

Fig. 6.16. The speed of response (t_{50}) of PPy-FePcTSA materials towards 300 ppm CO.

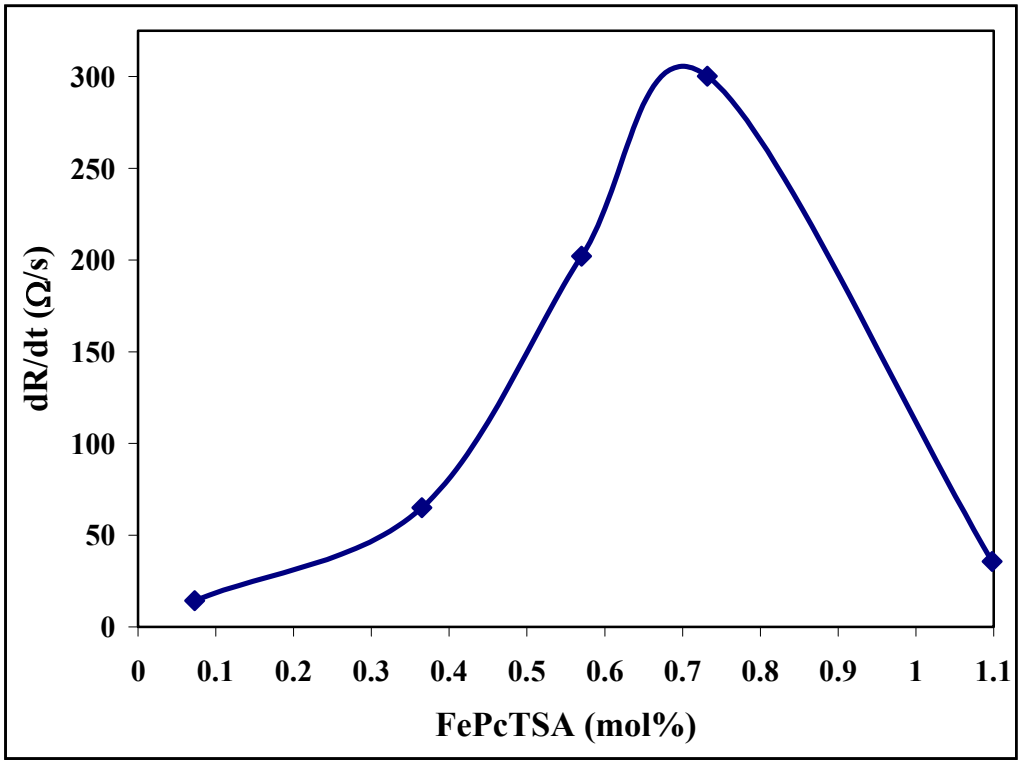

Fig. 6.17. Maximum change of resistance (dR/dt) experienced for the PPy-FePcTSA materials for the initial two seconds.

These observations are similar to the results obtained in the case of PPy-FeTPPCl described in chapter 5 wherein the sensitivity was found to be highest and the response fastest at certain composition of the functional additive. However, in the present case the actual values of response factor and the speed at much superior to those obtained earlier.

6.4. Electrochemical Incorporation of FePcTSA into PPy

The polymeric films of polypyrrole and those containing phthalocyanine were deposited on gold coated PET interdigitated substrates, as described in section 4.4.2. The thickness of the deposited films depends upon the time of deposition, which was maintained same in all cases. These films were characterized by cyclic voltammetry technique. The films from the same set were used for 300 ppm CO gas sensitivity measurements.

The cyclic voltammogram of iron phthalocyanine (0.1 mmol) is carried out in dimethyl sulphoxide (DMSO) containing 0.1 M tetrabutylammonium perchlorate ($TBAClO_4$) as electrolyte, shown in Fig. 6.18. It is showing characteristic oxidation as well as reduction peaks at –670 mV and –890 mV respectively. These two peaks are due to the oxidation of

Fe^{III} to Fe^{II} of phthalocyanine. The potentiodynamic growth of modification of PPy with FePcTSA is done with 0.1 M tetrabutylammonium perchlorate on Pt working electrode with a scan rate of 50 mV/s. It is shown in Fig. 6.19. (see section 4.5.B. for the CV of pure PPy). The oxidation and reduction peaks for FePcTSA is experienced slight shift to –636 mV and –970 mV respectively. The polypyrrole oxidation and reduction peaks observed at 20 mV and 420 mV respectively. The modified films were deposited on $FeCl_3$ activated gold coated interdigited PET substrate by chronoamperometry method. The potential given for the deposition of conducting film on interdigited electrodes is 900 mV. The cyclic voltammogram study of FePcTSA modified PPy film was carried out as a confirmational tool in 0.1 M TBAP electrolyte in acetonitrile solvent with a scan rate of 50 mV/s. Here, it gives a clear distinct oxidation as well as reduction peaks at 60 mV and –800 mV are assigned for PPy oxidation and phthalocyanine reduction respectively. The FePcTSA modified PPy film shows a slight shift of the FePcTSA from –890 mV to 800 mV. This is evident from the cyclic voltammogram of pure polypyrrole film and phthalocyanine solution. The CV of the modified film is shown in Fig. 6.20.

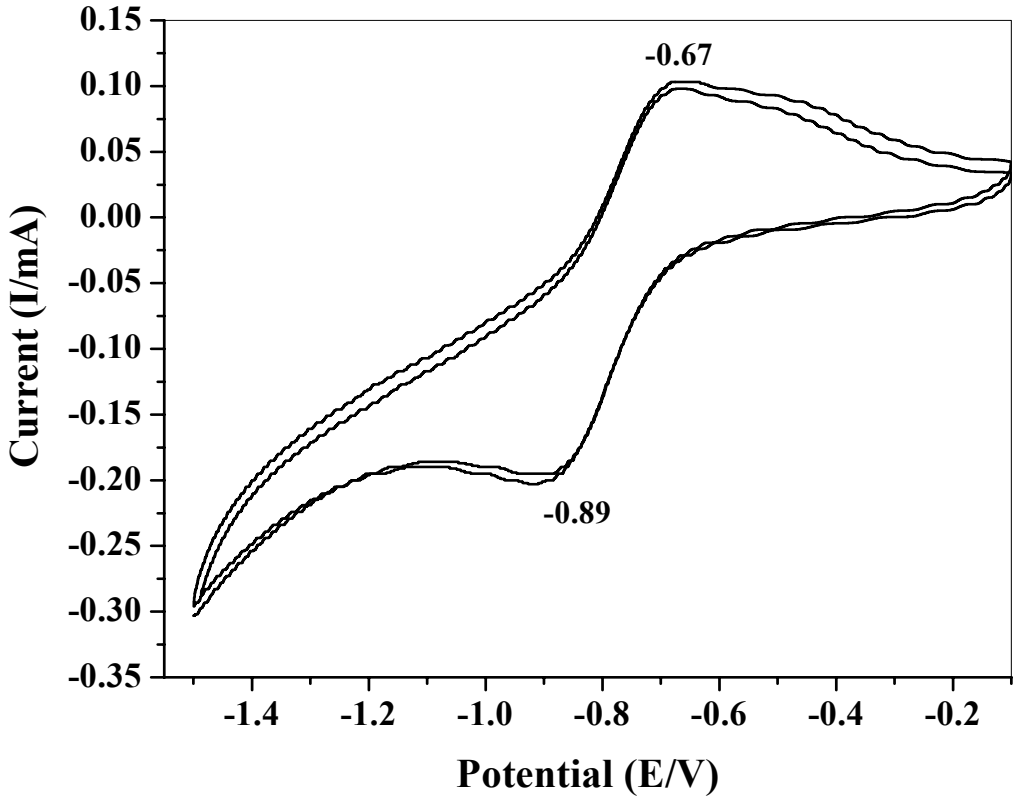

Fig. 6.18. Cyclic voltammogram of FePcTSA in DMSO containing 0.1 M TBAP as electrolyte. Electrodes: Pt, reference electrode: Calomel. Scan rate: 50 mV/s.

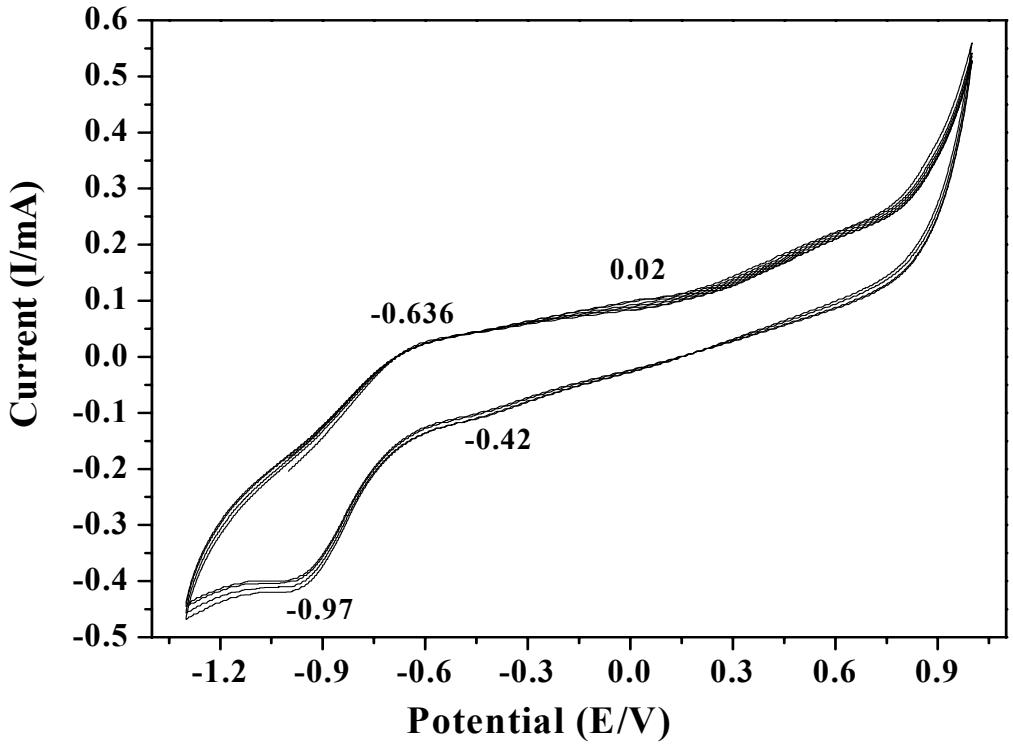

Fig. 6.19. Potentiodynamic growth of polypyrrole in 0.1 M TBAP dissolved in DMSO with the addition of 0.1 mmol FePcTSA in the electrolyte. Scan rate: 50 mV/s.

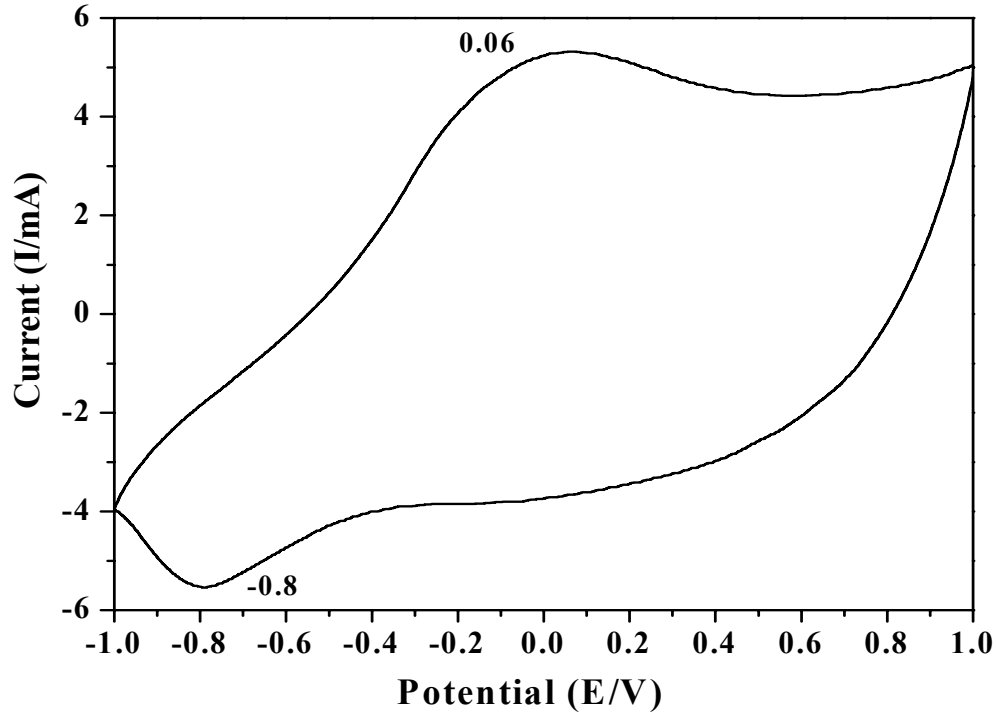

Fig. 6.20. Cyclic voltammogram of FePcTSA modified PPy film on Pt electrode in 0.1 M TBAP electrolyte in acetonitrile with a scan rate of 50 mV/s.

6.4.A. CO Gas Sensitivity Measurement of Electrochemically Modified PPy Films

The surface cells prepared with PPy films containing various levels of FePcTSA as co-dopant were tested for their response to 300 ppm carbon monoxide gas. The initial resistance (R_0) of the PPy-FePcTSA material electrochemically coated on the interdigited electrode is given in Table 6.10. Fig. 6.21. shows the response curve obtained in these cases.

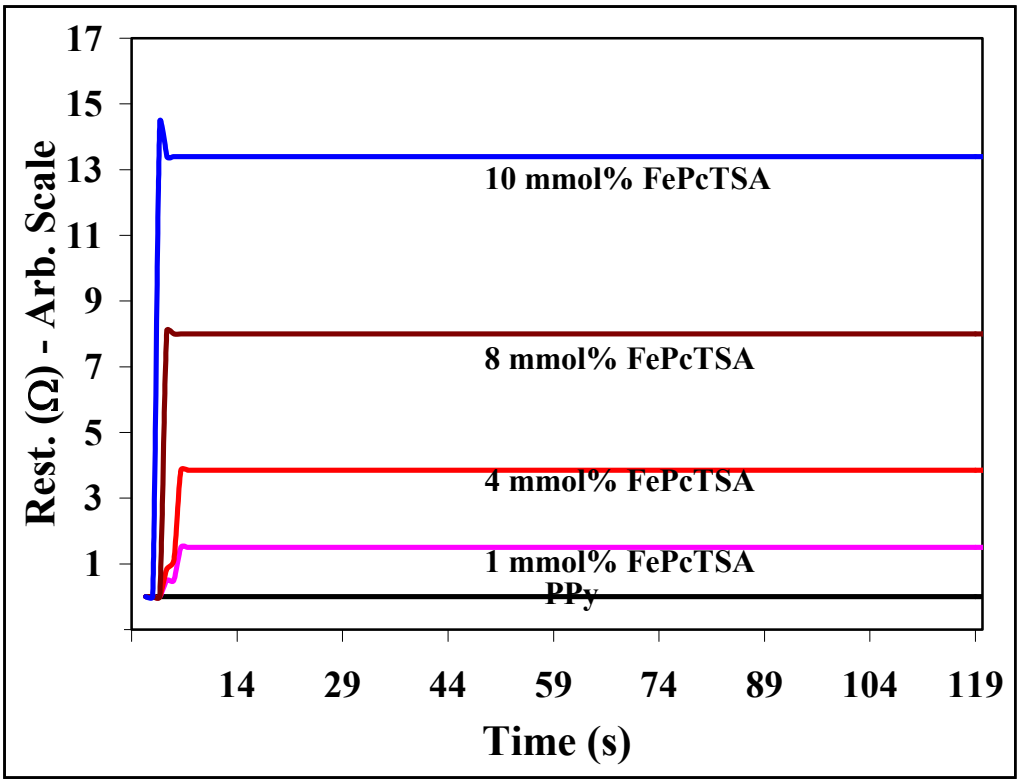

Fig. 6.21. Response curves for the surface cell containing PPy films doped with different concentrations of phthalocyanine, exposed to 300 ppm CO gas.

It is clear from the above figure that PPy deposited electrochemically with SO_4^{2-} as dopant alone is not at all sensitive to carbon monoxide gas, where as there is a sudden increase of resistance is observed for FePcTSA incorporated PPy materials, immediately after exposure to CO gas. Further, the change in sample resistivity at constant CO level depends on the concentration of the co-dopant present in PPy. The response factor [($\Delta R / R_0$)X100] for these electrochemically deposited films of PPy-FePcTSA is seen to depend critically on the co-dopant concentration. It is found to be highest (12.08%) for PPy film

with 10 mmol% of the FePcTSA with respect to monomer pyrrole, while it is practically 0 for PPy alone. The response factor (%) vs. composition plot is shown in Fig. 6.22.

FePcTSA content (mmol%)	Initial resistance, R_0 (Ω)
1	1430
4	901
8	432
10	119.2

Table 6.10. The initial resistance (R_0) of the electrochemically deposited films on interdigited electrode.

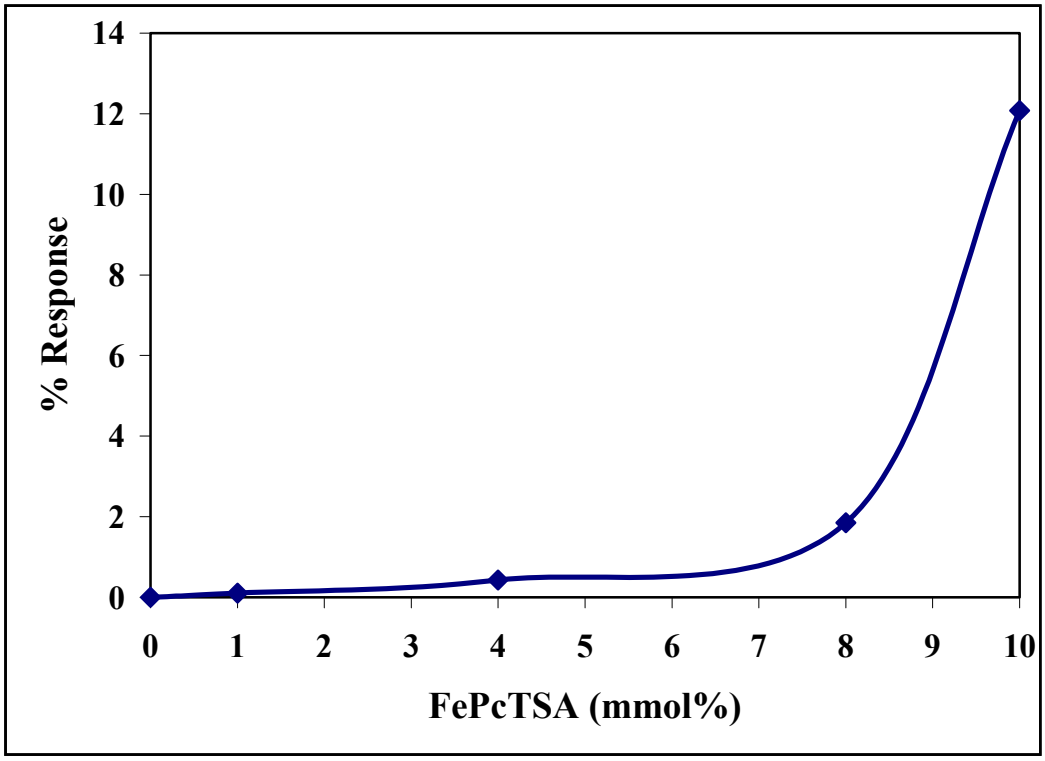

6.22. Response factor with respect to composition of PPy containing phthalocyanine exposed to 300 ppm carbon monoxide gas.

The speed of response (Fig. 6.23.) determined from the t_{50} value is quite low (0.487 s) for composition of 10 mmol% phthalocyanine in PPy film. In this case also it follows a similar trend as observed with electrochemically deposited PPy-FeTPPCl films. The low

concentration level of FePcTSA incorporated into PPy is good enough to give CO response. The CO response trend obtained for the electrochemically functionalized films of iron complexes used in all cases are similar, the explanation given for the sensing mechanism (sections 4.5.B.1 and 5.3.B.1.) holds good in this case also. Decrease in conductivity (increase of resistivity) when exposed to CO gas, depends on the concentration of phthalocyanine in the polymer. Hence, CO interaction with FePcTSA is dominating rather than with pyrrole moieties in the present samples.

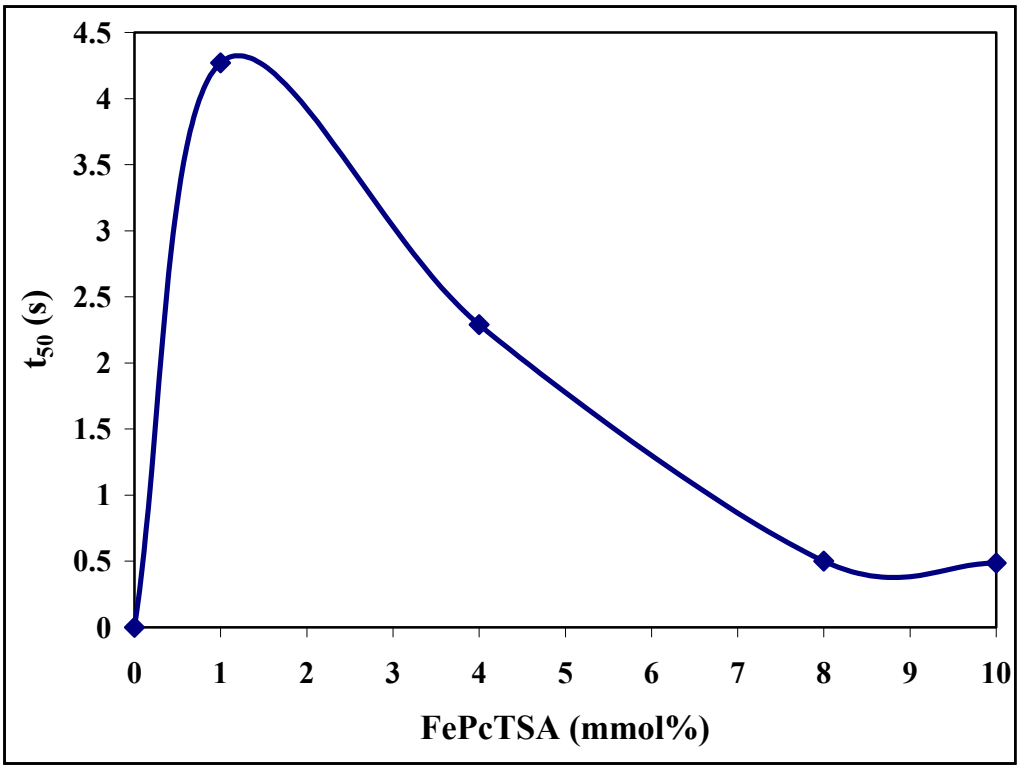

Fig. 6. 23. Compositional dependence of response time (t_{50}) for PPy with FePcTSA exposed to 300 ppm carbon monoxide gas.

In this case, the response is fast and so the initial 4 s is only crucial (because of the major change in resistance obtained at this stage only) for the detection of CO gas. The change of resistance (dR) over the initial 4 s (dt) is plotted against mmol% of FePcTSA in PPy is shown in Fig. 6.24. It is found that 3.59 Ω/s is the highest for 10 mmol% of FePcTSA concentration in PPy.

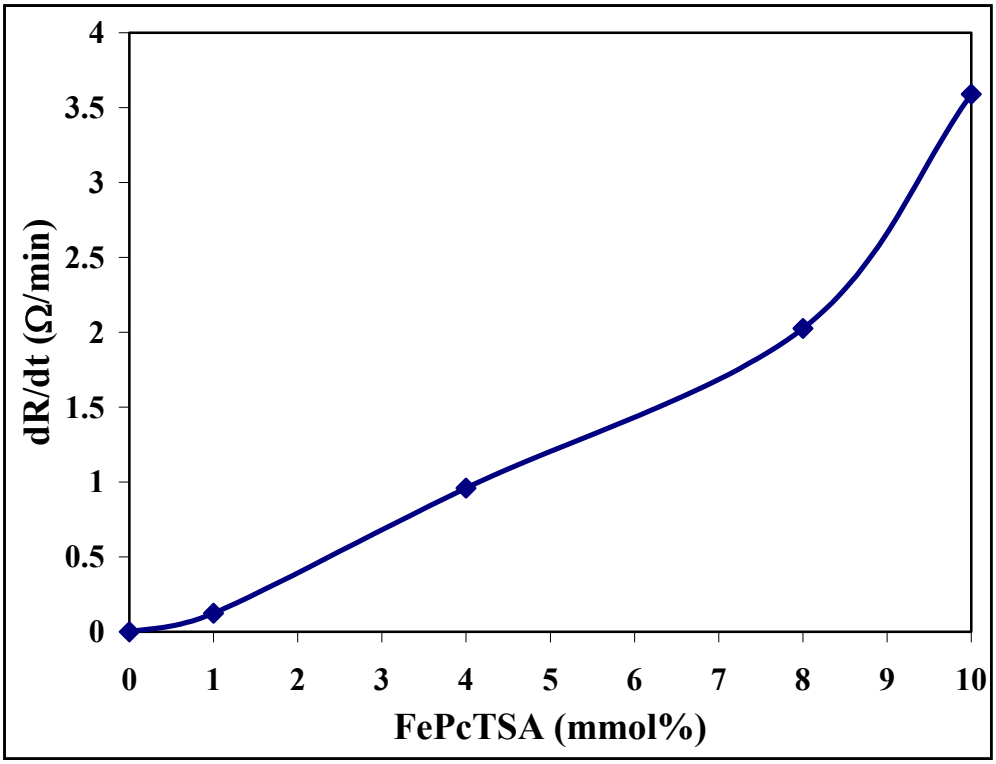

Fig. 6.24. Change of resistance for the initial 4 seconds of the PPy-FePcTSA materials.

6.5. Conclusions

The incorporation of phthalocyanine into polypyrrole has been successfully carried out, using both chemical as well as electrochemical method. The chemically doped PPy with FePcTSA were well characterised by different techniques and finally derived a most probable structure of phthalocyanine doped PPy. The major aim of enhanced CO gas sensitivity is achieved with the addition of phthalocyanine into the PPy matrix. Requirement of an optimum concentration of phthalocyanine in PPy for the higher CO gas response is confirmed from these results and analysis. It is confirmed from the UV-Vis. spectroscopy of the modified PPy powder, ESCA studies and electrical property measurements that the phase separation happens when FePcTSA concentration increases beyond certain limit. This is confirmed with the results of CO gas response characteristics experienced with the materials. PPy containing 1.098 mol% FePcTSA material experiences a major reduction in CO response due to the phase separation of phthalocyanine. The sensing mechanism in this regard for the PPy-FePcTSA materials

with CO gas is essentially the interaction of the CO molecules with Fe central atom and transfer of electrons leading to decrease in free carrier (holes) density of PPy .

The change of resistance during exposure to 300 ppm CO gas is very rapid and remarkable (691 Ω/0.51 s for 0.732 mol% FePcTSA containing PPy sample). It should be particularly noted that this sudden change occurred at RT and ordinary atmospheric conditions in a very short period of time. Not only the response, but also the recovery is spontaneous and immediate when the material is flushed with excess air.

The electrochemical activity of the PPy is enhanced by the incorporation of phthalocyanine into the PPy chains. Potentiodynamic depositions as well as cyclic voltammograms of the modified PPy film confirm the incorporation of phthalocyanine in the synthesized polymers. Further, the CO gas response of these materials is almost similar to the chemically doped samples i.e. it is equally fast in both the cases. This is in contrast to the observations made for FeTPPCl incorporated PPy where the electrochemically prepared samples gave faster response than the chemically prepared ones. The amount required to incorporate for obtaining the maxiumum CO gas response is also much lower than earlier cases. Thus, Fe-phthalocyanine appears to be much more effective in the enhancement of sensitivity of PPy to CO gas. Further, there is no loss of conductivity of the original PPy by the incorporation of this compound, which very much desired for device application.

6.6. References

[1] S. Rapi, V. Bochi, G. P. Gardini, Synth. Met. 24 (1988) 217.

[2] T. H. Chao, J. March, J. Polym. Sci., Polym. Chem. Ed. 26 743 (1988).

[3] S. P. Armes, Synth. Met. 20 (1987) 365.

[4] M. G. Kanatzidis, L. M. Tonge, T. K. Marks, H. O. Maecy, C. R. Kannewurf, J. Am. Chem. Soc. 109 (1987) 3797.

[5] M. Zagorska, A. Pron Synth. Met. 18 (1987) 43.

[6] Y. A. Bufitsky, B. A. Zhubanov, G. G. Maresch, Synth. Met. 41-43 (1991) 373.

[7] J. Ochmanska, P. G. Pickup, J. Electroanal. Chem. 271 (1989) 83.

[8] J. Grimshaw, S. D. Perara, J. Electroanal. Chem. 281 (1990) 125.

[9] A. Deronzier, R. Devaux, D. Limosin, J. M. Latour, J. Electroanal. Chem. 324 (1992) 325.

[10] S. Kuwaba, K. Okamoto, H. Yoneyama, J. Chem. Soc., Faraday Trans.I 84 (1988) 2317.

[11] D. T. McQuade, A. E. Pullen, T. M. Swager, Chem. Rev. 100 (2000) 2537.

[12] T. Kudo, M. Kimura, K. Hanabusa, H. Shirai, T. Sakaguchi, J. Porphyr. Phthalocyanines 3 (1999) 65.

[13] J. K. O'Rourke, J. S. Brooks, N. A. Bell, J. Cawley, S. C. Thorpe, Sens. Actuators B 13–14 (1993) 690.

[14] J. D. Wright, P. Roisin, G. P. Rigby, R. J. M. Nolte, M. J. Cook, S. C. Thorpe, Sens. Actuators B 13-14 (1993) 276.

[15] C. Gu, L. Sun, T. Zhang, T. Li, X. Zhang, Thin Solid Films 327–329 (1998) 383.

[16] S. L. Vilakazi, T. Nyokong, Polyhedron 17 (1998) 4415.

[17] A. Elzing, A. Van Der Putten, W. Visscher, E. Barend, J. Electroanal. Chem. 233 (1987) 113.

[18] A. Coutanceau, P. E. Hourch, J. Crouigneau, M. Leger, C. Lamy, Electrochim. Acta. 40 (1995) 2139.

[19] P. N. Mashazi, K. I. Ozoemena, T. Nyokong, Electrochim. Acta 51 (2006) 3489.

[20] P. Peumans, S. R. Forrest, Appl. Phys. Lett. 79 (2001) 126.

[21] J. P. Viricelle, A. Pauly, L. Mazet, J. Brunet, M. Bouvet, C. Varenne, C. Pijolat, Mat. Sci. Eng. C 26 (2006) 186.

[22] J. Brunet, A. Pauly, L. Mazet, J. P. Germain, M. Bouvet, B. Malezieux, Thin Solid Films 490 (2005) 28.

[23] C. L. Honeybourne, R. J. Ewen, J. Phys. Chem. Solids 44 (1983) 833.

[24] B. Bott, T. A. Jones, Sens. Actuators B 5 (1984) 43.

[25] T. A. Jones, B. Bott, Sens. Actuators B 9 (1986) 27.

[26] B. Tieke, Adv. Mater. 3 (1991) 532.

[27] J. K. O'Rourke, J. S. Brooks, N. A. Bell, J. Cawley, S. C. Thorpe, Sens. Actuators B 15–16 (1993) 91.

[28] C. F. Van Nostrum, R. J. M. Nolte, Chem. Commun. (1996) 2385.

[29] H. Laurs, G. Heiland, Thin Solid Films 149 (1987) 129.

[30] S. Radhakrishnan, S. D. Deshpande, Sensors 2 (2002) 156.

[31] H. Varela, R. L. Bruno, R. M. Torresi, Polymer 44 (2003) 5369.

[32] C. D. L. Fuente, J. A. Acuna, M. D. Vazquez, M. L. Tascon, P. S. Batanero, Talanta 49 (1999) 441.

[33] M. Han, Y. Chu, D. Han, Y. Liu, J. Colloid Interf. Sci. 296 (2006) 110.

[34] B. Tion, G. Zerbi, J. Chem. Phys. 92 (1990) 3892.

[35] G. B. Street, in 'Handbook of Conducting Polymers'. Skotheim, T.A.(Ed.), Marcel Dekker, New York, (1986), P-265.

[36] J. A. Asensio, S. Borros, P. Gomez-Romero, J. Polym. Sci.: Part A: Polym. Chem., 40 (2002) 3703.

[37] J. H. P. Utley, C. Z. Smith, J. Mater. Chem. 10 (2000) 2642.

[38] L. M. Huang, C. H. Chen. T. C. Wen, A. Gopalan, Electrochim. Acta. 51 (2006) 2756.

[39] Carbon monoxide: Environmental Health Criteria 13, Geneva, WHO, 1979.

[40] L. J. Folinsbee, Human Health Effects of Air Pollution, Environmental Health Perspectives 100 (1992) 45.

CHAPTER VII

SUMMARY AND CONCLUSION

Summary and Conclusion

Conducting polymers are finding many applications in the field of microelectronics, MEM's, sensors, actuators etc. From the industrial safety and health point of view, it is essential to continuously monitor the levels of polluting and toxic gases like carbon monoxide. The sensor used for this purpose should be rapid, highly sensitive and selective in room temperature operating conditions. Also, the equipment associated with this should not be too complicated. Hence, the active material is essential to be in the semiconducting range, stable, having sensitivity, selectivity, immediate recovery and cost effective. Polypyrrole possesses these characteristics but needs to be tailored accordingly with proper dopants in order to increase the sensitivity and selectivity to carbon monoxide. The present work is aimed to study various types of functional groups, which can be incorporated in polypyrrole and their effect on the sensing characteristics when exposed to low quantity of carbon monoxide.

The dopant molecules were selected from a series of iron based organometallic complexes with iron as the central atom since these would be expected to respond to carbon monoxide. Ferrocene is one of the important known iron metallocene molecules, iron porphyrin and iron phathalocyanine are macrocyclic structured molecules. Here, the prominent factor is the effect of dopants in CO sensitivity in terms of its molecular structure. The general approach has been to synthesize polypyrrole incorporated with ferrocene and the ferrocene derivative, iron porphyrin and iron phthalocyanine, followed by thorough characterization of the modified polymer and then study the response of the change in conductivity (or sample resistance) using surface cell type sensor after exposure to low levels of CO gas.

In order to incorporate ferrocene moieties in polypyrrole, a number of methods were tried: i) direct incorporation during polymerization, ii) synthesis of ferrocene derivative and incorporation during electrochemical polymerization and finally iii) ferrocene derivative containing pyrrole so that it can be co-polymerized and introduced in the main chain.

Ferrocene was derivatised to *trans*-1-{4[2-(1-ferrocenyl)vinyl]phenyl}pyrrole, which contain an potentially oxidisable moiety, pyrrole at one end. This is expected to be easily

copolymerised with pyrrole and improve the sensitivity due to the direct linkage between the functional group and the main chain. It was seen that there is a remarkable change in sensitivity experienced for ferrocenyl derivatised copolymer with polypyrrole. A small resistance change is observed for PPy-Fc material, where as the ferrocenyl-pyrrole copolymer experienced much larger change in resistance after exposure to 300 ppm CO gas (see chapter 4). It also shows improvements in speed of response (t_{50}); ferrocenyl-pyrrole copolymer is faster (47 s) compared to PPy-Fc (96 s).

These PPy samples containing different dopants/functional groups were characterized by various techniques. The detailed analysis of the results indicated not only the incorporation of the Fe-complexes was successful but also their role in the modification and effects on polymer formation as well as the properties. The rate of polymerization was estimated from the real time UV-Vis spectra of polypyrrole formation and its modification with Fc, FeTPPCl and FePcTSA. It was found that the rate of polymerization increases in presence of the Fe-complexes and follows according to the order as Py-Fc < Py-FeTPPCl < Py-FePcTSA (giving the rate as 4.24 X 10^{-3}, 6.4 X 10^{-3} and 9.26 X 10^{-3} respectively). This suggests that the improved conversion rate of pyrrole monomer into modified polymer is associated with the catalytic activity of the Fe-complex present during polymerization. The actual amount of the Fe-complex present inside the polymer is also calculated by UV-Vis. spectroscopic method after obtaining the calibration graph. The FTIR spectra gave clear indication of the presence of functional groups inside PPy and characteristic vibrational frequencies of the dopants (PPy-Fc – 1108, 999, 811, 476 cm^{-1}; PPy-FeTPPCl – 1600, 1203, 1175, 1072, 1004, 805, 750 cm^{-1}; PPy-FePcTSA – 3436, 2920, 1147, 1110, 1040, 746, 700 cm^{-1}) were observed in corresponding samples. The EDAX and GFAAS studies for the elemental detection studies also confirmed the presence of the Fe-complexes in the samples with proportional increase in iron content with increasing content of Fc, FeTPPCl and FePcTSA in the polymer. A consistent increase of sulphur content is also seen for PPy-FePcTSA materials

The TGA data for PPy-Fc system shows the thermal degradation of the modified polymer occurs is almost tallying with the degradation of Fc at the temperature limit of 60 and 140^0C, where the degradation of Fc starts at 90^0. In case of PPy-FeTPPCl system, the

thermal degradation studied between the temperature (350 and 600^0C) of major degradation happens for the FeTPPCl. The onset of degradation for FeTPPCl is 410^0C. In this case, the thermal stability of the material increased with the increase in porphyrin content and also the percentage degradation was tallying with the expected value for the higher porphyrin content in PPy. For the PPy-FePcTSA system, the thermal degradation studies were analysed between 200 and 400^0C, which gave the experimentally observed percentage weight loss was always less than the expected value. This suggested that the phthalocyanine is bound to the polymer due to the interaction between the sulphonic acid groups and pyrrole nitrogen which stabilises the polymer by reducing the rate of degradation.

The XRD data shows that ferrocene is highly crystalline but there is no long range order when it is incorporated into PPy. Similar observations were made for phthalocyanine (FePcTSA) which is originally crystalline but the PPy doped with this compound is only amorphous. On the other hand, the crystalline peaks were observed in PPy-FeTPPCl materials at higher concentrations. The intensity of peaks decreases with decreasing content of FeTPPCl in the polymer. This indicates that there are tiny crystals of porphyrin still present inside the polymer. The ESCA analysis gives core level C_{1s} and N_{1s} spectra and percentage of charged carbon and nitrogen with shift in binding energies corresponding to C_1, C_2, C_3 and N_1, N_2, N_3 species. These data suggested higher level of charge transfer interaction between the FePc-TSA and PPy than other dopants.

The activation energy values were calculated from the temperature dependence of conductivity of the pellets of PPy-Fc, PPy-FeTPPCl and PPy-FePcTSA materials. It was observed that the incorporation of iron ferrocene and iron porphyrin led to decrease of conductivity of the material with coresponding increase of activation energy. The room temperature conductivity decreases with increasing content of ferrocene and porphyrin in PPy, but there is a slight increase in conductivity observed for PPy-FePcTSA materials. This happens mainly because of the sulfonate groups in FePcTSA, which give additional doping and charge transfer to PPy. However, above an optimum level of 10 wt.%, there appears to be aggregate formation giving rise to two activation energies: lower one for the doping effect in PPy-FePcTSA (Ea = 0.061 eV) and higher one due to phase separated phthalocyanine (Ea = 0.28 eV) in 15 wt.% PPy-FePcTSA sample. The decrease

in the conductivity of PPy after incorporation of ferrocene or FeTPPCl was also supported by the corresponding blue shift in the bipolaronic peak in UV-Vis spectra. Some of the samples also exhibited additional peaks corresponding to the Fe-complex used with some changes in the nature of the peaks, which could be associated with the charge transfer interaction with PPy matrix.

The electrochemical preparation of the PPy doped with different Fe-complexes was carried out directly on gold coated interdigited substrates to form the sensor. Ferrocenyl methyl trimethylammonium iodide, porphyrin and phthalocyanine were used in small quantities during the electrochemical polymerization of pyrrole in suitable electrolyte. The concentrations used were in between 1–10 mol% for ferrocenyl derivative and 1–10 mmol% for FeTPPCl and FePcTSA respectively with respect to pyrrole monomer. The modified films were deposited by chronoamperometry method. The potentiodynamic deposition of PPy modified films with respective iron complexes were carried out as a tool for characterization. The modified films are deposited on Pt electrode and the cyclic voltammetry of the same was performed in order to check the characteristic oxidation/reduction peaks potentials for the incorporated species. In all cases, it was confirmed that the Fe-complex was successfully incorporated by this technique. The electrical resistance values for the electrochemically deposited films were very low, much less than the chemically prepared samples. This was attributed to the highly doped state of the films prepared by ECP route.

The main focus of this work was the application of the modified PPy for carbon monoxide sensors. Hence, studies were carried out on the sensitivity and response time with respect to composition with the modified PPy materials using surface cell configuration for both chemically and electrochemically prepared polymers. The various compositions of PPy modified with iron complexes were coated on interdigited electrodes and exposed to 300 ppm CO gas, which is well inside the toxic limits. In all the cases, it is observed that there is an increase in resistance when these materials were exposed to CO gas. There is a large increase of resistance observed for PPy-Fc, PPy-FeTPPCl and PPy-FePcTSA materials while the original unmodified PPy showed only slight decrease in resistance for the same exposure to CO gas. The response time for these materials was seen to decrease from ferrocene (96 s) to porphyrin (48 s) and further in

phthalocyanine (0.51 s) doped PPy materials. The rate of change of resistance was extremely rapid for PPy–FePcTSA and it took only 0.5 seconds to attain about 3 orders of magnitude change. There was no permanent change in the material since the resistance value recovered quickly after the samples were exposed to normal air. Also, these materials were capable of sensing as low as 21 ppm CO gas. In the case of PPy-FePcTSA, the sensitivity factor was clearly shown to depend on the CO concentration. It was observed that a sensitivity factor of 25.74, 45.6 and 51.8 was obtained for 21 ppm, 100 ppm and 300 ppm CO gas respectively.

The CO sensitivity and response of the electrochemically deposited films were found to have similar trends as those made by chemical polymerization route i.e. increase of resistance observed during exposure to CO gas, optimum concentration of the functional dopant at which maxiumum sensitivity and fast response was obtained. The electrochemically deposited pure PPy film was not at all sensitive to carbon monoxide gas. Although these films did not exhibit as high value of sensitivity as the chemically prepared samples, considering the very low concentration of Fe-complex used (in mmole levels), the films gave good response to CO gas. This can be due to the fact that the electrochemically deposited films have densely packed PPy structure where the CO interaction takes place mainly on the surface of the modified film. In case of chemically deposited films, it is a bulk phenomena, where the CO gas penetrates into the polymer particulate matrix and interacts with the doping agent present at large number of sites. Nonetheless, the electrochemically prepared films have great advantage in that these can be directly deposited from monomer on to the interdigited electrode giving the sensor where as the chemically prepared PPy particles have to be first separated from reaction mixture, then dispersed and coated to form as sensors. Further, very low levels of costly functional Fe-complexes are required for PPy deposited by electrochemical technique.

In all the cases studied in the present work for the dopants/functional groups introduced in polypyrrole, it was observed that there is an optimum concentration of the dopant needed to get high sensitivity when exposed to low levels (300 ppm) of carbon monoxide. The optimum concentration depends on the actual iron complex used, it is 1.3 mole% for ferrocene but for porphyrin it is 0.946 mol% and for phthalocyanine it is 0.732 mol% at which highest sensitivity is obtained. In order to understand the mechanism for

the observed increase in resistance during exposure to CO gas, it is essential to look at the charge generation and transport in these functionalized polymer after exposure to CO gas molecules. When polypyrrole is exposed to CO gas, it is seen that there is a very slight increase in conductivity or decrease in resistance but when it is modified with Fc, FeTPPCl and FePcTSA, the change in resistance is totally reversed i.e. there is large increase of resistance. The reason due to this reverse in trend is due to the interaction of CO molecules with the Fe center of the dopant species rather than the main PPy chain. In case of PPy, the interaction is between CO and nitrogen atom of the polymer, which is expected to lead to generation of more number of free carriers. This would lead to increase in conductivity or decrease in resistance but the actual change of resistance during exposure in pure PPy is very less. This indicates pure PPy is a poor sensor material, which needs improvements. On the other hand, when the iron complex such as ferrrocene, iron porphyrin or iron pthalocyanine is present in the polypyrrole matrix, CO molecules interact with these leading to transfer of electron and trapping of holes from the conducting polypyrrole. Since all the iron complexes used here is have a conjugated structure, it is expected that there are effective communication between dopant and the polymer when CO interacts with iron center. The iron atom of Fe complexes containing vacant *d*-orbitals. When CO enters, it is capable of contribute electrons to the vacant *d*-orbital of the central metal atom. Subsequent electron transport takes place leading to increase in resistance of p-type polypyrrole.

Material	Molecular Dimension (Å)	Sensitivity factor (max.)	Response time (max.), t_{50} (s)	Concentration of dopant (mol%)
PPy	—	0.76	936	—
PPy-Fc	4.3	25.8	96	1.32
PPy-FeTPPCl	15.5	10.8	169	0.946
PPy-FePcTSA	19.5	51.8	0.51	0.732

Table 7.1. Comparison of molecular dimensions of dopants and sensor characteristics.

It may be interesting to compare the effect of these various iron complexes used as functional dopants for enhancement of sensitivity of polypyrrole to carbon monoxide. Table – 7.1 depicts such a comparison for these molecules when incorporated in PPy. It may be noticed that there appears to be some systematic variation between the size of the functional group and the sensitivity factor, response time as well as the concentration at which highest sensitivity is obtained. It should be pointed out that all of these contain conjugated π electrons and central iron atom. As the molecular dimension of the functional group increases, the sensitivity as well as the speed of response increases. Also, the concentration of the functional dopant at which maximum sensitivity is obtained lower as its size is higher i.e. ferrocene having smaller size has to be added more for obtaining higher sensitivity while FePcTSA being bigger size gives higher sensitivity even at low concentration in polypyrrole. These observations and comparisons of the results suggest that the increase of sensitivity of PPy by the incorporation of functional molecules is brought about by two processes: (1) ease of diffusion of CO molecules into the polymer and (2) efficient charge transport between the functional group and the PPy chain. From the present studies, FePcTSA (sulfonated phthtalocyanine) has been found to be most effective in increasing the sensitivity of PPy to carbon monoxide because of its size as well as better doping effect. The former gives rise to large interchain separation of PPy molecules leading to ease of CO diffusion in and out of polymer film while the latter factor leads to large changes in electrical resistivity after exposure to CO gas. That the morphology also plays an important role in controlling the sensitivity is clearly seen from the fact that higher crystallinity of Fe porphyrin doped PPy gave lower sensing characteristics. Also, ferrocene being small molecule does not cause much openings between the PPy chains and CO molecules diffuse slowly into the polymer films leading to much slower response characteristics as compared to FeTPPCl and FePcTSA doped PPy.

The present studies have given deeper understanding regarding the various factors, which control the sensing behaviour of conducting polymer such as polypyrrole. Typical case of CO gas detection was taken because of its direct relevance to industrial and environmental safety. Also, room temperature operating fast sensors for this toxic gas are not easily available. As such, conducting polymers are not very sensitive to carbon

monoxide as compared to other gases such as ammonia, chlorine etc. which have direct doping/undoping effects on conducting polymers. Hence, the additional functional groups have to be introduced so as to increase the sensitivity of these polymers. The present studies clearly demonstrate how this can be achieved leading to a very useful and promising material for these applications. The basic principles have also been brought forth in the present studies: 1) appropriate dopant/functional group which can interact with the molecules to be detected, 2) its association with conducting polypyrrole in terms of doping, changes in morphology, increase of interchain separation etc. 3) optimization of the concentration of the functional dopant and 4) appropriate technique for sensor fabrication which give the best results. The judicious selection of the materials also has been brought out. The best performance material may be used directly for fabricating micro machined (MEM's) devices for higher sensitivity. The surface cell configuration can be useful as an alternative for other existing sensors available in the market, because the ceramic based sensors requires heating element to make it working, while the proton conducting membrane type sensors do not have long life. The present studies open up a new area and methodology for developing such sensors with better sensitivity and faster response.

PATENTS, PUBLICATIONS AND SYMPOSIA PRESENTATIONS

A) List of Publications

1) S. Radhakrishnan, **Santhosh Paul**, "*Conducting Polypyrrole Modified with Ferrocene for Applications in Carbon Monoxide Sensors*", ***Sens. Actuators B*** (in press) 2007.

2) **Santhosh Paul**, N. N. Chavan, S. Radhakrishnan, "*A Rapid Carbon Monoxide Sensor Based on Conducting Polypyrrole Functionalized with Ferrocenylmethyltrimethyl ammonium iodide* ", ***J. Anal. Chem.*** (communicated) 2007.

3) **Santhosh Paul**, S. Radhakrishnan, "*Iron(III)Phthalocyanine (FePcTSA) Doped Polypyrrole for Rapid Sensing of Carbon Monoxide Gas"*, ***Sens. Actuators B*** (communicated) 2007.

B) List of Patents

1) Santhosh Paul, S. Radhakrishnan, "*Carbon Monoxide Sensor Based on Conducting Polymer*", US, Europe and Indian Patents Appl. **Ind.Pat. NF 217 /2005**

C) Symposia Presentations

1) Participated for the **International Conference,** ICEP-2007 conducted by Indian Society of Electroactive Polymers (ICEP) and Material Research Development in Goa, India, 19–24, February, 2007.

2) **Santhosh Paul,** S. Radhakrishnan**,** "*Properties and applications of Iron(III) phthalocyanine doped polypyrrole as carbon monoxide sensor*", Society of Polymer Science (**SPS**), India at NCL, Pune, 17–20, December 2006.

3) **Santhosh Paul**, S. Radhakrishnan, *"Carbon Monoxide Sensor based on Conducting Polypyrrole",* National Seminar on Physics and Technology of Sensors at University of Pune from 27th February to 1st March, 2006.

4) **Santhosh Paul**, S. Radhakrishnan, "*Online spectrochemical monitoring of synthesis of conducting polypyrrole*", Society of Polymer Science, at National Chemical laboratory, Pune in august, 2005.

5) Participated **International Conference** on polymers **MACRO-2004**, Society of Polymer Science, India at Regional Research Laboratory, Thiruvananthapuram, Kerala in December 2004.